THE UNIVERSITY OF HULL


**Continuous Flow Processes on Single Magnetic
and Diamagnetic Particles in Microfluidic Devices**


being a Thesis submitted for the Degree of

Doctor of Philosophy

in the University of Hull


by


Mark Duncan Tarn MChem


April 2011

# Table of contents

# Acknowledgements

Firstly, I would like to say a special thank you to my supervisor, Nicole Pamme, for giving me the chance to study for this PhD, and for all of your support and advice over the last three years. I've learned so much and grown in a number of ways both professionally and personally as a result of the PhD, and I thank you so much for your considerable part in that. Although, I'm not sure I'll ever able to take the words "It's not as bad as it looks" seriously ever again when I'm handed back a piece of corrected work…just kidding.

I give special thanks to Sally Peyman, who started as my mentor in Lab C217, helping me find my way in a research environment, and became my best and closest friend. Thank you so much for all your fantastic support over the years and for all the amazing times both inside and outside of work. You made the lab way more fun than a place of work has any right to be, it just was never the same with you gone. Thanks also to Lou Evans who, along with Sal and Tom Dearing, was there to help me right at the start of the PhD, and who has been a close friend ever since.

I would also like to show my gratitude to my good friends and colleagues past and present in the analytical department including Alex Iles, Martin Vojtíšek, Francesco De-Leonardis, Emily, Entesar, Sam, Jane, Amy, Grant, Chris, Jenny, Cordula, Ivón, and the

numerous project students who passed through the doors of C217. Special thanks as well to Kirsty Evershed for the help and laughs in out of work, and for the reliable trips to the Gardener's Arms every Friday evening along with her husband, Mike.

From a more professional viewpoint, I would like to thank various people in the department, including Nigel Parkin and Mike Dunn from the workshops who made all manner of contraptions for me, Steve Clark for showing me how to fabricate my own chips (it's not too bad once you get over the crippling fear of using HF), Vesko Paunov for discussions regarding colloidal suspensions and surface chemistry, and to Rawil Fakhrullin for the provision of the magnetic cells. Furthermore, I would like to say 'arigato gozaimasu' to Noriyuki Hirota and Yoshio Sakka from NIMS for giving me the fantastic opportunity to work in Japan for those couple of months. To Hirota-san I am particularly grateful for his help with the practical side of things, I'm sorry I kept you at work until the early hours when I was too busy with experiments. Also, the opportunity to stand on a 38 T hybrid magnet (turned off) and see the cooling towers and planks of copper required to power it was awe-inspiring to say the least. Domo.

Outside of work I would like to thank my friends who have been there to support me over the years of this project, particularly Reg and Bec (who satiated my hunger for curry with regular trips to The Last Viceroy), Taz and John, Ian and Alice, Sophie and Simon, Anthony, Seb, Kirstie, Elaine, and my oldest friend from home, Lee Tinkler.

Finally, I give extra special thanks to my family for their support in everything I've achieved so far, to my parents Gary and Ann Tarn, and my sister Jaff Tarn. Thank you so much, and I hope I can make you proud.

# Glossary

| | |
|---|---|
| $1^o$ Ab | Primary antibody |
| $2^o$ Ab | Secondary antibody |
| APTES | (3-Aminopropyl)triethoxysilane |
| **B** | Magnetic flux density (T) |
| BA | Barrier filter wavelength (nm) |
| CRP | Recombinant human C-reactive protein |
| COC | Cyclic olefin copolymer |
| $C_W$ | Viscous drag coefficient on a particle in a microchannel (dimensionless) |
| $d$ | Depth of a channel (m) |
| $D$ | Molecular diffusion coefficient ($m^2 s^{-1}$) |
| DEP | Dielectrophoresis |
| DM | Dichromatic mirror cut-on wavelength (nm) |
| DNA | Deoxyribonucleic acid |
| EDC | (*N*-(3-Dimethylaminopropyl)-*N'*-ethylcarbodiimide hydrochloride |
| ELISA | Enzyme-Linked Immunosorbent Assay |
| EOF | Electroosmotic flow |
| EX | Excitation filter wavelength (nm) |

| | |
|---|---|
| $f\mathrm{R_e}$ | Coefficient of friction |
| $\mathbf{F_{ac}}$ | Acoustic force on a particle (N) |
| $\mathbf{F_{DEP}}$ | Dielectrophoretic force on a particle (N) |
| FDTS | Trichloro(1$H$,1$H$,2$H$,2$H$-perfluorooctyl)silane |
| FEMM | Finite Element Method Magnetics |
| FITC | Fluorescein isothiocyanate |
| FGA | Fluoresceinyl glycine amide |
| $\mathbf{F_{grav}}$ | Gravitational force on a particle (N) |
| $\mathbf{F_{mag}}$ | Magnetic force on a particle (N) |
| $\mathbf{F_{opt}}$ | Optical force on a particle (N) |
| $\mathbf{F_{vis}}$ | Viscous drag force on a particle (N) |
| $g$ | Acceleration due to gravity (9.81 m s$^{-2}$). |
| $\mathbf{H}$ | Magnetic field (A m$^{-1}$) |
| $\mathbf{H_c}$ | Coercivity (A m$^{-1}$) |
| $K$ | Constant of an Ubbelohde viscometer (m$^2$ s$^{-1}$) |
| $k_B$ | Boltzmann constant (1.3806504 x 10$^{-23}$ J K$^{-1}$) |
| $l$ | Length of a channel (m) |
| LbL | Layer-by-Layer |

| | |
|---|---|
| M | Molar mass (g mol$^{-1}$) |
| **M** | Magnetisation (A m$^{-1}$) |
| **M$_r$** | Magnetic remanence (A m$^{-1}$) |
| **M$_s$** | Saturation magnetisation (A m$^{-1}$) |
| MES | 2-(*N*-Morpholino)ethanesulfonic acid buffer |
| NdFeB | Neodymium-iron-boron |
| OTS | Octadecyltrichlorosilane |
| $\Delta p$ | Pressure drop (Pa) |
| PAH | Poly(allylamine hydrochloride) |
| PAH-FITC | Poly(fluorescein isothiocyanate allylamine hydrochloride) |
| PBS | Phosphate buffered saline |
| PC | Poly(carbonate) |
| PEEK | Poly(ether ether ketone) |
| PEG-silane | 2-[Methoxy(polyethyleneoxy)propyl]trimethoxysilane |
| PEG-SPA | Poly(ethylene glycol)-succinimidyl propionate |
| PDADMAC | Poly(diallyldimethylammonium chloride) |
| PDMS | Poly(dimethylsiloxane) |
| pI | Isoelectric point |

PMMA        Poly(methylmethacrylate)

PSS         Poly(4-styrenesulfonic acid)

PTFE        Poly(tetrafluoroethylene)

QAS         Quaternary ammonium silane

            (Dimethyloctadecyl[3-(trimethoxysilyl)propyl]ammonium chloride)

$r$           Radius of a particle (m)

$r_h$          Hydraulic diameter of a channel (m)

$R$           Gas constant (8.314472 J K$^{-1}$ mol$^{-1}$)

$R_\phi$          Flow resistance in a microchannel (kg m$^{-4}$ s$^{-1}$)

$R_\phi$(tot)      Total flow resistance in a microchannel (kg m$^{-4}$ s$^{-1}$)

$R_{sep}$        Separation distance between particle centres (m)

RCA         Rolling circle amplification

Re          Reynolds number

Re$_p$         Particle Reynolds number

$t$           Time (s)

$T$           Temperature (K or °C)

$w$           Width of a channel (m)

$x$           Distance (m)

$x_c$          Distance from the centre of a channel (m)

| | |
|---|---|
| $\mathbf{u_{defl}}$ | Deflection velocity of particle (m s$^{-1}$) |
| $\mathbf{u_{hyd}}$ | Particle velocity due to hydrodynamic flow (m s$^{-1}$) |
| $\mathbf{u_{mag}}$ | Particle velocity due to magnetic field (m s$^{-1}$) |
| $v$ | Velocity of a fluid (m s$^{-1}$) |
| $v_k$ | Kinematic viscosity (m$^2$ s$^{-1}$) |
| $v_p$ | Average velocity of a particle (m s$^{-1}$) |
| $V_m$ | Volume of magnetic material (m$^3$) |
| $V_p$ | Volume of a particle (m$^3$) |
| $\chi$ | Volume magnetic susceptibility (dimensionless) |
| $\chi_p$ | Volume magnetic susceptibility of a particle (dimensionless) |
| $\chi_m$ | Volume magnetic susceptibility of the medium (dimensionless) |
| $\chi_{mass}$ | Mass magnetic susceptibility (m$^3$ kg$^{-1}$) |
| $\chi_{mol}$ | Molar magnetic susceptibility (m$^3$ mol$^{-1}$) |
| $\delta$ | Hydrodynamic diameter of a channel (m) |
| $\phi$ | Applied flow rate (m$^3$ s$^{-1}$) |
| $\eta$ | Absolute (dynamic) viscosity of a fluid (kg m$^{-1}$ s$^{-1}$) |
| $\mu$ | Permeability (H m$^{-1}$) |
| $\mu_0$ | Permeability of free space ($4\pi$ x $10^{-7}$ H m$^{-1}$) |

$\zeta$        Zeta potential (V)

$\rho$        Density (kg m$^{-3}$ or g cm$^{-3}$)

$\rho_m$        Density of media (kg m$^{-3}$ or g cm$^{-3}$)

$\rho_p$        Density of a particle (kg m$^{-3}$ or g cm$^{-3}$)

$\nabla$        Del operator

$\zeta$        Zeta potential (V)

$\rho$        Density (kg m$^{-3}$ or g cm$^{-3}$)

# Abstract

Magnetic microparticles have seen increasing interest in (bio)chemical processes in recent years due to their various surface functionalities, high surface-to-volume ratio, small sizes, and ease of manipulation via magnetic fields. However, conventional reactions and assays that use magnetic particles as solid supports are typically performed in multi-step procedures that require consecutive reaction and washing steps. While offering high capture efficiencies, these are batch processes that, due to the consecutive steps required, are typically time-consuming and laborious. Their incorporation into microfluidic devices has brought about benefits including finer control over the movement of particles and reagent/sample solutions, as well as the ability to place a magnet closer to the area of interest. However, most instances of on-chip magnetic particle based procedures rely on trap-and-release methodology, essentially requiring the same stepwise routine as with conventional systems. A method of reducing these inefficiencies is to perform the reaction or separation in continuous flow, thereby allowing continuous sample introduction and analysis of the process in rapid times, and with minimal reagent consumption and waste production.

Two methods of performing continuous flow procedures on single particles in microfluidic devices via the application of magnetic forces were investigated: 1) the use of magnetic microparticles as mobile solid supports for performing rapid separations, reactions, and immunoassays via magnetic attraction, and 2) the use of diamagnetic repulsion forces for performing similar procedures on non-magnetic particles, with a view to the label-free processing of diamagnetic species such as polymer particles and biological cells, based on their intrinsic properties.

For the magnetic attraction experiments, a study into the effect of temperature on magnetic particle deflection behaviour and separations was performed, whereupon it was found that an increased temperature of the system yielded increased deflection distances and separation resolution due to the reduced viscous drag. This was followed by several investigations into the deflection of particles through laminar flow streams containing alternating reagents and washing buffers for performing multistep reactions and assays. The setup was used to demonstrate amide bond formation and polyelectrolyte deposition in continuous flow, before being used to detect clinically relevant levels (5 and 10 $\mu$g mL$^{-1}$) of the inflammatory biomarker, C-reactive protein. Thus, these findings show great potential for rapid, continuous processing of particles for a number of chemical and biological applications, as well as in clinical diagnostics.

For the diamagnetic repulsion studies, diamagnetic polystyrene particles were suspended in paramagnetic media and deflected away from a magnetic field in continuous flow. The effect of particle size and the magnetic susceptibility of the paramagnetic media on particle deflection were investigated using high magnetic fields, where it was found that larger particles in a medium with higher susceptibility yielded the greatest deflection. This work was extended via a proof-of-principle setup in which polystyrene particles were repelled out of a reagent stream and into a buffer stream using permanent magnets, with a view to performing continuous flow reactions through laminar flow reagent and washing buffer streams, akin to those achieved via magnetic attraction. Finally, flow focussing of polystyrene particles and label-free cells was achieved via diamagnetic repulsion forces applied by permanent magnets, demonstrating the ability to manipulate cells in continuous flow by magnetic forces based on their intrinsic properties. This work could be applied to the label-free processing of particles and cells for separations, reactions, and assays.

# 1 Introduction

## *1.1 Microfluidics and micro total analysis systems (μTAS)*

Microfluidic and lab-on-a-chip technology has increased dramatically in popularity in the last two decades. It concerns the manipulation of fluids with volumes smaller than the nanolitre range in networks of channels in a solid substrate, with the channels having dimensions of tens to hundreds of micrometres.[1,2] Microfluidics has been employed in a wide variety of chemical and biological procedures,[3,4] including: organic synthesis,[5,6] forensic analysis,[7,8] DNA extraction[9,10] and analysis,[11] polymerase chain reaction (PCR) amplification,[12] the interrogation of cells[13] and tissue,[14] chemical and biological assays,[15,16] environmental monitoring,[17,18] and various sample pre-treatment, separation and detection techniques in analytical chemistry.[19,20] Indeed, analytical chemistry is one of the major interests in microfluidics research, with even the first microfluidic device being a miniaturised gas chromatography system, fabricated on a silicon wafer by Terry *et al.*[21] in 1979. However, at the time the concept had little impact on the analytical chemistry community due to its poor performance compared to conventional gas chromatography.

In 1990, Manz *et al.*[22] developed a miniaturised open tubular liquid chromatography device on a silicon wafer, and even though no actual separation was performed, the theoretical gains of the system were made evident with the ability to achieve higher separation efficiencies than conventional methods. With this development came also the concept of micro total analysis systems (μTAS or microTAS) by Manz *et al.*,[23] in which a sample could be pretreated, separated, and detected, all on the same microfluidic device, effectively replacing conventional, bulky benchtop systems. This idea was well-received and sparked a new era in analytical technology, which has since

seen a phenomenal increase in interest with the miniaturisation of conventional methodologies and the development of new ones.

Despite being in a relatively early stage of development, microfluidics is already encouraging revolutionary techniques, particularly in the last decade, in chemical and biological processes that are difficult or even impossible to perform on the macroscale.[2] This can be most easily evidenced by the biennial publication, since 2002, of reviews into recent advances in microfluidic technologies and applications by the research group of Manz,[24-28] which in its most recent iteration even had to be split into two separate topics focussing on chemical[29] and biological[30] developments, respectively, such was the wealth of new information on offer. As further proof of the revolution in microfluidic research, a Web of Science search for the keyword *microfluid\** for the year 2000 gives 235 results, while for the year 2010 the same search yields 2,998 hits.

There are several reasons as to why microfluidic technology has experienced such popularity:

1) As alluded to by the name, microfluidics allows small volumes of solutions to be used to perform the same operations that would require substantially greater volumes in conventional systems. A chromatography setup that would require litre volumes of solutions on the bench could now be performed using a fraction of the volume in a small syringe or reservoir of a microdevice, whilst also producing less waste. Even procedures that would normally be considered to use "small volumes", such as assays performed in Eppendorf tubes, would typically occur in the microlitre or millilitre range, whereas on-chip the same assay would require nanolitres of solution or less. Hence, the amounts of reagents used can be reduced, which can be very cost-effective when dealing with expensive reagents. Another benefit of the

smaller volumes is that it adds extra safety to a procedure, since any hazardous material will only be present in a small amount.

2) Reaction and analysis times are decreased due to the shorter diffusion distances between different species in the confined spaces of a microchannel, giving better mass transfer. This is also beneficial for reactions/analysis on solid-supports in the channel, or on the channel surface itself, as species not only have less distance to travel before encountering the support, but with solutions being constantly pumped through the channel the support is constantly exposed to fresh reagent while any waste and unbound material is washed away. Additionally, the high surface-to-volume ratio enables better heat transfer to/away from the liquid inside the channel, a useful feature when trying to perform temperature-based operations (e.g. PCR) or to disperse heat, respectively.

3) Flow in microchannels is laminar, the physical parameters of which are well known, therefore precise control can be achieved over the processes taking place in the system compared to batch methods (e.g. the mixing of reagents). Additionally, reactions and assays can be performed in continuous flow, allowing high throughput and real-time monitoring of products and analyses, and an automated feedback system can be used to continually alter parameters to provide optimal results.[31-33]

4) The ability to integrate various devices into a chip for separation, assays or detection. Examples include integrated magnetic and magnetisable components,[34] electrodes for particle/cell manipulation,[35] and electrochemical sensors.[34] This allows the components to be situated as close to the area of interest as required, and to have all the necessary apparatus in the device itself.

5) A small footprint, requiring less laboratory space, and allowing portability and point-of-care diagnostics. Since the devices are on a very small scale, and can feature integrated microvalves[36] and micropumps,[37] they offer the potential to be taken directly to a patient's bedside or to a crime scene where the analysis can be performed on-the-spot. This offers shorter "time-to-results" since it would allow a "sample in – answer out" process to take place on the spot, in comparison to having to send samples to a normal laboratory for analysis.

6) Potentially low fabrication costs (depending on the method and material), giving the possibility for inexpensive mass production of the devices. This has the advantage that many prototypes can be produced whilst a technique is optimised, and the final design can be fabricated in large numbers, having greater cost advantages for single-use point-of-care devices. The low cost could also potentially allow systems to be "scaled out" rather than "scaled up", with regards in particular to chemical synthesis. When conventional reactions are scaled up for industrial production there are typically problems with the scaling process, such as bulk mixing. However, by scaling out, multiple microfluidic devices of the same type can be placed in parallel, allowing small-scale reactions to take place in such numbers as to generate large volumes of product in total.[38]

With these numerous advantages it is clear why microfluidic devices have received such interest in recent times, having great potential for revolutionising chemical and biological processes.

### 1.1.1    Microfabrication

Microfluidic chips can be fabricated from a number of materials, with the choice of substrate depending on the desired properties and function of the device.  Glass is a popular choice due to its optical transparency and stability to harsh chemicals.  Silicon is used less commonly than glass due to its lack of transparency.  Glass and silicon chips are generally fabricated using a photolithography and wet etching method derived from the semiconductor industry, which is described in greater detail in Section 2.3.[39-41]

Hard polymers have become popular as substrates over the years, including poly(carbonate) (PC),[42] poly(methyl methacrylate) (PMMA),[43] and cyclic olefin copolymer (COC).[44,45]  The downside of polymers is that they are generally not as stable to harsh chemicals and reaction conditions as glass, hence their use in chemical processes can sometimes be limited.[46,47]  Importantly, however, replication technologies can be applied to polymers that allow inexpensive and rapid production of disposable point-of-care systems.  Current methods of fabrication for polymers include injection moulding,[45,48] imprinting,[43] hot embossing,[43,49] and laser ablation.[50]

Poly(dimethylsiloxane) (PDMS)[51] is probably the most popular material for chip fabrication in research labs due to its fast and easy fabrication method that allows rapid prototyping, though it is not so useful for mass fabrication.  PDMS chips are prepared via soft lithography.[51,52]  Briefly, a "master" is prepared that features the chip design as positive relief, typically from SU-8 photoresist (a photocurable epoxy), and the elastomer precursor and curing agent are simply mixed and poured over the master. The device is allowed to cure, then peeled off the master and sealed onto a cover plate such as glass or PDMS.

## 1.1.2   Laminar flow and diffusion

Mixing chemicals in a beaker or flask is achieved via turbulence in the liquid, in which the flow is chaotic and unstable. However, in the confined channels of microfluidic systems, laminar flow predominates, with well-defined streamlines flowing side-by-side (Fig. 1). When flow is laminar, mixing between solutions occurs only due to the diffusion of co-flowing streams into each other.
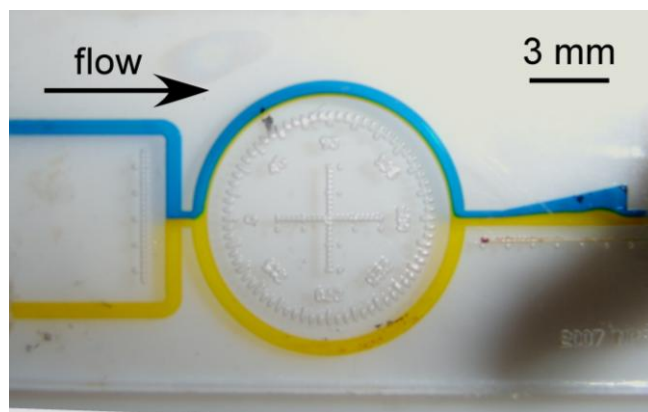


**Fig. 1   Example of laminar flow in a microfluidic device between blue and yellow inks. The design featured 500 μm wide and 100 μm deep channels.**

Laminar flow occurs when the viscous forces in the system dominate the inertial forces.[45,53] Whether a flow regime is laminar or turbulent can be determined by the calculation of its Reynolds number, Re (dimensionless), as shown in Equation 1. When Re < 2000 the flow is laminar, and when Re > 2000 the flow is turbulent.

$$\text{Re} = \frac{\rho \, r_h \, v}{\eta} \qquad \qquad \textbf{Equation 1}$$

where $\rho$ = density (kg m$^{-3}$), $\eta$ = dynamic viscosity (kg m$^{-1}$ s$^{-1}$), $r_h$ = hydraulic diameter of the channel (m), and $v$ = average fluid velocity (m s$^{-1}$). The hydraulic diameter can

be calculated using Equation 2, where $A$ = the cross-sectional area of the channel (m$^2$) and $P$ = the wetted perimeter of the channel (m).[53]

$$r_h = \frac{4A}{P}$$  **Equation 2**

The extent of diffusion of molecules can be determined using the Einstein-Smoluchowski equation (Equation 3).[54]

$$x = \sqrt{2D\,t}$$  **Equation 3**

where $x$ = distance (m), $D$ = diffusion coefficient (m$^2$ s$^{-1}$), and $t$ = time (s). Knowledge of this equation allows chips to be designed in such a way as to enhance or reduce mixing in the microchannels, depending on the purpose of the system.

Microfluidic devices have been shown to have several advantages over conventional systems. Areas in which they have been very successfully applied are the fields of separations and chemical or biological assays. In the latter case, the large surface-to-volume ratio of a microchannel allows surface-based assays, in which antibodies attached to the channel surface are used to capture antigens, to be performed very efficiently due to the reduced diffusion distances of antigens to the surface. In addition to these advantages, the surface-to-volume ratio can be further increased by employing functionalised microparticles within a microchannel, enabling further increases in reaction efficiency.[55] The next section explains how such particles are incorporated into these devices and the mechanisms by which they can be manipulated for performing a number of procedures, including bioassays and separations.

## *1.2     Microparticles*

## 1.2.1    Properties and theory

Particles can be fabricated from a number of materials including polymers, glass, silica, gold, and inorganic crystals, depending on the requirement, and are available in a range of sizes (1 nm to ~100 μm).[56,57]  Particles with diameters of 1 nm to 1 μm dispersed in a liquid medium are known as colloidal suspensions, and are used in the manufacture of paints, adhesives and rubbers, among other things.  Particles between 1 μm and 100 μm are commonly referred to as microparticles, and when suspended in a liquid medium they are called coarse suspensions.

Polymer microparticles, in particular those made from polystyrene, are a popular choice for many processes, including bioanalysis and chemical procedures, due to their versatility.  A review by Kawaguchi describes the fabrication methods and applications for which such particles can be employed.[56]  As well as their range of sizes, they can also be functionalised with a variety of chemical (e.g. amine, carboxylic acid, epoxy) or biological (e.g. antibodies, antigens, single-stranded DNA) groups, which enable target species to bind to or react with them (Fig. 2).  Their small volume and diameter result in large surface-to-volume ratios, giving a large surface area that is available for reactions to be performed on when appropriately functionalised.  The small size also means that particles can respond quickly to stimuli (temperature, pH, electric fields etc.), and they are highly mobile in solution due to the low viscous drag forces affecting them.  Indeed, some particles featuring soft layers allow water to penetrate the layer, further decreasing the fluid resistance on their movement.

| antibodies | antigens | single-stranded DNA | oligo dT | chemical groups |
|---|---|---|---|---|
| assays Ag isolation cell isolation | assays Ab isolation | DNA hybridisation DNA isolation | mRNA isolation cDNA synthesis | org. synthesis protein isolation |
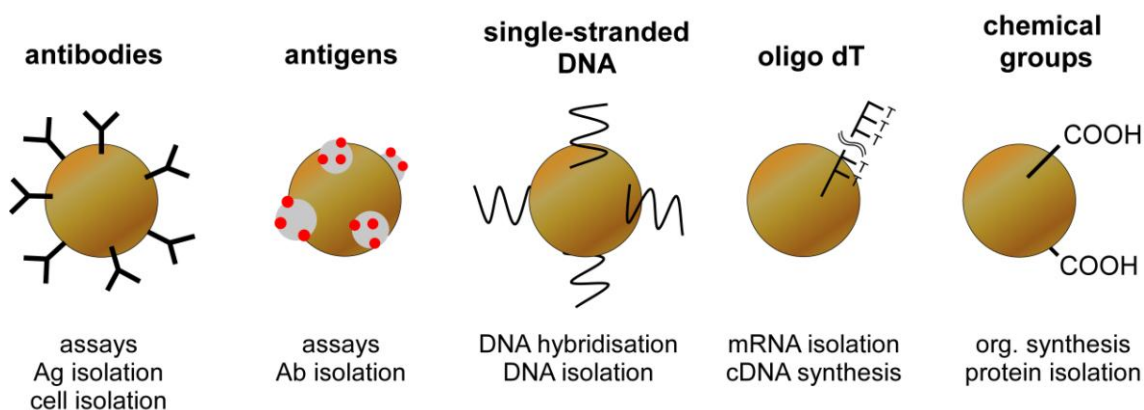
**Fig. 2  Microparticles functionalised with a wide variety of surface groups for performing a number of (bio)chemical procedures.**

With a range of surface properties and the aforementioned physical benefits of microparticles, they are commonly employed as solid supports for performing a number of (bio)chemical procedures including separations, immunoassays, and chemical reactions.[55,56,58] Typically, such processes are performed by introducing particles into a reagent solution or sample matrix and allowing the target species/reagent to bind to the surface, before separating the particles from the solution via sedimentation, decantation, centrifugation, and filtration. However, despite the advantages of using microparticles for performing assays etc., these traditional methods of separating them from the bulk mixture are time-consuming, laborious, and inefficient, particularly when the process must be repeated several times during the washing of the particles.

In recent years, microparticle separation and assay techniques have been incorporated into microfluidic devices, reducing diffusion distances whilst maximising binding efficiency (even more so than already possible in a surface functionalised microchannel), and allowing great control over the fluid flow and particle movement. In the following chapters, the theory of particle stability will be explained, and the

literature related to the use of microparticles in microfluidic systems will be reviewed, focussing on continuous flow procedures.

## 1.2.2    Stability of a particle suspension

When preparing or using a suspension of particles it is of paramount importance that the suspension be stable, lest the particles start sticking to each other and/or the surfaces of the container, or that they sediment (sink) or cream (rise) to the extent that they cannot be properly dispersed in the solution. Particle suspensions are thermodynamically unstable with respect to the bulk solution, with particles attracting each other via long-range forces (van der Waal's interactions) that work to agglomerate the particles into a single ball.[54] However, other factors oppose this attraction (such as electrostatic repulsion). Whether particles will attract to each other and agglomerate or repel each other and remain stable in solution depends on which of the forces are greater, as described by DLVO theory. These attraction-repulsion effects and their relation to DLVO theory are described below, as is non-DLVO theory, which explains "anomalous behaviour" with respect to classic DLVO theory. Additionally, sedimentation and creaming will be described since, while not inter-particle forces, they are also important for the stability of a particle suspension.

### Van der Waal's forces of attraction

These attractive forces occur between the electric dipoles of molecules, or in the case of particles the interactions between the molecules in each particle. There are three classes of van der Waal's forces: dipole-dipole (*Keesom*) interactions, dipole-induced-dipole (*induction*) interactions, and induced-dipole-induced-dipole (*dispersion*) interactions.

The first two classes only occur when some of the molecules in a system have permanent dipoles and so are not considered in DLVO theory, whereas dispersion interactions, also called London forces, are always present between molecules. In this scenario, electrons in a non-polar molecule "flicker" into an arrangement that results in an instantaneous dipole, which in turn polarises another non-polar molecule and causes the two dipoles to attract. While each dipole only contributes a weak attractive force, the sum of the molecules in a microparticle yields a significant force overall, resulting in the attraction of microparticles to each other. Van der Waal's forces have a range up to around 100 nm from a surface, and the strength of these forces is dependent on the particle material and the medium they are suspended in.

**Electric double-layer forces of repulsion**

An electrical double layer exists when ions build up a layer of charge on an oppositely charged surface. When two particles have electrical double layers featuring the same arrangement of charges, they are electrostatically repelled. Conversely, when two particles feature electrical double layers with opposing charge, they are attracted to each other. These electrostatic interactions are known as Coulomb forces.

When a particle features a charged surface, co-ions in solution are repelled from the surface while counterions are attracted to it and segregate into a layer of charge adjacent to the layer of surface charge (Fig. 3).[54,59] The rigid layer of adsorbed counterions is known as the Stern layer or Helmholtz layer (with a thickness approximately the diameter of a hydrated ion),[60] and the electric potential across this layer drops linearly with distance from the charged surface.
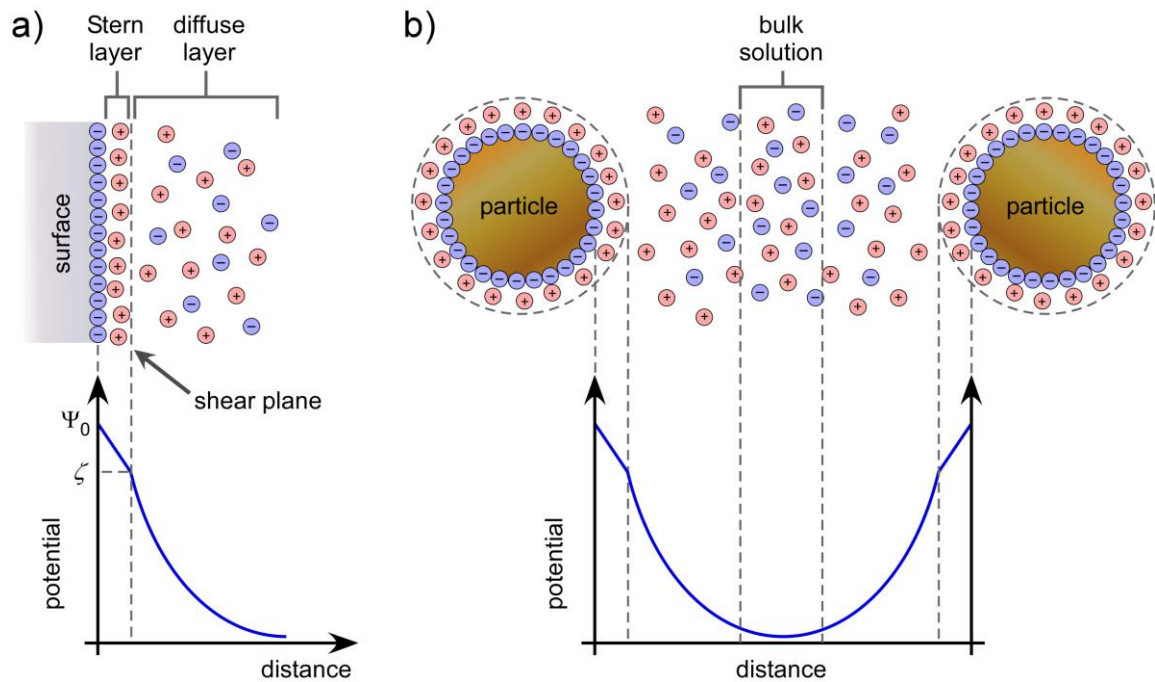
**Fig. 3  a) Electric double layer formation on a charged surface (with a surface potential designated $\Psi_0$). A rigid adsorbed layer of counterions forms on the surface, known as the Stern layer, across which the potential drops linearly. A second layer, the diffuse layer, then extends into the bulk solution, with the potential dropping exponentially. The surface potential at the shear plane is known as the zeta potential ($\zeta$). b)  Electrical double layers of two particles in a suspension. Electrostatic repulsion occurs between the particles when the double layers start to overlap.**

Beyond the Stern layer, a diffuse layer (Gouy-Chapman layer) is formed that consists of an excess of ions with opposite charge to that of the particle surface. The diffuse layer extends into the bulk solution, with potential now dropping exponentially with distance from the particle surface until it reaches zero, the point at which there is no excess of one charge over another in the bulk solution. The boundary between the Stern layer and the diffuse layer is known as the radius of shear, also called the shear or slipping plane).

The potential at the radius of shear relative to its value in the bulk material is known as the zeta potential, $\zeta$ (in volts), of the particle. The diffuse layer extends into the bulk solution with a thickness between a few and several hundred nm, as determined by the Debye length, $\kappa^{-1}$ (in nanometres), which gives the thickness of the electrical double layer (Equation 4).[61]

$$\kappa^{-1} = \frac{0.304}{\sqrt{I}} \qquad \textbf{Equation 4}$$

where $I$ = the ionic strength of the solution (M) of a 1:1 electrolyte solution (e.g. NaCl) at 298 K, as defined by Equation 5.

$$I = \frac{1}{2}\sum c_i \ z_i^{\ 2} \qquad \textbf{Equation 5}$$

where $c_i$ = concentration of ion $i$ (M), and $z_i$ = charge number of ion $i$. Equation 4 shows that the thickness of the electrical double layers increases with decreasing ionic concentration. For example the Debye length is 30.4 nm when [NaCl] = 1 x $10^{-4}$ M, whereas it is 0.96 nm at [NaCl] = 0.1 M. Thicker Debye layers are better for maintaining particle suspension stability as this allows electrostatic repulsion over longer distances, keeping the particles away from each other and stopping their agglomeration due to van der Waal's forces of attraction. With this in mind, low concentrations of ionic salt solutions are preferable for maintaining particle stability in microfluidic devices where the particles are in a confined region of space. Additionally, electrical double layers can form on the surfaces of microfluidic chips, hence the charge on the surface should be considered when introducing particles into such a device. For example, in the case of glass in a buffer solution with pH > 4, protons are dissociated from the silanol groups, rendering the surfaces negatively charged, and so the relative surface charge of the particles must also be considered.

**DLVO theory**

The overall theory of stability in a particle suspension considers both the attractive van der Waal's forces (with potential energy $V_A$) and the repulsive forces due to the overlap of the electrical double layer (with potential energy $V_R$). It was developed by Boris **D**erjaguin and Lev **L**andau in the Soviet Union (1941), and independently by Evert **V**erwey and Theo **O**verbeek in the Netherlands (1948), hence **DLVO** theory.[54,62] The total potential energy, $V$ (in Joules), of the two interactions is the sum of their individual potentials, as shown in Equation 6:

$$V = V_R + V_A \hspace{4cm} \textbf{Equation 6}$$

The potential energy of the particles due to the attractive ($V_A$) and repulsive ($V_R$) interactions are shown in Fig. 4, as is the resultant DLVO summation of the these energies ($V$). In the case shown, the resultant energy has a sufficient contribution from $V_R$ to repel particles from each other at long distances. However, at a short distance between the particles there exists a potential energy barrier.[59] If the barrier is large compared to the thermal energy of the particles, $k_B T$ (where $k_B$ is the Boltzmann constant of 1.381 x $10^{-23}$ J K$^{-1}$, and $T$ is the temperature in K), then the particles are unable to overcome this barrier and so the repulsion effect dominates, thus maintaining a kinetically stable suspension in which the particles remain separate. However, if the repulsion energy is low and the kinetic energy of the particles is sufficient to overcome the energy barrier, then the attractive forces will dominate and particles will coagulate, i.e. stick together irreversibly.

Thus, in order to maintain a stable particle suspension it is important to ensure that the repulsive forces are high enough to create a sufficient energy barrier.
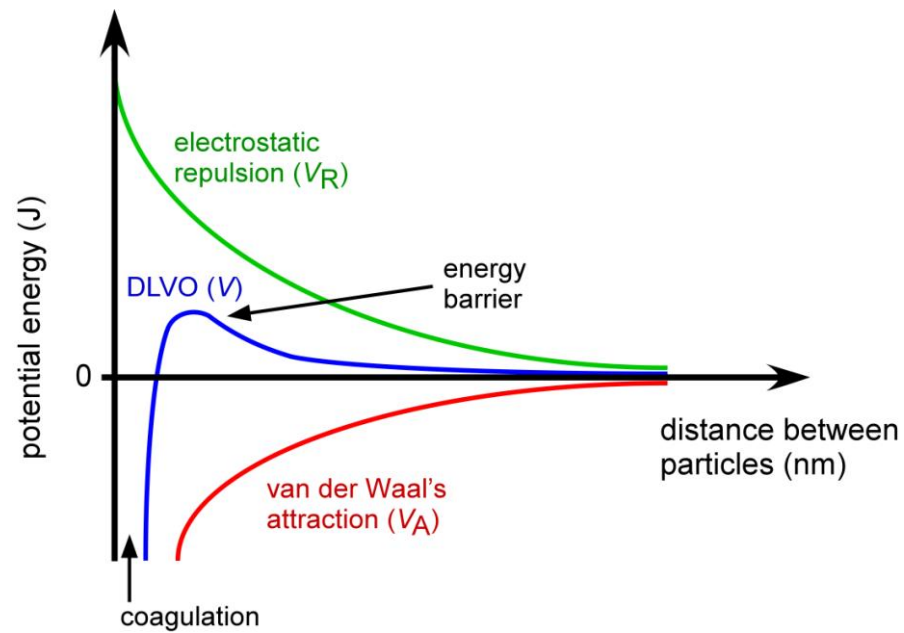
**Fig. 4  DLVO theory, demonstrating the combined effects of van der Waal's attraction and electrostatic repulsion over increasing separation distance between two particles.  As particles get closer together they experience an energy barrier; if their translational kinetic energy is sufficient to overcome this barrier they will coagulate.  If they do not overcome the barrier the particle suspension will remain stable.**

## Non-DLVO interactions

Although DLVO theory provides an excellent account of the major forces acting on particles and the stability of a colloidal suspension, there are other repulsive and attractive interactions that exist which deviate from expected DLVO theory.  These can be grouped together as non-DLVO interactions (also called Extended DLVO).  These interactions can typically be classified into three different types: oscillatory structural forces, steric polymer adsorption forces, and solvent association forces (hydrophobic and hydration forces).  However, the forces and physical causes behind many of these interactions are as yet unknown, and so there have been many theories as to why some

of the effects are observed. A review by Grasso *et al.*[63] details the non-DLVO interactions and summarises the theories that have been put forward, while several colloid science textbooks also contain chapters discussing the subject.[64,65] Additionally, Volume 14 of the journal *Colloids and Surfaces B: Biointerfaces* (1999), a special issue on DLVO theory, includes a number of publications concerning non-DLVO studies in order to extend the classical theory. Some of the non-DLVO interactions that are more relevant to this thesis will be outlined in brief in this section, while those not described here include: oscillatory structural forces, adhesion and capillary forces, and counter-ion only electrical double layer interactions.

*Hydrophobic attraction forces:* A form of solvent association forces, in this case describing attractive forces between hydrophobic surfaces. These have been observed to vary widely in range and magnitude, though they are measurable between ~10 and 250 nm and are much stronger than van der Waal's forces of attraction. The mechanism behind this particular type of interaction is unknown, though theories have included the presence of nanobubbles on the surfaces that bridge the gap between them, and the ejection of entropically disfavoured water from between two surfaces since water cannot form hydrogen bonds with them. It may be that several mechanisms contribute to an overall effect, or that different mechanisms occur in different experimental conditions.

*Hydration repulsion forces:* Another type of solvent association force, in this case the surfaces repel each other due to strongly bound water molecules on each surface (for example, the surfaces may feature ionic or hydrogen bonding groups), forming

hydration layers. The effective range of these forces is very short, typically ~3 nm between the surfaces. However, the actual cause and mechanism behind the repulsion is not understood on either a physical or theoretical level, though a basic explanation is that two hydrophilic substances prefer to be in contact with water rather than each other, hence they experience a repulsive force between them.

*Steric interactions due to polymer adsorption:* In this scenario, a polymer is introduced into the particle suspension, whereupon interactions due to the added polymer will dominate the other interactive forces between particles. The type of interaction depends on whether the polymer adsorbs to the particle surfaces, and the extent to which it does. When particles adsorb polymers onto their surface and approach each other, they experience so-called "steric" interactions between the polymers on their surfaces, which can be either attractive or repulsive. If a particle adsorbs a high density of polymer with a wide coverage, the polymer-coated particles repel each other due to overlapping and deformation of the polymer chains. However, when particles only adsorb polymers sparsely, bridging attraction can occur when the same polymer chain adsorbs to two different particles. Therefore, when using polymers in colloidal dispersions it is important to achieve a high density of polymer chains on the particle surfaces in order to obtain a stable suspension. While this describes the application of neutral polymers to particle suspensions, the use of charged polymers (polyelectrolytes) is less well understood due to lack of appropriate surfaces on which measurements can be performed. However, atomic force microscopy (AFM) experiments have suggested that the use of polyelectrolytes results in both steric and electrostatic contributions to interactions between surfaces.[64,66,67]

***Presence of surfactants:*** Surfactants are amphiphilic molecules that feature a hydrophilic "head" group (which may be anionic, cationic, non-ionic, or zwitterionic), and a hydrophilic "tail", thereby possessing parts that are soluble in aqueous solution and parts that are soluble in organic solvents. They can be added to colloidal systems to reduce sticking between particles and/or surfaces. However, their effect on a system is complicated as their presence alters the Debye length ($\kappa^{-1}$) of electrical double layers. Additionally, two surfaces with adsorbed surfactants featuring exposed hydrophilic headgroups can experience hydration repulsion or hydrogen bonding, while two surfaces consisting of exposed hydrophobic tailgroups will experience hydrophobic attraction. Depending on the surfactant concentration, the properties of a surface can be reversed, e.g. hydrophilic $\leftrightarrow$ hydrophobic, positive $\leftrightarrow$ negative. Micelles can also form in the solution, whereby the hydrophobic tails of multiple surfactant molecules group together to form a sphere, which features an outer surface of hydrophilic head groups and a hydrophobic region within the sphere. Hence, the addition of surfactants to a particle suspension affects a number of surface behaviours, and a complete overview of the effects has not yet been found. However, it is known that the addition of low concentrations of surfactants to a particle suspension will typically help to reduce particle sticking and agglomeration, though appropriate surfactants may need to be carefully selected.

## Sedimentation and creaming

When particles are suspended in a solution they can be prone to sinking to the bottom of the container (known as sedimentation), or rising to the surface (known as creaming), depending on a number of factors. The migration of a particle due to gravity depends on the gravitational force, $\mathbf{F_{grav}}$ (in Newtons), as shown in Equation 7:[59,60]

$$\mathbf{F_{grav}} = (\rho_p - \rho_m) \, V_p \, g \; = \; \Delta\rho \, V_p \, g \qquad\qquad \textbf{Equation 7}$$

where $\rho_p$ = the density of the particle (kg m$^{-3}$), $\rho_m$ = the density of the media (kg m$^{-3}$), $V_p$ = the volume of the particle (m$^3$), and $g$ = acceleration due to gravity (9.81 m s$^{-2}$). When the density of a particle is greater than the density of the liquid media, the resultant $\Delta\rho$ is positive and indicates that the particle will <u>sediment</u>. However, if the liquid media is more dense than the particle, $\Delta\rho$ becomes negative and the particle will <u>cream</u>, migrating to the top of the container.

When particles move through a solution they also experience a viscous drag (frictional) force, $\mathbf{F_{vis}}$ (in Newtons), that opposes their migration through the media. Stokes' law can be used to determine this frictional force, and is shown in Equation 8:

$$\mathbf{F_{vis}} = 6 \, \pi \, \eta \, r \, \mathbf{u_p} \qquad\qquad \textbf{Equation 8}$$

where $\eta$ = the viscosity of the medium (kg m$^{-1}$ s$^{-1}$), $r$ = the particle radius (m), and $\mathbf{u_p}$ = the velocity of the particle (m s$^{-1}$). When all parameters are kept constant (i.e. steady-state conditions), $\mathbf{F_{grav}} = \mathbf{F_{vis}}$, and the resultant equation can be rearranged such that the velocity at which particles sediment or cream can be determined (again, a positive value gives the sedimentation velocity, while a negative value gives the creaming velocity), as per Equation 9:

$$\mathbf{u_p} = \frac{2 \, \Delta\rho \, g \, r^2}{9 \, \eta} \qquad\qquad \textbf{Equation 9}$$

As typical examples relevant to the work in this thesis, if a Dynabeads M-270 (2.8 μm diameter) magnetic particle is suspended in phosphate buffered saline (PBS) solution, the particle will have a $\mathbf{u_p}$ value of +2.57 μm s$^{-1}$, indicating that it will sediment.

However, a 10 μm diameter polystyrene particle in 10 % w/v manganese chloride (II) solution would have a $\mathbf{u_p}$ of -1.32 μm s$^{-1}$, hence it would cream.

This sedimentation/creaming effect is important since, if the velocity is very high (in either the positive or negative direction), the particles will not stay suspended throughout a solution for very long, and would require methods to redisperse them throughout the media again, such as by shaking and other agitation techniques.

## 1.3    *Particle handling on-chip*

Having established the classical DLVO theory describing the stability of microparticle suspensions and the anomalies of the non-DLVO interactions, this next chapter will describe the applications of microparticles in microfluidic devices, and the mechanisms by which they are manipulated.  The methods and benefits of utilising microparticles in microfluidics have been reviewed by Verpoorte[55] and Peterson.[68]   The uses of microparticles in microfluidics for performing immunoassays have also been reviewed by Lim and Zhang.[69]   There are two main methods concerning the manipulation of particles in microchannels: (i) trapping, and (ii) continuous flow.

## 1.3.1    Particle trapping in microchannels

A common method of performing particle-based processes in microfluidic channels is by using a "trap-and-release" method.  Here, particles are pumped into a microchannel and trapped.  Depending on the procedure being performed, a reagent solution may be pumped over the particles, allowing (bio)chemical reactions to take place on the particle surfaces.  The particles can then be washed and either detected as they are, or released

for further downstream processing. A review of particle and cell trapping methods in microfluidic systems was recently published by Nilsson *et al.*.[70] Due to the focus of this thesis being continuous flow particle procedures, trapping methods will only be briefly summarised here. There are two major techniques by which trapping can be achieved; by the use of physical barriers or the application of forces.

The simplest method of retaining particles in microchannels is to create a dam or barrier that halts the movement of particles through the chip without stopping the fluid flow, after which assays or reactions can be performed on the particle surfaces (Fig. 5).[71] Particles can also be packed into chambers between two weirs, whereupon solutions can be pumped over them, allowing solid phase extraction and chromatography techniques to be executed. [72-74] Solid-phase extraction chips may also be formed by immobilising particles in a channel with sol-gel.[75] Further trapping of particles can also be achieved by other, less common methods: the fabrication of pillars to form a filter-chamber (as opposed to a solid dam) to reduce clogging,[76] the employment of the keystone effect,[77] and the use of well-based traps in microfluidic channels.[44]
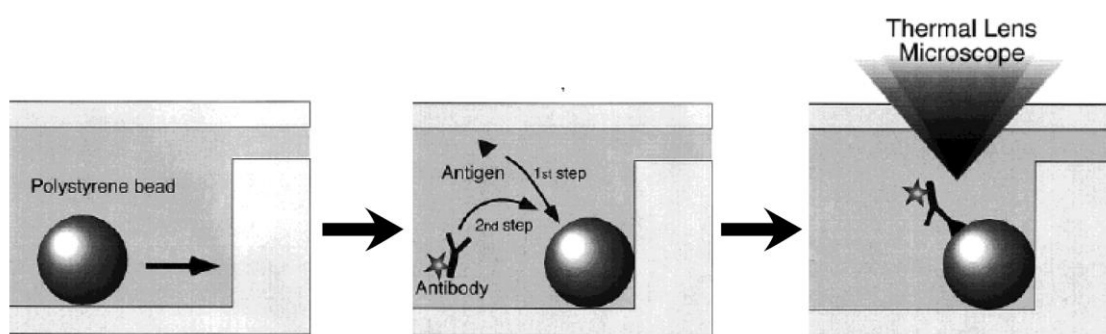


**Fig. 5  The use of a dam to trap particles in a microfluidic channel, whereupon reagents can be flushed over the particles to perform assays and reactions.  Image adapted from Ref. 71.**

A further method by which particles can be trapped is via the application of various types of forces. Adhesive forces can be used, whereby areas of a channel are treated such that the surfaces can capture particles either by chemical bonds,[78,79] electrostatic attraction,[80,81] or hydrophobic attraction.[82] Another method is to make use of the fluid flow itself, either hydrodynamic or electroosmotic or both, to retain the particles in areas of recirculating liquid.[83-86] Most commonly, however, particle retention is achieved by utilising external forces that capture and hold the particles in place without needing to contact the particles themselves. These forces can be applied to an entire chip or to specific locations within a microchannel, allowing fine control over particle location, while often the intensity of the force can also be changed to suit the procedure being performed. An example is shown in Fig. 6, in which a cell is selected and trapped for interrogation by optical forces provided by lasers,[87] though the principle is the same for particles. As well as optical forces,[87-96] trapping can be achieved in the same manner by employing a number of forces, including those generated by dielectrophoresis,[97-105] acoustics,[106-112] magnetism,[34,113-124] and diamagnetism.[125-130] The latter two examples will be explained in more detail later in the thesis.
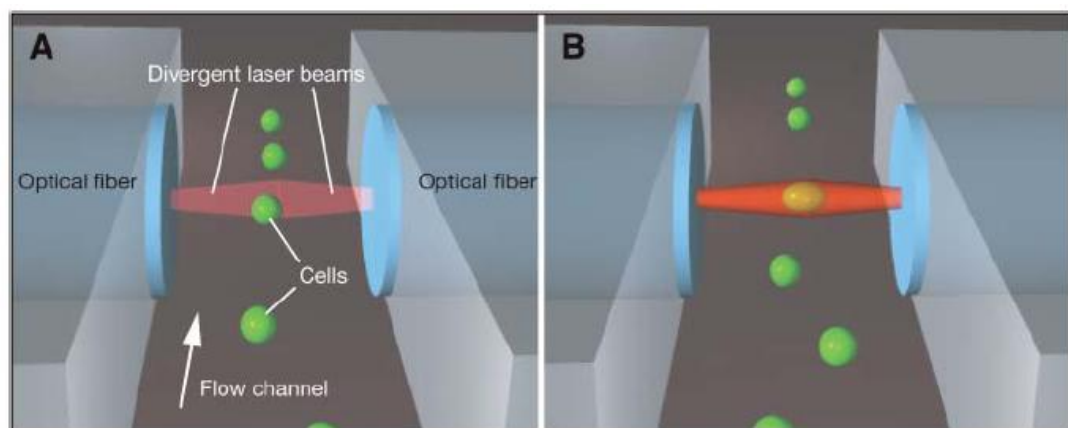


**Fig. 6 Principle of force-based trapping in microchannels, demonstrated here by the trapping of a cell by optical forces. (A) Cells flow freely through the channel, and (B) the laser intensity is increased, trapping a cell and allowing its subsequent interrogation.[87]**

Thus, particle trapping in microchannels can be achieved via a number of means. Each method has their own individual advantages and disadvantages, as summarised in Table 1. However, while trapping offers a simple means by which processes can be performed on the surfaces on the particles, in each case the trapping procedures are batch methods, requiring multiple reaction and washing steps that are labour-intensive and time-consuming. Such processes often necessitate the changing of solutions via the replacement of syringes or by valve operation, which in turn results in the system needing to equilibrate before any changes can be made in order to ensure that particles do not escape the trap, or that bubbles are not introduced into the system. In addition, each procedure uses set reaction/separation times and sample volumes, with the results of an experiment only given after all steps have been completed. Hence, parameters can only be changed after a procedure is finished, at which point an entire experiment needs to be performed again using the new parameters.

**Table 1  Summary of the different methods of trapping particles in microchannels, with the advantages and disadvantages of each and examples of their application.**

| Trapping method | Advantages | Disadvantages | References |
|---|---|---|---|
| Barriers | • On-chip integration<br>• No need for external forces | • Complex fabrication<br>• Risk of blockages and increased backpressure<br>• Difficult to regenerate<br>• Limited to specific areas in the device | 44, 71-77, 131-144 |
| Adhesion | • Less risk of blockages<br>• Control over trapping regions and the number of particles trapped | • Chemical modification of surface required<br>• Adhesion is often permanent | 78-82 |
| Flow | • Label-free<br>• No external forces | • Often requires complicated chip designs and careful control of flow regimes | 83-86 |
| Optical | • Label-free<br>• Contactless<br>• Allows precise control over individual particles/cells | • Requires external power supply and laser setup | 87-96 |
| Dielectro-phoretic | • Label-free<br>• Can easily control forces by adjusting electric field | • Electrodes typically require contact with buffer solution<br>• Requires external power supply<br>• Joule heating | 97-105 |
| Acoustic | • Label-free<br>• Contactless | • Requires external power supply and ultrasonic transducer | 106-112 |
| Magnetic | • Contactless<br>• Can use simple and cheap magnetic setup | • Requires magnetic properties or labelling | 34, 113-124 |
| Diamagnetic | • Label-free<br>• No contact with magnets | • Weak forces<br>• Typically requires paramagnetic medium | 125-130 |

## 1.3.2   Continuous flow processing of particles in microchannels

The exciting concept of continuous flow particle processing has seen an emergence in the last decade as a means of reducing the inherent inefficiencies of batch methods.  The vast majority of such methods are currently applied to the continuous *separation* of particles or cells, though there have been some recent developments for performing continuous flow *reactions* on particles, which will be discussed separately in Section 1.5.  Such is the level of interest in continuous flow separations in microfluidic devices, that a number of review articles have recently been published detailing the various methods available for performing them, including those by Pamme,[145] Lenshof and Laurell,[146] Kersaudy-Kerhoas *et al.*,[147] Tsutsui and Ho,[148] and Gossett *et al.*.[149]

Typically, particles are pumped continuously into a chamber, whereupon a force applied perpendicular to the flow causes the particles to move laterally across the width of the chamber (Fig. 7).  The particles migrate in this way to different extents depending on their interaction with the applied field, and are thus separated continuously.  There are several advantages to the use of continuous flow separation devices:[145] (i) a sample is continuously introduced into the device rather than in a small plug (such as in chromatography or capillary electrophoresis), which means that is no limit to the amount of sample that can be processed, (ii) the separation efficiency can be monitored in real-time, which allows on-line feedback that can be used to adjust parameters such as fluid flow and the forces on the particles without needing to stop-and-start the process, (iii) particles are separated laterally across the width of a chamber, allowing the continuous and simultaneous collection of fractions via the use of multiple outlets whilst allowing waste to be constantly removed.  Hence, separations are determined via signal versus position measurements rather than signal versus time measurements as in conventional chromatography methods.   Additionally, it is feasible to direct

particles/cells to certain outlets for further downstream applications. (iv) Due to the continuous introduction and collection of particles, it is relatively easy to integrate other upstream or downstream processes, such as particle focussing or continuous reactions. (v) In many cases the separation is "label-free", in that it is based on the intrinsic physical properties of the particles or cells, thereby requiring no labelling step before introduction into the device.
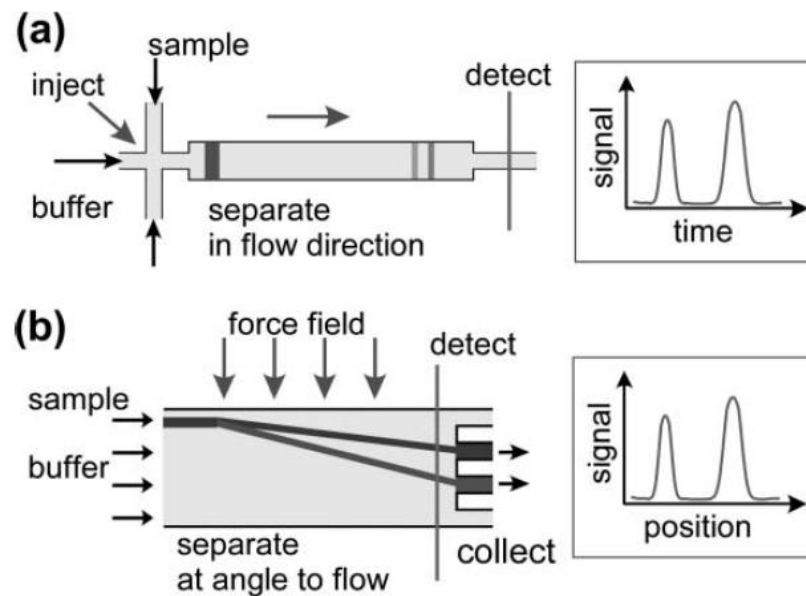


**Fig. 7  a) Batch separation method in which a small sample plug is injected into a column and detection performed after separation of the components.  Continuous flow separation procedure in which the sample is continuously injected into a chamber, whereupon the components are separated via a force applied perpendicular to the flow, allowing continuous and simultaneous detection of the separated materials.[145]**

A range of continuous separation methods exist due to the numerous forces that can be applied, typically the same types of forces as described for trapping in Section 1.3.1. Here, an overview of these various forces will be given, with examples of their use from literature published within the last decade.

## Continuous separation via physical objects

While most often used as dams, weirs and filters as explained in Section 1.3.1, physical objects and barriers can also be used to deflect particles in continuous flow. One such method of achieving this is known as "deterministic lateral displacement" (DLD), introduced by Huang *et al*. in 2004,[150] which utilises an array of microposts throughout a microfluidic chamber, with each row of posts off-set slightly from the last one. Small particles follow the laminar flow streamlines through the chamber, essentially weaving around the posts in a relatively straight line in the direction of flow. However, larger particles, above a critical size, are unable to follow the streamlines upon encountering a post, and are instead "bumped" in the direction perpendicular to flow (Fig. 8). The method has been used for the size-based separation of particles (0.80, 0.90 and 1.03 μm) and DNA (61 and 158 kbp),[150] the separation red blood cells, white blood cells and platelets from blood plasma,[151] the assessment of platelet size and morphology in whole blood,[152] and in-depth studies into flow regimes and particle separations.[153-155]
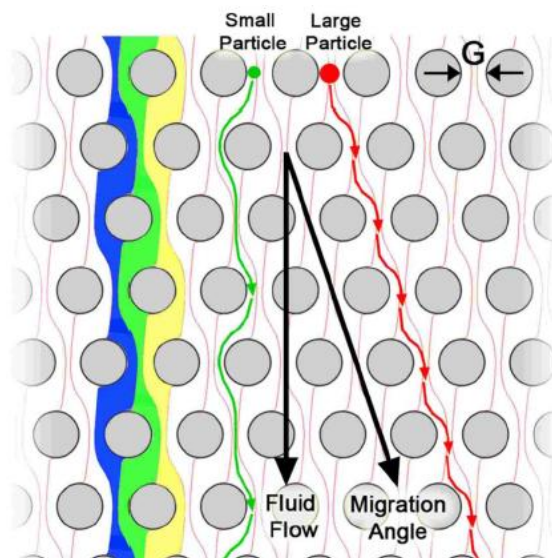


**Fig. 8 Principle of Deterministic Lateral Displacement (DLD). Microposts are arranged in asymmetric rows, allowing small particles to follow the direction of laminar flow while larger particles are "bumped" in the direction perpendicular to flow, resulting in size-based separation.[153]**

Another method utilising obstacles for particle and cell separation was developed by Choi and Park in 2007,[156,157] and termed "hydrophoretic separation". The device consisted of a focussing region followed by a filtration region. In the focussing region, slanted obstacles across the width of the channel were placed alternately on the top and bottom surfaces of the channel, which drove all of the particles to the sidewall. In the filtration region, the slanted features also featured cut-aways at the opposite sidewall to the particle stream. Small particles were able to pass over the obstacles whilst maintaining their focussed direction, but larger particles that could not pass over the obstacles were instead diverted to the cutaways. This allowed the continuous separation of 9 and 12 μm particles, and the device was also used to separate red and white blood cells.

Lillehoj et al.[158] developed a system in which particles were introduced into a chamber and flowed along the near wall, whereupon they encountered barriers with different-sized gaps between them (Fig. 9). The smaller particles were able to pass through the first gap and enter the top outlet, while larger particles were unable to fit and so migrated along the barrier until they could pass through a suitably sized gap and exit via the middle outlet. The largest particles were unable to pass through any barriers and were directed into the bottom outlet. Polystyrene particles of 90, 175 and 275 μm diameter were separated, as were three size groups of mouse embryoid bodies (EBs).

Obstacle based continuous separation devices allow label-free particle and cell sorting regardless of surface charges, and the pH and ionic strength of the buffer. However, these devices require careful design and fabrication considerations, and only allow the separation of a narrow range of particle sizes without having to change the channel and obstacle geometry.
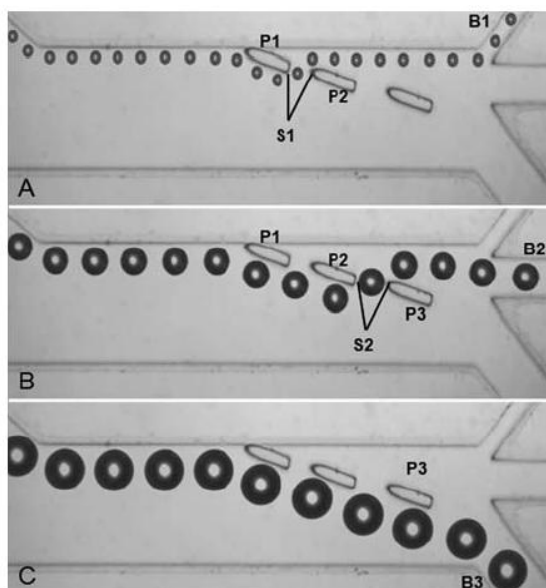
**Fig. 9 Separation of polystyrene particles via the use of barriers with different sized gaps between them, here used to separate (A) 90 μm, (B) 175 μm, and (C) 275 μm particles. The flow of the particle suspension is left to right.[158]**

## Continuous separation via flow effects

By employing novel channel designs, it is possible to use the flow regime itself to continuously separate particles. In 2002, Blom *et al.*[159,160] developed an on-chip hydrodynamic chromatography device in which particles were introduced into a channel and separated according to size. This was based on the parabolic profile caused by pressure-driven flow, which allows smaller particles to migrate closer to the walls of the channel such that they have a slower average velocity than larger particles that are farther from the wall, thus achieving separation. However, since a sample was injected as a single plug, and because the fractions eluted one after the other rather than simultaneously, this was in many ways a batch separation technique rather than a continuous technique. Pinched flow fractionation, a true continuous separation method, was developed by Yamada and Seki in 2004,[161] and allowed the continuous sorting of

15 μm and 30 μm particles. Here, a particle stream and a buffer stream were forced into a narrow channel, in which the particles were "pinched" against the sidewall. Due to the ability of the smaller particles to migrate closer to the wall compared to the larger particles, as they entered a widening chamber they followed different laminar stream lines, thereby allowing their separation (Fig. 10). The system was refined by asymmetric amplification of the flow in the system,[162] the incorporation of PDMS valves,[163] and by replacing pressure-driven flow with EOF.[164]
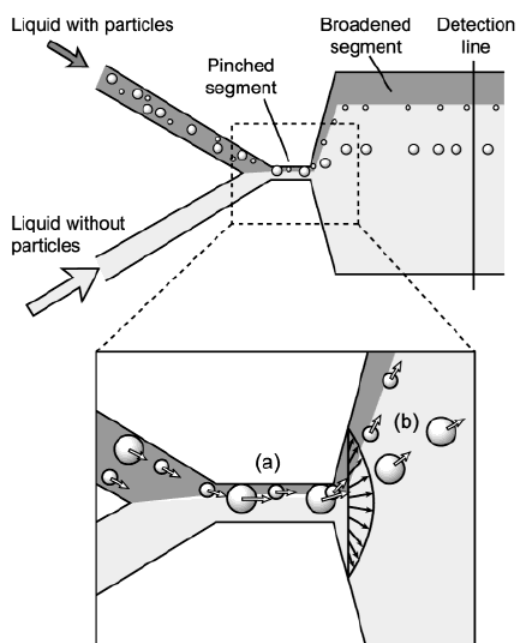


**Fig. 10 Pinched flow fractionation. (a) Particles are "pinched" against the sidewall of a narrow channel, then (b) separated according to their size upon entering a widening chamber.[161]**

Yamada and Seki[165,166] also developed a hydrodynamic filtration device that consisted of a main flow channel with a series of side branches. As particles flowed through the main channel, some of the liquid was directed out of the channel by the side branches,

depending on the flow resistance of these channels. This caused particle to migrate to the sidewall until the particles closest to the wall could exit via the side branches. The smallest particles exited first, followed by larger particles further down the main channel (Fig. 11). This allowed the separation of 1.0, 2.1, and 3.0 μm particles, and in later experiments the separation of leukocytes from diluted whole blood was also achieved.[165]
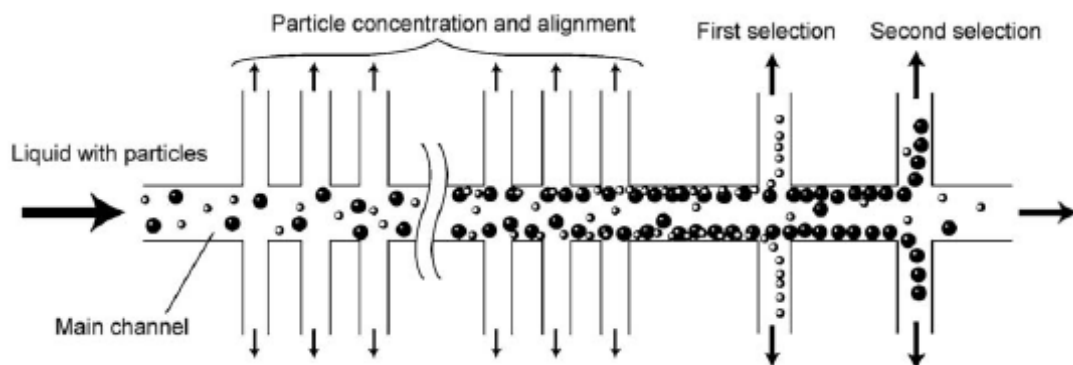


**Fig. 11 Principle of hydrodynamic filtration. A series of side branches remove liquid from a main channel, which first concentrates the particles to the sidewall of the channel. The smaller particles were then removed via a selection channel, before the larger particles were removed via a second selection channel.[165]**

Bhagat *et al.*[167] fabricated a spiral microfluidic device that utilised Dean flows to separate 7.32 μm from 1.9 μm particles, 1.9 μm from 590 nm particles,[168] and for the high-throughput counting of cells.[169] The flow at the inner walls of the spiral was faster than at the outer wall, creating circulating Dean flows that caused the smaller particles to migrate to the outer walls, while the larger particles moved to the inner walls due to inertial forces. Wu *et al.*[170] also demonstrated the use of inertial forces to separate bacteria from human blood cells, using an asymmetric sheath flow to generate a "soft

inertial force" that caused the deflection of larger particles while smaller ones were unaffected.

Sugino *et al.*[171-173] developed a chip in which mixtures of particles or *E. coli* cells could be separated by directing them into designated channels. While not a flow based method akin to the previous examples, the device used blocked channels to direct the flow into different outlets. Particles (or cells) exhibiting different colours were introduced into a microfluidic channel and focussed via two buffer streams, with each of the solutions containing thermoreversible gel polymer (TGP, which turns into a gel upon heating). The device featured five outlets, and when a particular coloured particle was detected, a laser heated the TGP in all but one channel, allowing the particle to exit via that channel only. Detection of different colours caused different outlets to be heated, thereby allowing separation of the particles.

Further examples of flow based separations take advantage of the tendency of red blood cells to flow in the centre of a channel, allowing continuous removal of plasma,[174] while the "Zeifach-Fung effect" ("bifurcation law") has been used to separate red blood cells from plasma as a result of red blood cells preferring to follow higher flow rates at a bifurcated region.[175] Rodríguez-Villarreal *et al.*[176] also demonstrated the ability to perform separations of whole blood by siphoning off plasma from a narrow side branch.

These examples have shown how flow regimes can be used in novel ways to perform continuous particle and cell separations, typically based on size and colour. However, these methods typically require complex chip geometries in order to carefully manipulate the flows. Additionally, the chip designs are only suitable for a certain range of particles outside of which a redesign is required, while the thermoreversible gel method necessitated the use of a complicated setup of lasers, optics and feedback systems to enable particle sorting.

**Continuous separation via external forces**

As with the trapping methods, external forces can be applied to particles to manoeuvre them in continuous flow, such that different types of particles are deflected to different extents and thereby facilitating their separation, as shown in Fig. 7. This section will describe the various types of external forces that can be applied to continuous flow separations, with examples of their uses in each case.

Two developments of note for the separation of particles and cells are the macroscale methods of Field Flow Fractionation (FFF) and the closely related Split Thin (SPLITT) flow fractionation. Although used for performing separations in devices with wide channel dimensions (i.e. tens to hundreds of millimetres long and wide, though they may only be hundreds of microns deep), they will be briefly discussed here due to their influence on microfluidic systems. Developed by Giddings in 1966,[177] FFF is a technique that can be operated using a variety of external forces, including electrical,[178] thermal,[179,180] gravitational,[181] magnetic[182-187] and cross flow forces, to direct particles towards the wall of a channel. Separation is based on particle size, with particles that can migrate closer to the wall travelling slower than the larger particles that cannot enter the slower flow streams.[188,189] Particle fractions are then collected at the outlet, with the faster particles eluting first (under most circumstances). Due to the wide ranges of particle sizes and external forces that can be applied, FFF has been successfully applied to the separation of polymer particles,[190,191] proteins,[190] cells,[188] and viruses.[188] However, FFF is not strictly speaking a continuous separation technique since the sample is injected all at once, and separated fractions are collected one after the other.

Split-flow lateral-transport thin (SPLITT) fractionation was also developed by Giddings in 1985,[192] as an advancement of FFF for the continuous flow separation of particles and cells. As with FFF, particles are introduced into a channel and an external force

acts laterally on the particles, causing them to migrate. However, rather than moving to the channel wall, the particles affected by the force field instead pass through an inlet into an adjacent channel containing a stream of carrier solution. Different particle types are affected to different extents by the applied force, such that some particles do not pass into the adjacent stream while other particles do, allowing them to exit via different outlets and thus providing a separation. As with FFF, SPLITT is a generic separation technique that can be achieved using a number of different forces including electrical,[193] acoustic,[194,195] gravitational,[196,197] centrifugal,[198] hydrodynamic,[199] and magnetic forces,[200-203] and has been applied to the separation of particles,[204] proteins,[193] and cells.[199] While SPLITT fractionation is a macroscale technique, the general principle behind it, i.e. that of applying lateral forces to particle streams, can be easily implemented in microfluidic devices.[205] Indeed, many microfluidic separation systems have been derived from the principles of SPLITT fractionation, as will be described in the following sections.

### *Optical forces*

Optical forces, best known for their application as optical tweezers,[206] arise due to "radiation pressure" exerted on a particle by a laser, whilst simultaneously a gradient force drives particles with a higher refractive index than the surrounding media towards the region of maximum optical intensity. In general, the optical force, $\mathbf{F_{opt}}$ (in Newtons), on a particle can be expressed by Equation 10:[89,207]

$$\mathbf{F_{opt}} = \frac{n_1 \, P}{c} \, Q \qquad\qquad \textbf{Equation 10}$$

where $n_1$ = the refractive index of the surrounding medium, $P$ = the laser power incident on the particle, $c$ = the speed of light (2.998 x $10^8$ m s$^{-1}$), and $Q$ = the trapping efficiency factor that depends on the size, shape, material, and position of the particle with respect to the spatial profile of the beam. The use of optical forces in microfluidics is often referred to as optofluidics, and recent reviews on the topic can be found by Hunt and Wilkinson,[88] Jonáš and Zemánek,[89] and by Ozkan *et al.*,[90] while two special issues (1 and 2) in Volume 14 of the journal *Microfluidics and Nanofluidics* are devoted to various research papers and review articles on the subject.

Whilst normally used for particle or cell trapping, optical forces can also be applied to continuous flow separations. In 2003, MacDonald *et al.*[208] developed a microfluidic device for separating particles in a "fractionation chamber", before splitting them into two outlets (Fig. 12). A three-dimensional optical lattice was created in the chamber using five laser beams created by the splitting of one beam. As particles passed through the chamber, some were deflected by the lattice into one of the outlets while unaffected particles passed into the other. This allowed the size-based separation of 2 μm and 4 μm protein microcapsules, and also the refractive index-based separation of 2 μm silica and polystyrene particles. The setup was also applied to the separation of erythrocytes from lymphocytes,[209] and the sorting of four different silica particle sizes (6.8, 5.2, 3.0 and 2.3 μm) into parallel laminar flow streams.[210] The same group also demonstrated the separation of 5 μm particles from 1 and 3 μm particles using an area of evanescent waves generated on the glass-water interface in the microfluidic device, via a near-infrared laser beam passed through a total internal reflection (TIR) objective.[211] Ladavac *et al.*[212] developed a similar device to the optical lattice of McDonald *et al.*,[208] in which an array of twelve lasers were used for optical fractionation of objects.

**Fig. 12   An on-chip continuous flow separation system utilising optical forces.   The technique was applied to the separation of particles of differing refractive index, and to protein microcapsules of different sizes.**[208]

*Free-flow electrophoresis and isoelectric focussing*

Free-flow electrophoresis (FFE) and free-flow isoelectric focussing are methods of manipulating charged species in continuous flow by the application of lateral, homogeneous electric fields.[145,213]   A recent review by Kohleyer *et al*.[213] details the theory and application of these techniques in microfluidic devices.   In free-flow electrophoresis, a sample solution is continuously pumped through a microfluidic chamber, between two adjacent streams of buffer solution (Fig. 13a).   A homogeneous electric field is generated perpendicularly across the chamber, causing charged analytes to deflect towards either the positive electrode (if the object is negative) or the negative electrode (if the object is positive), while uncharged materials pass through the chamber without being deflected.   Thus, these objects can be separated according to their mobility, which depends on their mass-to-charge ratios.   However, particles are not typically separated by FFE, with the technique instead used to sort amino acids and proteins.   Free-flow isoelectric focussing (FF-IEF) operates via a similar principle

except that the buffer streams are used to generate a pH gradient across the chamber (Fig. 13b).[214] Here, charged species migrate towards the electrodes until they reach the pH at which they exhibit no net charge, which is known as the isoelectric point (pI). This allows amino acids, proteins, and cells such as bacteria to be separated in continuous flow based on their individual pI values.

These methods will not be discussed in detail here since they are not used for particle separations, but are nonetheless worth mentioning as examples of continuous flow sorting via applied forces. Additionally, the "free-flow" principle and terminology has been adopted by a number of processes, albeit using different forces.
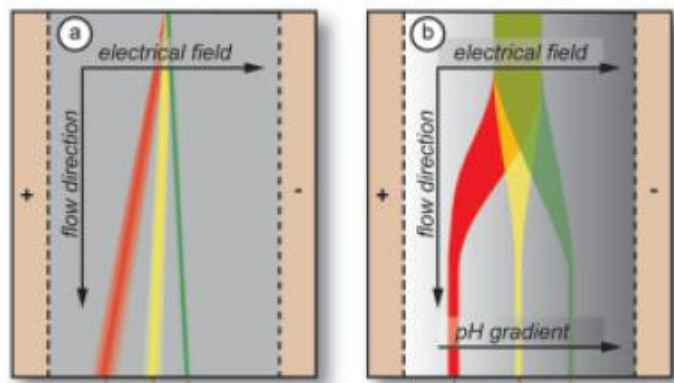


**Fig. 13   a) Free-flow electrophoresis (FFE), in which charged species are continuously separated in continuous flow via an applied electric field.   b) Free-flow isoelectric focussing, a similar process to FFE except that a pH gradient is generated across the chamber, and species are separated according to their isoelectric point.[213]**

*Dielectrophoresis*

While electrophoresis is the movement of charged particles in an electric field, dielectrophoresis (DEP) is the motion of uncharged but polarisable particles in an

inhomogeneous electric field.[215,216] Essentially, when placed in an electric field, dipoles are induced in the neutral material, which thus becomes polarised in the direction of the applied field. When placed in a homogeneous electric field the electrostatic forces on either end of the dipole are equal and there is no net movement, but when placed in an inhomogeneous field the forces on each side of the dipole are different, and the net force results in movement of the particle. The dielectrophoretic force, $\mathbf{F_{DEP}}$ (in Newtons), on a dielectric particle is given by Equation 11:[70,98,146]

$$\mathbf{F_{DEP}} = 2\ \pi\ \varepsilon_m\ r^3\ \mathrm{Re}(f_{CM})\ \nabla E_{rms}^2 \qquad \textbf{Equation 11}$$

where $\varepsilon_m$ = the absolute permittivity of a medium (F m$^{-1}$), where $\varepsilon_m = \varepsilon_r \varepsilon_0$ (in which $\varepsilon_r$ = the relative permittivity or dielectric constant of a medium, and $\varepsilon_0$ = the permittivity of free space), $r$ = the particle radius (m), $\nabla E_{rms}$ = the gradient of the root mean square (amplitude) of the electric field (where $E_{rms}$ has units of V m$^{-1}$), and $\mathrm{Re}(f_{CM})$ = the real component of the Clausius-Mossotti factor, given by Equation 12:

$$f_{CM} = \frac{\varepsilon_p^* - \varepsilon_m^*}{\varepsilon_p^* + 2\varepsilon_m^*} \qquad \textbf{Equation 12}$$

where $\varepsilon_p^*$ and $\varepsilon_m^*$ are the complex permittivity of the particle and the surrounding medium, respectively. When $f_{CM} > 0$, i.e. when $\varepsilon_p^* > \varepsilon_m^*$, the particles will experience a positive dielectrophoretic force (pDEP) and migrate towards the region of highest electric field. When $f_{CM} < 0$, i.e. $\varepsilon_p^* < \varepsilon_m^*$, the particles will experience a negative dielectrophoretic force (nDEP) directed away from the region of strongest electric field. Dielectrophoretic forces have been used extensively for the manipulation of particles and cells in microfluidic devices over the last decade, and reviews focussing on this work have been published by Pethig,[97,98] Khoshmanesh,[99] as well as Lapizco-Encinas and Rito-Palomares.[100] A few example applications will be given here.

Choi and Park[217] demonstrated a microfluidic device incorporating trapezoidal electrode arrays (TEA) for the negative dielectrophoretic (nDEP) separation of polystyrene particles. Particles in flow were deflected laterally by the TEAs, with the extent of deflection dependent upon the size of the particles, allowing the separation of 15 mm and 6 mm particles with >96 % efficiency. Kang *et al.*[218,219] utilised a rectangular obstacle placed in a microchannel to force particles into a narrow gap, with DEP forces applied that resulted in the migration of two different sized particles (combinations of 5.7, 10.35 and 15.7 μm diameters) in opposite directions as they exited the gap.

Chang and Cho[220] developed a system consisting of a "virtual" pillar array throughout a microfluidic chamber, similar to the Deterministic Lateral Displacement devices (DLD) described above. However, the posts in this case were generated by nDEP forces using electrode spots, rather than being physical pillars. The device was used to separate 5.7, 8.0, 10.5, and 11.9 μm diameter polystyrene particles, while red and white blood cells were also separated with >99 % efficiency.

Hu *et al.*[221] demonstrated the use of polystyrene particles as labels for the nDEP based separation of *E. coli* cells, and this was found to increase the forces on the cells by 100 times compared to unlabelled cells. A mixture of labelled and unlabelled cells was introduced into a channel and an electric field applied to gold electrode stripes in the chip, causing the separation of the two populations into different outlets with an efficiency of ~95 %, and a throughput of ~10,000 cells s$^{-1}$. The system was later improved by Bessette *et al.*[222] for the screening of a combinatorial peptide library, and by Pommer *et al.*[223] for the separation of platelets from blood cells.

DEP has also shown uses in the separation of viable and non-viable cells without the need for their labelling. Doh and Cho[224] showed that at low frequencies (and high medium conductivity), viable cells exhibited nDEP while non-viable cells exhibited

pDEP, while at higher frequencies the forces become reversed such that viable cells exhibit pDEP and non-viable cells exhibit nDEP. By embedding strips of gold electrodes into the chip, parallel to the flow direction, the authors were able to separate the cells using the latter scenario with an efficiency for viable cells of ~96 %, and for non-viable cells of ~65 - 74 %. Li *et al.*[225] demonstrated a similar principle in which hydrodynamically focussed yeast cells could be separated into viable and non-viable fractions using both pDEP and nDEP, via electrodes embedded into the chip. Braschler *et al.*[226] also performed the separation of viable and non-viable yeast, as well as *Babesia bovis* infected and uninfected red blood cells, by the continuous DEP focussing of cells into different streamlines, and also of red blood cells infected with *Babesia bovis* from those that were uninfected.

Kim *et al.*[227] developed a Multitarget Activated Cell Sorter based on DEP in which different cell types were labelled with particles of differing sizes, while some remained unlabelled (Fig. 14). A mixture of these species was introduced into a microfluidic chamber and deflected laterally via two areas of slanted electrodes. Cells featuring the largest labels were deflected further than those with smaller particles, while unlabelled cells were not deflected at all, allowing separation of the three populations into different outlets with ~1000 fold enrichment.

Dielectrophoresis has been employed to great effect for the separation of particles and cells in continuous flow, particularly since separation typically occurs due to the intrinsic properties of the species of interest, and because the electrodes are not required to be in contact with such species. High DEP forces can be applied, although high fields can result in Joule heating of the solution which can be detrimental to biological cells. Additionally, the configuration of the electrodes and their incorporation into the

microfluidic devices are typically very complex and require a great deal of consideration when designing the system.
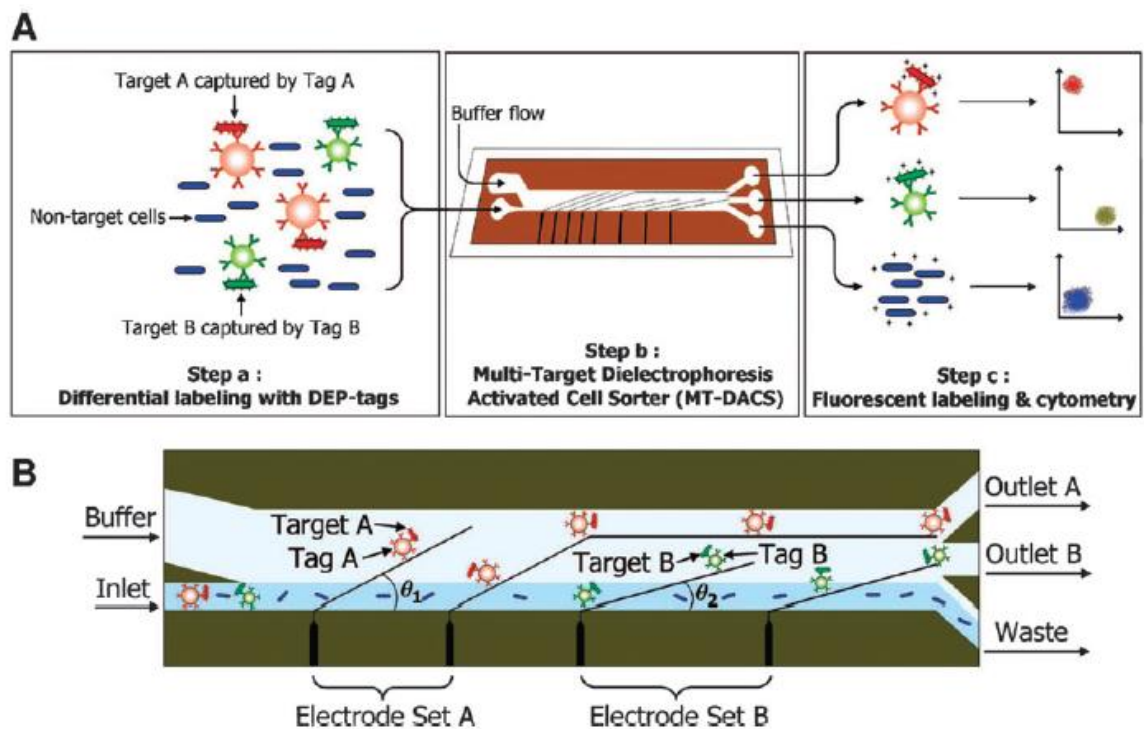


**Fig. 14 Multitarget Activated Cell Sorter for the continuous separation of cells labelled with different sizes of particles. A) The labelling of target cells with different tags. B) Cells are pumped through the device and deflected laterally by the electrodes in the sidewall of the chamber, such that the labelled cells are sorted according to the size of their labels.**[227]

*Acoustophoresis*

The application of ultrasonic standing waves generates stationary pressure gradients that exert radiation forces on particles and cells suspended in a media, with such objects moving to either a pressure node or to an anti-node, depending on the physical properties of the particles. The acoustic force, $\mathbf{F_{ac}}$ (in Newtons), on a particle is directed along the axis of the incident wave, and can be determined using Equation 13:[70]

$$\mathbf{F}_{ac} = p^2 \frac{\pi \, V_p \, \beta_m}{2 \, \lambda} \, \phi \, \sin\left(\frac{4 \, \pi \, x}{\lambda}\right)$$

**Equation 13**

where $p$ = pressure amplitude (Pa), $V_p$ = volume of the particle (m$^3$), $\beta_m$ = medium compressibility (Pa$^{-1}$), $\lambda$ = acoustic wavelength (m), and $\phi$ = acoustic contrast factor, given by Equation 14:

$$\phi = \frac{\rho_p - \rho_m}{2\rho_p + \rho_m} - \frac{\beta_p}{\beta_m}$$

**Equation 14**

where $\rho_p$ = density of the particle (kg m$^{-3}$), $\rho_m$ = density of the medium (kg m$^{-3}$), and $\beta_p$ = particle compressibility (Pa$^{-1}$). When $\phi < 0$, particles are attracted to the pressure node, while if $\phi > 0$ the particles will be attracted towards the anti-node. Most cells and particles exhibit negative $\phi$ values, while air bubbles and lipids have negative values and move towards the anti-nodes. A standing wave of a half wavelength is commonly employed in microfluidic devices, such that the pressure node is in the centre of the channel and the anti-nodes are at the walls. The use of acoustic forces in analytical biotechnology have been reviewed by Coakley,[228] and their application to the manipulation of particles and cells in microfluidic devices has been reviewed by Laurell *et al.*[112] A few examples of continuous flow acoustic separations will be given here.

In 2001, Hawkes and Coakley[229] fabricated a stainless steel microfluidic device (10 mm wide, 250 μm deep channel) with two outlets for the concentration of yeast cells (~5 μm). A standing acoustic wave was generated over the channel which continuously deflected the cells into one of the outlets, yielding enrichment of the cells by >1000 fold at a throughput of 2 x 10$^8$ cells min$^{-1}$. The group later constructed similar devices out of silicon and Pyrex,[230] as well as quartz and glass.[195]

The group of Laurell have performed a great deal of research into the application of acoustics for continuous flow processes in microfluidic devices. In 2004, Nilsson *et al.*[231] fabricated a flow channel with three outlets. By applying a standing wave, 5 μm particles were lined up along the nodes and directed into specific outlets, allowing the concentration of 90 % of the particles into two-thirds of the original liquid volume. Petersson *et al.*[232,233] used the same device to separate polyamide spheres with an efficiency of nearly 100 %, before applying the method to the separation of lipid particles (which followed the anti-nodes) from erythrocytes (red blood cells, which followed the node) in bovine blood. Lenshof *et al.*[234] also developed a reversed version of this system for "plasmaphoresis", in which blood cells were removed from the system to yield high quality plasma for clinical diagnostics. Additionally, Grenvall *et al.*[235] used an acoustic separation to precondition raw milk samples prior to lipid and protein content analysis, by enrichment or depletion of the lipids as desired.

Petersson *et al.*[236] later expanded the design to include multiple outlets, thereby allowing the separation and collection of multiple fractions of particle and cell types (Fig. 15), a procedure termed "free-flow acoustophoresis", akin to free-flow electrophoresis. Polystyrene particles of 2, 5, 8 and 10 μm diameters were continuously separated and collected into four outlets, with efficiencies of 62 - 94 % for each particle size. Particles of 3, 7 and 10 μm diameters were also separated into three outlets with efficiencies between 76 – 96 %. By adjusting the density of the media, the authors found it was also possible to separate normally acoustically inseparable materials, and this technique was applied to the separation of leukocytes, red blood cells and platelets. Kapishnikov *et al.*,[237] of a different research group, also demonstrated the size based separation of polyamide microparticles via acoustic forces, as well as the separation of red blood cells from plasma.

Acoustophoresis provides a relatively simple and contactless means by which label-free particles or cells can be separated in continuous flow. Additionally, particle surface charges and the ionic strength of the buffer solution are not important. However, careful consideration must be made of the channel dimensions and outlet positions for the objects of interest to be separated as desired, since the standing waves applied produce fixed nodes and anti-nodes.
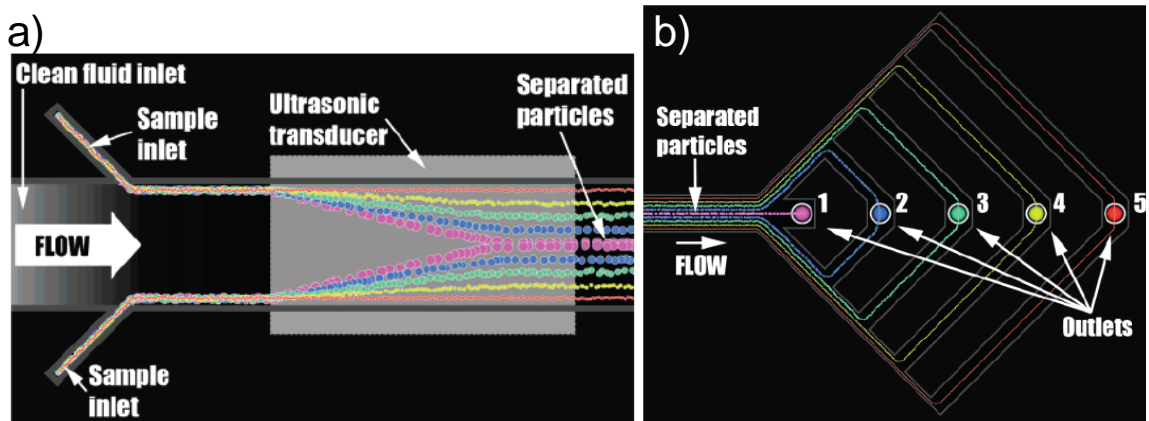


**Fig. 15 Principle of free-flow acoustophoresis. a) Particles are pumped into the chamber and an ultrasonic transducer is used to create acoustic pressure nodes and anti-nodes. The particles line up along these nodes and anti-nodes depending on their size, allowing them to be separated in continuous flow. b) After separation, the particles are collected via different outlets.[236]**

*Thermophoresis*

Thermophoresis describes the migration of particles toward either the hot or cold region in a temperature gradient (Fig. 16), depending on the type of electrolyte present in the solution. The thermophoretic mobility, $v_T$, of a particle depends on its thermal diffusion coefficient, $D_T$, and the temperature gradient, $\nabla T$, as shown in Equation 15:

$$v_T = -D_T \, \nabla T \qquad\qquad \textbf{Equation 15}$$

More detailed descriptions of the principles, theory and applications of thermophoresis can be found in reviews by Piazza[238-240] and Wiegand.[241] The effect has been utilised many times for field flow fractionation (FFF), and has been applied to some microfluidic systems for batch separations[242,243] and stopped flow studies.[244]
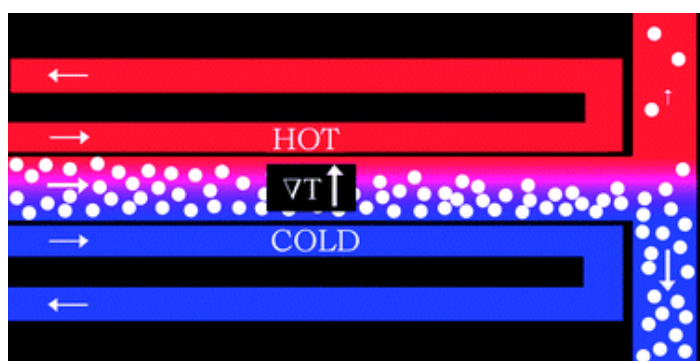


**Fig. 16   Principle of thermophoresis in a microfluidic device.   A thermal gradient is generated across the microchannel, and particles in flow migrate toward either the hot or cold region depending on the electrolyte present in the solution.   Figure from the table of contents for Ref. 239.**

In 2010, Vigolo *et al.*[245] developed microfluidic devices for studying the feasibility of thermophoresis for separations in continuous flow.   The temperature gradient was generated by either using hot and cold water running through side-channels, or by applying a voltage to side channels filled with silver-laden epoxy resin.   Particles (477 nm diameter) were pumped into the main channel and it was observed that when suspended in 100 mM NaOH they would migrate towards the hot region, while in 100 mM NaCl they migrated to the cold region.   No actual separations were performed, but the results suggested that the method could be applied to continuous separations like those illustrated in Fig. 16.

*Gravitational forces*

One type of force that has seen very little use in continuous particle processing, despite the fact that it inherently affects everything, is that of the Earth's own gravitational pull. However, the gravitational forces on polystyrene particles compared to the forces described previously are several orders of magnitude smaller, hence there has been very little application for this force in continuous flow separations.[145]  Despite this, in 2007, Huh *et al.*[246] reported a microfluidic device that utilised the sedimentation principles stated in Equation 9, by which larger particles settled faster than smaller ones.  20 μm polystyrene particles were separated first from 1 μm particles, and also from 3 μm particles (Fig. 17).
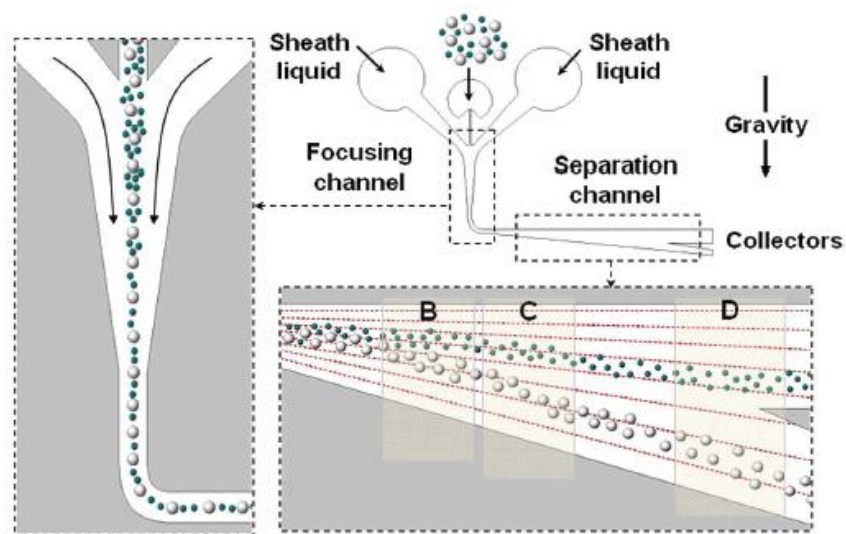


**Fig. 17  Gravity-based particle separation.  Particles are focussed into a narrow stream and guided into a widening chamber, where they separate due to gravity according to their sizes and are collected via different outlets.  20 μm polystyrene particles were separated from 3 μm and 1 μm particles in <1 min and with nearly 100 % efficiency.[246]**

The particle mixtures were pumped vertically through the chip, and focussed with a sheath flow into the centre of the channel. They were then guided 90° into a widening chamber, and as they traversed this channel their velocities were reduced. As the particles traversed the widening channel their velocities were reduced, allowing the different sized particles to separate over the length of the chamber due to the larger particles settling faster. Separation of the particle populations was achieved in <1 min, with an efficiency of <99.9 %.

*Magnetic forces*

A popular method for performing continuous flow separations and other processes is by the application of magnetic forces. Typically, the affected particles or cells feature a magnetic label that allows their deflection by attraction to an applied field. However, this may not always be the case, as diamagnetic repulsion forces have also been used to manipulate particles in continuous flow. Both of these methods will be explained in more detail in later chapters. Prior to that, however, the theory behind magnetism will first be explained.

**Summary of continuous flow particle separations**

Continuous flow separations have been demonstrated as a simple means of performing high throughput particle and cell sorting by the application of external forces or by the utilisation of physical objects or flow regimes. Balancing the respective forces is often relatively simple, particularly since the separation can be monitored in real-time and the parameters adjusted when necessary. Table 2 summarises the techniques detailed above

(adapted from Ref. 145), while the advantages and disadvantages of each method remain as described in Table 1.

A popular method of manipulating particles and cells, either for trapping or continuous flow separations, is by the use of magnetic forces, which have only briefly been mentioned in this chapter. The next chapter will give a detailed account of the properties of magnetic particles, the theory behind their manipulation in microfluidic devices, and their applications in such systems. Additionally, the phenomenon of diamagnetic repulsion will be explained, and its potential for performing on-chip procedures.

**Table 2  Summary of continuous flow separation techniques, and the types of sample they can be applied to.  Adapted from Ref. 145.**

| Method | Separation mechanism | Samples and applications | Refs. |
|---|---|---|---|
| Physical objects | • Obstacles <br> • Size of species | • Microparticles <br> • DNA <br> • Whole blood <br> • Embryoid bodies | 150-158 |
| Flow based methods | • Laminar flow <br> • Size of species | • Microparticles <br> • Cells <br> • Whole blood | 159-176 |
| Optical lattice | • Size and refractive index of species | • Microparticles <br> • Cells | 208-210, 212 |
| Free-flow electrophoresis (FFE) | • Homogeneous electric field <br> • Mass-to-charge ratio of species | • Amino acids <br> • Proteins | 213 |
| Free-flow isoelectric focussing (FF-IEF) | • pH gradient in homogeneous electric field <br> • Isoelectric point of species | • Proteins <br> • Cells | 214 |
| Dielectrophoresis (DEP) | • Inhomogeneous electric field <br> • Size and polarisability of species | • Microparticles <br> • Cells | 97-100, 217-227 |
| Acoustophoresis | • Acoustic pressure <br> • Size, density, and compressibility of species | • Microparticles <br> • Cells | 112, 195, 229-237 |
| Thermophoresis | • Species' thermal diffusion coefficient <br> • Thermal gradient <br> • Type of electrolyte | • Nanoparticles | 245 |
| Gravitational forces | • Sedimentation <br> • Size and density of species | • Microparticles | 246 |

## *1.4      Magnetic particles*

A large area of particle based microfluidic research involves the application of magnetic microparticles. Such particles offer all of the advantages of polymer particles as described in Section 1.2 (i.e. high surface-to-volume ratio, variety of surface functional groups, range of sizes etc.), but with the added attraction of being easy to manipulate by the application of external magnets. Before describing these particles in more detail, it is worth discussing some of the relevant magnetic theory.

## 1.4.1   Magnetism

Magnetism is one of the earliest recorded scientific discoveries by man, with Thales' writings *circa* 600 B.C. describing the attraction of iron to lodestone (magnetite), while it has also been claimed that the compass was used in China earlier than 2500 B.C.[247] Magnetism refers to the generation of a magnetic field in or around a magnetic body or a current-carrying conductor.[248] A magnetic field is always produced as a result of an electrical charge being in motion, either through electrical current flowing through a conductor (which is how electromagnets operate) or in a permanent magnet originating at the atomic level. In the latter case there exists no conventional electrical current, with the moving charge in fact being due to the spin of electrons (spin angular momentum),[249-251] and to a lesser extent the orbital motion of electrons around the nucleus of the atom (orbital angular momentum).[247] These momentums give rise to magnetic dipoles, consisting of a north pole and a south pole of equal strength, and a magnetic dipole moment ($\mathbf{m_d}$, in A m$^2$, or J T$^{-1}$) which describes the pole strength, separation between the poles, and direction of the "point-like" dipole pointing from south to north.

When a magnetic material is placed in a magnetic field, $\mathbf{H}$ (in A m$^{-1}$), the individual atomic dipole moments contribute to an overall response in the material that result in its magnetic induction, $\mathbf{B}$ (in Tesla, T, corresponding to N A$^{-1}$ m$^{-1}$, or Wb m$^{-2}$), which describes the force per metre on a conductor carrying a current perpendicular to the direction of the induction.[248,252] $\mathbf{B}$ is also known as the magnetic flux density, which is how it will appear throughout the remainder of this thesis. Magnetic parameters can be described using two systems of unit: the CGS (centimetre-gram-second) system and the SI (International System of Units) system. The SI system will be used throughout this thesis.

When an external magnetic field ($\mathbf{B}$) is applied to a magnetic dipole moment ($\mathbf{m}_d$), the dipole moment experiences a torque, $\tau$ (in N m, or J), as the $\mathbf{B}$ field tries to align the dipole such that the moment ($\mathbf{m}_d$) aligns parallel with the flux density (Equation 16).

$$\tau = \mathbf{m}_d \times \mathbf{B} \qquad \qquad \textbf{Equation 16}$$

The extent to which a medium responds to the magnetic field ($\mathbf{H}$) depends on the permeability of the material, $\mu$ (in Henry per metre, H m$^{-1}$, corresponding to N A$^{-2}$). The relationship between the $\mathbf{H}$, $\mathbf{B}$ and $\mu$ terms is given by Equation 17.[253]

$$\mathbf{B} = \mu \mathbf{H} \qquad \qquad \textbf{Equation 17}$$

In free space, the equation becomes $\mathbf{B} = \mu_0 \mathbf{H}$, where $\mu_0$ is the permeability of free space and is a universal constant ($\mu_0 = 4\pi \times 10^{-7}$ H m$^{-1}$).

The field of magnetic flux density ($\mathbf{B}$) consists of lines of magnetic flux, $\Phi_m$ (in Weber, Wb), within a unit area, hence a $\mathbf{B}$ field of 1 Tesla = 1 Wb m$^{-2}$. A greater number of lines per unit area gives a greater value of $\mathbf{B}$, indicating a stronger magnetic field exhibited by the magnetic body. The value of $\mathbf{B}$ decreases rapidly with increasing

distance from the surface of a magnet as the flux density lines move further apart, as shown in Fig. 18 for a typical rectangular (bar) magnet.
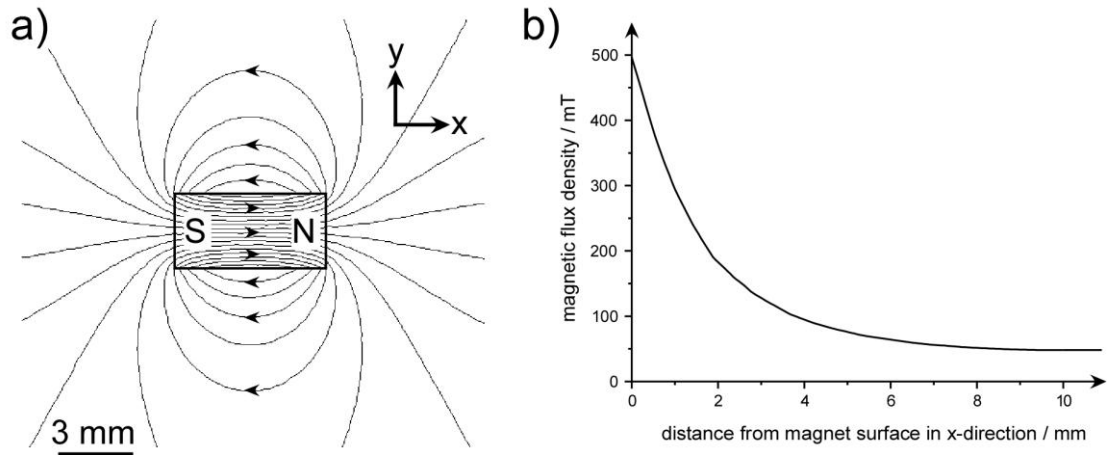


**Fig. 18  Characteristics of a typical rectangular magnet, illustrating a) the magnetic flux density, B, in and around the magnet, and b) the decrease in B with increasing distance from the magnet surface in the x-direction.**

Equation 18 and Fig. 19 describe how the dimensions of a rectangular magnet determine the value of **B** at a distance, $X$ (in m), from the surface.[254]

$$\mathbf{B} = \frac{\mathbf{B_r}}{\pi}\left( \tan^{-1}\frac{AB}{2X\sqrt{4X^2 + A^2 + B^2}} - \tan^{-1}\frac{AB}{2(L+X)\sqrt{4(L+X^2) + A^2 + B^2}} \right)$$

**Equation 18**

where $\mathbf{B_r}$ = the residual (remanence) magnetic flux density (T), $L$ = length or thickness of the magnet (m), $A$ = width of the magnet (m), and $B$ = the height of the magnet (m). The north and south poles are situated on the faces in the $X$-direction.
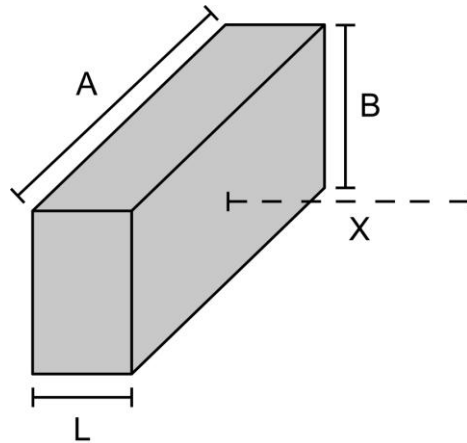
**Fig. 19  Dimensions of a rectangular magnet when determining the value of the magnetic flux density at a distance, $X$, from the surface, with the poles located on the $X$ faces of the magnet.  $L$, $A$, and $B$ signify the length (thickness), width, and height of the magnet, respectively.**

Equation 19 shows how to determine the magnetic flux density of a cylindrical magnet with radius $R$ and length $L$ at a distance $X$, with the dimensions given in Fig. 20.  The poles are situated on the faces of the magnet in the $X$-direction.

$$\mathbf{B} = \frac{\mathbf{B}_r}{2}\left( \frac{(L+X)}{\sqrt{R^2 + (L+X)^2}} - \frac{X}{\sqrt{R^2 + X^2}} \right) \qquad \textbf{Equation 19}$$
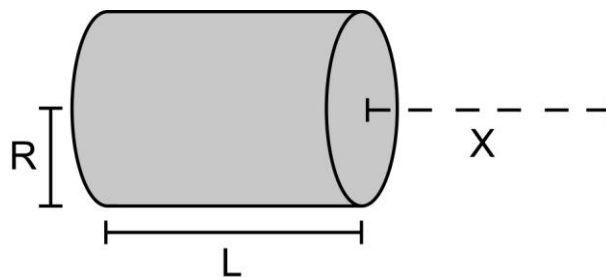


**Fig. 20   Dimensions of a cylindrical magnet for the determination of the magnetic flux density at a distance, $X$, from the surface.  The north and south poles are situated on the faces of the cylinder, and $R$ and $L$ are the radius and length of the magnet, respectively.**

Additionally, it is worth noting the effects observed when two permanent magnets are placed in close proximity, with the results depending on their relative orientation. Fig. 21a shows two magnets placed with their opposite poles facing, illustrating the lines of magnetic flux density (black lines), and the relative magnitude of **B** field based on the colour shown (where purple shows the highest value of **B**, and blue the lowest). Here, the lines of magnetic flux density pass from the north pole of one magnet to the south pole of the other across the gap in space, thereby allowing complete loops of flux lines from one magnet and through the other. The flux lines between the magnets are concentrated into a small space, and the result is an attractive force between them.
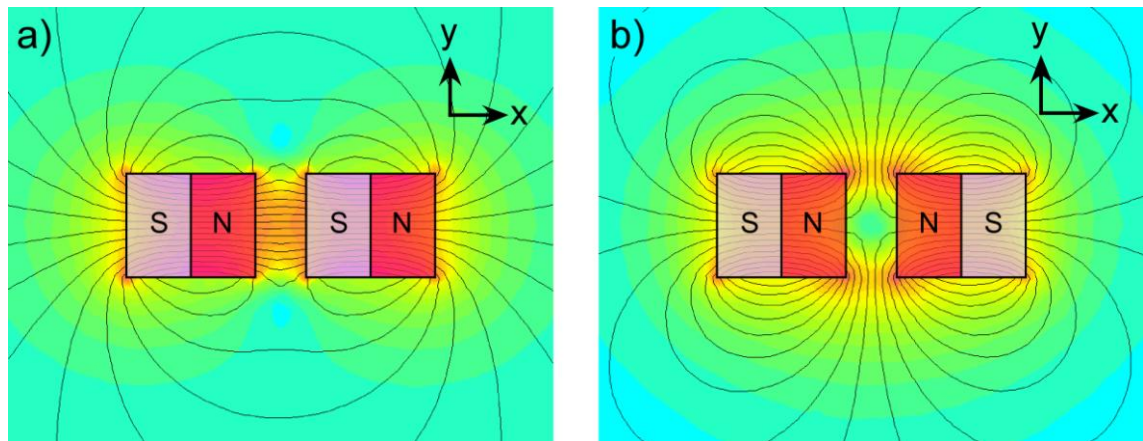


**Fig. 21 Magnetic flux lines and their density (B field) between two permanent magnets. a) When the opposite poles of two magnets are facing, the B field flows from the north pole of one magnet to the south pole of the other, and there is a resultant attractive force between the magnets. b) When the like poles of two magnets are facing, the field lines cannot cross, and they instead "push" against each other, generating a repulsive force between the magnets. Additionally, an area of low field is created between the facing poles.**

However, in Fig. 21b, the two magnets are shown with their like poles facing each other. Magnetic flux density lines are unable to cross one another, and so as the

magnets are brought close together the field lines of both magnets become "pressed" against each other, particularly at the corners where the field is strongest. This "compression" of the flux density lines creates a repulsive force between the two magnets, hence they are repelled from each other. In this scenario, a region of low field is also generated between the two magnets, as shown by the light blue and green region between the two north poles.

A magnetic field produced by a permanent magnet differs to that produced by a current-carrying capacitor as the former has a magnetisation, $\mathbf{M}$ (A m$^{-1}$), due to its having a net magnetic moment, whilst the latter does not.[248] The magnetisation ($\mathbf{M}$) is defined as the magnetic moment ($\mathbf{m_d}$) per unit volume of material, $V_m$ (m$^3$), as shown in Equation 20:

$$\mathbf{M} = \frac{\mathbf{m_d}}{V_m} \qquad \text{Equation 20}$$

The magnetisation ($\mathbf{M}$) is related to $\mathbf{B}$ in a similar manner to how $\mathbf{H}$ was above, as shown in Equation 21:

$$\mathbf{B} = \mu_0(\mathbf{H} + \mathbf{M}) \qquad \text{Equation 21}$$

Here, it can be seen that the magnetic field ($\mathbf{B}$) induced in the permanent magnet consists of contributions from both the applied magnetic field ($\mathbf{H}$) and the magnetisation of the material ($\mathbf{M}$). The magnetisation is related to $\mathbf{H}$ via the property of a material known as its magnetic susceptibility. There are three different, but related, forms of susceptibility: volume susceptibility ($\chi$, dimensionless), molar susceptibility ($\chi_{mol}$, m$^3$ mol$^{-1}$), and mass susceptibility ($\chi_{mass}$, m$^3$ kg$^{-1}$). The form used throughout this thesis will be the volume susceptibility ($\chi$). The susceptibility of a material describes the ease with which it becomes magnetised in an applied $\mathbf{H}$ field, as shown in Equation 22.

$$\mathbf{M} = \chi \ \mathbf{H}$$ 

**Equation 22**

Several different types of magnetism exist, which can each be described in terms of their magnetic susceptibility and magnetisation. Table 3 summarises the different types, and some of the more relevant types to this thesis are described below.

**Table 3  The different types of magnetism, with an overview of their atomic and magnetic properties.  Adapted from www.aacg.bham.ac.uk/magnetic_materials/type.htm.**

| Type of magnetism | Susceptibility | Atomic/magnetic behaviour | |
|---|---|---|---|
| Diamagnetism | - small<br>- negative<br>- ($\chi < 0$) | - atoms have no magnetic moments |  |
| Paramagnetism | - small<br>- positive<br>- ($\chi > 0$) | - atoms have randomly orientated magnetic moments |  |
| Ferromagnetism | - large<br>- positive<br>- ($\chi \gg 0$)<br>- function of applied field | - atoms have parallel aligned magnetic moments within domains |  |
| Anti-ferromagnetism | - small<br>- positive<br>- ($\chi > 0$) | - atoms have antiparallel aligned moments |  |
| Ferrimagnetism | - large<br>- positive<br>- ($\chi \gg 0$)<br>- function of applied field | - mixed parallel and antiparallel moments that do not totally cancel |  |

*Ferromagnetism*

This is the type most commonly associated with magnetism, being that it is encountered in everyday life in the form of fridge magnets and in children's action figures etc. Ferromagnetic materials exhibit a large and positive magnetic susceptibility ($\chi \gg 0$) due to unpaired electrons in their atomic or molecular orbitals. When unpaired electrons exist they are free to align their moments in any direction, and the application of a magnetic field will cause these spins to align in the direction of the field. This essentially creates a new magnet, with its magnetisation in the same direction as that of the applied field, giving rise to attraction, as seen in Fig. 21a.

Ferromagnetic materials (such as iron) feature net magnetic moments in their structures due to the alignment of magnetic moments into ordered arrangements that point in the same direction, even when there is no external **H** field present. However, rather than *all* of the moments aligning in the same direction throughout the material, they instead form microscopic regions of aligned moments, called magnetic "domains", or Weiss domains. If the material is in its demagnetised state, the domains are oriented in different directions, such that the bulk material exhibits no net magnetic moment, hence no overall magnetisation (Fig. 22a). Between each domain in the material there exists a domain wall, also called Bloch walls (or Néel walls below a critical thickness of the ferromagnetic material), which exist as transition layers between the domains. Here, the magnetic moments are gradually reorientated 180° or 90° across the layer (Fig. 22b), and typical domain wall thicknesses include 40 nm for iron and 100 nm for nickel.

When an external magnetic field is applied, the domains within the ferromagnetic material start to align with the field (with the moments within the domain walls orientating most easily), resulting in net magnetisation of the material. Increasing the field strength results in the alignment of more domains until they are all orientated in

the same direction (Fig. 22c). This point, at which all of the domains are aligned and the material cannot be further magnetised, is called the saturation magnetisation, $M_s$ (A m$^{-1}$). Additionally, when magnetised in an applied field, the magnetisation persists even after the removal of the field, as can be observed using a hysteresis loop. These loops can be produced as either **M-H** or **B-H** curves, and are generated by measuring either the magnetisation (**M**) or magnetic flux density (**B**) of a material as the applied magnetic field (**H**) is increased. Fig. 23 shows a typical example of an **M-H** curve (also known as a magnetisation curve) for a ferromagnetic material.
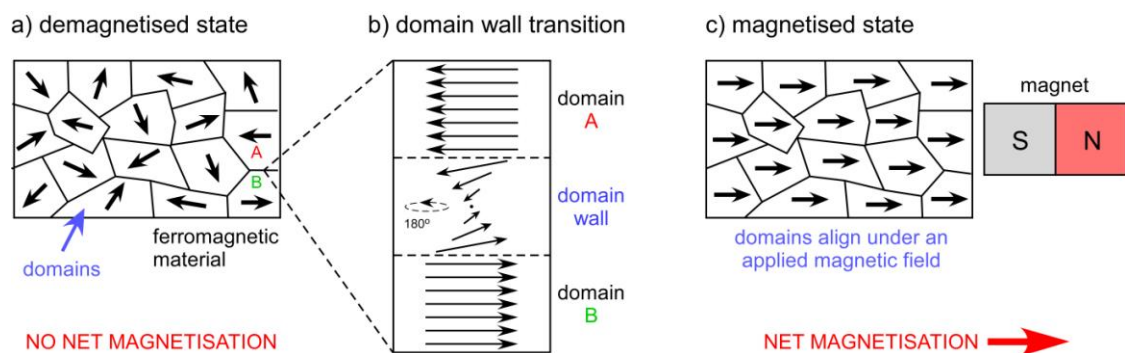


**Fig. 22    a) Domains point in random directions in the demagnetised state of a ferromagnetic material, resulting in no net magnetisation.  b) Domain wall transition of moments from one domain to another, with the moments in the wall gradually rotating throughout.  c) When a magnetic field is applied, the domains align in the same direction, resulting in a net magnetisation that persists even after removal of the applied field.**

If the material starts in its demagnetised state as seen in Fig. 22a, i.e. with no net magnetisation, then with zero applied field the magnetisation is also zero. As the applied field (**H**) is increased, the magnetisation (**M**) increases as the domains in the material start to align with the field until it reaches saturation magnetisation ($M_s$), and all the domains are aligned. When the applied field is reduced to zero, the

magnetisation does not return to the origin, instead decreasing to a value of known as the magnetic remanence, $\mathbf{M_r}$. This is the value of $\mathbf{M}$ when $\mathbf{H} = 0$, and thus it is now the material's magnetisation value now that it has become a permanent magnet. As the magnetic field continues to be increased in the opposite direction to that which it was originally applied, the material reaches the point at which half of the domains have been 'flipped' and the net magnetisation is zero. The magnetic field required to achieve this is known as the coercivity, $\mathbf{H_c}$. The same effects are observed as the magnetic field continues to be increased in this direction to another point of saturation magnetisation (at which all of the domains are oriented in the opposite direction to the original $\mathbf{M_s}$ value). The field is then increased again in the original direction until it reaches $\mathbf{M} = 0$, thus completing the hysteresis loop of the $\mathbf{M}$-$\mathbf{H}$ curve.
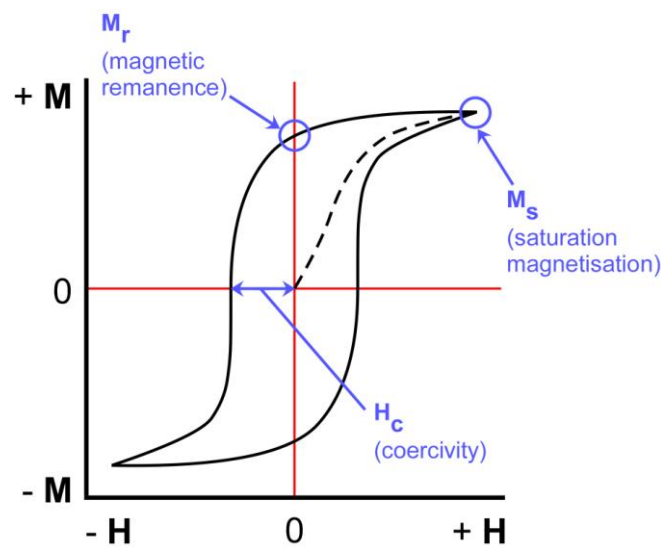


**Fig. 23 Hysteresis loop observed in the M-H curve for a ferromagnetic material. The magnetisation (M) of the material increases with the applied field (H), until it reaches saturation ($\mathbf{M_s}$). As the field is reduced to zero, the material remains magnetised to the value of its magnetic remanence. The field strength required to drive the magnetisation back to zero is known as the coercivity. The positive and negative values of H and M correspond to opposite directions, e.g. +M refers to the magnetisation in one direction while –M refers to the magnetisation in the opposite direction.**

A further property of ferromagnetic materials is that they possess a Curie temperature (or Curie point), $T_c$ (°C), above which the spontaneous magnetisation is destroyed, the permeability drops, and the magnetic remanence and coercivity become zero, causing the material to become paramagnetic.

*Paramagnetism*

Like ferromagnetic species, paramagnetic materials contain unpaired electrons, allowing them to be aligned in a magnetic field such that they form a net magnetic moment, hence their attraction to magnetic fields. However, unlike ferromagnets, and as seen by their **M-H** proportionality, they do not exhibit magnetic remanence upon removal of the field as the individual magnetic moments become randomised due to thermal energy ($k_B T$) and do not interact with each other. Thus, paramagnetic materials are only magnetised in the presence of an applied field, and once the field is removed the magnetisation is lost. Examples of paramagnetic materials include aluminium, several transition metal compounds, and some gases such as oxygen.

*Superparamagnetism*

Despite the suffix, this type of magnetism is actually observed in ferromagnetic and ferrimagnetic materials, most commonly the magnetite ($Fe_3O_4$) and/or maghemite ($\gamma$-$Fe_2O_3$) compounds found in the latter. However, a crucial factor is that the materials exist as small, single domain nanoparticles.[252,255,256] This means that all of the magnetic moments of the atoms in a particle align without the application of a magnetic field, thus forming a magnetic domain as seen in ferromagnetic materials. When the size of

the nanoparticle is smaller than that of a domain wall (typically 5 - 100 nm, depending on the material), only a single domain is able to exist, thus at an instantaneous point in time the particle has a net moment in one direction. However, due to the small size of the nanoparticles they are affected by thermal energy ($k_B T$) in the same manner as paramagnetic materials, with the thermal motion continuously causing the moment of the particle to randomly flip. Hence, the time-averaged moment of a particle without an applied magnetic field becomes zero.
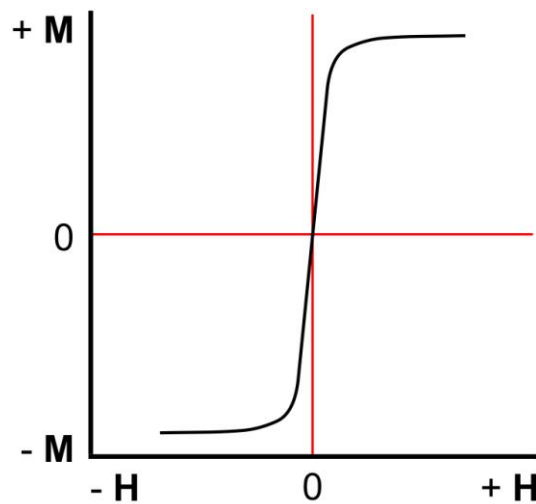


**Fig. 24 Magnetisation (M-H) curve for a superparamagnetic nanoparticle. As the applied field increases, so too does the particle magnetisation, until it is saturated. Unlike a ferromagnetic material, there is no magnetic remanence, meaning that upon removal of the field the particle essentially becomes non-magnetic.**

When a magnetic field is applied, the moments of the particles align with the direction of the field, thereby giving a net time-averaged magnetisation. Thus, the particles will migrate towards the region of highest field, and should the particles encounter each other they form chain-like structures. Additionally, since the materials in the particles are ferro- or ferrimagnetic, the magnetic susceptibility is very high and so the attraction

towards the field is very strong. However, when the field is removed, thermal energy is again able to affect the moments of the particles, returning them to their original state whereby they exhibit no time-averaged net magnetic moment. As a result, the particles lose their magnetisation and are able to disperse back into the media they are present in. Hence, the particles act like paramagnets, except with very large magnetic susceptibilities and magnetic moments, and thus they are known as superparamagnetic particles. Fig. 24 shows a typical **M-H** curve of a superparamagnetic nanoparticle, reaching saturation as seen in ferromagnetic materials but without the hysteresis, hence having no magnetic remanence (i.e. no magnetic "memory") and no coercivity.

*Diamagnetism*

In diamagnetic materials, magnetisation occurs in the opposite direction to the applied field, resulting in repulsive effects (as illustrated in Fig. 21b). Diamagnetism arises due to the presence of pairs of electrons in atomic orbitals in which the magnetic moments of the two electrons to cancel. Hence, diamagnetism is an inherent property of all matter, though should a material exhibit any other magnetic property (ferro-, para-, etc.) then the diamagnetic contribution is "masked". Diamagnetic materials include water, wood, gold, copper, plastics (such as polystyrene), and carbon.

The effect of diamagnetic repulsion has seen some interest in recent years as, although the phenomena is generally very weak, the development of high magnetic field superconducting magnets has made it possible to easily achieve such repulsion. One of the major applications for superconducting magnets in this area has been the magnetic levitation of a variety of diamagnetic objects against gravity inside a bore. In 1991, Beaugnon and Tournier[257] showed that a number of diamagnetic substances could be

levitated, including wood, plastics, graphite, antimony, bismuth, water, and organic solvents (ethanol and acetone). Geim[258] demonstrated the levitation of live frogs in 1997, while Guevorkian and Valles have shown the levitation and manipulation of frog embryos and paramecium in high magnetic fields.[259-265] This levitation effect is now commonly used to simulate a zero-gravity environment, which is of interest for studying biological effects and protein crystal growth in "space".[266,267] These have included research into levitated liquid oxygen[268] and large water droplets,[269] among other liquids.[267] A recent development saw the successful levitation of young mice, which shows promise for studies on the long-term effects of weightlessness in mammals.[269] Levitation has also been investigated for the diamagnetic orientation of biological systems,[270] the containerless growth of proteins,[271-273] inorganic crystal and water crystal growth,[274] the fabrication of glass spheres,[275] and the processing of other types of materials.[276-283]

## 1.4.2 Superparamagnetic particles

Superparamagnetic particles can be fabricated or bought commercially in a range of sizes and with differing magnetic properties. The synthesis of superparamagnetic nanoparticles has been reviewed previously by Lu,[284] Osaka,[285] and Gijs.[255,256] After synthesis of the magnetic particles themselves, they are typically coated with a layer of material (such as polymers, surfactants, silica, carbon, precious metals etc.) to prevent/reduce their agglomeration due to van der Waal's, magnetic and electrostatic forces. As well as these protective coatings, the surface can also be functionalised with a range of chemical or biological species (as with the microparticles in Section 1.2), including antibodies, antigens, DNA, chemical functional groups, and one of the most common functional groups: streptavidin. With such a variety of sizes and

functionalisations, magnetic nanoparticles have seen a number of applications, and the reader is directed to reviews by Pankhurst *et al.*[252] regarding their use in biomedicine, Osaka *et al.*[285] for their application to bioassays, and Palacek and Fojta[286] for their use in electrochemical DNA and protein biosensing. Additionally, reviews by Saiyed *et al.* and Safarik *et al.* detail the use of magnetic particles (both nano- and microparticles) in drug delivery and biomedicine,[287] and for the isolation and purification of proteins and peptides,[288] respectively. A recent review by Wu *et al.*[289] also summarises the most recent applications of magnetic nanoparticles in biomedicine, while a review by Krishnan[290] details their use in imaging, diagnostics, and therapy. Some of these applications include hyperthermia, drug targeting, MRI (magnetic resonance imaging) contrast enhancement, and cell/particle separations.[252,255]

Hyperthermia involves the treatment of cancer by heating of the malignant cells using magnetic particles introduced into the cancer.[291] MRI imaging is based on the relaxation times of the magnetic moments of protons in a tissue, and superparamagnetic particles can be used to enhance the contrast in images by affecting these relaxation times. Suitable functionalisation also allows superparamagnetic nanoparticles to be employed for drug delivery, whereby particles featuring a drug bound to their surfaces could be introduced into the blood stream, captured at a cancer site by an external magnetic field, and the drug released upon exposure to a stimulus. However, this method has limitations including particle toxicity, possible accumulation of particles to form a blockage in the body, lack of magnetic properties of the drug once released, and the large distances required for the magnetic field to reach in order to accumulate particles. Additionally, magnetic nanoparticles can be used for the magnetic labelling of biological cells, which are typically diamagnetic. This can be achieved by either functionalising the particles such that they are able to bind to the cell surface,[292] or by allowing cells to take the particles into themselves.[293,294] Hence, the cells would then

essentially become like superparamagnetic microparticles, being attracted to magnetic fields but exhibiting no magnetic properties upon removal of the field.[295,296] The ability to render cells magnetic allows their magnetic separation, which will be described in more detail later in this section.

Two important uses of magnetic particles (both nanometre and micrometre sized) are their application to bioassays and particle/cell separations. As both size ranges can be applied to these procedures, they will be explained in more detail after a description of the superparamagnetic microparticles that were used throughout the work in this thesis. Monodisperse magnetic microparticles can be purchased commercially from a number of sources, and the brand names include Dynabeads (Invitrogen, Paisley, UK), Micromer particles (micromod Partikeltechnologie GmbH, Rostock, Germany), Compel (Bangs Laboratories, Inc., Indiana, USA), MACS MicroBeads (Miltenyi Biotec GmbH, Bergisch Gladbach, Germany), Adembeads (Ademtech, Pessac, France), SiMAG (Chemicell, Berlin, Germany), as well as Seradyn and MagnaBind particles (Thermo Fisher Scientific, Inc., Illinois, USA).

Superparamagnetic microparticles (hereafter referred to simply as magnetic particles) are typically the same as polystyrene microparticles, as described in Section 1.2, except that, crucially, they contain either a core of iron oxide (Fig. 25a) or a dispersion of iron oxide nanoparticles throughout the particle (Fig. 25b). In the latter case, an extra layer of material is applied to the surface of the particle to seal the iron oxide inside, which in the case of Dynabeads (the particle type chosen for the work in this thesis), is a hydrophilic layer of glycidyl ether. Most commercially available superparamagnetic microparticles are fabricated with a dispersion of ferromagnetic nanoparticles rather than a single core, presumably to ensure that the superparamagnetic properties of the nanoparticles are retained rather than risking the generation of a large core that could be

too big to display superparamagnetism. As well as polystyrene, various other polymer matrices can be used to fabricate the particles, and, in the case of SiMAG, a silicon matrix can also be applied. The iron oxide core/nanoparticles are typically in the form of ferrimagnetic magnetite ($Fe_3O_4$) and maghemite ($\gamma$-$Fe_2O_3$), though sometimes other ferrites such as cobalt ferrite and manganese ferrite can be used.
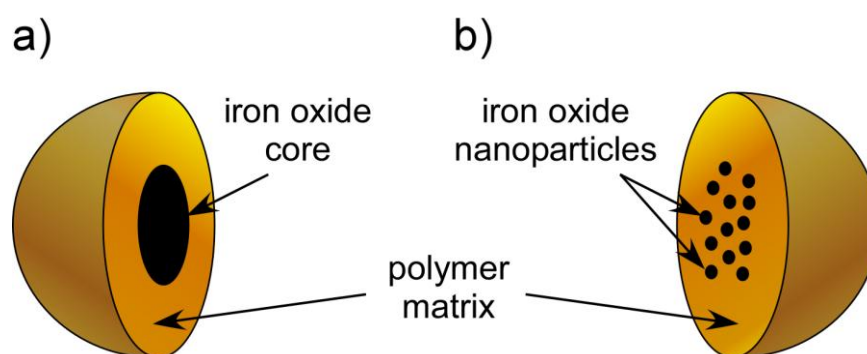


**Fig. 25 Cross-section of two types of superparamagnetic microparticle: a) an iron oxide core is encased in a polymer matrix, and b) iron oxide nanoparticles are dispersed throughout the polymer matrix, before being sealed inside with an extra layer of material.**

Due to the size of the iron oxide nanoparticles, the microparticle as a whole displays superparamagnetic behaviour in that they are attracted to magnetic fields but, once the field is removed, they are able to redisperse freely in solution. This property has revolutionised particle based separations and bioassays, and magnetic particles have become popular as mobile solid supports that can be easily manipulated with magnetic fields. The wide variety of possible surface functionalities, as with conventional polystyrene microparticles (Fig. 2), allows for their use in any number of reaction and/or separation procedures.
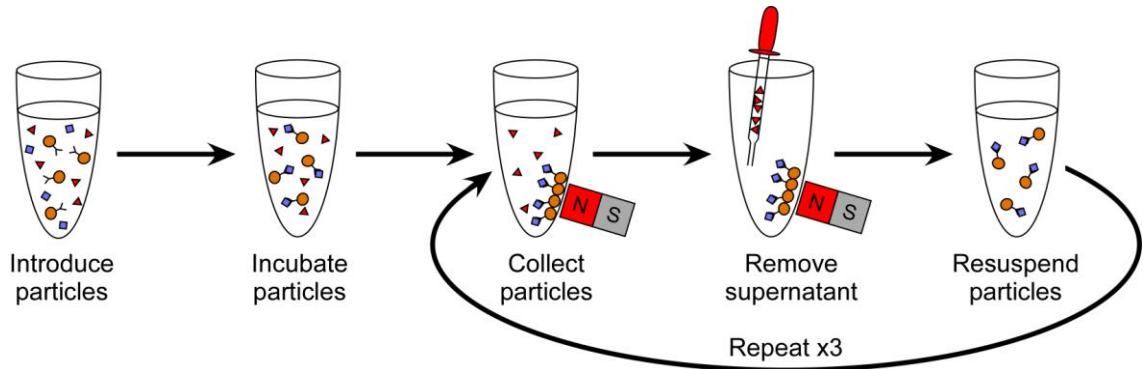
**Fig. 26 A typical reaction or separation using magnetic particles, where (1) the particles are introduced into the sample or reagent solution, (2) they bind to the target analyte/reagent, (3) the particles are collected using an external magnet, (4) the supernatant is removed, and (5) the particles are resuspended in fresh buffer solution. Steps 3-5 are repeated several times to ensure any unbound material is removed from the particle surfaces.**

A typical magnetic particle based bioassay or separation takes place in an Eppendorf tube or similar vessel, as shown in Fig. 26. The tube contains the reagent or sample of interest, into which the magnetic particles, featuring surface groups for binding specific targets, are introduced. The suspension is incubated with agitation, allowing the particles to bind to the target molecules, after which they are drawn to the side of the tube by an external magnetic field. The supernatant can then be removed and fresh buffer added, after which the particles are agitated, before again being drawn to the side of the tube and the supernatant removed. This washing step is repeated several times to ensure any unbound material is removed from the surfaces of the particles. Thus, the particles have successfully either removed the analyte of interest from the sample mixture, or been used to perform a bioassay on their surface followed by their

separation from the reagent solution. This provides extremely high capture efficiencies with a simple and easy method, which can also be applied to magnetically labelled cells.

This type of procedure has been used to perform a number of ELISA-type immunoassays. These have included the measurement and analysis of immunoglobulin concentrations in fluids,[297] schistosomal circulating anodic antigen in serum samples,[298] Cyclosporin A,[299] ligand and epitope adsorption,[300] biotin-binding capacity of streptavidin coated particles,[301] benomyl and carbenazim in water, soil, and fruit juice,[302] captan residues in water, peaches and apple juice,[303] antigen binding phage,[304] HIV-1&2 immunoassays,[305] free hCGβ in serum,[306] IgG immunoassays via chemilumiscent detection,[307] brain natriuretic peptide,[308] aflatoxin B1,[309] and many, many others. Similar procedures to that shown in Fig. 26 have been used also been used for the isolation of calcium phosphate crystals, known to be linked to destructive joint conditions, from complex synovial fluids.[310] In each of these cases, the particles were functionalised with surface groups suitable for binding to the analyte of interest.

A popular method of performing magnetic cell separations, though typically with magnetic nanoparticles, is by magnetic-activated cell sorting (MACS®),[311] developed in 1990 by Miltenyi et al.,[312] and now commercially available from Miltenyi Biotec. In this procedure, antibody labelled magnetic particles are introduced into a cell suspension, where they bind to the cell of interest. The suspension is then flushed through a high-gradient magnetic separation column. The column contains steel wool that is magnetised by the presence of an external permanent magnet, which traps the magnetically labelled cells on the wool whilst the unlabelled cells are allowed to pass through the column, thereby allowing their separation. The magnets can then be removed, allowing the magnetically labelled cells to be eluted from the column.

Having established the properties and behaviour of magnetic particles, and detailed their applications for separations and immunoassays, their use in microfluidic devices will now be discussed. On-chip trap and release methods of performing separations, assays and reactions will first be briefly described, followed by on-chip continuous flow separations. The applications of magnetic particles in microfluidic devices have been reviewed in more detail by Pamme[313] and Gijs et al.,[255,256] within a review of on-chip particle trapping methods by Nilsson et al.,[70] and in reviews of on-chip continuous flow particle separations by Pamme,[145] Lenshof et al.,[146] Gossett et al.,[149] Kersaudy-Kerhoas et al.,[147] and Tsutsui and Ho.[148]

### 1.4.3   On-chip magnetic trap and release procedures

As explained above, magnetic particle-based processes are a very efficient means of performing reactions, assays and separations. However, conventional batch procedures suffer from requiring multiple, sequential reaction and washing steps (Fig. 26) that render the procedures laborious and time-consuming, and often result in using relatively large volumes of potentially expensive reagents. Microfluidic methods of performing magnetic particle-based processes often employ a 'trap and release' technique (Fig. 27). Here, functionalised particles are pumped through a microchannel and trapped in a magnetic field, before having washing solutions or reagents flushed over them.

A common use of the trap and release method is for the on-chip separation of magnetic particles, that have been suitably functionalised to bind to a particular target analyte, from their original sample matrix. The particles are trapped and washed with buffer solution, which removes the unwanted non-magnetic material from the system, and they are then released for collection or downstream analysis. Such processes have been

achieved using permanent magnets,[314-319] integrated micro-electromagnets,[320-323] external electromagnets,[324,325] and integrated metallic or microcircuit structures that are subsequently magnetised by an external applied field.[326-328] These setups have typically only been used to separate magnetic particles from their carrier fluid, but it has also been shown that different magnetic particle populations can be separated and trapped when combined with dielectrophoresis,[316] and the successful separation and detection of magnetically labelled dengue virus has been reported.[315]
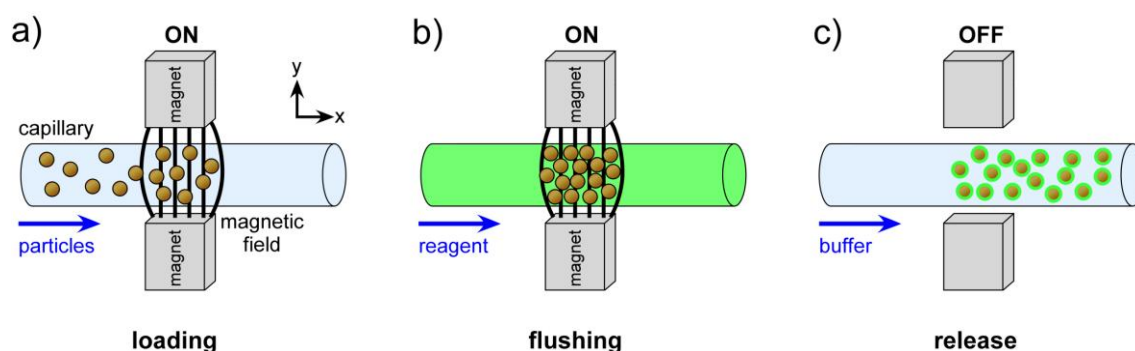


**Fig. 27 'Trap and release' method of magnetic particle handling in microchannels. a) Magnetic particles are loaded into the channel and trapped in a magnetic field. b) A sample or reagent is flushed over the trapped particles, allowing reactions to occur on the particle surfaces, before being washed with buffer solution. c) The field is removed and the particles released for downstream detection or further processing.**

However, the trap and release procedure has been employed to a far greater degree for performing reactions and bioassays on the surfaces of trapped particles. Here, functionalised particles are trapped in the microchannel by a magnetic field, and a reagent solution is flushed over them, allowing the reagent to bind to the particle surfaces. The reagent is replaced with buffer solution in order to wash the particles, which are then released from the magnetic field for downstream detection or other

applications. A number of reactions and assays have been performed using this method, and these include enzymatic assays and immunoassays for HIV-protease and anti-human growth hormone,[124] mouse IgG immunoassays,[34] simultaneous streptavidin-biotin and protein A assays,[114] parathyroid hormone and interleukin-5 sandwich assays,[115] purification and enrichment of dengue virus samples for RNA amplification and detection,[116] mRNA isolation,[117] DNA hybridisation[118-120] and separation,[329] purification of polymerase chain reaction (PCR) products for gene synthesis,[330] cell capture from blood followed by PCR amplification of the lysed cells and DNA detection,[331] human T cell capture from blood for PCR analysis,[332] reaction rate measurements,[333] and protein digestion.[113,121-123]

The above examples show a selection of microfluidic trap and release methods, that demonstrate the wide versatility, ease of use, and efficiency of the procedure. However, whilst the technique involves pumping solutions in flow over the surface of the particles, they still require multiple reagent and washing steps to be performed that require solutions to be changed sequentially. Therefore, the 'trap and release' is a batch method, and as such suffers from the same inefficiencies as off-chip methodologies in that they can be laborious and time-consuming due to the number of reaction and washing steps that must be performed. One method of reducing these inefficiencies is to perform the separations, reactions and assays in continuous flow. This offers the advantages of combining all of the reaction and washing steps into one single process, thereby decreasing the amount of time and labour required on behalf of the user, and rendering the procedure relatively automated once initiated.

### 1.4.4 On-chip magnetic particle separations in continuous flow

As described in the previous section, one of the major uses of magnetic particles is their separation from sample mixtures, since magnetic particles migrate towards a magnetic field (a process known as "magnetophoresis"), while non-magnetic material generally remains unaffected. However, as will be shown, it is also possible to continuously separate magnetic particles that exhibit different magnetic properties. Such separations are particularly useful in biomedical applications when the particles are bound to a target analyte.

Continuous flow separations offer the potential to eliminate some of the inefficiencies of batch microfluidic methods, allowing continuous introduction and separation of the sample, the advantages of which were described in Section 1.3.2. Thus, a selection of microfluidic devices that have been used for performing continuous flow magnetic particle separations will be highlighted. While not strictly microfluidic, the continuous flow separation of magnetic particles in the slightly larger systems of field-flow fractionation (FFF) and split-flow thin (SPLITT) fractionation should also be noted. The group of Zborowski and Chalmers have been developing both FFF[182,187,334,335] and SPLITT[203,336-338] devices for particle and cell separations for a number of years, and typically employ quadrupole magnetic fields to provide the lateral forces necessary for particle deflection. Latham et al.[184] used a 250 μm diameter capillary to perform field flow fractionation via the use of a permanent NdFeB magnet, which they applied to the separation of 3.5, 6.2 and 7.8 nm $Fe_2O_3$ nanoparticles, and 8.6 and 12.5 nm $CoFe_2O_4$ nanoparticles. Fuh et al.[200-202] developed SPLITT devices that also utilised an NdFeB magnet, and performed the separation of particles with varying magnetic susceptibilities obtaining separation efficiencies greater than 94 % for over 8 h of operation. In 1992, Hartig et al.[339,340] developed a free-flow magnetophoresis device based on a

conventional free-flow electrophoresis (FFE) chamber, with dimensions in the order of several millimetres. However, rather than applying electrical forces across the chamber, the force was instead supplied by an inhomogeneous magnetic field from an electromagnet. When magnetic particles were introduced into the chamber, they were continuously separated from non-magnetic particles due to their deflection from the sample stream, in a similar fashion to proteins in FFE devices. The device was used to separate magnetic particles with a throughput up to $10^9$ particles per hour, and with a sorting efficiency of >99 %. The method was also applied to the sorting of labelled B- and T-leukocytes (white blood cells).

In 1998, Blankenstein and Larsen[341] demonstrated a similar technique for the continuous separation of magnetic particles in a microfluidic device containing three parallel laminar streams, the middle stream of which consisted of a mixture of magnetic and non-magnetic particles. Magnets were placed beside the chip that deflected the magnetic particles into one of the adjacent buffer streams, while the non-magnetic particles remained in the central stream, thus separating the two particle populations in continuous flow. The system was only able to separate two different particle types into two different outlets, a design which has been replicated on many occasions, but the authors also stated that by splitting the flow channel into several outlet channels, labelled cells could potentially be distinguished and separated depending on their paramagnetic properties.

Kim and Park[342] fabricated a similar chip from PDMS, with two inlets that converged into a single main channel, before diverging into two outlets (Fig. 28), also known as a H-filter due to the shape of the design. Here, magnetic nanoparticles were attached to fluorescent polystyrene microparticles via antibody-antigen complexes and introduced into the chip. A magnet placed next to the main channel continuously deflected the

labelled microparticles into a buffer stream, whilst unlabelled microparticles remained in the same stream. Thus, if an analyte were present in the particle suspension before its introduction to the chip, the magnetic nanoparticles would become bound to the microparticle and allow their separation and detection of the analyte on-chip.
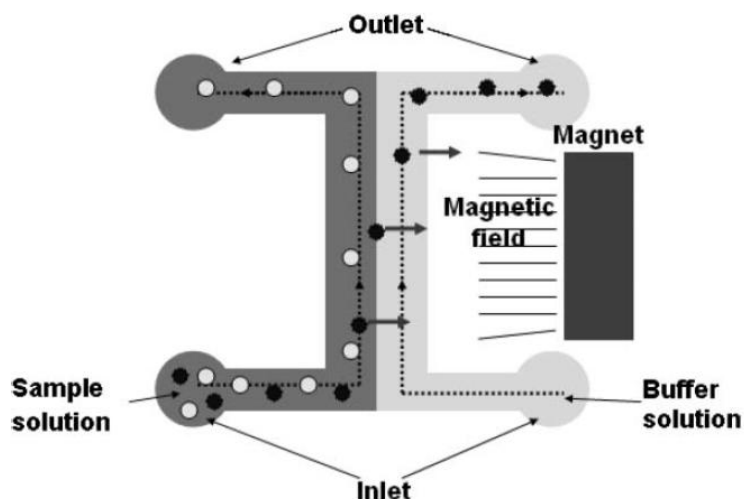


**Fig. 28  A common microfluidic method for continuous magnetic particle separation, known as an H-filter.  A particle mixture is introduced into a wide channel alongside a buffer stream, and a magnet used to deflect the magnetic particles into the buffer stream while the non-magnetic particles remain unaffected.  The two particle populations are thus separated via two outlets.[342]**

Xia *et al.*[343] also fabricated a two inlet, two outlet PDMS device with a single main channel, except that here they also incorporated a magnetic (NiFe) microneedle or a microcomb into the final structure.  When a permanent magnet was placed onto the chip, the microstructures generated a stronger magnetic field gradient across the chamber, which allowed magnetic particles to be deflected into the buffer stream at higher flow rates than when no magnetic microstructure was present.  The gradient

without any microstructures was 15 T m$^{-1}$ in the channel, while for the needle and comb they were >25 Tm$^{-1}$ and 50 T m$^{-1}$, respectively. The microcomb allowed particle separation efficiencies of 92 % at 40 μL h$^{-1}$, and the setup was then applied to the separation of magnetically labelled *E. coli* cells from a physiological concentration of red blood cells, with an efficiency of 78 % at 25 μL h$^{-1}$.

Yung *et al.*[344] developed a magnetophoresis device for the cleansing of blood, with a view to the prevention of sepsis in immunocompromised patients. Whole blood was spiked with *Candida albicans* fungi, a leading cause of sepsis-related deaths, and magnetic particles functionalised to capture the fungi. The mixture was pumped into the device alongside a buffer stream, and a magnetic field applied via an electromagnet that deflected the magnetically labelled fungi into the buffer stream, thus cleansing the blood with a separation efficiency of 80 % and at an impressive (at the microscale) volume flow rate of 20 mL h$^{-1}$. The system allowed devices to be multiplexed, such that in the example shown, four parallel chips were employed, with a view to stacking more chips on top of each other to increase throughput further.

Lai *et al.*[345] demonstrated a similar two-stream magnetic separation device, with "smart" magnetic nanoparticles being bound to model protein (streptavidin), the suspension introduced into the chip, and the labelled streptavidin deflected into an adjacent buffer stream. Interestingly, however, was the fact that the magnetic nanoparticles were pH responsive. Hence, in the sample solution (pH 7.4) they were successfully bound to streptavidin, but when deflected into the second buffer stream, which had a pH of 8.3, the nanoparticles were disaggregated from the protein. Thus, the proteins were separated from their original sample mixture with a separation efficiency of 81 %, while being simultaneously unlabelled in the process.

Han and Frazier[346-348] developed a "paramagnetic capture" (PMC) mode magnetophoretic microseparator that incorporated a nickel wire running along the centre of microfluidic chamber (Fig. 29a).
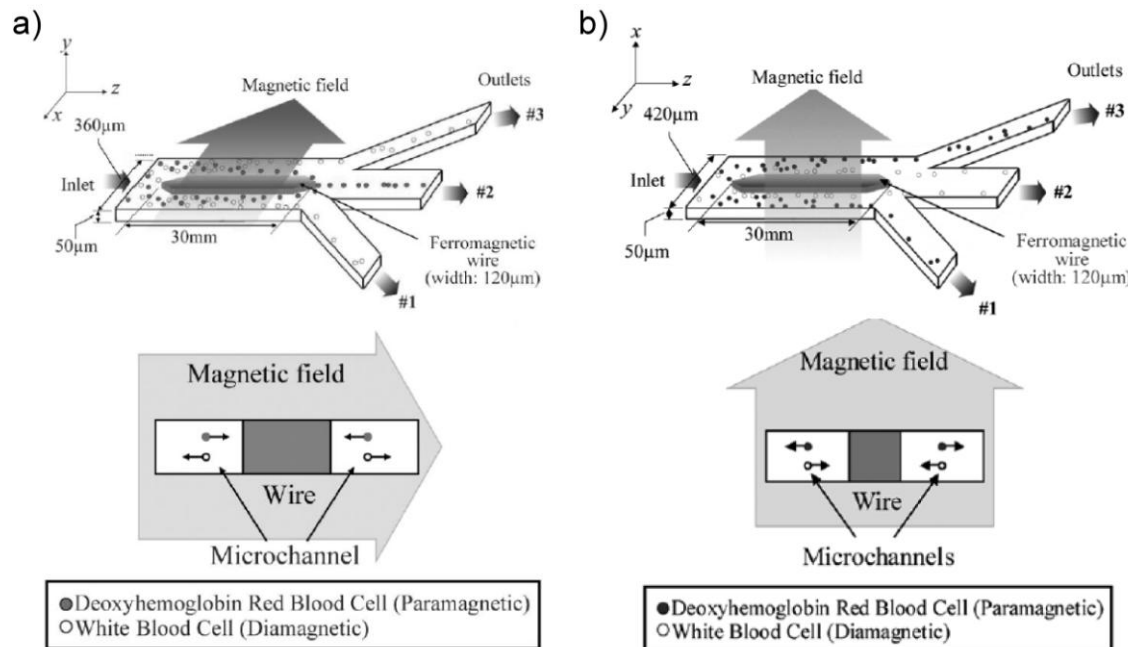


**Fig. 29 a) Paramagnetic capture mode magnetophoretic sorter. A nickel wire in the chamber is magnetised, causing red blood cells to be attracted and white blood cells to be repelled, allowing their collection at different outlets.[347,348] b) Diamagnetic capture mode magnetophoretic sorter. By orientating the applied field 90° to that shown in (a), red blood cells now migrate away from the wire whilst white blood cells move towards it, again allowing their separation by different outlets.[346,349]**

The chip featured three outlets that were used to separate red and white blood cells from diluted whole blood in continuous flow. The nickel wire was magnetised by an external permanent magnetic field, such that as the cells passed through the chamber the red cells were attracted towards the wire, forcing them towards the centre of the chamber

and therefore out of the middle outlet. However, the white cells were repelled by the field towards the outer edges of the chamber, exiting the chip via the upper and lower outlets, thereby achieving separation. Additionally, the setup could be altered such that it then became a "diamagnetic capture" (DMC) mode magnetophoretic microseparator (Fig. 29b).[346,349] By changing the direction of the applied magnetic field by 90°, the effect was reversed, with red cells migrating towards the edges of the chamber (exiting via the upper and lower outlets) while the white cells moved towards the centre of the chamber (exiting via the middle outlet). Qu *et al.*[350] demonstrated a similar device in which a nickel wire was situated inside the chamber of a microfluidic device and used to separate red and white blood cells by their respective attraction and repulsion.

Inglis *et al.*[351,352] performed a continuous immunomagnetic cell separation in a very different manner to those shown previously. Here, leukocytes (white blood cells) labelled with magnetic nanoparticles were separated from whole blood by the use of microfabricated ferromagnetic stripes that had been integrated into the microfluidic device. The stripes were angled 11° to the direction of fluid flow. A permanent magnet was used to magnetise the stripes, such that as the whole blood passed through the chip, the magnetically labelled leukocytes were attracted to the stripes. The leukocytes then flowed along the stripes away from the direction of flow of the red blood cells (which were not affected by the magnetic field), thus achieving separation of the leukocytes.

Adams and Soh *et al.*[353] designed a multitarget magnet activated cell sorter that offered the ability to separate cell types that had been labelled with magnetic particles of differing sizes and saturation magnetisations ($\mathbf{M_s}$). The device was akin to the multitarget dielectrophoresis activated cell sorted developed by Kim and Soh *et al.*,[227] described in Section 1.3.2, except that rather than having two sets of electrodes present in the device, it instead featured two sets of nickel strips. Unlabelled cells and those

tagged with the two different types of magnetic particles were pumped through the chip. The cells that exhibited no tag passed through the device without being affected, whilst the cells labelled with the larger particles (containing more magnetic material than the smaller ones) encountered the first set of nickel strips which, in the presence of an external magnetic field, caused these cells to deflect laterally across the chamber into an outlet channel. The second type of labelled cells, tagged with the smaller particles, were not greatly affected by this first set of nickel strips, but were instead deflected by the second set of strips into a different outlet, thus separating the three cell types. The device was used to successfully separate three sub-types of *E. coli* cells with greater than 90 % efficiency, and a throughput of $10^9$ cells h$^{-1}$.

Derec *et al.*[354] fabricated a microfluidic device in which the microchannels were etched into a layer of copper on an epoxy glass substrate, with a plastic top plate used to close the system, and featuring a main channel that branched into two outlets. The copper was etched such that thin strips ran alongside the channel, and when an electric current was applied to a copper strip, a magnetic field was induced that caused magnetic particles to deflect laterally as they flowed through the channel. The device was subsequently used to sort magnetically labelled tumour cells and unlabelled cells. The labelled cells were attracted to one side of the channel and out of the nearest outlet with an efficiency of >93 %, while the unlabelled cells exited out of both outlets equally, thus depleting the labelled cells from one of the collected fractions.

Siegel *et al.*[355] fabricated a device featuring a main channel and two parallel channels. The parallel channels were filled with molten solder which, when allowed to set, formed electromagnets when an electric current was passed through them. Magnetic fields up to 2.8 mT were generated, with gradients up to 40 T m$^{-1}$, and were first used for the trap and release of magnetic particles. The device was then used to sort the magnetic

particles into two different outlets by switching on/off the two electromagnets appropriately. Song et al.[356] developed a multi-layered microfluidic device in which separation occurred in the vertical direction. Here, the chip featured a bottom channel and a top channel, with a section overlapping between the two down the length of the chip. Electroplated copper microcoils were placed on top of the chamber that became electromagnets when electric current was passed through, causing the particles to deflect from the bottom channel to the top channel, whilst in the absence of a magnetic field the particles remained in the bottom channel. The integrated microelectromagnets were able to separate magnetically labelled Jurkat cells labelled from a sample solution, with an efficiency greater than 95 %.

Lou et al.,[357] from the group of Soh, redeveloped their earlier cell-sorting microfluidic device that utilised dielectrophoresis (Hu et al.[221]), by instead incorporating nickel strips into the chamber rather than the electrodes used previously. When the nickel strips were magnetised by an external magnet, magnetically labelled aptamers followed the direction of the strips (as demonstrated previously by Inglis et al.[351]), which allowed them to be separated from samples streams into a buffer stream, whereupon they exited the chip via a different outlet to the sample streams.

Most of the examples above have typically involved a variation of the H-filter design shown in Fig. 28, and usually simply involve the separation of magnetic particles from a sample stream and into a buffer stream. However, whilst reducing processing times and sample volumes by utilising these methods, they generally only allow one material to be separated from another. In many cases separation of multiple species may be required, which can be achieved, for example, by labelling/capturing the desired analyte with different types of magnetic particles and separating these magnetically. To achieve this, Pamme and Manz[358] developed a technique known as "on-chip free-flow

magnetophoresis", that allowed the simultaneous separation of magnetic particles from non-magnetic materials, as well as the separation of magnetic species from each other based on their sizes and magnetic susceptibilities.
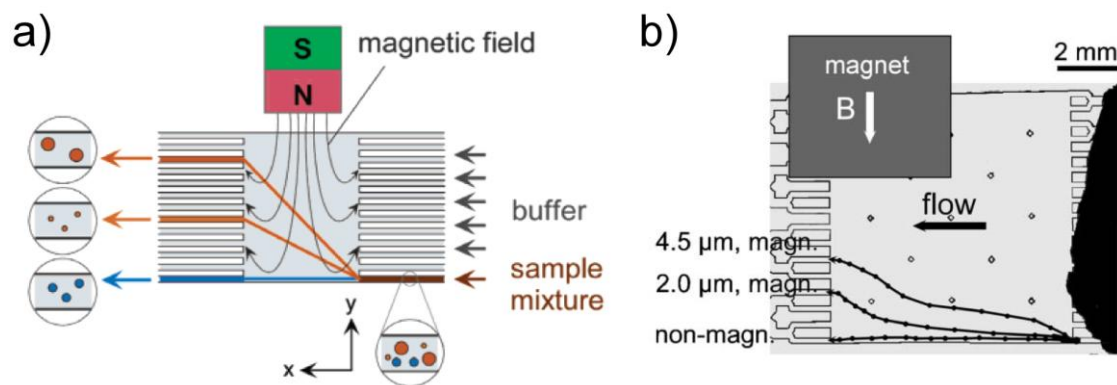


**Fig. 30 a) Principle of on-chip free-flow magnetophoresis. A mixture of particles is introduced into a microfluidic chamber and deflected laterally by a magnetic field, allowing different particle types to exit the chip by different outlets.[358] b) Experimental particle trajectories of 4.5 μm and 2.0 μm magnetic particles, as well as non-magnetic particles, demonstrating their separation as they traverse the chamber.[313,358]**

The on-chip free-flow magnetophoresis microfluidic device featured a wide chamber into which a mixture of particles were introduced into the bottom corner (Fig. 30). A series of inlets allow the introduction of a buffer stream parallel to the sample stream, with the two streams flowing side-by-side due to laminar flow, and a series of outlets provides a number of potential exit points for the particles, as well as allowing the removal of sample and buffer waste. An inhomogeneous magnetic field was generated across the chamber, perpendicular to the direction of laminar flow, via an external permanent magnet. When a mixture of magnetic particles of different sizes and magnetic susceptibilities were introduced into the chamber, they were deflected from

the direction of flow by the magnetic field, traversing the chamber diagonally until they exited via one of the outlets. However, the different particle types deflected towards the magnet to different extents, such that the two particle populations exited through different outlets, thus achieving a continuous, simultaneous separation of two types of magnetic particles.

One issue with the original design of the magnetophoresis chip was that, rather than the particles of one type exiting through one outlet, they actually left the chamber via as many as four outlets which in some circumstances could result in lack of complete separation. Hence the design was altered such that the inlet and outlets were tapered, thus allowing "smoother" entry and exit of the liquids and particles into and out of the chamber, respectively. This enabled the complete separation of 2.8 μm and 4.5 μm magnetic particles, which each exited the chamber over only two outlets, and particle deflection was observed either via a microscope or by laser light scattering.[359] Pamme and Wilhelm also used the technique to separate magnetically labelled cells.[360] Mouse macrophages and HeLa (human ovarian tumour) cells were each incubated separately with magnetic nanoparticles, which were taken into the cells via the endocytosis pathway. The deflection behaviour of both cell types was observed separately by pumping them into the chamber and tracking them as they migrated towards the magnet, out of the sample stream, and demonstrated that the magnetically labelled species could be successfully deflected laterally. This was followed by the introduction of a mixture of magnetically labelled and unlabelled mouse macrophages, which were separated due to the deflection of the labelled species while the unlabelled species simply followed the laminar flow direction.

Thus, the technique of on-chip free-flow magnetophoresis has been demonstrated for the simultaneous separation of different magnetic particle types, and for the deflection

and separation of magnetically labelled cells. In addition, Al-Hetlani, Tarn and Pamme *et al.*[361,362] recently showed that aqueous based ferrofluid (magnetic nanoparticles suspended in a carrier solution with a surfactant stabiliser to stop particle agglomeration) droplets in a fluorocarbon oil based media could be continuously deflected across a magnetophoresis chamber, opening up new potential for the use of magnetic forces in the rapidly growing field of droplet microfluidics.[363,364] Zhang *et al.*[365] also demonstrated the deflection of aqueous droplets containing superparamagnetic $Fe_3O_4$ nanoparticles (synthesised in-house) in an oil continuous phase, showing how the magnetic droplets could be directed to different outlets when deflected across a microfluidic chamber.

Since the development of on-chip free-flow magnetophoresis, several devices have been presented for continuous flow magnetic particle and cell separations on a larger scale (i.e. dimensions of several millimetres or centimetres). Schneider and Zborowski *et al.*[366,367] developed a "dipole magnetic flow fractionator" that, like on-chip free-flow magnetophoresis, operated via the introduction of a particle stream alongside a buffer stream into a separation chamber. NdFeB magnets placed above and below the chamber caused the magnetic species to be deflected to different extents and collected via the different outlets by which they exited. The device was used to continuously sort magnetically labelled Jurkat cells into different outlets based on their antigen expression level (i.e. a higher expression level allows a greater number of magnetic particles to become bound to the cell, thereby increasing the deflection distance),[367] and later applied it similarly to the sorting of a stem and progenitor cell population based on their surface CD34 expression levels.[366] Espy and Carr *et al.*[368,369] fabricated a similar device that was orientated vertically, with the magnetic field provided by a quadrupole setup of permanent magnets, and applied it to the sorting of superparamagnetic and

ferromagnetic microparticles across 8 outlets, and later the sorting of superparamagnetic and non-magnetic microparticles across between 8 and 25 outlets.

### 1.4.5 On-chip diamagnetic repulsion

The weak repulsion of diamagnetic objects from high magnetic field gradients is described in Section 1.4.1. However, when the diamagnetic materials are suspended in a paramagnetic medium (e.g. aqueous manganese (II) chloride solution, pressurised oxygen etc.), the repulsive effect from the magnetic field becomes larger due to the attractive force of the paramagnetic species towards the magnet. This phenomenon is known as the magneto-Archimedes effect,[370] or magnetic buoyancy.[125] While diamagnetic repulsion is usually only achievable to any noticeable degree when using high magnetic fields, such as those provided by a superconducting magnet, the magneto-Archimedes effect allows the repulsion to be achieved on a much smaller scale. As a result, diamagnetic repulsion has been of interest in recent years for the manipulation of objects via magnetic fields on a small scale, without the need for prior labelling of the objects with magnetic species.[313]

Kimura *et al.*[129,130] demonstrated the micropatterning of cells and particles suspended in aqueous paramagnetic solutions. The suspensions were placed atop a magnetic field modulator constructed from alternating layers of iron and aluminium, and application of the 1 T magnetic field (via two electromagnets) caused the particles and cells to migrate, forming periodic lines above the iron layers where the field was weakest. Winkleman *et al.*[128] investigated the behaviour of single cells in a paramagnetic solution of gadolinium (III) diethylenetriaminepentaacetic acid (Gd-DTPA), a biologically benign medium, used as an MRI (Magnetic Resonance Imaging) contrast agent. The

cells were trapped in a region of low magnetic field between two permanent magnets with their like poles facing each other. The same group also demonstrated the density-based separation of diamagnetic materials[371] in a similar fashion as previously presented using superconducting magnets.[370] They instead used permanent magnets with their like poles facing, placed above and below a cylinder in which the diamagnetic materials were suspended in paramagnetic solution, allowing the materials to levitate at different heights depending on their respective densities.[371] This work has since been adapted for the density-based determination of atomic-level differences in polymer compositions and chemical assay monitoring on diamagnetic particles,[372,373] density measurements of several solids and liquids,[374] and the characterisation of food and water samples.[375]

The above examples showed how the phenomenon of diamagnetic repulsion could be exploited with the use of electromagnets and conventional rare earth permanent magnets, rather than the bulky and expensive superconducting magnets used previously. Recently, diamagnetic repulsion has also been applied to microfluidic systems, allowing fine control over the movements of objects and enabling magnets to be situated closer to the regions of interest. Winkleman *et al.*[371] developed a microfluidic device based on their density-based diamagnetic separation method described above. Here, particles of differing densities were suspended in gadolinium (III) chloride solution ($GdCl_3$) and constantly introduced into a vertically orientated chamber that was positioned between two permanent magnets with their like poles facing. As the particles entered the chamber the more dense particles migrated along a plane lower than that of less dense particles, allowing the continuous flow fractionation and collection of different particles from a series of outlets at the end of the chamber (Fig. 31).

Watarai *et al.*[125-127] positioned NdFeB magnets around a capillary to trap particles and blood cells from flow, due to their inability to pass through the region of magnetic field.

As the flow rate was increased some of the particles/cells would escape the field, hence it was suggested that the system could be used to fractionate biological materials depending on their size and susceptibility. Additionally, the same group employed a similar system in which a capillary was placed in a superconducting magnet, allowing flowing particles to migrate back and forth across the width of the chamber as they passed through the magnet.[376]
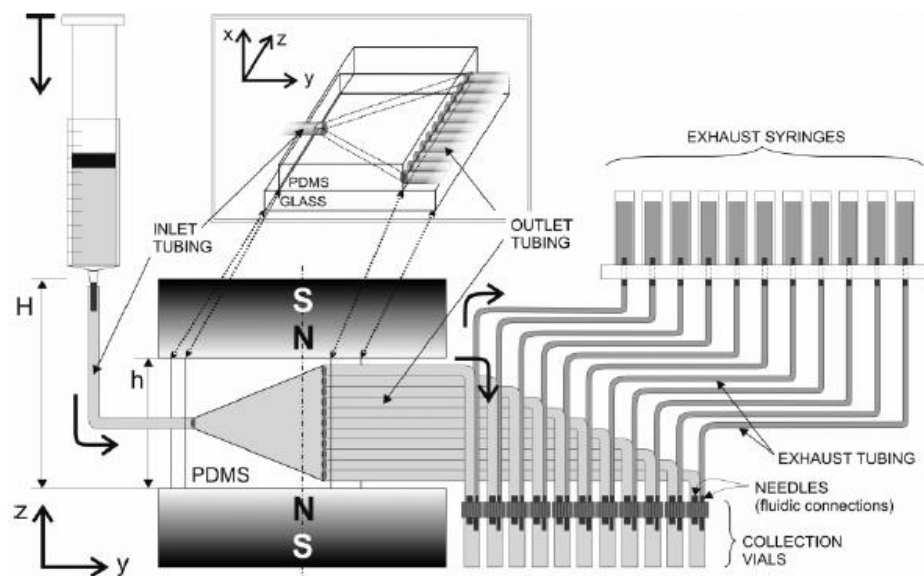


**Fig. 31 Density based continuous flow separation of diamagnetic polystyrene particles suspended in a paramagnetic medium (GdCl₃). Particles were pumped through a vertical microfluidic chamber between two permanent magnets with like poles facing, causing the particles to levitate at different heights as they traversed the chamber, allowing their collection at different outlets.**

Han and Frazier[346,349] developed a diamagnetic capture (DMC) mode microseparator in which a ferromagnetic wire integrated in a microfluidic chip was used to separate white blood cells (diamagnetic) and red blood cells (paramagnetic when deoxygenated) in

whole blood when exposed to a magnetic field (Fig. 29b). The white blood cells were repelled towards areas of low field around the wire, while the red blood cells migrated towards the outer edges of the chip, thereby allowing separation. However, the actual extent of migration of white blood cells was not commented upon, and so the separation may have mainly relied on the movement of the red blood cells. Furlani[377] also prepared a method, albeit theoretical, for the continuous separation of white and red blood cells in plasma via a microfluidic device containing permalloy elements.

Kang *et al.*[378] developed an "isomagnetophoresis" system (akin to isoelectrophoresis) in which a concentration gradient of Gd-DTPA was generated across a microfluidic chamber, creating a magnetic susceptibility gradient. Diamagnetic particles of differing magnetic susceptibility were then separated as they flowed through the chamber under a magnetic field, with each type migrating to the region where the difference between the magnetic susceptibility of the particle and the medium ($\Delta\chi$) was zero (see Section 1.4.6). Chetouani *et al.*[379] used diamagnetic levitation to guide microparticles and microdroplets along magnetic grooves without contacting the surface, and also to trap particles in magnetic wells. This work was expanded upon by Kauffmann *et al.*,[380] who levitated particles by diamagnetic repulsion and moved them via dielectrophoresis and magnetophoresis, allowing them to be positioned along linear magnetostatic traps.

Thus, the use of diamagnetic repulsion in microfluidics offers numerous applications, though most commonly involving the separation of cells and particles based on their intrinsic properties, without the need for magnetic labelling. However, it is somewhat more challenging to generate the same forces as those achievable by magnetic attraction, since diamagnetic repulsion is a weak force.

## 1.4.6    Theory of magnetic deflection of particles in flow

The magnetophoretic movement of magnetic particles through a fluid is a vital component of all of the examples of magnetically actuated continuous flow processes detailed in the last three sections, whether the migration of the particles was due to attractive or repulsive forces.  All of the experimental work described in this thesis utilises these same forces, and therefore these forces and their effect on continuous flow procedures will be described here.

Firstly, the magnetic force, $\mathbf{F_{mag}}$ (N), acting on a point-like magnetic dipole moment (such as that of a superparamagnetic microparticle), $\mathbf{m_d}$ (A m$^2$), in a field with magnetic flux density, $\mathbf{B}$, can be described by Equation 23:[252,255,337,381]

$$\mathbf{F_{mag}} \;=\; (\mathbf{m_d} \cdot \nabla)\mathbf{B} \hspace{3cm} \textbf{Equation 23}$$

where $\nabla$ = the del operator (m$^{-1}$), also known as the vector differential operator, which can be used to describe various properties of vector fields in three-dimensional space using the Cartesian coordinate system (*x*, *y*, and *z*-axis).  In this case it is used to describe the gradient of the magnetic flux density, and is written as $\nabla\mathbf{B}$ (T m$^{-1}$).

Thus, it can be seen that the force is dependent on both the magnetic dipole moment ($\mathbf{m_d}$) and the gradient of the magnetic flux density ($\nabla\mathbf{B}$).  Therefore, it is important to note that in order to cause a particle to migrate towards a magnet, the field must be inhomogeneous, meaning that it must have a gradient.  If no gradient exists then the field is homogeneous, and the dipole (particle) would experience no force. Inhomogeneous fields are used in applications such as nuclear magnetic resonance (NMR) analysis, and are achieved by the use of large magnets with respect to the size of the sample.[313]

As described in Section 1.4.1, $\mathbf{m_d}$ is related to the volume of magnetisable material ($V_m$) and its magnetisation ($\mathbf{M}$), and $\mathbf{M}$ in turn is related to the magnetic susceptibility of the dipole ($\chi$) and the external magnetic field ($\mathbf{H}$) as per Equation 22. However, when a superparamagnetic particle is suspended in a media, the magnetisation can be calculated using Equation 24:

$$\mathbf{M} = \Delta\chi \; \mathbf{H} \qquad\qquad \textbf{Equation 24}$$

where $\Delta\chi$ = the *effective* magnetic susceptibility of the particle, and is the difference between the susceptibility of the particle ($\chi_p$) and the susceptibility of the media ($\chi_m$), hence $\Delta\chi = \chi_p - \chi_m$. Additionally, since $\mathbf{B}$ is related to $\mathbf{H}$ via the permeability of free space ($\mu_0$), as shown by Equation 17, the force on a magnetic particle ($\mathbf{F_{mag}}$) can be determined by the combination of Equations 17, 20, 23, and 24 to give Equation 25:

$$\mathbf{F_{mag}} = \frac{\Delta\chi \; V_m \; (\mathbf{B}\cdot\nabla)\mathbf{B}}{\mu_0} \qquad\qquad \textbf{Equation 25}$$

Hence, the force on a magnetic particle ($\mathbf{F_{mag}}$) is dependent on the effective susceptibility of the particle ($\Delta\chi$), the volume of magnetisable material ($V_m$), the magnetic flux density ($\mathbf{B}$) and its gradient ($\nabla\mathbf{B}$), and the permeability of free space ($\mu_0$). However, this equation only holds true when the field is strong enough that the magnetisation of the particle reaches saturation ($\mathbf{M_s}$), while Shevkoplyas *et al.*[382] have developed an equation for the magnetic force on a particle that has not reached saturation.
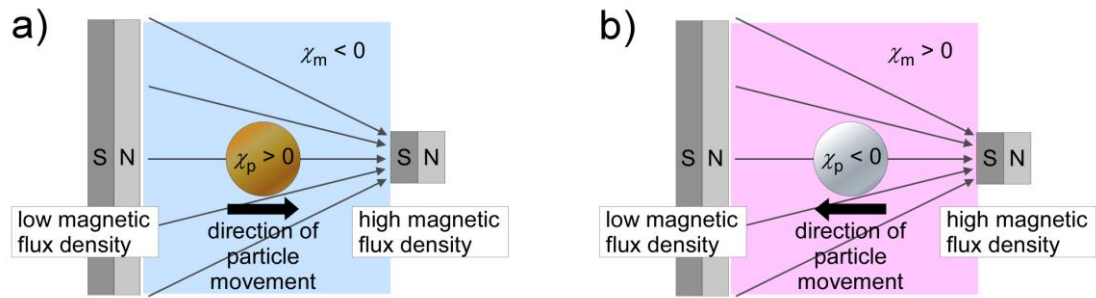
**Fig. 32  a) Attraction of a magnetic particle to a region of high magnetic field when the magnetic susceptibility of the particle is greater than that of the media.  b) Repulsion of a diamagnetic particle from a region of high field when the magnetic susceptibility of the particle is lower than that of the medium.**

Additionally, it should be noted that while this equation is typically used for the calculation of forces on magnetic particles, it can also be applied to magnetic forces on diamagnetic particles.  If the particle is superparamagnetic ($\chi > 0$) and the surrounding media is diamagnetic ($\chi < 0$), then the resultant $\Delta\chi$ is positive and the particle migrates towards regions of high magnetic fields, i.e. magnetic attraction (Fig. 32a).  However, if the particle is diamagnetic ($\chi < 0$) and the media is paramagnetic ($\chi > 0$), then $\Delta\chi$ becomes negative, and the particle would be repelled from regions of high field, i.e. diamagnetic repulsion (Fig. 32b).  It can also be seen that, by altering the constituents of the particle and media, $\Delta\chi$ can be manipulated such that paramagnetic particles could be repelled in paramagnetic media of higher susceptibility, while diamagnetic particles could be "attracted" towards a magnetic field when suspended in a media of lower susceptibility.

However, as a particle migrates through a media due to its attraction towards a magnetic field (assuming a superparamagnetic particle in a diamagnetic medium such as water), it

experiences an equal but opposite viscous drag force ($\mathbf{F}_{vis}$), as described in Section 1.2.2. It can be explained again here, albeit in terms of the magnetically induced velocity of the particle, $\mathbf{u}_{mag}$ (m s$^{-1}$), its radius, $r$ (m), and the viscosity of the medium, $\eta$ (kg m$^{-1}$ s$^{-1}$), as shown by Equation 26:[358,383]

$$\mathbf{F}_{vis} = 6\,\pi\,\eta\,r\,\mathbf{u}_{mag} \qquad \textbf{Equation 26}$$

Since $\mathbf{F}_{mag} = \mathbf{F}_{vis}$, Equation 25 can be rearranged to give the value of the magnetically induced velocity of the particle ($\mathbf{u}_{mag}$) towards the region of high field (Equation 27):

$$\mathbf{u}_{mag} = \frac{\mathbf{F}_{mag}}{6\pi\eta r} = \frac{\Delta\chi\,V_m\,(\mathbf{B}\cdot\nabla)\mathbf{B}/\mu_0}{6\,\pi\,\eta\,r} \qquad \textbf{Equation 27}$$

Hence, Equations 25 and 27 can be applied to the deflection of magnetic particles in the y-direction across an on-chip free-flow magnetophoresis chamber. However, an additional consideration when deflecting particles in microfluidic devices is that the particles experience a drag effect caused by the surfaces of the channels, which can be estimated by the viscous drag coefficient ($C_W$) due to the top and bottom surfaces of the chip as shown in Equation 28:[376,384,385]

$$C_W = [\,1 - 1.004(r/h_z) + 0.418(r/h_z)^3 + 0.21(r/h_z)^4 - 0.169(r/h_z)^5\,]^{-1} \qquad \textbf{Equation 28}$$

where $r$ = the particle radius (m), and $h_z$ = the distance halfway between the top and bottom surfaces of the chip. Thus, Equations 26 and 27 can be subtly altered to describe the $\mathbf{F}_{vis}$ and $\mathbf{u}_{mag}$ of a particle in a microfluidic device to give Equations 29 and 30, respectively:

$$\mathbf{F}_{vis} = 6\,\pi\,\eta\,r\,\mathbf{u}_{mag}\,C_W \qquad \textbf{Equation 29}$$

$$\mathbf{u_{mag}} = \frac{\mathbf{F_{mag}}}{6\pi\eta r C_W} = \frac{(\chi_p - \chi_m)\, V_m\, (\mathbf{B}\cdot\nabla)\mathbf{B}/\mu_0}{6\,\pi\,\eta\,r\,C_W}$$

**Equation 30**

In an on-chip free-flow magnetophoresis device, the particles also have a velocity in the x-direction due to the applied hydrodynamic flow, $\mathbf{u_{hyd}}$ (m s$^{-1}$), as shown in the schematic of the setup in Fig. 33. Thus, the particles have velocities in both the x-direction and y-direction, and the resultant deflection velocity, $\mathbf{u_{defl}}$ (m s$^{-1}$), is the sum of both $\mathbf{u_{mag}}$ and $\mathbf{u_{hyd}}$, as shown in Equation 31:

$$\mathbf{u_{defl}} = \mathbf{u_{mag}} + \mathbf{u_{hyd}}$$

**Equation 31**

Therefore, if the applied hydrodynamic flow rate ($\mathbf{u_{hyd}}$) is kept constant, the extent of deflection ($\mathbf{u_{defl}}$) depends only on the magnetically induced velocity ($\mathbf{u_{mag}}$). In turn, if the magnetic field properties (($\mathbf{B}\cdot\nabla)\mathbf{B}$) and the susceptibility of the medium ($\chi_m$) are kept constant, the deflection of the particles therefore depends on their size ($r$), magnetic susceptibility ($\chi_p$), and volume of magnetisable material ($V_m$), as well as the viscosity of the medium ($\eta$), according to Equations 27 and 30.

The differences in the properties of the particles alters the magnetic forces acting on them, resulting in different deflection velocities that allows their separation in an on-chip free-flow magnetophoresis device. Additionally, it has been described that the same forces and effects apply to the diamagnetic repulsion of particles, provided $\Delta\chi < 0$. It is also worth noting that the deflection velocities of magnetic particles have been modelled using simulation software, utilising the equations described here to allow visualisation of expected particle trajectories in continuous flow.[386,387]
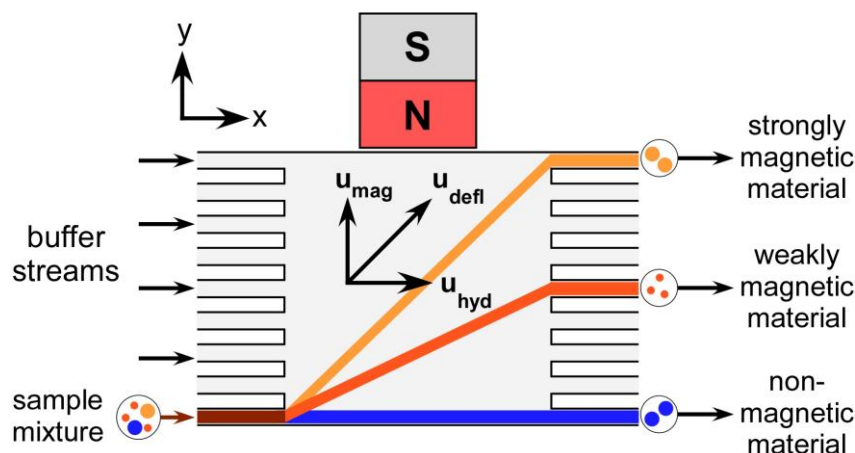
**Fig. 33   Principle of on-chip free-flow magnetophoresis, showing how the deflection velocity ($u_{defl}$) is the summation of the magnetically induced velocity of the particle ($u_{mag}$) in the y-direction, and the hydrodynamic velocity ($u_{hyd}$) in the x-direction.   When $u_{hyd}$ is kept constant, differences in deflection depends only on the $u_{mag}$ of the particles, allowing different particles to be deflected to varying extents and resulting in their separation.**

## *1.5     On-chip continuous flow reactions on mobile particles*

Multiple laminar flow streams have been generated across microfluidic chambers that can be utilised to perform reactions and studies on species by exposing them to different reagents in each stream.   Takayama and Whiteside *et al*.,[388] in 2001, used the laminar flow regime of microfluidic devices to perform the interrogation of a single bovine capillary endothelial cell trapped in a microfluidic channel (Fig. 34).   Three laminar flow solutions containing different labelling dyes were pumped simultaneously over different areas of the trapped cell and the effects on the labelled mitochondria inside the cell were studied for several hours.
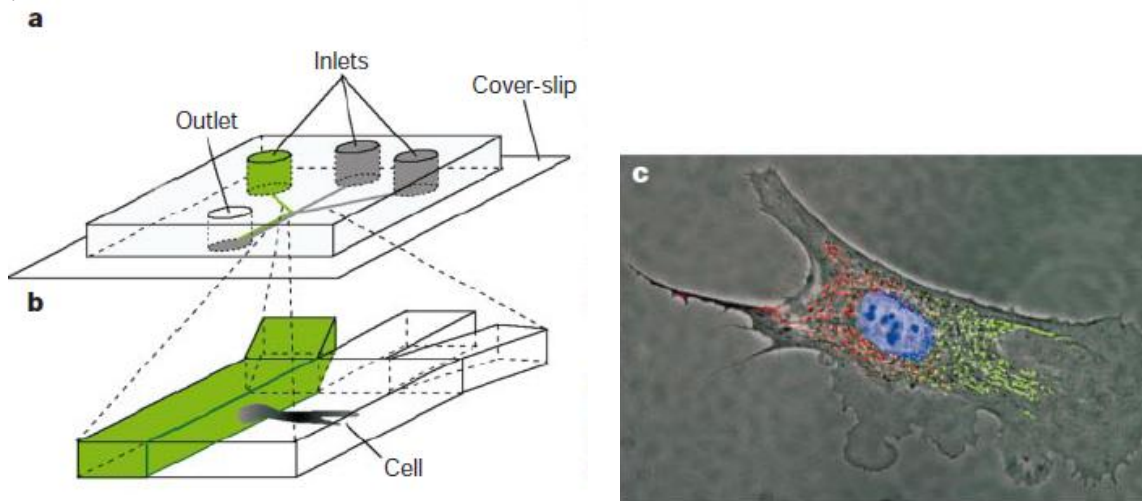
**Fig. 34 a,b) Laminar flow streams containing various dyes were pumped over different sections of a trapped cell. c) The mitochondria inside the cell were labelled, and their movement from each exposed region were examined over several hours.[388]**

Seger and Renaud *et al.*[389] developed a similar method in which cells were captured by a negative dielectrophoresis (nDEP) trap in the middle of a chamber. Two laminar flow streams were generated containing buffer solution and dye, respectively. By altering the pressure at each inlet, the cells were exposed to the dye by increasing its flow rate and allowing it to cross most of the chamber, before decreasing the flow rate again such that the cells were washed with the buffer stream (Fig. 35). This technique of "shifting" the laminar streams was also applied by Boer and Renaud *et al.*,[390] and by Eriksson *et al.*,[391] who each used optical trapping rather than DEP forces. Eriksson *et al.*[392] developed the technique further by maintaining the laminar flow rates, and moving an optically trapped cell back and forth between two streams of differing salt concentration to study the effect of the resultant osmotic shock.
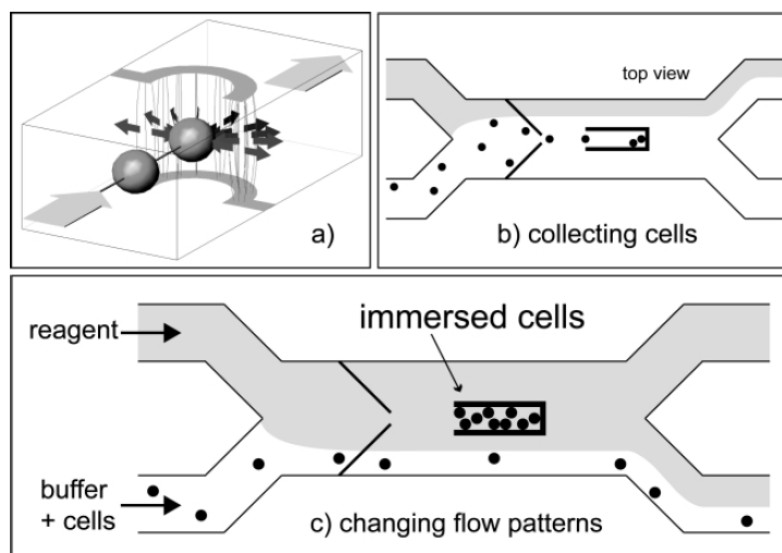
**Fig. 35 Principle of particle and cell immersion by a laminar flow reagent stream.[389] a,b) Particles or cells are trapped by dielectrophoretic forces. c) The reagent stream is shifted by increasing its flow rate, thus immersing the trapped object. The technique has also been performed using optical forces.[390,391]**

None of these examples were actually continuous flow processes since they required the trapping of particles or cells, hence they were actually batch processes, but they nonetheless laid the foundations for later continuous methods. Recent multiple laminar flow based methods have involved maintaining stable streamlines, and directing particles or cells through each of the streams in continuous flow, allowing reactions to occur on their surfaces as they pass through a reagent stream. In 2004, Seger and Renaud *et al*. [393] demonstrated the use of dielectrophoretic barriers to "dip" cells into and out of a reagent stream (Fig. 36). However, the "reagent" stream did not contain any actual reagents with which to study or perform reactions on the cells, and instead they simply contained a dye with which the coflowing streams could be visualised. The setup also required two arrays of electrodes to be integrated into the device, and there was also "*considerable*" diffusion of the dye across the microfluidic chamber.
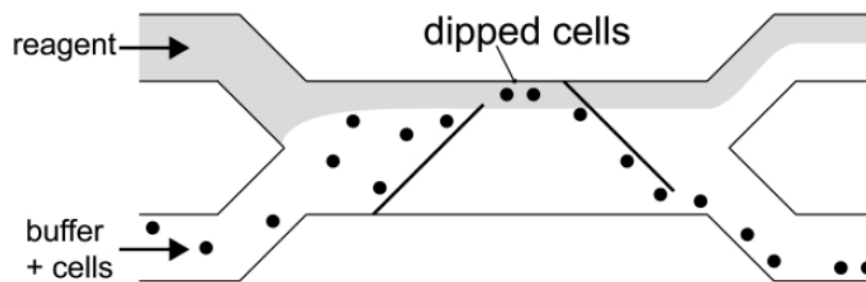
**Fig. 36 Principle of continuous flow cell dipping. Cells in a buffer stream are directed into a reagent stream via dielectrophoretic forces generated by integrated electrodes, before being diverted back into the buffer stream by a second set of electrodes.**[389]

In 2008, Peyman *et al*., of Dr Nicole Pamme's research group, developed a microfluidic platform for performing rapid reactions and assays on the surfaces of functionalised magnetic microparticles in continuous flow, by deflecting them through streams of reagent.[394] The system was derived from the free-flow magnetophoresis methods described previously (Section 1.4.3),[358,360,383,395] albeit with multiple inlet channels that allowed the generation of alternating laminar flow streams of reagents and buffer solutions across the microfluidic chamber. By introducing magnetic particles into the stream at the bottom edge of the chamber, particles could be deflected via a permanent magnet placed at the opposite side of the chamber such that they crossed each of the reagent and buffer streams. With the correct choice of functional groups on the particle surface, the particles act as mobile solid supports on which consecutive reactions occur as they pass from one reagent stream to the next. The principle of this "multilaminar flow" approach is shown in Fig. 37, which illustrates the mechanism for performing a typical sandwich immunoassay on appropriately functionalised magnetic particles.
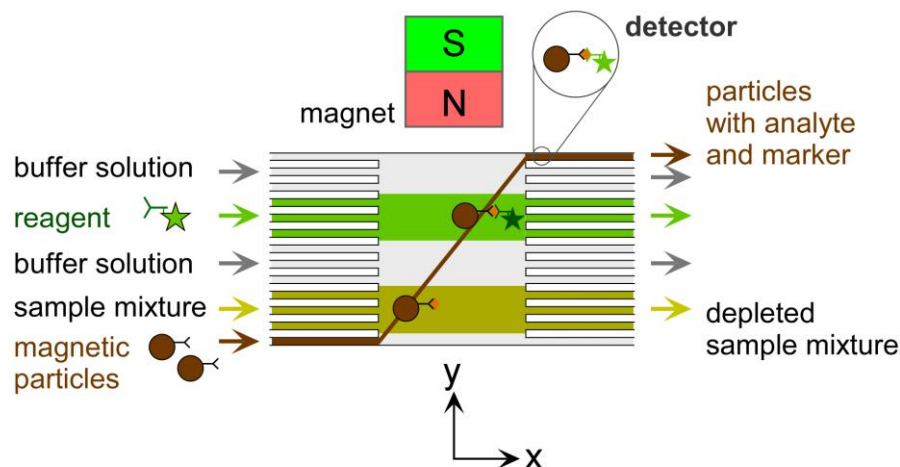
**Fig. 37 Principle of the multilaminar flow platform. Alternating reagent and buffer streams are generated across a microfluidic chamber and functionalised magnetic particles are deflected through each stream, allowing multiple consecutive reactions to occur on the particle surfaces.[394]**

The initial experiments involved a proof-of-principle study in which streptavidin coated particles were deflected out of the buffer solution in which they were suspended, through a single stream of fluorescently labelled biotin solution, and into a final washing buffer stream. Fluorescence analysis of the particles showed a significant increase in fluorescence after they passed through the reagent stream. This indicated that the biotin had become successfully bound to the streptavidin coated particles in an exposure time of only 15 seconds, a large reduction in processing time compared to the >20 min times required by batch microfluidic methods. Thus, the system demonstrated a continuous flow approach for performing rapid processes on magnetic particles, requiring only a simple setup of a syringe pump and a permanent magnet. Although this was only a first test of the system, it showed potential for performing a number of assays and reactions due to the variety of magnetic particle functionalisations available.

Since the publication of this technique by Peyman, and after the start of the multilaminar flow experiments described in this thesis, there have been many similar multilaminar flow devices reported. Around the same time that Peyman's work was published, Tornay and Renaud *et al*.[396] presented an updated version of the cell dipping method described previously.[389] Here, dielectrophoresis was used to deflect particles into a stream of fluorescent labelling solution. The particles then traversed a long channel to a separate chamber, where they were deflected back out of the reagent stream into a fresh buffer stream. With the presence of two chambers the technique was rather complex compared to the platform developed by Peyman,[394] in which the entire reaction process occurred in a single chamber. Later, the design was altered such that only a single, wide chamber was present,[35] although this design required the placement of electrodes across the chip.

Another type of multiflow method was developed later by Morton *et al*.,[397] using their deterministic lateral displacement method described previously (Section 1.3.2).[150,155] The device was first used to deflect 3 μm particles through a stream of 0.5 μm fluorescent particles that were too small to have their overall trajectories affected by the posts. Next, blood platelets were deflected across a stream of labelling dye, thereby rendering the platelets fluorescent (Fig. 38). Finally, *E. coli* cells were deflected through a cell lysis solution, where they were lysed and their components separated. This device allowed accurate control over the path of the cells and particles, but required careful calculations regarding the object sizes and post array geometry.
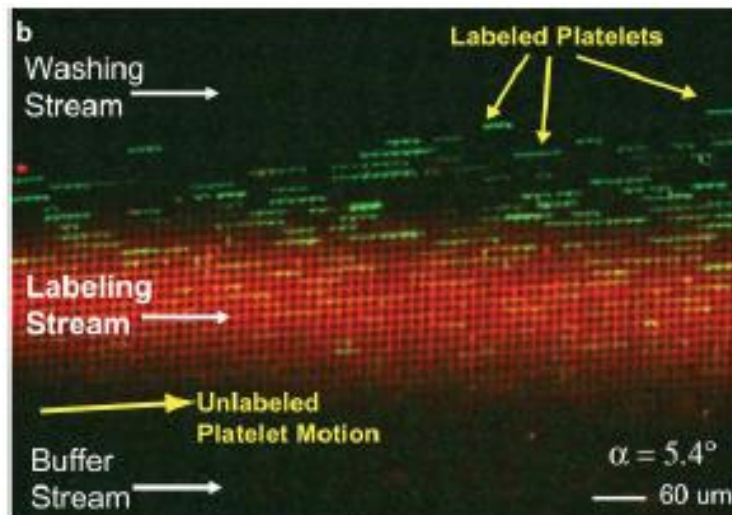
**Fig. 38 Continuous flow processing via deterministic lateral displacement. Blood platelets were deflected across a stream of labelling solution via a series of microposts, whereupon they were fluorescently tagged.[397]**

Augustsson *et al*.[398] developed a system consisting of a main channel along which particles were pumped, with many side channels introducing different buffer solution. As the particles traversed the channel they were deflected by acoustic forces towards the centre, such that they entered a new buffer solution rather than being carried out of a waste channel, thus performing a "buffer medium exchange" of the particles. The procedure was also applied to the washing of red blood cells from diluted whole blood.

Kim *et al*.[393] used biomolecular motors to transport microtubules laterally through a reagent stream, whereupon the microtubules were labelled with analyte and collected after passing through a washing buffer stream.

There have also been several magnetic particle based continuous flow processes reported very recently. Ganguly *et al*.,[399] in 2010, developed their own multilaminar flow system utilising magnetophoresis, in which streptavidin coated magnetic particles were deflected through a stream of biotinylated, fluorescently labelled oligonucleotide

reagent. After crossing the stream, the particles exhibited an increase in fluorescence which indicated successful binding. However, after the reaction, the particles were simply pulled to the side wall of the channel near the magnet and collected there, which meant the particles aggregated over time and in a real analysis scenario would give varying fluorescence intensity results depending on the point in time at which the particle plug was analysed. Additionally, photographs showed a very high degree of diffusion of the reagent stream, even diffusing as far as the outer edges of the particle plug which would give false results. The extent of diffusion may be due to low flow rates needed to deflect the Micromer-M particles across the channel, which have previously been shown to be less responsive in microfluidic systems than the Dynabeads used by Peyman *et al.*.[394,395]

Sasso *et al.*[400] generated streams of buffer and fluorescently labelled biotin solutions along a microchannel. Streptavidin functionalised magnetic particles were introduced and deflected towards the sidewall, into the biotin stream where they were labelled. At the end of the channel, the particles were deflected back into the buffer solution. The same technique was also used to perform an immunoassay of C3a antigen, which also included deflection of the particles into and out of a second reagent stream for fluorescent labelling of the captured antigen. The authors stated the advantages of this method were that the particles could be retained in the reagent stream for as long as required, thereby increasing the residence time of the particles, but it should be noted that to increase the number of possible multistep reactions on the particles the channel would need to be significantly lengthened, leading to an increase in backpressure. Great care would also be needed to ensure that no reagent from one stream was able to migrate further down the channel where it could contaminate the next reagent stream. Additionally, the method relied on particles rolling along the sidewall of the channel when in the reagent stream. Although acceptable for the assays reported, this may limit

the system since a number of procedures might involve the use species that cause particles to stick to the surface it is trying to roll against.

Karle *et al*.[401] developed a "phase transfer magnetophoresis" device in which magnetic particles featuring *E. coli* DNA bound to their surfaces were deflected consecutively into a washing buffer stream and then into an elution buffer stream to remove the DNA from the particle surfaces (Fig. 39). However, rather than a simple wide chamber as seen in previous examples, the system featured several spiral channels that intersected each other at various points, and the magnetic field was provided by a rotating permanent magnet to reduce agglomeration of particles against the sidewall.
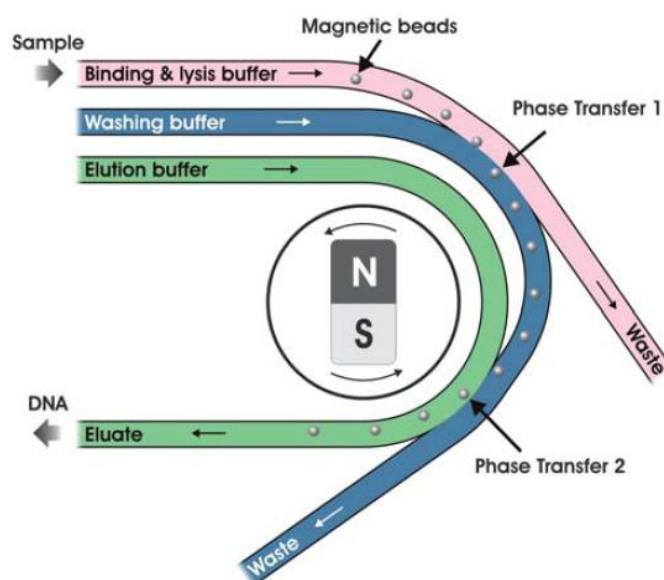


**Fig. 39 Schematic of the phase transfer magnetophoresis device for continuous DNA extraction. A rotating magnet was used to deflect particles featuring surface-bound DNA into consecutive washing and elution streams.[401]**

Continuous flow reactions and assays potentially allow a number of processes to be performed in rapid times and with reduced reagent consumption and waste production,

by deflecting particles through multiple streams of reagents and buffer solutions. However, many of the techniques described were not applied to any particularly useable situations, instead mostly involving proof-of-principle assays. Techniques involving dielectrophoresis[35,389,396] require complex electrodes to be integrated into the microfluidic device which, as well as complicating the fabrication procedure, means that the positions of the electrodes cannot be changed post-fabrication should different types of studies be desired. The deterministic lateral displacement[397] method suffers from a similar problem, since the geometries of the micropost arrays must be tailored for specific scenarios due to the critical size factors of the particles and cells to be deflected.

Additionally, the magnetophoresis method of Ganguly *et al.*[399] had the drawback that the particles were simply drawn to the side of the microchannel, which resulted in the formation of a plug that actually interacted with the reagent stream once it had gotten too big. The system developed by Sasso *et al.*[400] allowed deflection into and out of a reagent stream, but the addition of further reagent streams would result in longer channels with increased backpressure, and the risk of contamination between reagent streams if each reagent was not *completely* removed from the system after its use. The acoustophoresis method of Augustsson *et al.*[398] suffered from similar potential problems, as well as being limited by the position of the nodes and anti-nodes across the channel in terms of adapting the device further.

The magnetophoresis based method originally demonstrated by Peyman *et al.*[394] represented a simple setup that could potentially be applied to a range of biological assays and chemical reactions. The use of permanent magnets allows numerous sizes, types and positions to be utilised quickly and easily, and enables fast optimisation of the magnetic particle deflection even when changing other system parameters (e.g. flow

rate). The continuous deflection through a reagent stream potentially enables reproducible results on a particle-by-particle basis without the formation of plugs, and more reagent streams could be added by simply having more inlet and outlet channels, and without increasing the backpressure of the system. However, this device, as with all of the others described, had only been demonstrated for proof-of-principle experiments at the point when the PhD project described in this thesis was started.

## *1.6    Aims of the PhD project*

The aim of this project was to investigate the use of microparticles as mobile solid supports for performing a variety of microfluidic processes in continuous flow. Firstly, the effect of temperature on the deflection of magnetic particles and their separation by on-chip free-flow magnetophoresis was studied. Next, a series of investigations were undertaken to determine the potential of the multilaminar flow system developed by Peyman *et al*.[394] for performing continuous flow procedures on magnetic particles that would usually require long processing times. These included chemical reactions, the deposition of coatings onto particles, and sandwich immunoassays. In addition, the use of diamagnetic repulsion for performing similar types of procedures to those described above were investigated to determine whether it is feasible to perform such continuous processes on "non-magnetic" particles, with a view to the use of unlabelled biological cells in their place in the future.

The work performed throughout the PhD will be split into different sections in this thesis. Firstly, the materials and methods used will be detailed in the **Experimental** chapter. This will be followed by several **Results** chapters, which will be broken into two main sections describing those experiments performed using *magnetic attraction*,

followed by those performed using *diamagnetic repulsion*. A **Conclusions** chapter will summarise the work performed and present recommendations for the future of the work. **References** will then be listed, followed by an **Appendix** containing publications related to the work described here.

# 2 Experimental

This chapter describes the experimental setup and procedures utilised for the work in this thesis, detailing (2.1) the chemicals and particle suspensions employed, (2.2) the design of the microfluidic chips, (2.3) their fabrication, (2.4) treatment of the glass surfaces, (2.5) on-chip free-flow magnetophoresis experiments, (2.6–2.10) multilaminar flow procedures, and (2.11) diamagnetic repulsion studies.

## *2.1 Chemicals and particle suspensions*

### 2.1.1 Chemicals

Solid and liquid chemicals were purchased from the distributors shown in Table 4. Aqueous solutions were prepared in double-filtered (0.05 μm) water with a resistivity of 18.2 MΩ cm at 25 °C, obtained from an ELGA Option 4 that fed into an ELGA UHG PS water purification system (both devices from ELGA Process Water, Marlow Buckinghamshire, UK), unless otherwise stated. Prepared solutions were filtered through 0.20 μm syringe filters (Whatman, VWR, Lutterworth, Leicestershire, UK) prior to introduction into microfluidic devices. All chemicals were of analytical grade.

**Table 4  Chemicals, solvents and reagents used in chip fabrication and experiments.**

| Chemical | Supplier |
|---|---|
| *Solvents* | |
| Acetone | Fisher Scientific, Leicestershire, UK |
| Acetonitrile | Fisher Scientific, Leicestershire, UK |
| Chloroform | Fisher Scientific, Leicestershire, UK |
| Cyclohexane | Fisher Scientific, Leicestershire, UK |

| | |
|---|---|
| Ethanol | Fisher Scientific, Leicestershire, UK; Wako Pure Chemicals, Ibaraki, Japan |
| Hexadecane (anhydrous, 99+ %) | Sigma-Aldrich, Dorset, UK |
| Hexane | Fisher Scientific, Leicestershire, UK |
| Methanol | Fisher Scientific, Leicestershire, UK |
| Propan-2-ol | Fisher Scientific, Leicestershire, UK |
| Toluene | Fisher Scientific, Leicestershire, UK |
| 2,2,4-Trimethylpentane [*isooctane*] | Fisher Scientific, Leicestershire, UK |
| *Acids and bases* | |
| Boric acid (99+ %) | Sigma-Aldrich, Dorset, UK |
| Hydrochloric acid (36 %) | Fisher Scientific, Leicestershire, UK |
| Hydrofluoric acid (48 %) | Sigma-Aldrich, Dorset, UK |
| 2-(*N*-Morpholino) ethanesulfonic acid [*MES*] | Sigma-Aldrich, Dorset, UK |
| Phosphoric acid (85 %) | Fisher Scientific, Leicestershire, UK |
| Potassium hydroxide pellets, AnalaR | BDH (VWR), Leicester, UK |
| Sodium hydroxide pellets, analyt. grade | BDH (VWR), Leicester, UK |
| Sulphuric acid (98 %) | Fisher Scientific, Leicestershire, UK |
| *Buffers and salts* | |
| Glycine | Fluka, Dorset, UK |
| Phosphate buffered saline tablets [*PBS*] | Gibco (Invitrogen), Paisley, UK |
| Sodium bicarbonate | Sigma-Aldrich, Dorset, UK |
| Sodium chloride | Fluka, Dorset, UK |
| Sodium phosphate (98 %) | Sigma-Aldrich, Dorset, UK |
| *Surface treatments and silanising agents* | |
| Agarose (low melting point) | Sigma-Aldrich, Dorset, UK |
| (3-Aminopropyl)triethoxysilane [*APTES*] | Sigma-Aldrich, Dorset, UK |
| Dimethyloctadecyl[3-(trimethoxysilyl)-propyl]ammonium chloride (42 % wt. in MeOH) [*QAS*] | Sigma-Aldrich, Dorset, UK |
| Methoxypolyethylene glycol 5,000 propionic acid *N*-succinimidyl ester [*PEG-SPA*] | Sigma-Aldrich, Dorset, UK |
| 2-[Methoxy(polyethyleneoxy)propyl] trimethoxysilane [*PEG-silane*] | Fluorochem Ltd., Derbyshire, UK |
| Octadecyltrichlorosilane [*OTS*] | Sigma-Aldrich, Dorset, UK |
| Trichloro(1*H*,1*H*, 2*H*,2*H*-perfluorooctyl)silane [*FDTS*] | Sigma-Aldrich, Dorset, UK |
| 5,6-Carboxyfluorescein | Sigma-Aldrich, Dorset, UK |
| *Photolithography and wet etching* | |
| Ammonium fluoride (40 %) | Fisher Scientific, Leicestershire, UK |

| | |
|---|---|
| Chrome Etch 18 | Chestech Ltd., Warwickshire, UK |
| Hydrogen peroxide (30 % w/v) | Fisher Scientific, Leicestershire, UK |
| Microposit 351 Developer | Chestech Ltd., Warwickshire, UK |
| Microposit Developer Concentrate | Chestech Ltd., Warwickshire, UK |
| *Surfactants and additives* | |
| Bovine serum albumin [*BSA*] | Sigma-Aldrich, Dorset, UK |
| Hexadecyltrimethylammonium bromide [*CTAB*] | Sigma-Aldrich, Dorset, UK |
| Sodium dodecyl sulphate [*SDS*] | Wako Pure Chemicals, Ibaraki, Japan |
| Tween20 (polysorbate 20) | Sigma-Aldrich, Dorset, UK |
| *Fluorescamine reaction* | |
| Fluorescamine | Sigma-Aldrich, Dorset, UK |
| *Amide bond synthesis* | |
| Fluoresceinyl glycine amide [*FGA*] | Sigma-Aldrich, Dorset, UK |
| (*N*-(3-Dimethylaminopropyl)-*N'*-ethylcarbodiimide hydrochloride [*EDC*] | Sigma-Aldrich, Dorset, UK |
| *Polyelectrolyte deposition* | |
| Poly(allylamine hydrochloride) [*PAH*] | Sigma-Aldrich, Dorset, UK |
| Poly(fluorescein isothiocyanate allylamine hydrochloride) [*PAH-FITC*] | Sigma-Aldrich, Dorset, UK |
| Poly(4-styrenesulfonic acid) (18 wt%) [*PSS*] | Sigma-Aldrich, Dorset, UK |
| *C-reactive protein immunoassay* | |
| Biotinylated monoclonal mouse anti-human C-reactive protein [$1^o Ab$] | R&D Systems, Oxfordshire, UK |
| Polyclonal goat anti-human C-reactive protein conjugated to FITC [$2^o Ab$-*FITC*] | Abcam plc., Cambridge, UK |
| Recombinant human C-reactive protein [*CRP*] | R&D Systems, Oxfordshire, UK |
| *Diamagnetic repulsion and cell media* | |
| Biotin-4-fluorescein | Invitrogen, Paisley, UK |
| Dulbecco's Modified Eagle Medium [*DMEM*] | Sigma-Aldrich, Dorset, UK |
| Fetal calf serum [*FCS*] | Sigma-Aldrich, Dorset, UK |
| Gadolinium (III) chloride hexahydrate | Sigma-Aldrich, Dorset, UK |
| Gadolinium (III) diethylenetriamine pentaacetic acid [*Gd-DTPA*] | Sigma-Aldrich, Dorset, UK |
| L-glutamine | Sigma-Aldrich, Dorset, UK |
| Manganese (II) chloride tetrahydrate | Wako Pure Chemicals, Ibaraki, Japan; Sigma-Aldrich, Dorset, UK |
| Penicillin-streptomycin [*PS*] | Sigma-Aldrich, Dorset, UK |

## 2.1.2    Magnetic particles

Dynabeads superparamagnetic particles of 1 μm and 2.8 μm diameter were purchased from Invitrogen (Paisley, UK), and featured a variety of surface functionalities, as detailed in Table 5, which also shows the binding capacity/active surface functionality of each particle type, as obtained from the manufacturer's specifications.  Particles were supplied in a suspension of buffer apart from the M-270 Epoxy range, which were supplied as dry particles, and Dynabeads particles were chosen due to their superior on-chip response to magnetic fields.[395]   The radii, $r$ (m), of each particle type shown in Table 6 was used to calculate the volume of each particle, $V$ (m$^3$), using Equation 32. The mass, $m$ (kg), of each particle type was calculated from the particle densities, $\rho$ (g cm$^{-3}$), using Equation 33.

$$V = \frac{4}{3}\pi\ r^3 \qquad\qquad \textbf{Equation 32}$$

$$m = \rho\ V \qquad\qquad \textbf{Equation 33}$$

Dynabeads are polystyrene microparticles doped with iron oxide nanoparticles/crystals. The nanoparticles are a mixture of maghemite ($\gamma$-Fe$_2$O$_3$) and magnetite (Fe$_3$O$_4$) in an undisclosed ratio.  The magnetic properties of Dynabeads particles were characterised by Fonnum $et\ al.$,[402] who determined that maghemite was the predominant crystalline phase, with crystal sizes in the range of 8 nm.  The crystals were found to be evenly spread throughout the Dynabeads particles, and the inter-nanoparticle interactions were not sufficient for the Dynabeads to retain any magnetic remanence or coercivity in the magnetisation hysteresis loops, thereby demonstrating the superparamagnetic nature of the Dynabeads particles as a whole.

**Table 5  List of Dynabeads superparamagnetic particles employed in this work.  Details are given of the particle sizes, surface groups, stock concentrations, and active chemical functionality/binding capacity on the surface, all as stated by the manufacturer.**

| Particle type | Particle diameter ($\mu$m) | Surface group | Particle concentration (particles mL$^{-1}$) | Active chemical functionality/ binding capacity |
|---|---|---|---|---|
| Dynabeads MyOne Carboxylic Acid | 1.05 | Carboxylic acid (-COOH) | 7 - 12 x 10$^9$ | 0.6 mmol g$^{-1}$ |
| Dynabeads M-270 Carboxylic Acid | 2.80 | Carboxylic acid (-COOH) | 2 x 10$^9$ | 0.15 mmol g$^{-1}$ |
| Dynabeads M-270 Amine | 2.80 | Amine (-NH$_2$) | 2 x 10$^9$ | 0.1 – 0.2 mmol g$^{-1}$ |
| Dynabeads M-270 Epoxy | 2.80 | Epoxy (-C$_2$H$_3$O) | 6 - 7 x 10$^7$ mg$^{-1}$ (dry particles) | 0.1 – 0.2 mmol g$^{-1}$ |
| Dynabeads M-270 Streptavidin | 2.80 | Streptavidin | 6 - 7 x 10$^8$ | $\leq$ 10 $\mu$g biotinylated antibody per mg of particles |

| Particle type | Particle radius ($\mu$m) | Particle volume ($m^3$) | Particle density ($g\ cm^{-3}$) | Mass of particle (g) | Ferrite content (% wt.) | Mass of iron oxide per particle (g) | Approx. volume of iron oxide, $V_m$ ($m^3$) | Relative $V_m$ | Mass susceptibility, $\chi_{mass}$ ($m^3\ kg^{-1}$) | Particle volume susceptibility, $\chi_p$ (unitless) |
|---|---|---|---|---|---|---|---|---|---|---|
| **MyOne** | 0.525 | $6.06 \times 10^{-19}$ | 1.80 | $1.09 \times 10^{-12}$ | 37 | $4.04 \times 10^{-13}$ | $7.75 \times 10^{-20}$ | 1.0 | $8 \times 10^{-4}$ | 4.17 |
| **M-270** | 1.400 | $1.15 \times 10^{-17}$ | 1.60 | $1.84 \times 10^{-11}$ | 20 | $3.68 \times 10^{-12}$ | $7.06 \times 10^{-19}$ | 9.1 | $6 \times 10^{-4}$ | 3.13 |

**Table 6 Physical and magnetic properties of the Dynabeads MyOne and M-270 particles, either as stated by the manufacturer or derived as described in the text.**

While the precise volume of magnetic material ($V_m$) in the particles is not disclosed by the manufacturer, they do specify the iron oxide content (in weight percent) of each particle type, as shown in Table 6. From these weight percent values and the mass of the Dynabeads particles, the corresponding mass of iron oxide content was calculated and is also shown in Table 6. Since the exact density of the iron oxide in the particles is not known, an assumption can be made in which the density lies between that of $\gamma$-$Fe_2O_3$ (5.24 g cm$^{-3}$) and $Fe_3O_4$ (5.18 g cm$^{-3}$).[403] Thus, the average of these two densities was taken as an approximation, giving a value of 5.21 g cm$^{-3}$ that was subsequently used to calculate the volume of iron oxide in the Dynabeads (i.e. the volume of magnetic material in the particle, $V_m$) by rearranging Equation 33. Also given are the relative $V_m$ values of the two particle types with respect to the MyOne variety, in order to compare the amount of magnetisable material in the larger particles to that in the smaller particles.

Further magnetic properties can be determined from the manufacturer's specifications and from papers. The mass magnetic susceptibilities ($\chi_{mass}$) of the particles are given by Invitrogen and are shown in Table 6, alongside the volume magnetic susceptibilities of the particles ($\chi_p$) calculated using Equation 34 and the approximate density ($\rho = 5.21$ g cm$^{-3}$) of the iron oxide content given above.

$$\chi_p = \rho \; \chi_{mass} \qquad\qquad \textbf{Equation 34}$$

### 2.1.3   Diamagnetic particles

Polystyrene particles featuring no surface functionalisation and with diameters of 20 $\mu$m (Megabead NIST Traceable Size Standard), 10 $\mu$m (Megabead NIST Traceable Size

Standard) and 5 μm (Microbead NIST Traceable Size Standard) were obtained as aqueous suspensions from Polysciences Europe GmbH (Eppenheim, Germany). Streptavidin coated polystyrene particles with a diameter of 10 μm (Micromer Streptavidin) were purchased from Micromod Partikeltechnologie GmbH (Rostock, Germany) as a suspension in PBS buffer (pH 7.45). All diamagnetic particles had a volume magnetic susceptibility ($\chi_p$) of -8.21 x $10^{-6}$, since this is the susceptibility of polystyrene, and had a density of 1.05 g $cm^{-3}$. Details of the particle diameters, volumes, surface groups, and original concentrations are given in Table 7.

**Table 7  Types of diamagnetic polystyrene particles employed, and their diameters, volumes, surface groups, and particle concentrations.**

| Particle type | Particle diameter (μm) | Particle volume, $V_p$ ($m^3$) | Surface group | Particle concentration (particles $mL^{-1}$) |
|---|---|---|---|---|
| Microbeads | 5 | 6.55 x $10^{-17}$ | None | 1.21 x $10^8$ |
| Megabeads | 10 | 5.24 x $10^{-16}$ | None | 1.87 x $10^7$ |
| Megabeads | 20 | 3.14 x $10^{-15}$ | None | 4.55 x $10^7$ |
| Micromer Streptavidin | 10 | 5.24 x $10^{-16}$ | Streptavidin | 4.60 x $10^7$ |

## 2.2    Microfluidic chip designs

Five different chip designs were employed for the work described in this thesis, though all featured common traits of a central separation/reaction chamber, as well as a particle inlet channel, multiple buffer/reagent channels and several outlet channels. Each of the

designs will be described here and given a designation which will be referred to throughout the remainder of the thesis.

The free-flow magnetophoresis chip design, labelled FFM1, was utilised for on-chip free-flow magnetophoresis experiments, and featured a 6 mm x 6 mm separation chamber supported by 13 square posts that were each 200 μm x 200 μm (Fig. 40). 16 buffer inlet channels and a single sample (particle) inlet channel were situated opposite 16 outlet channels, and each channel was 100 μm wide. The buffer inlets were branched to allow introduction of the buffer from a single reservoir and to spread the buffer evenly over the width of the chamber. The outlets were branched in a similar fashion to allow pumping via a single withdrawing syringe. This outlet system inevitably recombined any separated particles, but was nonetheless suitable for proof of principle experiments and had the added advantage of requiring only one syringe.
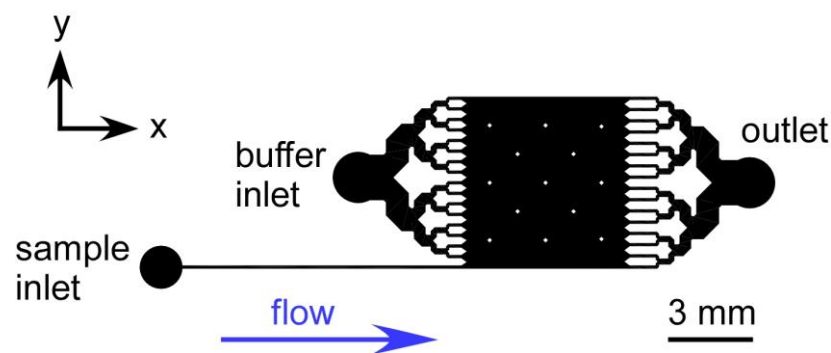


**Fig. 40 Schematic of the free-flow magnetophoresis chip design FFM1, featuring a 6 mm x 6 mm chamber, a single sample inlet channel, 16 buffer inlet channels and 16 outlet channels.**

A second type of free-flow magnetophoresis design, labelled FFM2, was used for diamagnetic repulsion experiments. This chip design was a modified version of FFM1,

featuring the same separation chamber and post setup (Fig. 41). 16 particle inlet channels were situated opposite 17 outlet channels, with all channels being of 100 μm width. However, for the purposes of the diamagnetic repulsion experiments, the chip was rotated 180° so that the inlets became the outlets and vice versa. Thus, the inlet channels were branched from a single inlet access hole, allowing particles to be introduced via one syringe and then enter the chamber across its entire width. The outlet system featured two branched channels and a single channel, originally designed as a particle inlet channel.
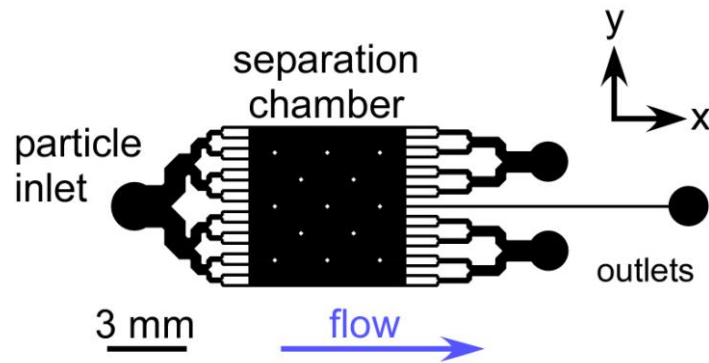


**Fig. 41 Schematic of chip design FFM2, which featured a 6 mm x 6 mm separation chamber, a branched particle inlet system with 16 inlets, and 17 outlet channels.**

Two chip designs were employed for the multilaminar flow experiments, designated MLF1 and MLF2. MLF1 featured a 6 mm x 3 mm reaction chamber and four inlets (Fig. 42). Inlet 1 was a particle inlet channel of 100 μm width. Inlets 2 to 4 were reagent/buffer channels of 400 μm width that each branched into two channels of 200 μm width, which in turn branched into two further channels of 100 μm width. The outlet system consisted of a single particle channel of 100 μm width at the opposite corner of the chamber to the particle inlet channel, and twelve outlet channels that

diverged into a single channel for the collection of waste reagents and washing solutions. The single particle outlet channel was designed to allow collection of particles after a reaction, while the branched waste outlet system was designed to allow easy setup by reducing the amount of tubing required, and to enable collection of the waste solutions into a single vial. This chip was designed for performing one-step reactions, with reagent introduction via inlet 3 and buffer introduction via inlets 2 and 4.
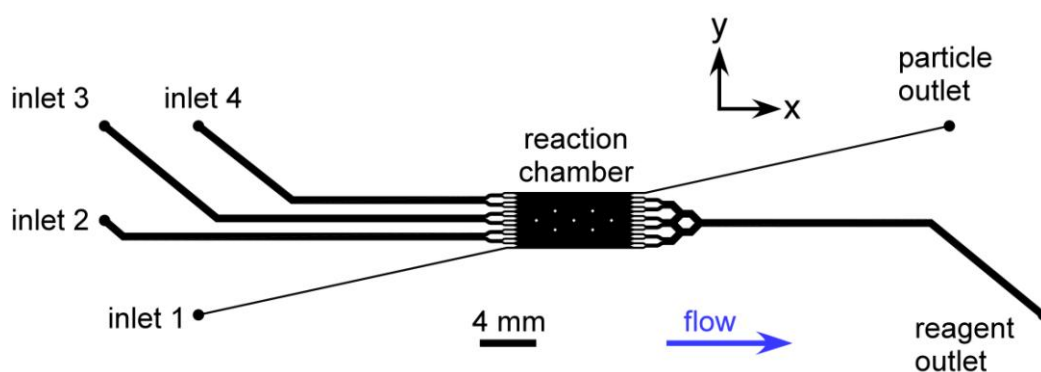


**Fig. 42  Schematic of chip design MLF1, created for one step reactions.  The chip featured a 6 mm x 3 mm reaction chamber, a single particle inlet, three reagent/buffer inlets, a single particle outlet, and a branched waste outlet.**

MLF2 was created for performing two step reactions and featured an 8 mm x 3 mm reaction chamber with a symmetrical inlet and outlet system of five channels (Fig. 43). Each of the inlet and outlet channels was 240 μm wide, before branching into two 120 μm wide channels prior to the reaction chamber.  Inlet 1 was used for the introduction of particles into the chamber, with inlets 2 to 5 used as reagent and buffer inlet channels, depending on the experiment being performed.
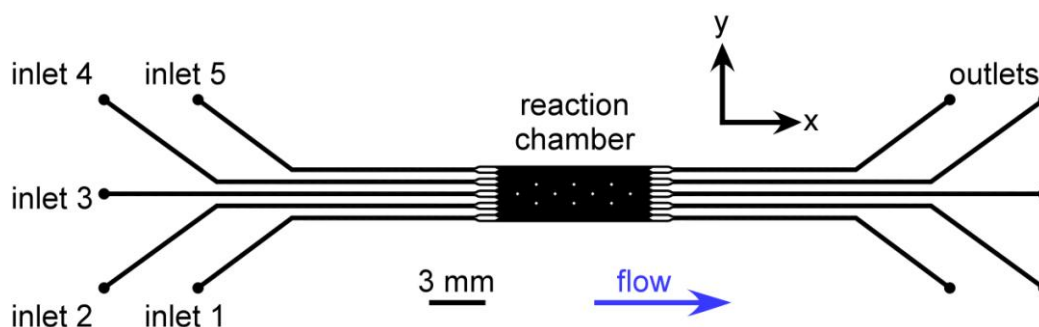
**Fig. 43 Schematic of chip design MLF2, featuring an 8 mm x 3 mm reaction chamber, five inlets, and five outlets.**

The final chip design was labelled MLF3, a variation of the previous multilaminar flow devices designed to increase the number of possible reagent streams and to focus the particles as they entered the chamber (Fig. 44). However, MLF3 was utilised here instead for performing diamagnetic repulsion experiments. The design featured an 8 mm by 5.24 mm reaction chamber supported by 17 square posts that were each 200 μm x 200 μm. Solutions were introduced via 10 inlets that incorporated a flow focussing design into the inlets at the top of the design, and waste solutions were removed via 9 outlet channels. The flow focussing part of the chip consisted of two buffer channels fed by a single inlet hole, which diverged around a single particle inlet hole, with both buffer channels then converging on either side of the particle inlet channel. Each of the flow focussing channels was 240 μm wide at the inlet hole, before each tapered into a 120 μm wide channel at the entrance to the chamber. The remaining 8 inlet channels were 240 μm wide at the inlet holes, before each split into two parallel 120 μm wide channels at the entrance to the chamber. The outlet channel in the opposite corner to the flow focussing channels was a single channel designed to collect particles that traverse the entire width of the chamber, and was 120 μm wide at the exit of the chamber before

tapering out to 240 μm at the outlet hole. The other 8 outlet channels were 240 μm wide at the outlet holes, then splitting into two 120 μm wide channels before the chamber, as with the inlet channels.
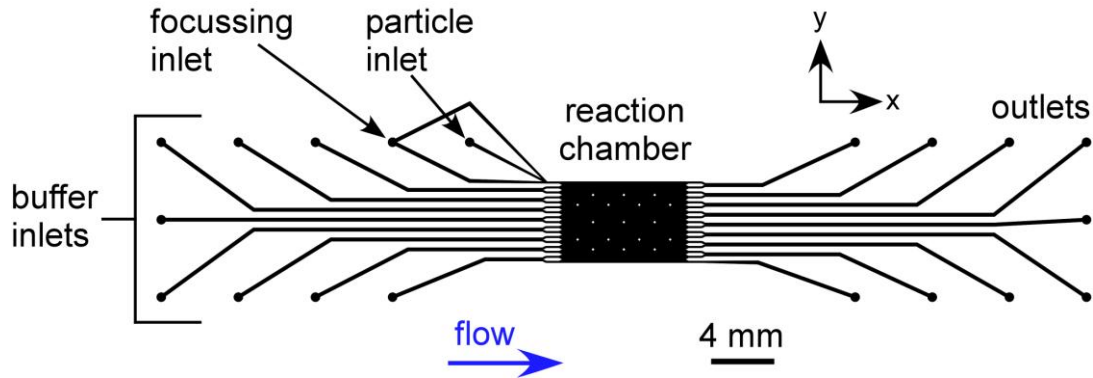


**Fig. 44 Schematic of the 10 inlet chip design (MLF3), which featured an 8 mm x 5.24 mm chamber, 10 inlets which incorporated particle focussing channels, and 9 outlets.**

## 2.2.1 Pressure calculations

An important consideration when designing microfluidic devices is the pressure across the system when pumping liquids through the channels, which can result in high backpressure that cause difficulties in the introduction of fluids. As a liquid flows through a pipe or channel the pressure decreases from one end of the channel (the source of the pressure) to the other due to frictional forces, an effect known as the pressure drop. These frictional forces arise from a resistance to the flow exerted by a channel based on its dimensions and the viscosity, $\eta$ (kg m$^{-1}$ s$^{-1}$), of the fluid flowing through it. The pressure drop in a microfluidic device can be calculated by first determining the flow resistance, $R_\phi$ (kg m$^{-4}$ s$^{-1}$), as shown in Equation 35:[404,405]

$$R_\phi = \frac{2 \; f\,R_e \; l \; \eta}{w \; d \; \delta^2}$$

**Equation 35**

where $l$ = channel length (m), $w$ = channel width (m), $d$ = channel depth (m), $f R_e$ = the friction coefficient which is related to the shape of the microchannel (assumed to be 24 for a microfluidic chamber).[405] The hydrodynamic diameter, $\delta$ (in m), can be calculated for a rectangular cross-section using Equation 36:

$$\delta = \frac{2 \; w \; d}{w + d}$$

**Equation 36**

The pressure drop, $\Delta p$ (Pa), is then determined from the flow resistance, $R_\phi$, and the applied flow rate, $\phi$ ($m^3$ $s^{-1}$), using Equation 37. This can be also be likened to the calculation of the voltage, or potential difference ($V$), from the current ($I$) and resistance ($R$) in an electronic circuit according to Ohm's law, $V = I\,R$.

$$\Delta p = \phi \; R_\phi$$

**Equation 37**

As in an electrical circuit, the flow resistance of multiple channels in a microfluidic chip may be treated like electrical resistors, and Kirchhoff's laws can be applied to find the total flow resistance, $R_\phi(tot)$, for the chip and its individual sections. When the channels in a microfluidic chip are in a serial arrangement (i.e. one channel follows another) the total flow resistance can be calculated using Equation 38, where $R_1$, $R_2$ etc. refer to resistance values for individual channels.

$$R_\phi(tot) = R_1 + R_2 + R_3 + ... + R_i$$

**Equation 38**

When the channels are in a parallel arrangement (e.g. when a single channel splits to give two parallel channels) the total resistance can be calculated by determining the

value of $1/R_\phi(\text{tot})$ from each of the parallel channels as shown in Equation 39, before

taking the inverse of this number to give $R_\phi(\text{tot})$.

$$\frac{1}{R_\phi(tot)} = \frac{1}{R_1} + \frac{1}{R_2} + ... + \frac{1}{R_i}$$

**Equation 39**

## 2.3     *Fabrication of microfluidic chips*

Chip designs FFM1, MLF1, MLF2 and MLF3 (each drawn using AutoCAD software) were patterned onto glass wafers using conventional photolithography and wet etching methods of chip fabrication, using white crown B-270 glass.[39,40,406] Wafers of 1 mm thick B-270 glass were purchased precoated with a 1200 Å thick layer of chromium and a layer of AZ 1518 "positive" photoresist, from Telic Company (Valencia, CA, USA). The photoresist was exposed to ultraviolet light (LV204 UV Exposure Unit, Mega Electronics, Cambridge, UK) for 60 s through a photomask (JD Photo-Tools, Oldham, Lancashire, UK) featuring the desired chip design, printed from the AutoCAD file provided (Fig. 45).   The wafer was then placed into a bath of photodevelopment solution consisting of Microposit Developer Concentrate in a 1:1 ratio with purified water for 60 seconds.  UV irradiation alters the chemical structure of the exposed areas of a positive photoresist, making it soluble in the photodevelopment solution such that after the 60 seconds had passed the exposed area had dissolved, leaving the chip design visible on the chromium layer beneath.  The wafer was then immersed in a solution of Microposit Chrome Etch 18 solution for 60 seconds, which etched away the exposed chromium layer to now leave the chip design visible on the glass itself.
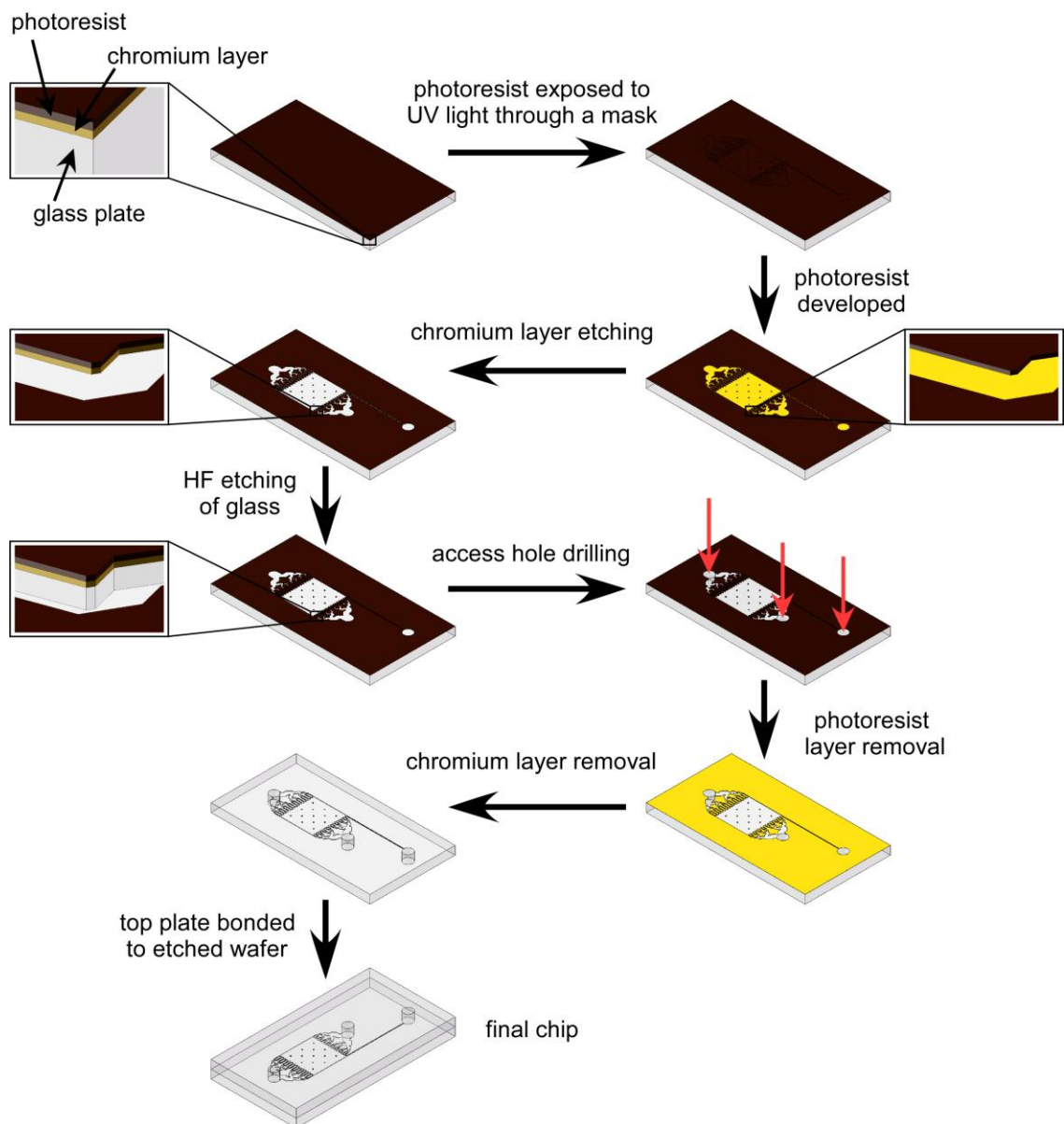
**Fig. 45   Conventional photolithography and wet etching method of microfluidic chip fabrication.   A glass wafer coated with chromium and photoresist layers is exposed to UV light through a mask featuring the channel design, whereupon the exposed region is dissolved in photodeveloper.   The revealed chromium is removed and the design etched into the glass using hydrofluoric acid.   Access holes are drilled, the photoresist and chromium layers are dissolved, and the etched plate is thermally bonded to a top plate.**

The wafer was immersed in a glass etching solution consisting of 1.3 % hydrofluoric acid, 13.3 % phosphoric acid and 85.3 % purified water. The etching solution was prepared by first adding 10 mL hydrofluoric acid and 100 mL phosphoric acid to 140 mL water, then adding 50 mL of this stock solution to 100 mL water to give the final concentrations. The etch rate of this solution was around 0.13 $\mu$m min$^{-1}$. A low concentration (~1 %) of hydrofluoric acid is favourable as, although the etching rate becomes slower, it yields a smoother etched surface on the glass than when using higher concentrations. It should also be noted that the glass etching occurs isotropically, by which the etching occurs in all directions in the glass. After subsequent rinsing with sodium bicarbonate solution (1.2 M, to neutralise the acid) and deionised water, access holes of 368 $\mu$m diameter were drilled into the glass wafer for the inlets and outlets of the multilaminar flow chips, and access holes of 1 mm diameter for the FFM1 and FFM2 chip designs. 368 $\mu$m diameter carbide and 1 mm diameter diamond drill bits, as well as the drill itself, were purchased from Drill Service Ltd. (Horley, Surrey, UK). The wafer was rinsed with water, dried using a nitrogen gas line, and immersed in acetone until the photoresist layer was entirely dissolved, before rinsing again with water and removing the chromium layer by immersion in Chrome Etch 18 solution.

The wafer was rinsed and dried, then underwent a rigorous cleaning process to ensure any grease and dirt was removed before the final bonding procedure. The etched wafer, and an unetched piece of glass cut to the same size that would be a top plate for the chip, were immersed consecutively in solutions of acetone and propan-2-ol for 15 min each, then cleaned in piranha solution for 1 h at 65 °C. Piranha solution was prepared by the slow addition of hydrogen peroxide (30 % w/v) to a vessel containing sulphuric acid (98 %) in a 3:1 $H_2SO_4$:$H_2O_2$ ratio (e.g. 60 mL $H_2SO_4$, 20 mL $H_2O_2$). After this final washing step, the glass plates were allowed to cool, rinsed with purified water, and brought together under a stream of running water. The plates were aligned and clamped

together using bulldog clips, then placed in a 60 °C oven until dry. They were removed, allowed to cool, and Impega invisible tape (Lyreco, Shropshire, UK) used to hold the edges of the plates in place so that the clips could be removed.

The aligned glass plates were placed onto a stainless steel plate, and a flat, stainless steel weight was placed on top of the glass, with the amount of weight required depending on the size of the chip and type of glass it was made from. This assembly was placed in a furnace (EF3, Vecstar Furnaces, Chesterfield, UK) and heated to 590 °C for 3 hours. Occasionally, this bonding process had to be repeated several times to ensure the entire chip was properly bonded.

## 2.4    Surface treatments

In an effort to reduce the sticking of particles to the glass surfaces of the microfluidic channels during some experiments, several treatments were performed to modify the glass. Initial attempts to perform surface treatments involved the introduction of chemicals through fused silica capillaries. However, it was found that this also treated the capillaries themselves, and always resulted in increased back pressure and difficulties in introducing particles into the chips. It was hypothesised that this was due to the presence of water (possibly from moisture in the air) that reacted with the silanising agent to form residues that partially blocked the capillaries. Silanisation of a glass surface requires a minute amount of water to be present, but too much water will cause the formation of powdery residues, hence the agents were stored in a desiccator when not in use, and were typically only used for $2 - 3$ weeks after being opened. Due to the suspected blocking of the capillaries, subsequent attempts to treat the chips involved pumping the required solutions directly into the chip via the following

methods. Two types of surface treatments were investigated: silanisation and agarose

gel coating.

**Table 8  Silanising agents and their properties.  References show where the application methods for each agent were adapted from.**

| Silanising agent | Abbrev. | Leaving group | Solvent | Effect on glass surface |
|---|---|---|---|---|
| Octadecyltrichlorosilane [407,408] | OTS | -Cl | 4:1 Hexadecane: Chloroform | Hydrophobic; uncharged |
| Trichloro(1*H*,1*H*,2*H*,2*H*-perfluorooctyl)silane [409,410] | FDTS | -Cl | Isooctane (2,4,4-trimethyl-pentane) | Hydrophobic; fluorophilic; lyophobic; uncharged |
| 2-[Methoxy (polyethyleneoxy)propyl] trimethoxysilane [411] | PEG-silane | -OMe | Toluene | Hydrophilic; uncharged |
| (3-aminopropyl) triethoxysilane [412] | APTES | -OEt | Ethanol | Positively charged at low pH |
| Dimethyloctadecyl[3-(trimethoxysilyl)propyl] ammonium chloride [413] | QAS (quaternary ammonium silane) | -OMe | Methanol | Positively charged |

A chip, having been cleaned via a furnace (500 °C for 6 h) and/or in piranha solution,

and with no tubing attached, was flushed with acetone by placing a syringe directly over

one of the inlet holes, then a syringe filled with air used to remove the acetone. The

chips were placed in a 60 °C oven overnight to ensure that the surfaces were dry. These

steps were to ensure that no water was present in the chips during silanisation

treatments, where the presence of water can produce unwanted byproducts and cause

blockages. For the silanisation procedure, solutions were prepared by dissolving the

silanising agent in an appropriate solvent to a concentration of 1 % v/v (Table 8).

**Table 9  Chemical structures of the silanising agents.**

| Silanising agent | Chemical structure |
|---|---|
| OTS |  |
| FDTS |  |
| PEG-silane |  |
| APTES |  |
| QAS |  |
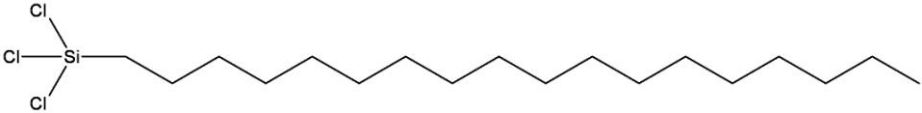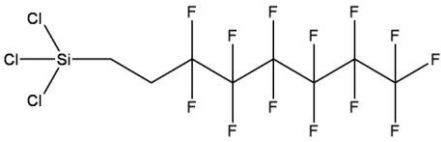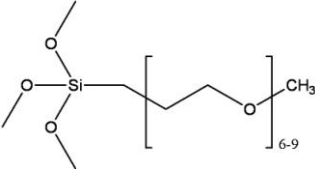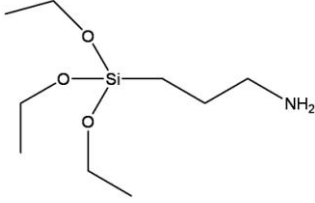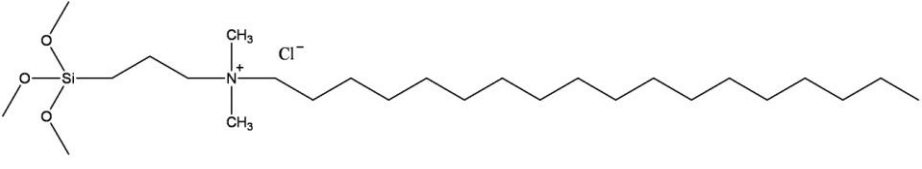
The chips were flushed first with the pure solvent via a syringe, before filling them with the silanisation solution and leaving it to react for 10 min.  Finally, the chips were flushed with the solvent again, followed by acetone and then water, leaving the chip ready for use in experiments.  The silanising agents were used to render the glass chip surfaces hydrophobic, hydrophilic (more so than regular glass), or positively charged, depending on the type of agent used.  Each agent featured a silane group with four substituents, one of which was the group (-R) responsible for conferring the desired physical effect on the system, and the other three of which were hydrolysable leaving

groups of either methoxy (-OMe), ethoxy (-OEt) or chlorine (-Cl), used to link the silane to the glass surface. Table 8 shows the different silanising agents used in this work, together with their abbreviations, the effect on the glass surface, the leaving group, and the solvents used to prepare the 1 % v/v solutions. Table 9 shows the chemical structures of each of the silanising agents.

Fig. 46 shows the mechanism by which silane modification takes place on a surface featuring hydroxyl groups (-OH), such as the surface groups on glass.[414-416] Firstly, the alkoxy (methoxy, -OMe, or ethoxy, -OEt) leaving groups of the silane are hydrolysed by water to form silanols. Hence, a small amount of water is typically required in the system to perform the surface treatment, and may come from the atmosphere or be present in small quantities on the surface of the glass. For those silanising agents featuring chlorine leaving groups, anhydrous alcohols are usually used as the solvent, and the chlorosilane reacts with the alcohol to produce an alkoxysilane and hydrochloric acid. Some of the hydrochloric acid then reacts with the alcohol to produce small quantities of alkyl halide and water, the latter of which causes formation of silanol groups from the alkoxysilanes. Thus, whether an alkoxysilane (with methoxy or ethoxy groups) or a chlorosilane (with chlorine groups) is used as the starting material, both become silanols as a result of hydrolysis, albeit by slightly different mechanisms. In general, the reactivity of the silanising agents with the hydroxylated groups of the substrate surface is greater for the chlorosilanes than the alkoxysilanes, but nevertheless the latter type are the most widely used due to the non-corrosive and volatile byproducts, and for the methoxysilanes there is the advantage that they are able to modify surfaces under dry conditions.
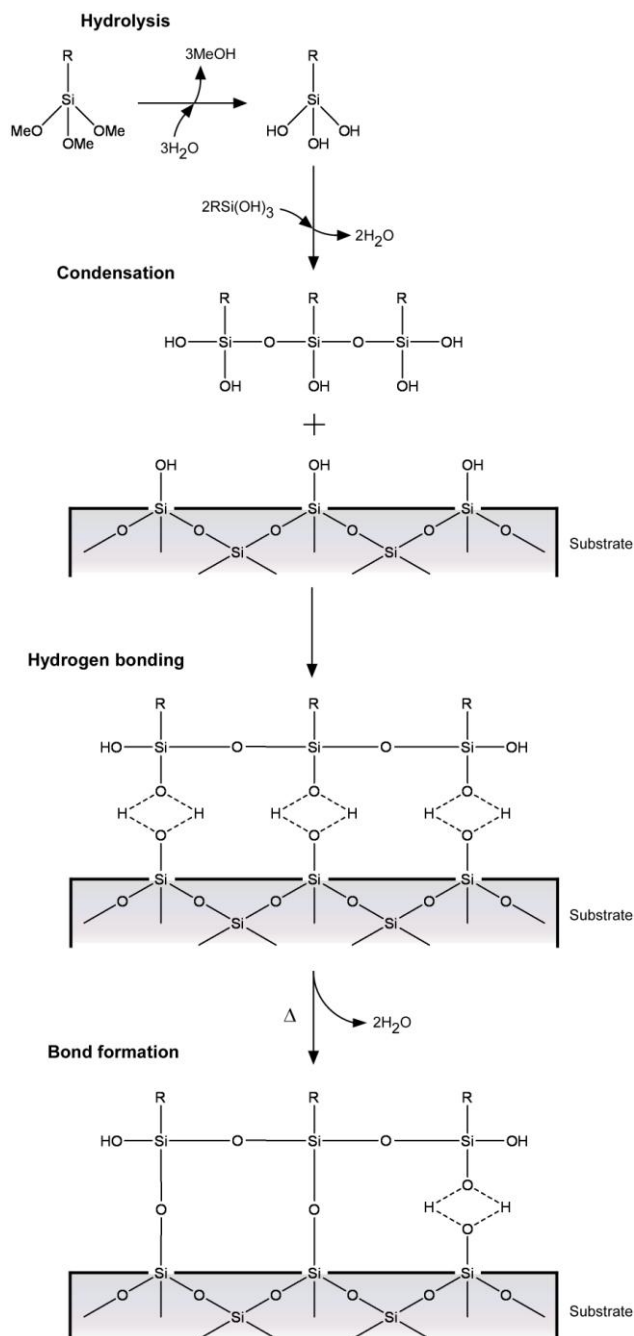
**Fig. 46  The deposition of silanising agents onto a glass substrate.  The example shows an alkoxysilane featuring three hydrolysable methoxy groups.  Reproduced from Refs. 415 and 416.**

Once hydrolysis of the silanes has been performed, the silanols produced undergo condensation to form oligomers, which in turn hydrogen bond with the hydroxyl groups of the substrate.  Finally, a covalent bond is formed with the substrate due to loss of

water by drying or curing, securing the silane and the properties of its R group to the glass surface. These steps are described sequentially, but can actually occur simultaneously after the hydrolysis step. Chips silanised with a hydrophobic treatment were tested by examining the water-air interface in a channel to observe the contact angle, where it was found that hydrophobic surfaces gave a contact angle of around 90° while untreated surfaces exhibited contact angles of < 30°. Surfaces treated with a positive charge were exposed to 5,6-carboxyfluorescein, a negatively charged fluorescent dye, before being washed with water. The negative dye coated the positive surface of the chip due to electrostatic attraction, demonstrating successful coating of the positively charged silanising agent onto the chip. However, this method was only useful for showing that the silanisation procedure worked since it left the surface unsuitable for subsequent experiments, and so the silanisation was repeated with another chip that was then not exposed to 5,6-carboxyfluorescein.

Aside from the silanisation treatments, other methods of modifying the glass surfaces were also performed in order to render the channels of the microfluidic chips more hydrophilic. One method of modification utilised of methoxypolyethylene glycol 5,000 propionic acid $N$-succinimidyl ester (also called polyethylene glycol-succinimidyl propionate, PEG-SPA).[412] Firstly, the microfluidic chip was silanised using APTES as described above, before curing for 3 h at 120 °C in an oven, thus bestowing primary amine groups onto the glass surfaces. In the next step, a 1 mg mL$^{-1}$ solution of PEG-SPA was prepared in sodium phosphate buffer (20 mM, pH 8), and the APTES-modified chip was filled with this solution and left to react at 4 °C for 24 h. Finally, the channels were flushed with purified water and the chip stored at 4 °C until ready for use. The PEG was covalently bound to the amine groups of the silane-modified glass as, at a pH above neutral, the $N$-succinimidyl ester is subject to nucleophilic substitution by the primary amine, as shown in Fig. 47. This yielded a hydrophilic surface, although

Chuang *et al*., who used this method to study electrophoretic mobility shift assays on PEG-modified glass chips, also stated that the surface exhibited a slight positive charge under buffer conditions of pH 7.5, which may be because not all of the primary amine groups on the surface undergo the reaction with the PEG-SPA.
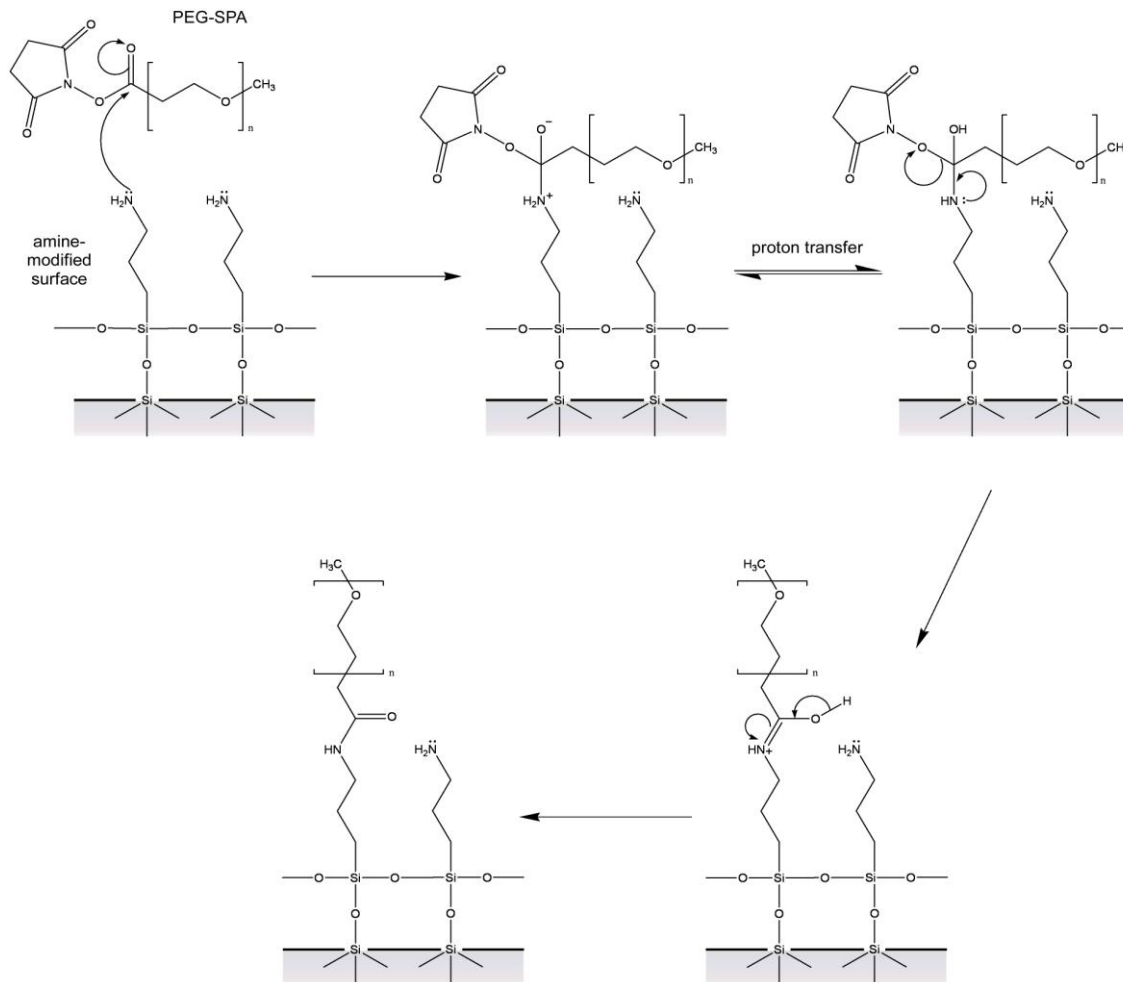


**Fig. 47 The bonding of PEG-SPA to a primary amine-modified glass surface via nucleophilic substitution of the *N*-succinimidyl ester to give PEGylated surfaces.**

A further method of surface modification to render glass more hydrophilic was to coat it with a thin layer of agarose gel (a linear polymer of alternating D-galactose and 3,6-anhydro-L-galactose units, Fig. 48), which is widely used for its hydrophilic properties. The gel was prepared as per manufacturer's instructions (Sigma-Aldrich). A 1 % w/v

solution of low gelling temperature agarose (melting point ~ 65 °C, gel point ~ 30 °C) was prepared by adding 50 mg of agarose powder to 5 mL of water in a sample vial with stirring to avoid clumping of the solid. The sample vial was covered with parafilm and a hole pierced for ventilation, and was placed in a beaker of water. The beaker was heated above 65 °C with occasional swirling of the sample vial until all of the powder had dissolved, whilst simultaneously a microfluidic chip was placed on a separate hot plate and heated to around 65 °C. A portion of the agarose solution was taken up into a syringe and immediately injected into an access hole of the chip, filling the entire device. A compressed air line was then held to the same access hole and air pumped through the chip until no "clumps" of the solution could be seen in the chip, and leaving only a thin coating on the glass.
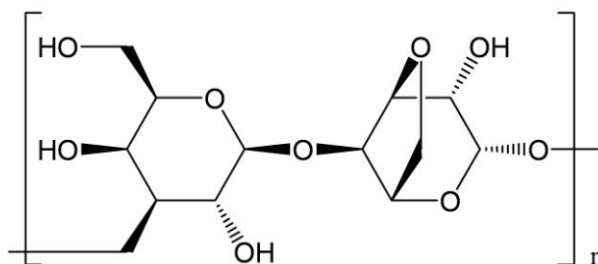


**Fig. 48  The structure of agarose gel, used here as a hydrophilic surface treatment.**

Finally, the chip was removed from the hot plate and allowed to cool so that a thin layer of agarose gel formed on the surfaces, which could be observed as a "smear" on the glass. However, due to the method by which the film was applied to the microfluidic chip, it was not possible to control the thickness of the agarose layer produced, though future studies could involve characterisation of the procedure and the resultant gel using such surface analytical techniques as ellipsometry.

## *2.5      On-chip free-flow magnetophoresis*

This section describes the experimental parameters, chemicals, particles, and setup for the study of magnetic particle deflection behaviour and separation resolution in a microfluidic chamber with varying buffer solution viscosity (by controlling the system temperature).

## 2.5.1    Buffers and solutions

Three concentrations of glycine saline buffer were employed, each with different roles, for the on-chip free-flow magnetophoresis work.  All glycine saline solutions were prepared by the addition of glycine powder and sodium chloride powder to water, with solutions adjusted to pH 8.3 by the addition of 0.1 mM sodium hydroxide and the use of a pH meter (Navi D-53, Horiba Instruments Ltd., Northampton, Northamptonshire, UK).  Table 10 shows the role and concentration of each glycine saline solution prepared.  Bovine serum albumin (BSA) was dissolved in the 0.1x glycine saline assay running buffer to a concentration of 0.01 % w/v in order to avoid particle-particle and particle-surface interactions that would otherwise cause particles to stick to each other and to the microfluidic surface.  PBS solution was prepared as per manufacturer's instructions.  Briefly, a 5 g PBS tablet was dissolved in 500 mL water, yielding the following concentrations of each species in the solution: 0.14 M NaCl, 0.01 M $PO_4^{3-}$, and 0.003 M KCl.  The pH of the standard solution was 7.45.

**Table 10  Concentration and role of glycine saline solutions.**

| Solution designation | Concentration of glycine | Concentration of NaCl | Role of solution |
|---|---|---|---|
| 10x glycine saline | 100 mM | 150 mM | Blocking buffer for epoxy particle surface groups |
| 1x glycine saline | 10 mM | 15 mM | Particle storage buffer |
| 0.1x glycine saline | 1 mM | 1.5 mM | Assay running buffer |

## 2.5.2  Magnetic particle suspensions

Dynabeads M-270 Epoxy particles (2.80 μm diameter), as described in Section 2.1.2, were purchased from Invitrogen as a dry powder, and prepared as per the manufacturer's instructions.  3 mg of particles (~ 2 x $10^8$ particles) were dispersed in 1 mL of PBS buffer in a 1.5 mL Eppendorf tube (VWR, Leicestershire, UK), and underwent the following particle washing procedure: the suspension was vortexed for 20 s, the particles collected at the side of the tube via an external magnet, the supernatant removed, and fresh PBS added (see Fig. 26).  This washing process was repeated twice more, and once the supernatant had been removed for the last time the particles were resuspended in 10x glycine saline blocking buffer, vortexed for 20 s, and incubated overnight with agitation.  The glycine thus coated the particle surface and deactivated the reactive epoxy groups by covalently binding to them (Fig. 49).
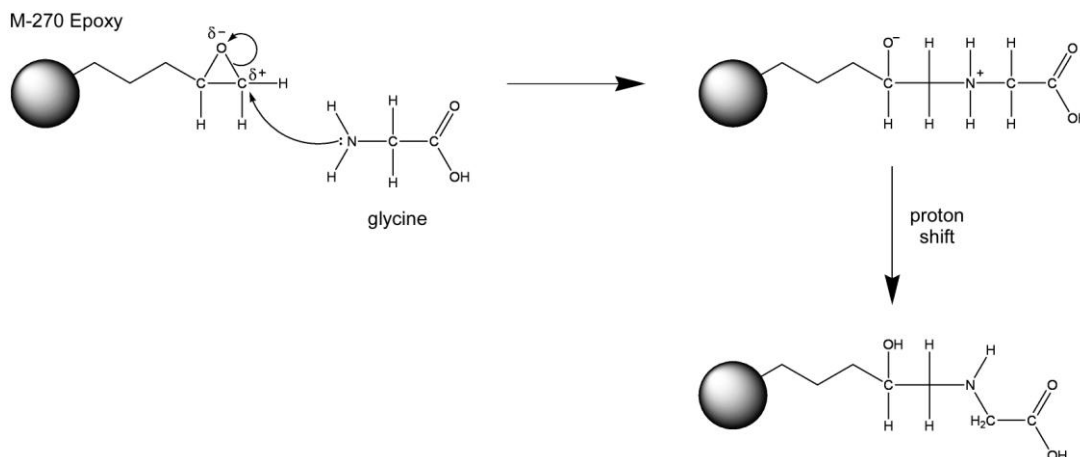
**Fig. 49  The reaction of the epoxy groups on the surface of the M-270 Epoxy particles with glycine, the simplest amino acid.**

The glycine coating procedure began with the addition of 10 μL of the stock particle solution to 990 μL of the 1x glycine saline storage buffer to give a concentration of 2 x $10^6$ particles mL$^{-1}$, stored at 4 °C.  Prior to experiments, the particle suspension was diluted a further ten times using 0.1x glycine saline assay running buffer, giving a final concentration of 2 x $10^5$ particles mL$^{-1}$.  The pI of glycine is 6.07.[417]  Hence, the glycine on the surface of the particles was mostly negatively charged in the pH 8.3 glycine saline buffer, rendering the particles themselves negatively charged and, due to electrostatic repulsion, reducing the possibility of particle agglomeration (Section 1.2.2).

Dynabeads MyOne Carboxylic Acid particles (1.05 μm diameter) were purchased as a suspension of 1 x $10^{10}$ particles mL$^{-1}$.  20 μL of this stock suspension was diluted in 980 μL of the 10x glycine saline solution to give 2 x $10^8$ particles mL$^{-1}$, of which 10 μL was then diluted in 990 μL of the 1x glycine saline solution to give a concentration of 2 x $10^6$ particles mL$^{-1}$.  This suspension was stored at 4 °C prior to experiments, at which time it was diluted a further ten times in 0.1x glycine saline solution to give a final

concentration of 2 x $10^5$ particles $mL^{-1}$. A reaction between the surface carboxylic acid groups and the glycine in the solution would not have occurred due to the lack of a carbodiimide to promote a coupling reaction, hence the particles remained coated with carboxylic acid during experiments. With a pKa value of around 5 for a carboxylic acid on an alkyl chain,[418] the particles were negatively charged in the pH 8.3 solution, thus reducing the possibility of agglomeration as described above for the M-270 Epoxy particles.

### 2.5.3   Viscosity and density measurements

The absolute viscosity, $\eta$ (kg $m^{-1}$ $s^{-1}$), of the 0.1x glycine saline solution (including 0.01 % w/v BSA) at temperatures of 5, 10, 20, 30 and 40 °C, was determined over a series of experiments by the measurement of the kinematic viscosity and density of the solutions. The relationship between these parameters will be shown in Section 3.2.1. The kinematic viscosity, $v_k$ ($m^2$ $s^{-1}$), of the glycine saline solution and of purified water were measured using an Ubbelohde viscometer, or "suspended level" viscometer (Fisher Scientific). Fig. 50 shows the operation of an Ubbelohde viscometer, which features a U-bend with one arm containing a narrow capillary with a bulb at the top, and a third arm extending from the bottom of the capillary that is open to air. Liquid was introduced into the viscometer until the U-bend was full, whereupon suction (via a standard pipette filler) was used to draw the liquid up through the capillary, filling the bulb. The bulb features a mark at the top and a mark at the bottom, and once the liquid had passed the top mark the suction was removed, allowing the liquid to flow back down the capillary, emptying the bulb. The time taken for the meniscus of the liquid to pass from the top mark to the bottom mark was recorded, and the procedure repeated twice more to give an average value. Additionally, this method was also used to

determine the density of 6 % and 10 % w/w solutions of manganese (II) chloride (Section 9.2.2).

The density of the 0.1x glycine saline solution and of purified water were measured at the same temperatures shown above, using a hand-held density meter (DMA 35N, Anton Paar Ltd., Hertfordshire, UK).  A tube attached to the instrument was simply inserted into a solution, a small volume taken up into the device, and the density given on the display.  The temperature of the solutions for both the viscosity and density measurements was controlled by immersing the solutions/viscometer in refrigerated circulator thermostat baths (LTD6G, Grant Instruments, Cambridge, UK).
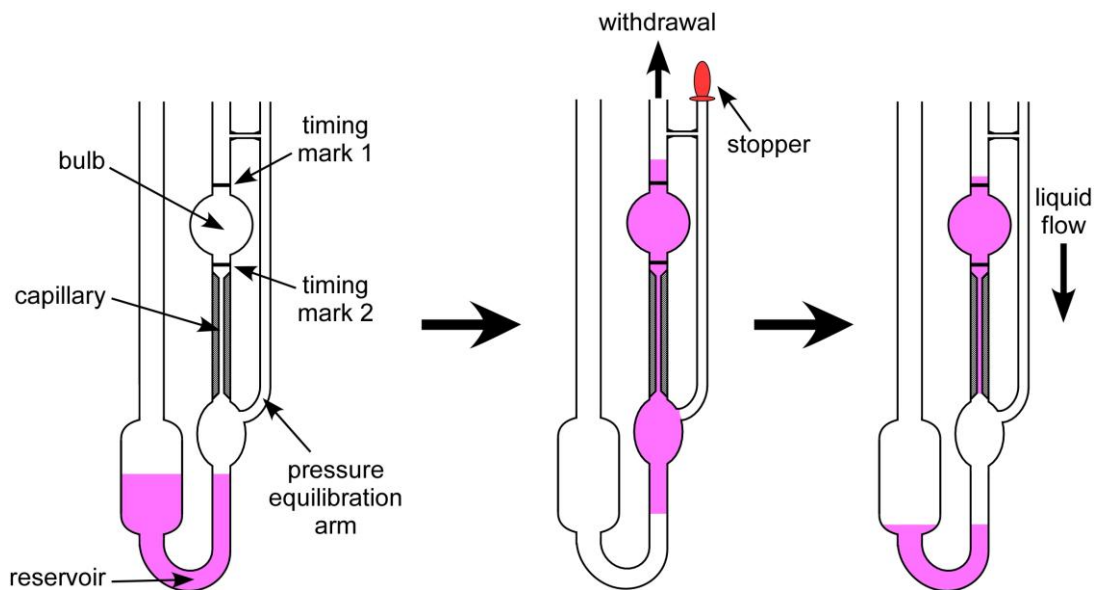


**Fig. 50  Operation of an Ubbelohde viscometer.  Liquid (shown in purple) was introduced into the viscometer, drawn into a bulb via suction, and allowed to flow out of the bulb with the time taken for the meniscus to pass the two timing marks recorded.**

## 2.5.4    Microfluidic chip setup and interfacing

Chip design FFM1 was utilised for the on-chip free-flow magnetophoresis experiments, and was fabricated in 1 mm thick B-270 glass using the method described in Section 2.3, to a depth of 20 μm. Buffer and sample reservoirs were prepared from plastic pipette tips (50 mm, VWR, Leicestershire, UK), which were cut to an appropriate size and glued over the sample inlet and buffer inlet holes of the microfluidic chip using epoxy resin (Araldite Rapid, RS Components, Northamptonshire, UK) (Fig. 51). A 1 cm length of poly(ether ether ketone) tubing (PEEK, 0.5 mm i.d., 1.6 mm o.d., Cole-Parmer Instrument Co., London, UK) was glued into the outlet hole of the chip and interfaced to a 5 mL syringe (Henke-Sass Wolf (HSW) polypropylene syringe, VWR), via a 6 cm length of Tygon tubing (1.0 mm i.d., 1.8 mm o.d., Cole-Parmer). A syringe withdrawal rate of 400 μL h$^{-1}$ (930 μm s$^{-1}$ in the chamber) was applied using a syringe pump (Pump 11 Plus, Harvard Apparatus, Kent, UK). A 10 mm Ø x 5 mm disc neodymium-iron-boron (NdFeB) magnet (Magnet Sales UK, Swindon, UK) was placed on the chip, halfway over the separation chamber, as shown in Fig. 51.
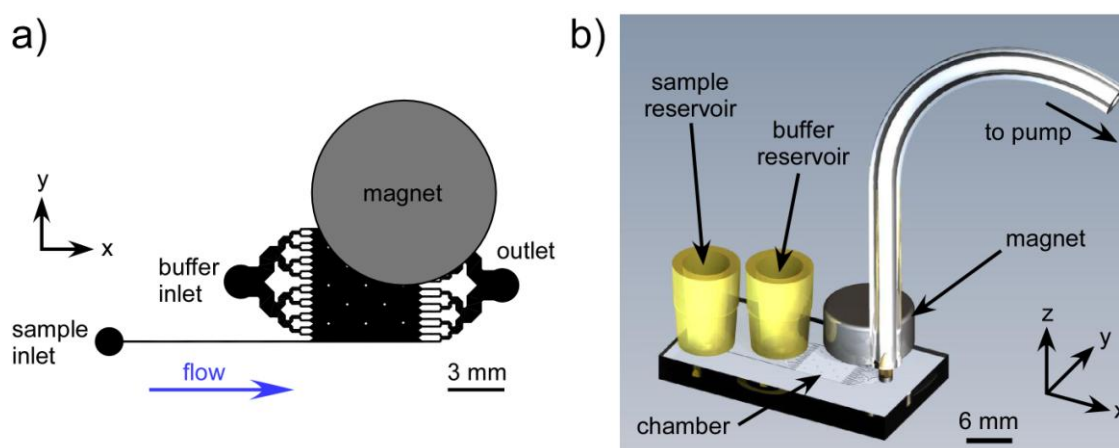


**Fig. 51  a) Position of the 10 mm Ø x 5 mm NdFeB disc magnet on the microfluidic chip. b) Setup of the device, featuring the sample and buffer reservoirs over the inlet holes, tubing for interfacing the outlet to a syringe pump, and the NdFeB magnet.**

## 2.5.5   Magnet setup

The magnetic flux density (**B**) over the separation chamber was simulated using Finite

Element Method Magnetics software (FEMM 4.2, http://femm.foster-miller.net) (Fig.

52), and using the theoretical value of **B** at the magnet surface (435 mT) calculated

using Equation 19.   The average value of **B** across the half of the chamber that the

particles traversed was determined to be 205.7 mT, with a gradient of ~10.5 mT mm$^{-1}$.

Thus, the product of (**B**·∇)**B** was estimated to be 2.16 T$^2$ m$^{-1}$.
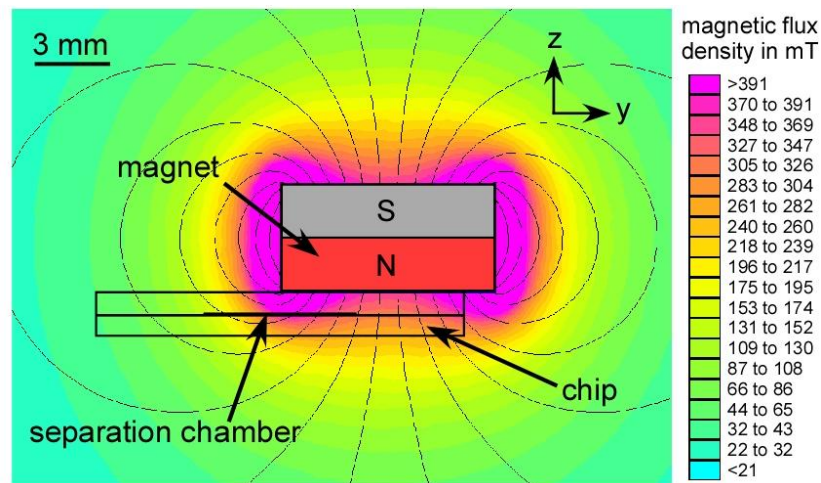


**Fig. 52   Two-dimensional simulation of the magnet flux density, B, over the separation chamber, as observed from a side-on view.   FEMM software was used to generate the model.**

## 2.5.6   Temperature control

A Peltier element (Thermo Module 127 TEC1-12708, Akizukidenshi, Tokyo, Japan)

was sandwiched between two aluminium blocks acting as heatsinks, and the chip was

placed atop one of the blocks (Fig. 53).   Adjusting the voltage supplied to the Peltier

element via a DC power supply (SM5020, Digimess, Berkshire, UK) allowed control

over the temperature of the aluminium blocks. When temperatures of 20 °C and above were required, the blocks were placed into a plastic clamp to hold them in place. However, when temperatures of less than 20 °C were required, the blocks were taken out of the clamp and placed onto a computer heat sink and cooling fan to remove heat and thus allow better control over the temperature. The temperature of the microfluidic device was measured using a hand-held infrared temperature sensor (Precision Gold, Maplin Electronics, Barnsley, UK).
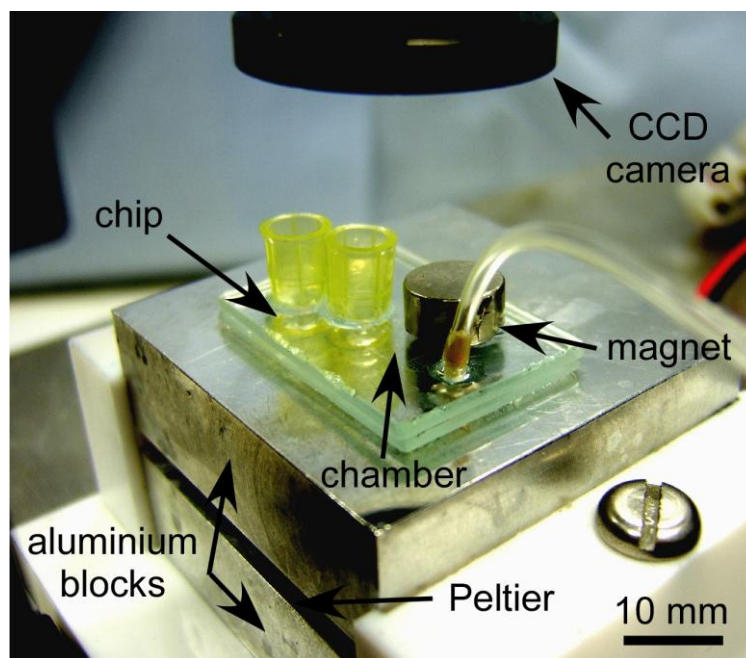


**Fig. 53 Photograph of the experimental setup for determining the effect of temperature on particle behaviour, utilising a Peltier element sandwiched between two aluminium heat sinks.**

Additional readings were taken with a thermocouple (K-type, TM-301 Dual Thermometer, AS ONE, Japan) used to measure the top surface of the chip and the surface of the aluminium block.

### 2.5.7 Particle visualisation

Observation of the particles in the separation chamber was achieved using an overhead zoom CCD camera (PV10, Olympus, Japan) connected to a television (1485T, Bush, UK), with videos recorded by VCR (SV-5000W, Samsung). After confirming the temperature of the apparatus during an experiment, a small piece of black carbon copy paper was inserted beneath the chip to allow the particles to be seen as bright white spots on the dark background when an external lamp (MegaLight 100, SCHOTT Nippon K.K., Tokyo, Japan) was positioned to illuminate the chip. Particles were difficult to observe without the lamp and carbon copy paper being present.

### 2.5.8 On-chip particle deflection experiments

Prior to performing particle experiments, the microfluidic chip was pretreated by consecutively washing with IPA-KOH solution, water, and finally 0.1x glycine saline solution, each for 15 min. IPA-KOH solution was prepared by dissolving 0.6 g potassium hydroxide in 20 mL isopropyl alcohol (propan-2-ol) with stirring. The solution was filtered using a Whatman 0.20 μm syringe filter (VWR) before introduction into a chip. Fresh solution had to be prepared every three days as the solution would form crystals that could block the microfluidic channels. Introduction of the solution into the chip also had to be performed carefully and without generating too much pressure, as this would cause crystals to drop out of solution in the separation chamber of the chip, which would hinder particle experiments. The purpose of the IPA-KOH wash was to simultaneously clean the channels of the microfluidic device, and also to render the surface of the glass negatively charged (due to the presence of the hydroxide), thus increasing the effect of electrostatic repulsion on the negatively

charged particles and thereby reducing the possibility of particles sticking to the surfaces of the chip. The water wash was used to remove the IPA-KOH solution, before the introduction of the 0.1x glycine saline running buffer. The solutions were introduced consecutively into the sample and buffer reservoirs on the chip, and pulled through the chamber by negative pressure at a rate of 100 $\mu$L h$^{-1}$ (230 $\mu$m s$^{-1}$ in the chamber), before the solution was pipetted out, leaving only a small volume covering the access holes so that no air could enter the chip. The reservoirs were then refilled with the next washing solution. Subsequently, the glycine saline solution in the sample reservoir was pipetted out and replaced with a suspension of particles. The flow rate was increased to 400 $\mu$L h$^{-1}$ (930 $\mu$m s$^{-1}$ in the chamber) and, once a steady stream of particles could be observed across the separation chamber, the magnet was positioned as described above.

As the particles traversed the separation chamber they experienced a deflection from laminar flow towards the magnet, exiting the chamber via one of the 16 outlets.[358,383] The outlet directly opposite the sample inlet was labelled outlet 1, with the remaining outlets numbered consecutively until outlet 16, which was furthest away from the sample inlet and actually underneath the magnet. Two studies were undertaken using this experimental setup. Firstly, the effect of temperature on the deflection behaviour of M-270 particles was investigated over a range of 5 – 50 °C, with the number of particles exiting the chamber recorded with respect to the outlet that they passed through. Secondly, the effect of temperature on the separation of M-270 and MyOne particles from a mixture was determined at 5, 20 and 50 °C.

## 2.5.9 Theoretical particle trajectories
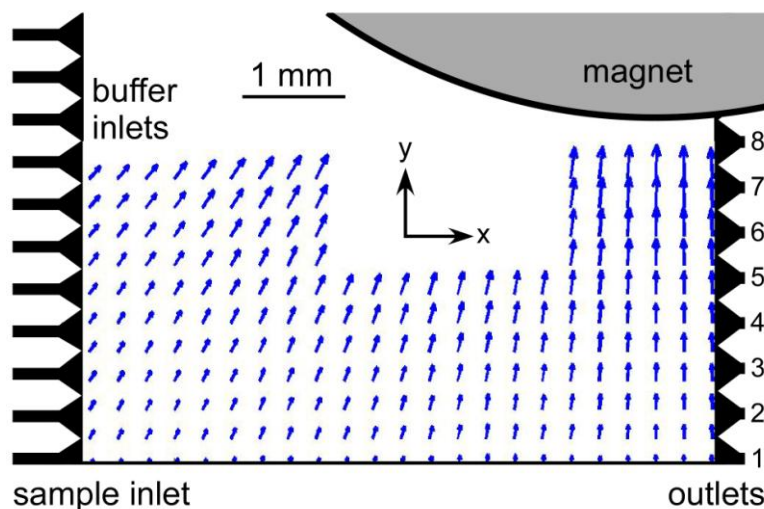


**Fig. 54  Map of the magnetic gradient over the FFM1 magnetophoresis chip, with blue arrows representing the magnitude and direction of the gradient.  An arrow of 1 mm length on the given scale represents a gradient of 60 T m$^{-1}$, hence the gradient in the chamber ranges from ~7 T m$^{-1}$ in the bottom-left corner to ~21 T m$^{-1}$ in the top-right corner.  Only eight outlets are shown as the magnet was placed over the remaining eight.**

Theoretical trajectories of the particles were calculated and simulated by Damien Robert (Université Paris-Diderot, Paris, France) using a Runge-Kutta algorithm that allowed the particle paths to be determined under given conditions, i.e. flow rate, viscosity of the solution, and particle type.  The program utilised a map of the magnetic field gradient across the separation chamber, as described by Pamme *et al.*[360]  To obtain the magnetic field map, particles were introduced into the separation chamber of the chip and, in the absence of applied hydrodynamic flow, became stationary.  The 10 mm Ø x 5 mm disc magnet was moved quickly into position using a micromanipulator, and the subsequent movement of the particles towards the magnet was recorded.  The measured particle velocities, along with magnetic saturation data and particle radii, were used to determine

the strength of the magnetic field in different areas across the chip, thus allowing the gradient map to be prepared. The resultant gradient across the chamber is shown in Fig. 54, with the magnitude and direction of the gradient illustrated with blue arrows. An arrow of 1 mm length on the given scale would be equivalent to a 60 T m$^{-1}$ gradient, thus typical gradients in the chamber were ~7 T m$^{-1}$ in the weakest regions to ~21 T m$^{-1}$ in the strongest regions.

## *2.6    Multilaminar flow processes*

This section describes the general setup and experimental conditions for performing investigations into multilaminar flow processes on mobile magnetic particles.

### 2.6.1    Microfluidic chip setup and interfacing

Chip designs MLF1 and MLF2 were utilised for the multilaminar flow investigations. For most of the experiments described here, 16 cm lengths of fused silica capillaries (150 μm i.d., 363 μm o.d., Polymicro Technologies LLC, Composite Metal Services Ltd., Shipley, UK) were inserted into the inlet holes and glued in place using Araldite Rapid Glass & Ceramic epoxy resin (B & Q, Hull, UK). 1 cm sections of capillary (150 μm i.d.) were glued into each of the access holes of design MLF2. However, due to the outlet system of chip design MLF1, a 10 cm length of capillary (100 μm i.d.) was glued into the particle outlet hole, while a 1 cm piece of capillary (150 μm i.d.) was glued into the reagent waste hole. This was to increase the back pressure in the narrower particle outlet to ensure even pressure distribution throughout the chip.

To avoid long gluing times and problems with blocked channels when glue seeped into the inlet or outlet holes, two chip holders were fabricated late in the project in which chips could be fixed in place and the capillaries introduced and sealed without the need for glue. Both chip holders were designed by the author in collaboration with Nigel Parkin (Workshop manager, Department of Chemistry, University of Hull), and were fabricated in-house from aluminium. Chip holder (A) was built in two identical sections, each consisting of a bottom plate onto which the chip was placed, with a top plate placed over the inlet holes of the chip and screwed into the lower plate (Fig. 55a). The top plate featured a matrix of holes, each 5 mm apart, such that the access holes of the chip could be aligned to allow capillaries to be connected to the chip. The two sections of chip holder were held together by a pole that passed through a hole in each of the bottom plates, which allowed the sections to moved closer together or further apart to accommodate a range of chip sizes.

Chip holder (B) differed in that the bottom plate was one large piece with a viewing hole in the centre (Fig. 55b). Here, the chip was placed over the viewing hole, then top plates screwed over the inlet and outlet holes, again featuring a matrix of holes (5 mm apart) that aligned with the chip access holes. The bottom plate featured multiple holes for the top plates to screw into, thereby allowing a range of chip sizes to be used in the device. For both chip designs, capillaries were interfaced to the chip by inserting the end of a piece of capillary into a NanoPort Ferrule (6-32 Flat Bottom-360/510µm, Presearch Limited, Hampshire, UK), placing this through a hole in the top plate, and screwing a TinyTight PEEK nut (Super Flangeless Fittings for 6-32 FB (Flat Bottom) Ports, Presearch Limited) into the hole that forced the ferrule against the chip surface, thus sealing the capillary against the chip (Fig. 56).
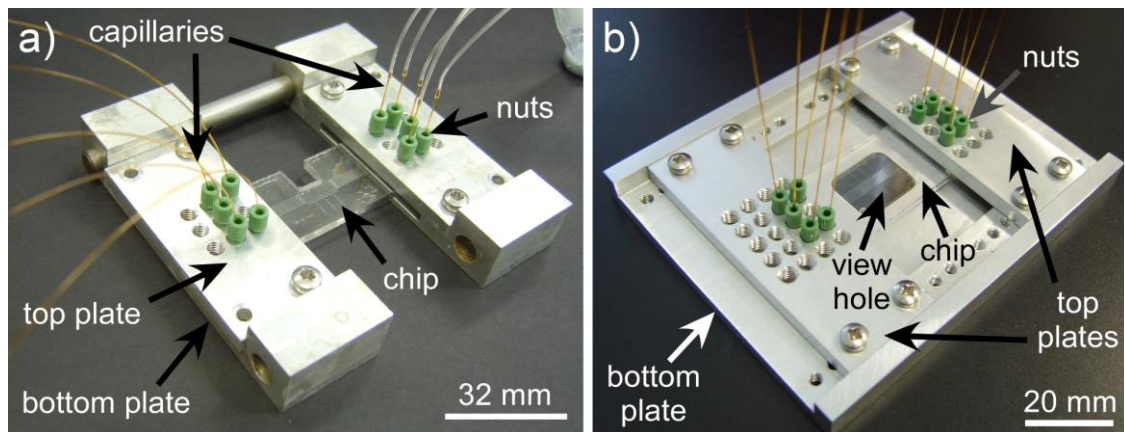
**Fig. 55** **Photographs of the chip holders fabricated in-house, and the nuts used to connect the capillaries to the chip.  a) Chip holder design (A), consisting of sliding sections to accommodate different sized chips.  b) Chip holder design (B), which consisted of a single bottom plate with a viewing hole, and multiple screw holes for connecting to the top plates, allowing different sized chips to be inserted.**
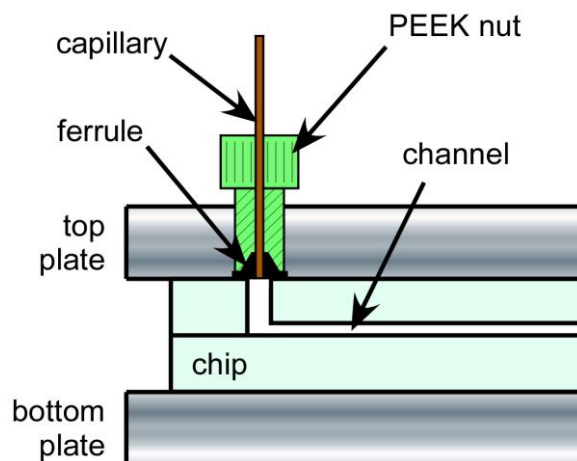


**Fig. 56   Schematic demonstrating the interfacing of capillaries to a microfluidic device when using a chip holder.  The capillary is held by a ferrule that covers the inlet hole of the chip, and the ferrule is sealed against the chip by a PEEK nut that screws directly into the chip holder.**

As well as reducing chip setup times, the holders had the advantage of reducing the problems encountered due to air bubbles. On many occasions before using the holders, despite care taken during experiments to exclude air from entering the system, it was not always possible. Air bubbles would sometimes become "stuck" behind a capillary that was glued into a hole, introducing the possibility of smaller air bubbles breaking away from the stuck bubble and entering the chamber. Air bubbles in the chamber could affect the laminar flow and particle trajectories, and the effect was particularly prominent when using negative pressure. When using the chip holders the capillaries were held in place above the hole, which therefore prevented air bubbles from becoming trapped.

Whether the capillaries were glued into a chip or a holder was used for the connections, the subsequent steps remained the same for each setup. Tygon tubing (0.254 mm i.d., 0.762 mm o.d., Cole-Parmer) was attached to each of the outlet capillaries and fed into a sample vial for waste collection. Tefzel ferrules (1/16 inch, Anachem Ltd., Bedfordshire, UK), with a sleeve of poly(tetrafluoroethylene) tubing (PTFE, 0.3 mm i.d., 1.58 mm o.d., Supelco, Dorset, UK) inside them, and PEEK nuts (1/16 inch, Anachem Ltd.) were attached to the ends of each inlet capillary by inserting the capillary into the PTFE sleeve, and the chips then underwent a washing procedure. The washing solutions varied depending on the experiment. A PEEK syringe adaptor (1/4-28 Female to Female Luer adaptor, Anachem Ltd.) was screwed onto the nut of one of the capillaries, and the first washing solution was pumped through the chip via a 1 mL syringe (BD Plastipak, Becton Dickinson UK Ltd., Oxford, UK). When finished, the syringe was carefully removed from the adaptor with slight pressure on the plunger, such that the adaptor was filled with liquid as the syringe was removed. A syringe containing the next solution was then pushed into the adaptor, with the liquid on the end of the syringe and that in the adaptor contacting before the syringe was fully inserted,

ensuring that no air was between the two solutions when the connection was finished. These steps were repeated for each washing step, then the PEEK syringe adaptors were attached to the remaining inlet capillaries and the liquid in the syringe was pushed carefully through the chip such that the adaptors became filled with the solution. The syringe was then removed from the adaptor, again while filling the adaptor with solution in the process. At this point, the chip was set up for using either positive or negative pressure.

When positive pressure was used, syringes of the appropriate particles and reagents were loaded onto a syringe pump with a multi-syringe rack (PHD 22/2000, Harvard Apparatus). Pressure was applied until each syringe had a drop of liquid on the end of the syringe. The adaptors on each capillary were carefully connected to each syringe, with the liquid at the end of each syringe and in the adaptors ensuring that the connections took place in liquid to minimise the possibility of air entering the system. The syringe pump was activated to start pumping the particle suspensions, reagents and buffers through the chip if using positive pressure. When using negative pressure, the same process was applied except that the syringes simply contained a small volume of washing buffer solution Negative pressure was only used with chip design MLF2, and involved particles, reagents and washing buffers being contained in Eppendorf tubes and fixed near the outlets of the chip. A 1 cm length of fused silica capillary (250 μm i.d., 363 μm o.d., Composite Metal Services Ltd.) was inserted into the open end of each piece of Tygon tubing connected to the chip, as particles would not enter the Tygon tubing itself without the capillary present, possibly due to some electrostatic repulsion effect with the plastic tubing. Once the short lengths of capillary were inserted, pressure was applied to the syringes until a drop of solution was on the end of each capillary. They were then placed into the appropriate Eppendorf tubes and negative pressure applied via the syringe pump to draw the solutions through the chip.

## 2.6.2    Magnet setup

Most commonly, a 4 x 4 x 5 mm$^3$ rectangular NdFeB magnet (Magnet Sales UK) was placed on top of the chip, next to the chamber, as shown in Fig. 57. The magnetic flux density at the surface of the 4 x 4 x 5 mm$^3$ magnet was determined to be 561 mT with Equation 18, while the value for the 6 mm Ø x 3 mm disc magnet was 435 mT. Using the surface flux density value and FEMM 4.2 software, the magnetic flux density was simulated across the chamber in two orientations, the first from a top-down perspective (Fig. 58a) and the second from a side-on view (Fig. 58b). The average value of **B** across the chamber was calculated to be 135.5 mT, with a gradient ($\nabla$**B**) across the chamber of 43.8 mT mm$^{-1}$, and an estimated (**B**·$\nabla$)**B** value of 5.9 T$^2$ m$^{-1}$.
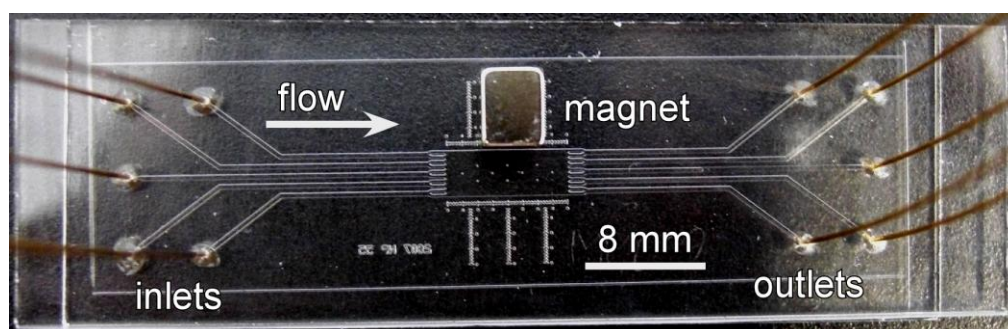


**Fig. 57  Photograph of chip design MLF2 with the 4 x 4 x 5 mm$^3$ NdFeB magnet placed on top of the chip, next to the reaction chamber, and fused silica capillaries in the access holes.**
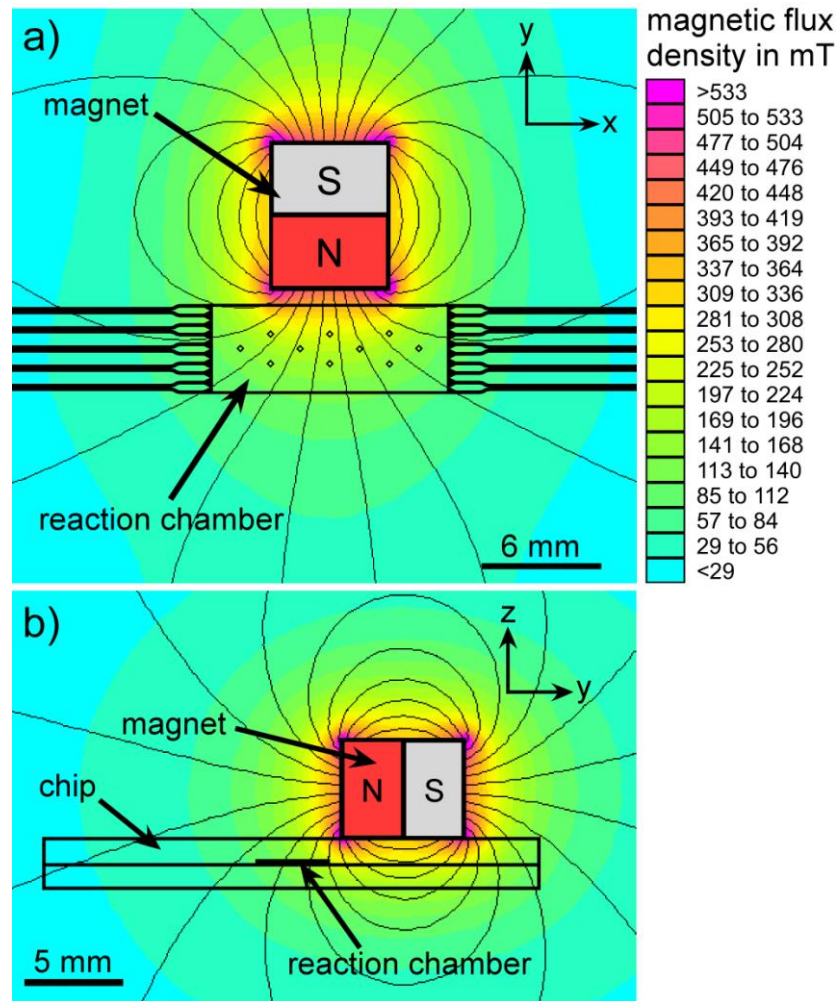
**Fig. 58  FEMM simulation of the magnetic flux density of a 4 x 4 x 5 mm³ NdFeB magnet across the microfluidic chamber from a) a top-down viewpoint, and b) a side-on cross-sectional view.**

When a magnet was placed onto the chip surface, magnetic particles in the chamber experienced not only an attractive force in the y-direction but also upwards, in the z-direction, which could result in particles being drawn towards the top of the chamber and becoming stuck against the surface of the chamber.  Therefore, by positioning a magnet in the same horizontal plane as the particles they would experience no upwards force, and so should flow through the chamber without being pulled against the chip surfaces, thus helping to reduce sticking.  With this in mind, some of the MLF2 design

chips had a section of glass cut out next to the chamber so that the magnet could be placed in line with the chamber. An example of a chip with a section of glass cut out is shown in the chip holder in Fig. 55a. When this setup was used, a 6 mm Ø x 3 mm NdFeB disc magnet was placed in this position rather than the rectangular magnet used above, and a FEMM simulation of this is shown in Fig. 59. The average value of **B** across the chamber was 122.4 mT, with a gradient ($\nabla$**B**) of 83.3 mT mm$^{-1}$, giving an estimated (**B**·$\nabla$)**B** value of 10.2 T$^2$ m$^{-1}$.
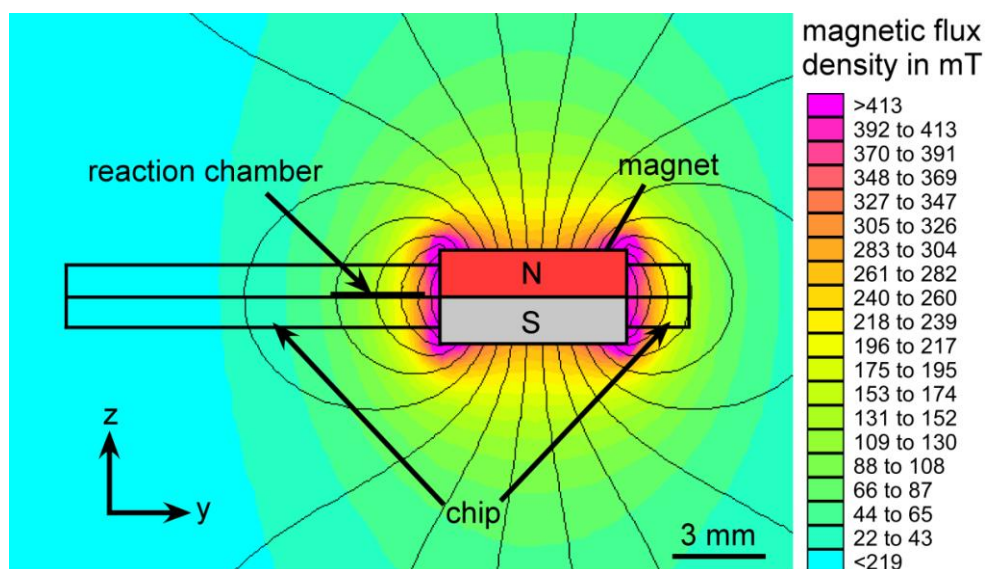


**Fig. 59  Cross-sectional FEMM simulation of the magnetic field across the chip when a 6 mm Ø x 3 mm disc magnet was placed in the same plane as the microfluidic chamber.**

### 2.6.3   Particle visualisation

The chips were placed onto the stage of either a Nikon TE-2000 or Nikon Ti inverted fluorescence microscope (Nikon Instruments Europe B.V., Surrey, UK), equipped with 2x, 4x, 10x, 20x, and 40x objectives (Fig. 60). Videos and images were captured using either a high sensitivity, black and white, cooled CCD camera (Retiga-EXL, QImaging,

Media Cybernetics UK, Buckinghamshire, UK) and Image-Pro Plus 6 software (Media Cybernetics UK) on the TE-2000 microscope, or a lower sensitivity, colour CCD camera (MTV-63V1N, Mintron Enterprise Co. Ltd., Taipei Hsien, Taiwan) and WinDVD Creator 2 software (InterVideo (Corel UK Ltd.), Berkshire, UK) on the Ti microscope. Therefore, the TE-2000 microscope was used when high sensitivity was required for capturing images with low fluorescence signals, whilst the Ti microscope was used when high sensitivity was not necessary and/or when a colour image was required. Fluorescence images were obtained by employing either an ultra-violet filter cube (UV-2A, excitation filter wavelengths (EX) = 330-380 nm, dichromatic mirror cut-on wavelength (DM) = 400 nm, barrier filter wavelength (BA) = 420 nm) or a blue light filter cube (B-2A, EX = 450-490 nm, DM = 500 nm, BA = 515 nm) on the microscope, depending on the fluorescent tag being observed.
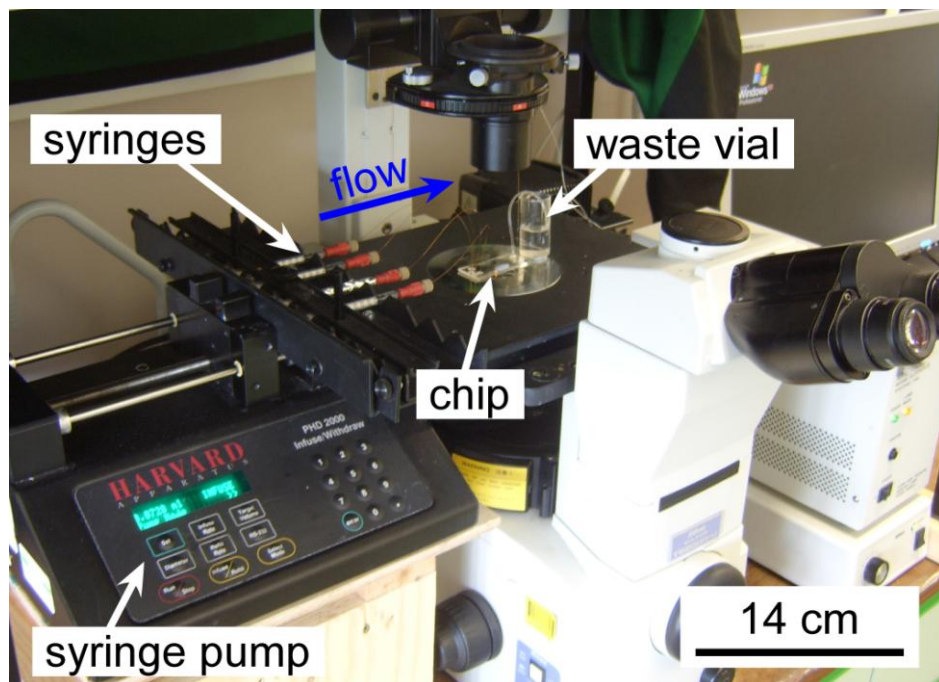


**Fig. 60  Photograph of the chip setup on the stage of an inverted fluorescence microscope (Nikon TE-2000), with a syringe pump for the introduction of particles and solutions.**

This setup was used to study the following processes in continuous flow: (i) a fluorescamine reaction, (ii) amide bond formation via carbodiimide coupling, (iii) polyelectrolyte deposition onto magnetic templates, and (iv) a C-reactive protein sandwich immunoassay.

## *2.7 Fluorescamine reaction*

### 2.7.1 Buffers and solutions

Borate buffer was prepared by the dropwise addition of 3 M sodium hydroxide to a solution of 0.16 M boric acid to give a final pH of 9.60, as measured by a pH meter. Tween20 was added to a concentration of 0.1 % w/w. A 1.8 mM (501 $\mu$g mL$^{-1}$) solution of fluorescamine was prepared by dissolving 50 mg fluorescamine (Fluram, $\lambda_{ex}$ = 390 nm, $\lambda_{em}$ = 475 nm, Sigma-Aldrich) in 100 mL acetone. A solution of blue coloured ink was prepared by diluting filtered fountain pen ink (Parker, Staples, Hull, UK) ten times in borate buffer.

### 2.7.2 Magnetic particle suspensions

Dynabeads M-270 Amine particles (2.8 $\mu$m diameter), as described in Section 2.1.2, were purchased from Invitrogen as an aqueous suspension. 10 $\mu$L of Dynabeads M-270 Amine particle (2.8 $\mu$m diameter) suspension was pipetted into an Eppendorf tube. 990 $\mu$L borate buffer solution was added, and the suspension was vortexed for 20 s. The particles were washed by collecting them to one side of the tube via an external permanent magnet, removing the supernatant, and adding fresh borate buffer. This

process was repeated twice more to ensure that the particles were thoroughly washed. Finally, they were resuspended in 1000 μL borate buffer to give a concentration of 2 x $10^7$ particles mL$^{-1}$, and stored at 4 °C until ready to use.

### 2.7.3    Off-chip tests

To ensure that the reaction worked using the prepared solutions, it was first tested in an off-chip experiment.  100 μL of the aqueous 2 x $10^7$ particles mL$^{-1}$ was added to 100 μL of the 1.8 mM fluorescamine solution in a 1.5 mL Eppendorf tube.  Two tests were performed, with the fluorescamine dissolved in either acetone or ethanol to check that the reaction was feasible in each solution.  The suspensions were covered in tin foil to avoid photobleaching, vortexed for 20 s, and allowed to incubate for 5 min with agitation.  The particles were collected at the side of the tube for 2 min using a magnet, the supernatant removed, and the particles washed three times with borate buffer, before being resuspended in buffer.  A drop of the suspension was added to a microscope slide, covered with a cover slip, and observed under the fluorescence microscope (UV-2A filter).  Unreacted particles were also observed under the microscope in borate buffer to compare particle fluorescence intensities before and after the reaction.

### 2.7.4    On-chip tests

For the one-step fluorescamine reaction, chip design MLF1 (see Fig. 42) was used with surfaces either left untreated, or treated with OTS or FDTS silanising agents (see Section 2.4) to render them hydrophobic and uncharged.  The chip was washed by flushing consecutively with ethanol, water and borate buffer solution.  The setup was as

described in Section 2.6.2, with a 4 x 4 x 5 mm$^3$ NdFeB magnet placed on top of the chip, next to the chamber, and capillaries glued into the access holes. The particle suspension was introduced into inlet 1, borate buffer (washing solution) in inlets 2 and 4, and 1.8 mM fluorescamine (in acetone) in inlet 3 (Fig. 61). The principle of this setup was that the amine functionalised particles would enter the chamber and deflect in the y-direction towards the magnet, thus crossing the fluorescamine stream and entering the borate buffer washing solution in stream 4. A TE-2000 microscope was used to capture bright field and fluorescence (via a UV-2A filter cube) images of the particles in the chamber, and the flow rate applied by the syringe pump was 15 $\mu$L h$^{-1}$ (278 $\mu$m s$^{-1}$).
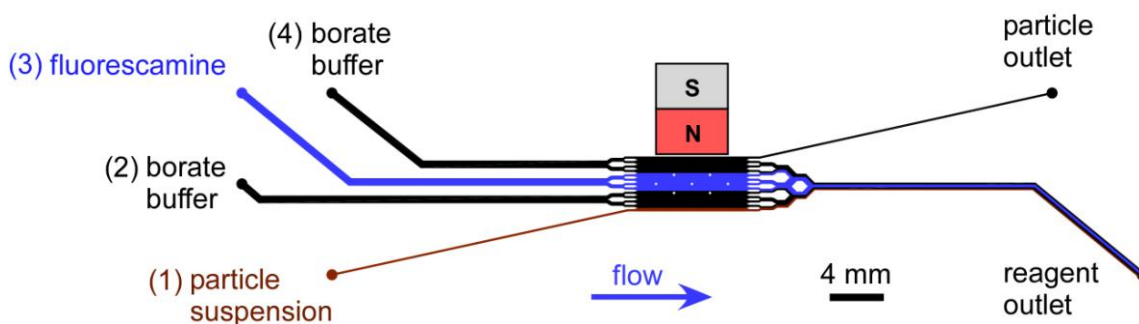


**Fig. 61    Schematic of the setup of chip design MLF1 for performing a one-step fluorescamine reaction in continuous flow.  Magnetic particles were pumped into inlet 1, and fluorescamine solution in inlet 3.**

## *2.8    Amide bond formation*

### 2.8.1    Buffers and solutions

A 100 mM solution of MES buffer was prepared by dissolving 2.13 g of 2-(-*N*-morpholino)ethanesulfonic acid (MES) in 100 mL water, and adjusted to pH 5. This

solution was diluted to 25 mM, and the pH adjusted to a range between 5 and 7. PBS buffer was prepared by dissolving a 5 g PBS tablet in 500 mL water, and the pH of the solution was varied between 6.45 and 8.45. Tween20 was added to a concentration of 0.1 % w/w. For some of the experiments, the cationic surfactant CTAB was added to a concentration of 0.01 % or 0.1 % w/v. A 10 $\mu$g mL$^{-1}$ (24.73 $\mu$M) solution of fluorescently labelled glycine was prepared by dissolving 1 mg of fluoresceinyl glycine amide (5-(aminoacetamido)fluorescein, FGA, Invitrogen) in 100 $\mu$L MES buffer. EDC (*N*-(3-dimethylaminopropyl)-*N*'-ethylcarbodiimide hydrochloride, Sigma-Aldrich) was prepared immediately prior to use by dissolving 10 mg of solid EDC in 500 $\mu$L cold buffer solution (either MES, PBS or purified water).

## 2.8.2 Magnetic particle suspensions

10 $\mu$L of Dynabeads M-270 Carboxylic Acid particle suspension (Section 2.1.2) was pipetted into a 1.5 mL Eppendorf tube and 990 $\mu$L PBS buffer (pH 7.45, with 0.1 % w/v Tween 20) was added. The particles were washed three times with PBS buffer, giving a 2 x 10$^7$ particles mL$^{-1}$ concentration that was stored at 4 °C. Particles at this point were used either in one-step or two-step reactions on-chip. Immediately prior to one-step reactions, 200 $\mu$L of the particle suspension was added to a 1.5 mL Eppendorf tube, the particles collected via a magnet, and the supernatant removed. 200 $\mu$L of freshly prepared EDC solution was added and the suspension incubated for 30 min with agitation. The supernatant was removed, the particles washed quickly with cold washing buffer (MES, PBS or water) and finally resuspended in 200 $\mu$L cold buffer.

### 2.8.3 Off-chip tests

To test that the reaction worked, off-chip tests were performed. 100 μL of the EDC-activated particles were added to an Eppendorf tube, the particles collected via a magnet and the supernatant removed. 100 μL of the fluoresceinyl glycine amide (FGA) solution (in MES buffer, except where stated) was added, the tube wrapped in aluminium foil to avoid photobleaching of the fluorescent tag, then vortexed for 20 s and incubated for 15 min with agitation. The particles were collected to the side of the tube for 5 min using an external magnet and washed three times with PBS buffer solution (except where stated). The fluorescence intensities of the particles were measured (i) before EDC activation, (ii) after EDC activation, and (iii) after the FGA reaction, using the Nikon TE-2000 microscope with a B-2A filter, as described in Section 2.6.3. In some cases, CTAB surfactant was added to a concentration of 0.01 % or 0.1 % w/v, at first in an attempt to reduce particle sticking, and later due to the effect of added CTAB on the observed particle fluorescence. Additionally, off-chip tests were performed to evaluate the effect of different pH buffers on the reaction, which included studying the effect of MES buffer pH on the reaction between pH 5 and 7, and the effect on detection of suspending the fluorescent particles in MES buffer between pH 5 and 7 and in PBS buffer between pH 6.45 and 8.45. The lifetime of EDC-activated particles were also examined by first activating a suspension of particles, then reacting a portion of these particles with FGA every 10 min to determine the time after which the FGA reaction would not work.

## 2.8.4    On-chip one-step reaction

Chip design MLF2 was used to perform one-step amide bond formation reactions (Fig. 43). The chip was set up as described in Section 2.6.1, with capillaries glued into the access holes, a 4 x 4 x 5 mm$^3$ NdFeB magnet placed next to the chamber, and solutions were pumped through the chip using either positive pressure (flow rate = 10 - 12 $\mu$L h$^{-1}$ (232 - 278 $\mu$m s$^{-1}$ in the chamber)) or negative pressure (flow rate = 10 $\mu$L h$^{-1}$ (232 $\mu$m s$^{-1}$ in the chamber)). Prior to experiments, the chip was flushed consecutively with IPA-KOH solution, water, and buffer solution, either MES or PBS depending on which was to be the main washing solution throughout the experiment. Since the chip design was symmetrical, the numbering of inlets remained the same whether positive or negative pressure was used. EDC-activated particles were introduced into inlet 1, washing buffer into inlets 2, 4 and 5, and FGA solution into inlet 3 (Fig. 62). Initial experiments were performed using MES buffer for all solutions, but in later studies PBS was used for all solutions except for the FGA, which was dissolved in MES buffer.
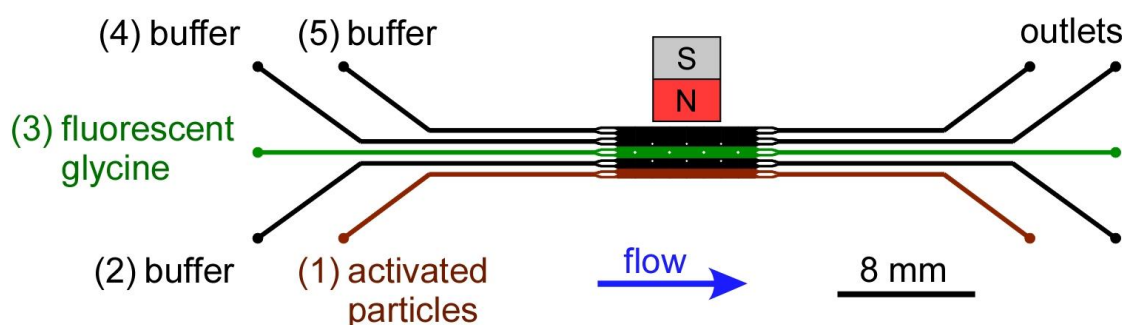


**Fig. 62   Schematic of the chip setup for performing one-step peptide synthesis in chip design MLF2.   Carboxylic acid particles were activated with EDC off-chip before being pumped through the device.   The schematic demonstrates the process as performed using positive pressure, when using negative pressure the solutions were introduced into the access holes on the right and pumped towards the left.**

To increase the residence time of particles in the FGA stream, an experiment was performed in which FGA solution in MES buffer was introduced into inlets 2 to 4. CTAB surfactant was added to all solutions for some experiments to a concentration of 0.1 % w/v. Some experiments involved the use of a chip with a section of glass cut out so that the magnet could be placed in line with the chamber, and in some experiments the chip surfaces were treated with either OTS, FDTS, PEG-silane, PEG-SPA or QAS solutions (see Section 2.4) to try to reduce the extent to which particles stuck to the chip surfaces. If the chip was treated with a silanising agent, it was flushed consecutively with ethanol, water and buffer solution prior to experiments, rather than using IPA-KOH in order to avoid potential damage to the coating.

### 2.8.5 On-chip two-step reaction

Chip design MLF2 was used for two-step peptide synthesis reactions, and either positive or negative pressure was applied. The chip was flushed as described previously. Capillaries were glued into the chip, and the 4 x 4 x 5 mm$^3$ NdFeB magnet was placed on top of the chip, next to the chamber. Here, particles were not activated with EDC prior to their introduction into the chip, with the EDC step now incorporated into the on-chip reaction. Carboxylic acid particles were pumped through inlet 1, EDC solution through inlet 2, fluoresceinyl glycine amide through inlet 4, and washing buffer through inlets 3 and 5 (Fig. 63). In the initial experiments, all of the solutions were prepared in MES buffer, while in later experiments only the FGA solution was prepared in MES buffer and the remaining solutions in PBS buffer.
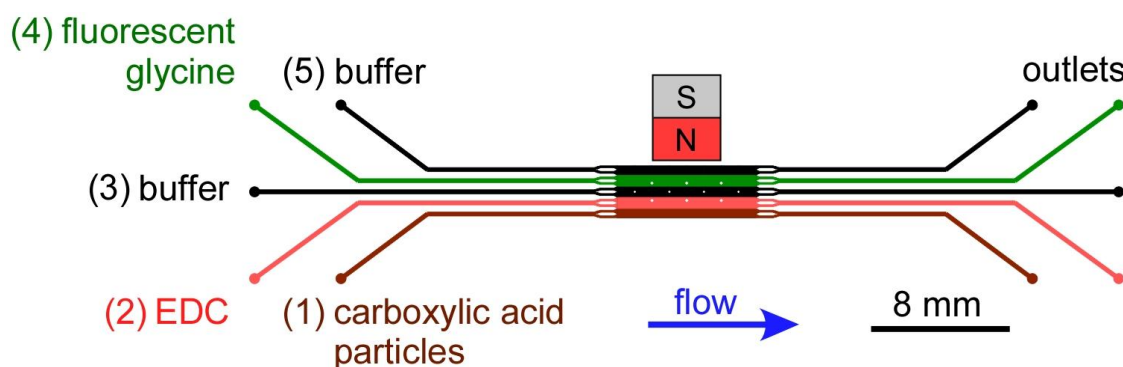
**Fig. 63 Schematic of the two-step peptide synthesis reaction. Carboxylic acid particles are pumped into the chip and deflected through streams of carbodiimide (EDC) and fluorescently labelled glycine.**

## *2.9 Polyelectrolyte deposition*

## 2.9.1 Buffers and solutions

Poly(fluorescein isothiocyanate allylamine hydrochloride), a fluorescently labelled and positively charged (cationic) polyelectrolyte (PAH-FITC, Sigma-Aldrich) was prepared to a concentration of 20 μg mL$^{-1}$ (357.14 nM) in 0.01 M sodium chloride solution (BDH Laboratory Supplies). 0.01 M sodium chloride solution was used as the washing buffer. 0.1 % w/w Tween20 was added to all solutions to help reduce particle sticking to each other and to the chip surfaces.

## 2.9.2 Magnetic particle and cell suspensions

For the polyelectrolyte deposition experiments, two types of magnetic templates were employed: particles and cells. Dynabeads M-270 Carboxylic Acid particles were

washed and diluted from the $2 \times 10^9$ particles mL$^{-1}$ stock suspension to a concentration of $1 \times 10^7$ particles mL$^{-1}$ in 0.01 M NaCl. The suspension was stored at 4 °C. Magnetic yeast cells were supplied by Dr Rawil F. Fakhrullin (Department of Biochemistry, Kazan State University, Tatarstan, Russian Federation, and the Department of Chemistry at the University of Hull).[419] In brief, Baker's yeast cells (*S. cerevisiae*), negatively charged in water, were coated with the cationic polyelectrolyte, poly(allylamine hydrochloride) (PAH, Sigma-Aldrich, $\lambda_{ex}$ = 495 nm, $\lambda_{em}$ = 521 nm), followed by the anionic polyelectrolyte, poly(4-styrenesulfonic acid) (PSS, Sigma-Aldrich). Concentrations of PAH and PSS were 10 mg mL$^{-1}$ in 0.5 M NaCl, and each solution was incubated with the cell solution for 10 min before being centrifuged and washed three times with purified water. Another PAH layer was added, before the cells were added to a suspension of anionic tetramethylammonium-stabilised $Fe_3O_4$ magnetic nanoparticles (MNPs) for 15 min and washed with water. A layer of PAH and a final layer of PSS were added to the cells, yielding negatively charged magnetic yeast cells with the following architecture: cell/PAH/PSS/PAH/MNPs/PAH/PSS.

### 2.9.3  Off-chip tests

The polyelectrolyte deposition procedure was tested off-chip for the Dynabeads M-270 Carboxylic Acid particles. 100 μL of the suspension prepared above was added to 100 μL of PAH-FITC in an Eppendorf and incubated for 15 min. The particles were collected for 5 min using an external magnet, washed three times with NaCl, and resuspended in 100 μL NaCl. Fluorescence images of the coated and uncoated particles were taken using the Nikon TE-2000 microscope.

## 2.9.4    On-chip tests of particles and cells

Chip design MLF1 and MLF2 were used for the polyelectrolyte deposition experiments, and the setup was identical for both types of magnetic templates. The chips were prepared by washing consecutively with ethanol, water, and 0.01 M NaCl solution. Magnetic templates were introduced into inlet 1 and polyelectrolyte solution into inlet 3 (Fig. 64). Sodium chloride washing solutions were pumped through inlets 2 and 4 (and 5 when using chip design MLF2). Particles were deflected using either a 4 x 4 x 5 mm$^3$ NdFeB magnet placed on top of the chip, or a 6 mm Ø x 3 mm NdFeB disc magnet situated in line with the microfluidic chamber. Experiments were performed in an untreated chip, an FDTS treated chip, and a PEG-silanised chip.
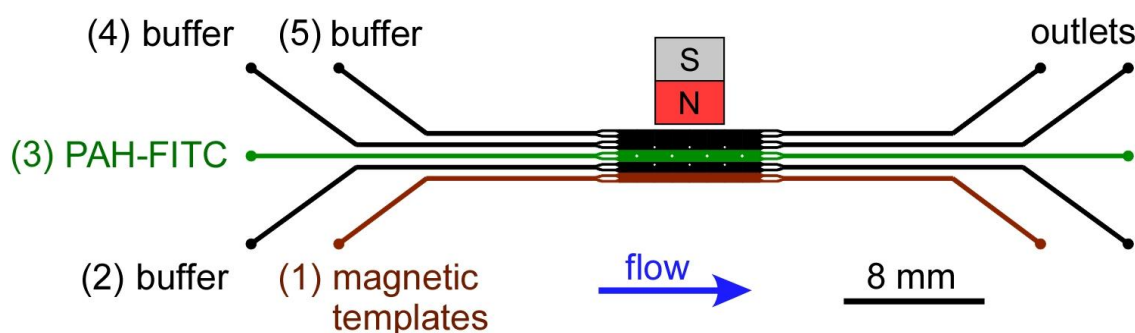
**Fig. 64  Schematic of MLF2 used for performing cationic polyelectrolyte deposition (inlet 3) onto anionic magnetic particles or cells (inlet 1).**

## *2.10    C-reactive protein immunoassay*

### 2.10.1  Buffers and solutions

PBS buffer (pH 7.45) was prepared as described previously, with 0.01 % w/v bovine serum albumin (BSA, Sigma-Aldrich) added to reduce non-specific binding of reagents and particle sticking.  The primary CRP antibody, biotinylated monoclonal mouse anti-human C-reactive protein (1° Ab), was purchased from R&D Systems (Oxfordshire, UK) as a lyophilised powder and reconstituted in PBS to a concentration of 50 $\mu$g mL$^{-1}$. Recombinant human C-reactive protein (CRP) was also purchased from R&D Systems as a lyophilised powder, and was reconstituted in tris buffer (20 mM, pH 8) with 0.1 % BSA (as per the manufacturer's instructions) to a concentration of 200 $\mu$g mL$^{-1}$.  The secondary CRP antibody, polyclonal goat anti-human C-reactive protein conjugated to fluorescein isothiocyanate (2° Ab-FITC, $\lambda_{ex}$ = 495 nm, $\lambda_{em}$ = 521 nm) was purchased from Abcam plc. (Cambridgeshire, UK) as an aqueous solution at a concentration of 10 mg mL$^{-1}$.  Prior to performing experiments the 1° Ab, CRP and 2° Ab-FITC solutions were each diluted in PBS to a concentration of 10 $\mu$g mL$^{-1}$.

### 2.10.2  Magnetic particle suspension

Dynabeads M-270 Streptavidin magnetic particles were purchased from Invitrogen as described in Section 2.1.2.  10 $\mu$L of Dynabeads M-270 Streptavidin particle suspension was added to an Eppendorf tube, followed by 200 $\mu$L of the 10 $\mu$g mL$^{-1}$ 1° Ab solution, and the mixture was incubated for 30 min with agitation to ensure that the biotinylated antibodies became bound to the streptavidin groups on the particles.  The particles were

then washed three times with PBS and resuspended in 1000 μL PBS buffer (containing 0.01 % BSA) to give a final concentration of 6.7 x $10^6$ particles $mL^{-1}$.

### 2.10.3  Off-chip tests

The CRP sandwich immunoassay was tested by performing off-chip studies.  200 μL of the activated (1° Ab) particle suspension was added to an Eppendorf tube, the supernatant removed, and 200 μL of the CRP solution added.  The particle suspension was incubated for 15 min with agitation, then washed three times with PBS buffer. After the PBS solution was removed for the last time, 200 μL of the 2° Ab-FITC solution was added and the particles incubated with agitation for a further 15 min.  The particles were then washed three times with PBS and the fluorescence intensity of the particles before and after the reaction were measured using a Nikon TE-2000 microscope with a B-2A filter, as described in Section 2.6.3.  A negative test was also performed in which the above steps were repeated minus the CRP step, to check that no fluorescence increase was observed when no CRP was present.

### 2.10.4  On-chip tests

Chip design MLF2 was used for the CRP sandwich immunoassays, and was set up as described in Section 2.6.1, with either positive or negative pressure applied, and a 4 x 4 x 5 $mm^3$ NdFeB magnet placed on top of the chip, next to the chamber.  Initial experiments were performed using untreated chips with glued capillaries, and the devices were washed consecutively with IPA-KOH solution, water and PBS buffer.  In later experiments the chip was treated with agarose gel, the procedure for which is

detailed in Section 2.4, and a chip holder was employed. In the latter scenario, the chip was washed consecutively with ethanol, water and PBS buffer. Magnetic particles with $1°$ Ab bound to the surface were pumped through inlet 1 of the chip, CRP solution (10 $\mu$g mL$^{-1}$ or 5 $\mu$g mL$^{-1}$) through inlet 2, $2°$ Ab-FITC solution through inlet 4, and PBS washing buffer through inlets 3 and 5 (Fig. 65). A Nikon TE-2000 microscope was used to capture fluorescence images with a B-2A filter.
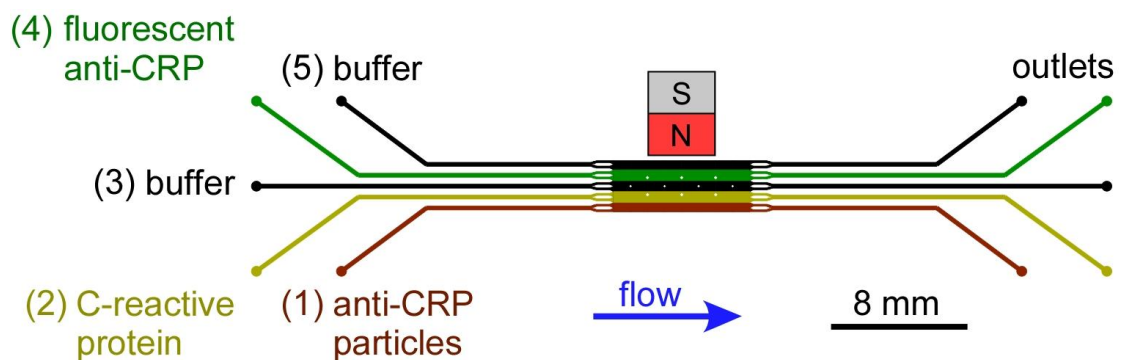


**Fig. 65 Schematic of the setup of chip design MLF2 for performing a C-reactive protein sandwich immunoassay in continuous flow. Particles featuring primary CRP antibodies were deflected across a stream of CRP, where the reagent became bound to the particles, before being labelled in a stream containing fluorescently labelled CRP secondary antibodies.**

## *2.11    Diamagnetic repulsion*

The following sections describe experimental setups for using diamagnetic repulsion to manipulate particles and cells in continuous flow, by suspending them in paramagnetic media and applying relatively high magnetic fields and gradients. Investigations included studies into (i) the deflection behaviour of polystyrene particles in manganese

(II) chloride solution, (ii) the deflection of streptavidin coated polystyrene particles out of a biotin reagent stream, towards performing multilaminar flow reactions, and (iii) continuous flow focussing of polystyrene particles and cells using magnets.

### 2.11.1 Particle deflection behaviour

**Manganese (II) chloride solution**

Solutions of 6 %, 10 % and 20 % w/w paramagnetic aqueous manganese (II) chloride ($MnCl_2$) were prepared by dissolving the appropriate mass of manganese (II) chloride tetrahydrate in water to give final concentrations corresponding to 0.48 M, 0.79 M, and 1.59 M, respectively.  0.01 % w/v sodium dodecyl sulphate (SDS) surfactant was added to all solutions to prevent particles from sticking to each other and to the microfluidic surfaces.  The solutions were degassed using a vacuum pump prior to further use. Viscosity measurements of the 6 % and 10 % $MnCl_2$ solutions were undertaken at 20 °C as described for the glycine saline solutions in Section 2.5.3.  The density data was provided by Dr Noriyuki Hirota (National Institute for Materials Science (NIMS), Tsukuba, Japan).

**Preparation of particle suspensions**

Polystyrene particles of 5 μm and 10 μm diameter (Section 2.1.3) were obtained with concentrations of $1.21 \times 10^8$ and $1.87 \times 10^7$ particles $mL^{-1}$, respectively.  These were diluted 5 in 1000 times in the appropriate $MnCl_2$ solution (e.g. 100 μL particle suspension in 20 mL $MnCl_2$) to yield final particle concentrations of $6.05 \times 10^5$ particles $mL^{-1}$ and $9.35 \times 10^5$ particles $mL^{-1}$ for the 5 μm and 10 μm particles, respectively.

**Microfluidic chip setup and interfacing**

Chip design FFM2 was utilised for these experiments (Fig. 66). Fabrication of the chips was performed as described in Section 2.3, although here they were fabricated by Dr Nicole Pamme rather than the author, and so the following exceptions to the described method took place: (i) the design was patterned onto the photoresist of 1.5 mm soda-lime glass (Nanofilm, Inc., Westlake Village, CA, USA) using a direct write laser lithography system (DWL, Heidelberg Instruments, Heidelberg, Germany) rather than a photomask and UV lamp,[358] and (ii) the etched plate was pressure-bonded[406] to the top plate rather than thermally-bonded. The channel depth was 20 μm.
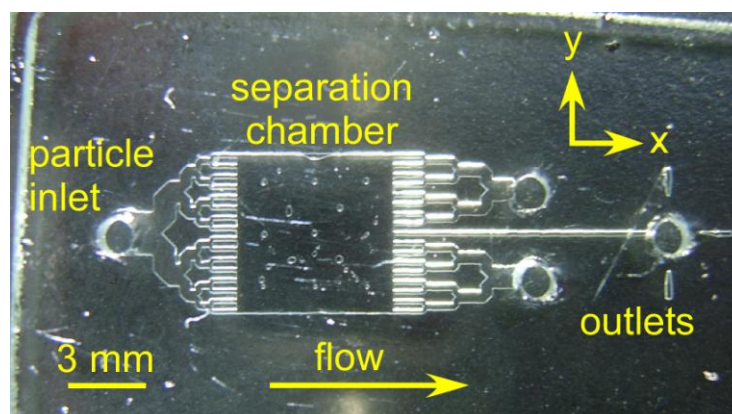


**Fig. 66  Photograph of the microfluidic design FFM2, fabricated in soda-lime glass to a depth of 20 μm, and featuring a chamber, 16 inlet channels, and 17 outlet channels.**

PTFE tubing (0.3 mm i.d., 1.58 mm o.d., Supelco) of a length of 7 mm were tapered using a scalpel and glued into each of the access holes of the microfluidic chip with Araldite Rapid. Sections of 1.5 cm long fused silica capillary (150 μm i.d., 363 μm o.d.), were inserted into each of the PTFE "sleeves" in the outlet holes, and connected to a 2 m length of Tygon tubing (1 mm i.d., 1.8 mm o.d.) via short sections of PTFE

tubing. The Tygon tubing fed into a waste bottle. A 3 m length of PEEK tubing (0.5 mm (0.02 in.) i.d., 1.6 mm (1/16 in.) o.d., Supelco) was connected to the PTFE sleeve in the inlet hole via a 7 cm long piece of capillary (150 μm i.d., 363 μm o.d.), while the other end of the PEEK tubing was interfaced to a 5 mL HSW syringe.

The chip was first flushed consecutively with water, ethanol, water, and finally a solution of manganese (II) chloride. The PEEK tubing was also flushed with water, $MnCl_2$ solution, and particle solution, then interfaced to the particle inlet of the chip via the piece of capillary attached to the PEEK. Particles were introduced into the chip through the PEEK tubing from a 5 mL syringe and pumped at 400 μL h$^{-1}$ (930 μm s$^{-1}$) through the chamber using a syringe pump (Pump 11 Plus).

**Particle visualisation**

The chip was attached to a setup designed to be inserted into the bore (100 mm diameter) of a superconducting magnet (JMTD-series Jastec Superconductor 13 T, Japan Superconductor Technology Inc. (Jastec), Tokyo, Japan). The apparatus consisted of an aluminium alloy rail (DryLin W, Igus Inc., Tokyo, Japan) onto which a prism was fixed (Fig. 67). The chip was placed on top of the prism and an LED (K40CWB-05, HOTHINK, Japan) was fixed over the chip to provide illumination. A CCD camera (MN43H camera, with a T416MB lens, Elmo Company Ltd., Aichi, Japan) was set beside the prism, such that the light from the LED passed through the separation chamber of the chip and was reflected by the prism into the CCD, allowing visualisation of the particles inside the chamber. The CCD camera was interfaced to a DVD video recorder (DMR-E100H, Panasonic, Tokyo, Japan) for capturing videos of particle behaviour inside the chip.
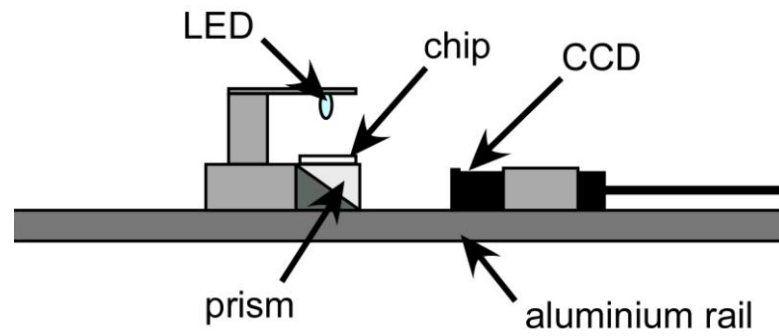
**Fig. 67  Apparatus for the visualisation of the chip inside the magnet bore.  Light from the LED passed through the chamber and was reflected by the prism into the CCD camera.**

## Magnet setup

The rail was inserted into the bore of the superconducting magnet such that the position of the chip inside the magnet could be changed by simply sliding the rail to the desired position in the bore (Fig. 68).  The magnetic flux density of the superconducting magnet was maintained at 10 T for all experiments.
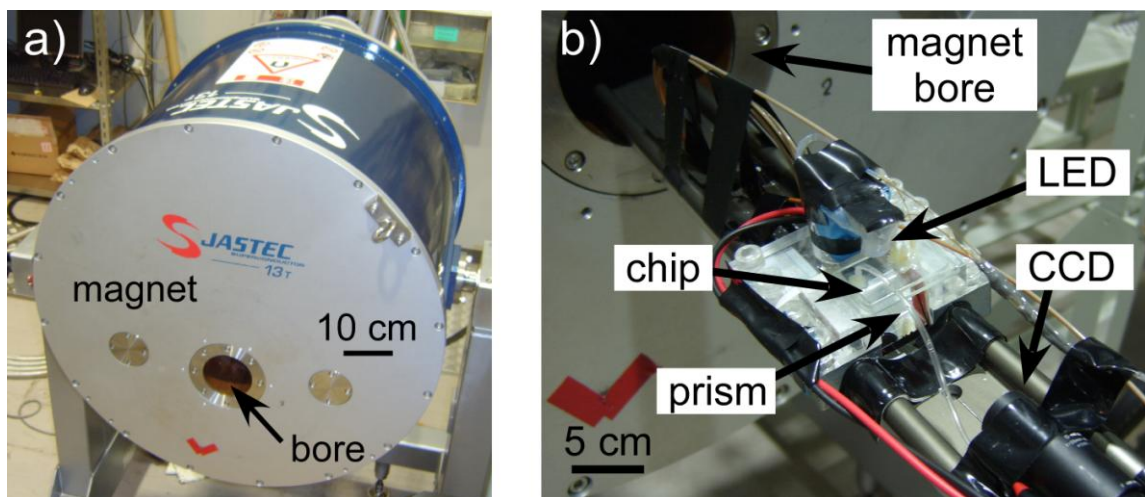


**Fig. 68  a) Superconducting magnet, maintained at 10 T, and featuring a 10 cm diameter bore.  b) The introduction of the rail holding the visualisation apparatus into the bore of the superconducting magnet.**
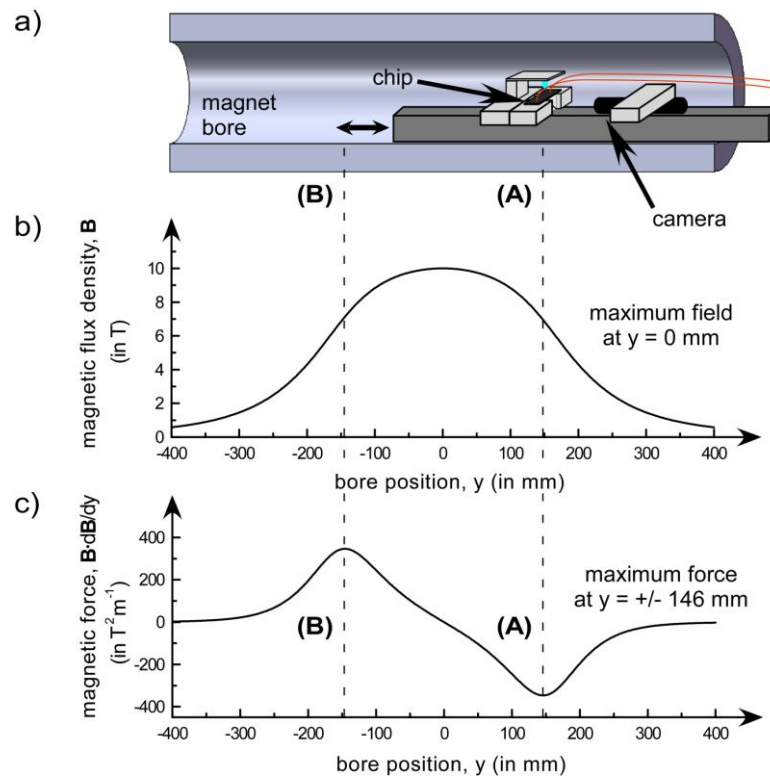
**Fig. 69 a) Schematic of the magnet bore, showing how the chip was moved in the bore using the aluminium rail, such that the chip was positioned at either location (A) or (B). b) The magnetic flux density across the length of the bore, with the highest value in the centre of the magnet. c) The product of the magnetic flux density and its gradient over the length of the bore. This product was greatest at y = ± 146 mm from the centre of the bore.**

The position of the chip was alternated between three positions in the bore, one of which was at the centre (y = 0 mm), while the other two positions were designated (A) and (B) and were situated 146 mm from the centre of the bore on either side. The positions of (A) and (B) are illustrated in Fig. 69, alongside a plot of the magnetic flux density, **B**, across the length of the bore (the y-direction), and a corresponding plot of the product of the magnetic flux density and the gradient, **B**(d**B**/dy). Markings on the rail were used to position the chip at (A) and (B). Fig. 69b shows that the maximum value of the magnetic flux density (10 T) was at the centre of the bore (y = 0 mm).

However, while the maximum **B** value was at the centre of the bore, the lack of a gradient in that position means that the resultant $\mathbf{B}(d\mathbf{B}/dy)$ value was zero; hence, the particles in the chip would experience no repulsion from the field.

On the other hand, Fig. 69c shows that at a position of 146 mm either side of the centre of the bore, the $\mathbf{B}(d\mathbf{B}/dy)$ is at its greatest, giving a value of 347 $T^2$ $m^{-1}$, and thus the particles in the chip would experience the greatest repulsive effect when in either of these positions. It was for this reason that positions (A) and (B) were chosen at +/- 146 mm for performing the experiments. Also of note is that position (A) has a negative value of 347 $T^2$ $m^{-1}$ while position (B) has a positive value, which indicates that the particles would be repelled in different directions from the centre of the magnet bore.

A series of experiments was undertaken in which the velocities of the polystyrene particles in the y-direction (i.e. due to the magnetic field), $\mathbf{u_{mag}}$, were determined in different concentrations of manganese (II) chloride at positions (A) and (B) in the magnet bore, and also at the centre of the bore. Table 11 illustrates the experiments performed using different sizes of polystyrene particles.

**Table 11  The combinations of MnCl$_2$ concentration, particle diameter and bore position investigated in the diamagnetic repulsion of polystyrene particles in continuous flow.**

| MnCl$_2$ concentration | Particle diameter | Bore position |
|---|---|---|
| 6 % | 5 µm | A |
| | | B |
| | 10 µm | A |
| | | B |
| 10 % | 5 µm | A |
| | | B |
| | 10 µm | A |
| | | B |
| 20 % | 10 µm | A |
| | | B |

## 2.11.2  Repulsion from a reagent stream

**Preparation of solutions**

10 % (0.79 M) $MnCl_2$ solution was prepared in water as described above, except that 0.01 % w/w Tween20 rather than SDS was added to reduce particle sticking.  This was due to the discovery that, over time, SDS promoted the formation of needle-shaped crystals in $MnCl_2$.  Also, 0.01 % w/v BSA was added to all solutions to reduce non-specific binding of biotin onto the particle surfaces.  A solution of fluorescently labelled biotin was prepared by dissolving 1 mg of biotin-4-fluorescein ($\lambda_{ex}$ = 494 nm, $\lambda_{em}$ = 521 nm in water) in 100 mL $MnCl_2$ to give a final concentration of 1 μg $mL^{-1}$ (1.55 μM).

**Preparation of particle suspensions**

Polystyrene particles of 10 μm diameter and featuring streptavidin surface groups were obtained from Micromod Partikeltechnologie, as described in Section 2.1.3.  6.5 μL of the 4.6 x $10^7$ particles $mL^{-1}$ stock solution was diluted in 1000 μL of the 10 % $MnCl_2$ solution to give a final concentration of 3 x $10^5$ particles $mL^{-1}$.

**Microfluidic chip setup and interfacing**

Chip design MLF3 was used for these experiments.  The chip was fabricated in 1 mm thick B-270 glass to a depth of 20 μm, thus increasing the width of each channel by a further 40 μm.  As described in Section 2.2, this design was originally created to increase the number of reagent streams that could be generated for the multilaminar flow procedure, whilst also incorporating a flow focussing design that would keep the

particle trajectories across the chamber more reproducible. This design was chosen for the diamagnetic repulsion of particles based entirely on the presence of the flow focussing channels, where narrow streams of reagent could be generated such that the particles would have less distance to travel to exit the reagent. Hence, most of the remaining inlets were not required for these experiments, and were only present due to the intended original purpose of the chip.

Fused silica capillaries (150 μm i.d., 363 μm o.d.) of 25 cm and 1 cm lengths were glued into the inlets and outlets, respectively, using Araldite Rapid epoxy glue. 1 cm long sections of PTFE tubing (0.3 mm i.d., 1.58 mm o.d.) were inserted into 10 cm lengths of Tygon tubing (1 mm i.d., 1.8 mm o.d.) and the outlet capillaries of the chip inserted into the PTFE tubing to allow removal of waste from the chip into a sample vial.

The inlet capillaries of the chip were interfaced to syringes using the same method as described in Section 2.6.1. The chip was flushed consecutively with ethanol, water and 10 % w/v $MnCl_2$ solution, after which the syringe adaptors were connected to reagent and buffers syringes loaded on a syringe pump with a 10-syringe rack (Harvard PHD 22/2000). A 250 μL glass syringe (SGE, Sigma-Aldrich) was filled with particle suspension, a 100 μL glass syringe (SGE) with biotin-4-fluorescein, and eight 1 mL plastic syringes (BD Plastipak) were filled with 10 % w/v $MnCl_2$ solution. Plastic syringes were used rather than glass syringes for the washing solutions as it was found that the Luer tip design of the former was easier to attach without air bubbles entering than the Luer Lock design of the latter. A flow rate of 1 μL h$^{-1}$ was applied to the syringes, relative to the 1 mL plastic syringes. Respective flow rates for the 100 μL and 250 μL glass syringes were 0.33 μL h$^{-1}$ and 0.52 μL h$^{-1}$, giving a combined total of 0.85 μL h$^{-1}$. The total linear flow velocity of solution in the chamber was 217 μm s$^{-1}$.

**Magnet setup**

A 20 mm Ø x 5 mm NdFeB disc magnet was placed on top of the chip such that the very edge of the magnet was positioned at the top edge of the chamber, with the centre of the magnet lined up with the centre of the chamber in the y-direction, and the field lines orientated in the z-direction (Fig. 70.). The magnetic flux density, **B**, at the surface of the magnet was determined by Equation 19 to be 275 mT, and this value was used for FEMM simulations of the magnetic field across the chip from a frontal (Fig. 71a) and a side-on view (Fig. 71b). From the simulation, it was estimated that the average value of **B** in the region of the chamber where the particles would be present was 307.0 mT, with a gradient of 47.9 mT mm$^{-1}$ that gave a value of 14.7 T$^2$ m$^{-1}$.
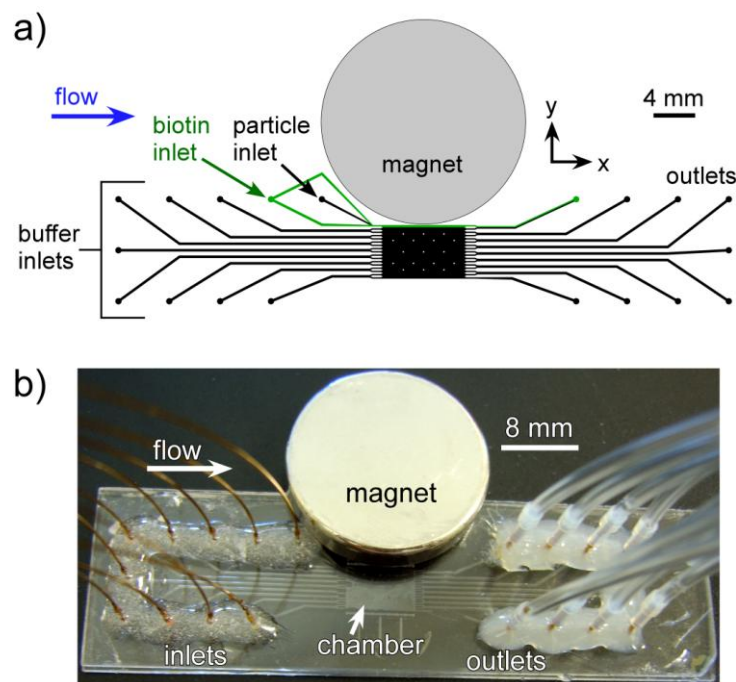


**Fig. 70   a) Schematic of the experimental setup, showing the magnet position on chip design MLF3, and the flow focussing section used for the biotin and particle introduction. b) Photograph of the chip, demonstrating the placement of the 20 mm Ø x 5 mm NdFeB disc magnet, and the capillaries glued into the access holes.**
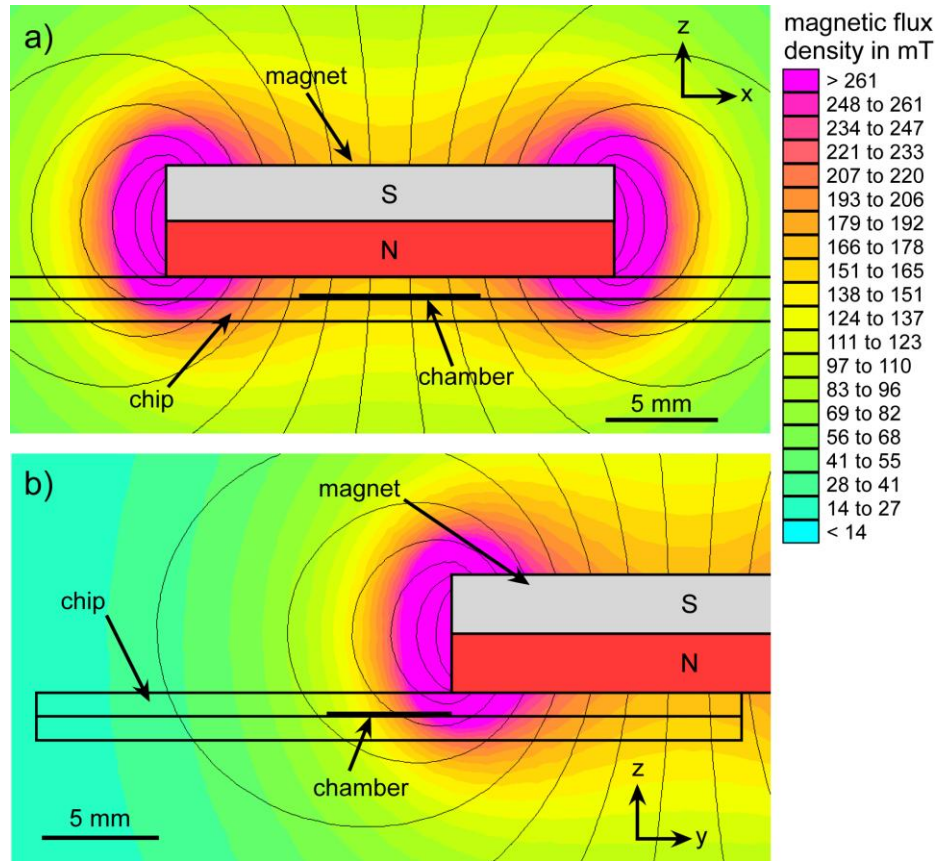
**Fig. 71 Finite Element Method Magnetics (FEMM) simulations of the magnetic field across an MLF3 chip and its reaction chamber from a 20 mm Ø x 5 mm NdFeB disc magnet. Due to software limitations, the field could not be shown from a view above the chamber, and so the views shown are a) a frontal view of the chip, and b) a side-on view of the chip.**

## Particle visualisation

The chip was placed on the stage of an inverted fluorescence microscope (TE-2000), as in Fig. 60, and the inside of the chamber viewed using a 10x objective. Fluorescence images were acquired using a blue light filter (B-2A), and a high sensitivity CCD camera (Retiga-EXL). Image-Pro Plus 6 software was used to capture videos and images. Streptavidin particles were pumped into the chip. They were exposed to the

fluorescently labelled biotin stream at the flow focussing junction, before entering the chamber where they then encountered the magnetic field. Particle fluorescence intensities before and after the reagent stream were measured using ImageJ software.

## 2.11.3 Flow focussing of particles and cells

These experiments were performed by Angeles Ivón Rodríguez-Villarreal, a visiting PhD student from the University of Barcelona, but were closely supervised by the author who had a great deal of input into the experimental setup and procedures, as well as the theoretical understanding of the work.

**Preparation of solutions**

Manganese (II) chloride tetrahydrate and gadolinium (III) chloride hexahydrate were purchased from Sigma-Aldrich and dissolved in purified water to give concentrations of 0.79, 0.56, 0.40, 0.24, 0.079 and 0.039 M. Tween20 (Sigma-Aldrich) was added to the solution to a concentration of 0.01 % w/w to reduce particle sticking. Concentrations of 0.24, 0.079 and 0.039 M $MnCl_2$ and $GdCl_3$ were also prepared in PBS buffer solution. Gadolinium (III) diethylenetriaminepentaacetic acid (Gd-DTPA) was purchased from Sigma-Aldrich and prepared to concentrations of 0.24, 0.079 and 0.039 M in PBS buffer. A cell culture medium was prepared, consisting of 4.5 g $L^{-1}$ high glucose Dulbecco's Modified Eagle Medium (DMEM), 10 % fetal calf serum (FCS), 1 % penicillin-streptomycin (PS) and 1 % L-glutamine.

**Preparation of particle suspensions**

10 μm and 20 μm diameter polystyrene particles were purchased from Polysciences Europe, as described in Section 2.1.3. Stock particle suspensions were ten times diluted in each of the MnCl$_2$ and GdCl$_3$ concentrations, giving final concentrations of 1.87 x 10$^6$ and 4.55 x 10$^6$ particles mL$^{-1}$ for the 10 and 20 μm particles, respectively. The particle suspensions were stored at 4 °C until ready for use.

**Preparation of cell suspensions**

Spontaneously immortalised human skin keratinocyte (HaCaT) cells, with diameters of around 10 μm, were grown in the DMEM media and incubated at 37 °C in a Petri dish. Cells were detached from the dish using trypsin, then washed with PBS solution and resuspended in solutions of PBS buffer with either MnCl$_2$, GdCl$_3$ or Gd-DTPA.

**Cell viability studies**

In order to test the viability of the cells over the course of an experiment, a CellTiter 96$^®$ AQ$_{ueous}$ One Solution Cell Proliferation Assay (MTS) was purchased from Promega Corporation (Southampton, UK) and used to determine the percentage of the living HaCaT cells in paramagnetic buffer solutions (MnCl$_2$, GdCl$_3$, or Gd-DTPA in PBS) over four hours.

**Capillary setup and interfacing**

A 20 cm length of fused silica capillary (150 µm i.d., 363 µm o.d., Composite Metal Services Ltd.) was held briefly over a cigarette lighter until the polyimide coating was burned off. The burned coating was wiped off using an ethanol soaked tissue, leaving the affected area of the capillary transparent and thus allowing visualisation of particles or cells within the microchannel. The capillary was placed on a custom made aluminium platform with x-y-z translational stages, and was held in place using a holder fabricated from pipette tips (Fig. 72).
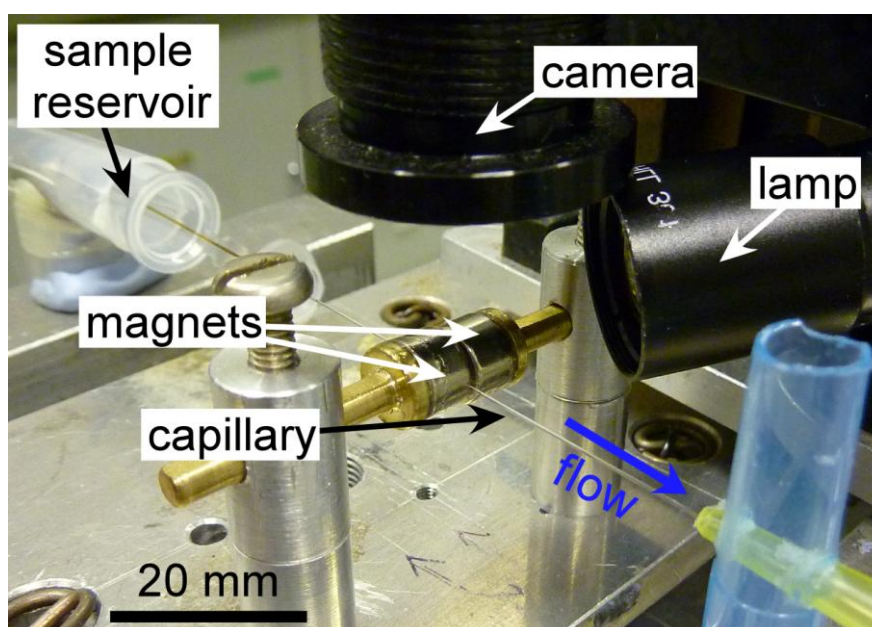


**Fig. 72 Photograph of the particle focussing setup. A fused silica capillary was positioned on a custom made setup between two NdFeB magnets with their like poles facing. Particle suspensions were pumped through the microchannel from a sample reservoir via negative pressure. Visualisation was achieved using an external lamp and a CCD camera.**

The capillary was interfaced to a syringe pump (Pump 11 Plus) via a length of Tygon tubing (0.254 mm i.d., 0.762 mm o.d) and a 1 mL syringe (BD Plastipak) containing a

paramagnetic solution of $MnCl_2$, $GdCl_3$ or Gd-DTPA. The capillary was flushed with the paramagnetic solution using positive pressure to wet the inner surfaces of the microchannel and ensure that no air bubbles were present. The open end of the capillary was placed into a sample reservoir (1.5 mL Eppendorf tube) containing a suspension of particles or cells, and negative pressure was applied to draw the suspension through the microchannel. Flow rates of 30, 40 and 50 $\mu$L h$^{-1}$ were applied, corresponding to flow velocities of 0.47, 0.63 and 0.78 mm s$^{-1}$, respectively.

**Magnet setup and cell visualisation**

Visualisation of the particles and cells was achieved via an overhead zoom CCD camera (PV10) with an external lamp (Mega Light 100) used for illumination of the microchannel. Videos were captured using WinDVD Creator 2 software, and particle/cell positions in the capillary were measured at distances of 3 mm before and 3 mm after the pair of magnets using ImageJ software. To analyse the particle distributions across the microchannel, the width of the capillary was divided into seven sections and the number of particles counted in each section. The capillary was positioned between two NdFeB magnets (Magnet Sales) with like poles facing each other 300 $\mu$m apart. The magnetic fields were generated by pairs of 4 x 4 x 5 mm$^3$ rectangular magnets (**B** at surface = 561 mT), or 10 mm Ø x 5 mm disc magnets (**B** at surface = 435 mT). FEMM simulations of the magnetic field between the magnets were created, with the simulation for the pair of 4 x 4 x 5 mm$^3$ magnets shown in Fig. 73.

The value of **B** at a distance from one of the magnets towards the centre of the capillary at the entrance to the magnet pairs was determined to be 1,121 mT, with a gradient ($\nabla$**B**) of 1,502 mT mm$^{-1}$, giving an estimated (**B**·$\nabla$)**B** value of 1,684 T$^2$ m$^{-1}$. These values are

very high due to the fact that the magnetic field is strongest at the edges of a magnet, and in this case the field lines are repelled by the opposing magnetic field, thereby forcing them into a narrow area closest to the magnet to give a high value of **B** near to the magnet.   The repulsion of the two opposing fields also creates an area of low magnetic field midway between the two magnets, thus exhibiting a very large gradient between the high field near the magnet and the low field midway between the opposing magnets.  The corresponding values for the setup of two 10 mm Ø x 5 mm disc magnets were $\mathbf{B} = 1263$ mT, $\nabla \mathbf{B} = 409$ mT mm$^{-1}$, and $(\mathbf{B} \cdot \nabla)\mathbf{B} = 517$ T$^2$ m$^{-1}$.  These values show that $(\mathbf{B} \cdot \nabla)\mathbf{B}$ for the smaller rectangular magnets was more than twice that of the larger disc magnets (due to the higher concentration of field lines near the surface of the smaller magnets compared to the larger ones), hence the force on the particles should have been greater as they first approached the magnetic setup.   However, the larger magnets were two and a half times wider than the block rectangular magnets, and so at the same flow rate the particles would have a residence time between the magnets 2.5x longer for the disc magnets.
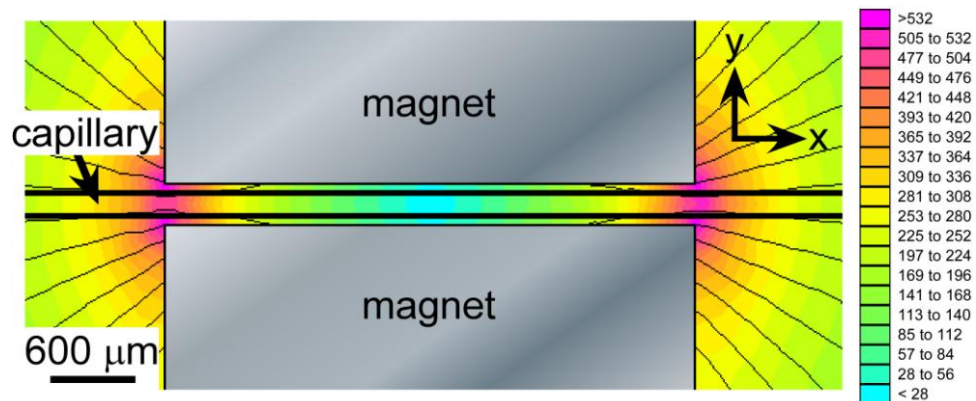


**Fig. 73  FEMM simulation of the magnetic field when two 4 x 4 x 5 mm$^3$ NdFeB magnets were placed with like poles facing each other.  The strongest field was at the corners of the magnets, with the space between the corners exhibiting a slightly lower flux density that the particles migrated towards.  The scale on the right shows the flux density, B (mT).**

This setup was used to determine the effect of several factors on the efficiency of the particle focussing method: (i) concentration and type of paramagnetic salt, which altered the magnetic susceptibility ($\chi_m$) of the solution, (ii) the flow rate of the medium applied by the syringe pump, (iii) the sizes of the particles used, and (iv) the residence time of the particles under the influence of the magnetic field by increasing the width of the magnets. Subsequently, the results of these experiments were applied to the flow focussing of HaCaT cells.

# 3      On-chip free-flow magnetophoresis

This section describes the effect of temperature on magnetic particle deflection behaviour and separations in on-chip free-flow magnetophoresis systems, and has been published in the Journal of Magnetism and Magnetic Materials.[395]

## *3.1      Introduction*

On-chip free-flow magnetophoresis, as described in Section 1.4.3, is a continuous flow separation method that is able to simultaneously sort magnetic particles from each other and from non-magnetic particles,[358,383] as well as magnetically labelled cells from unlabelled cells.[360]  By introducing particles into a separation chamber in the x-direction, and applying a magnetic field in the y-direction, the particles can be deflected laterally from the direction of flow, with different species deflecting to different extents and thus allowing their collection from different outlets as they exit the chamber (Fig. 33).  Simultaneously separating different particle types has the advantage that several target species can be separated and collected at the same time by utilising the surface functionalisation of the particles.  Separation systems that feature only two outlets are only able to sort one type of magnetic particle, and therefore only one target analyte in a sample matrix, hence to separate multiple species the sample would have to be reintroduced into the chip with a new type of particle in order to collect each analyte.

As explained in Section 1.4.5 and Equation 30, the extent of deflection depends on several factors, including: the volume of magnetisable material in the particle ($V_m$), the radii of the particles ($r$), the difference between the magnetic susceptibility of the particle ($\chi_p$) and that of the medium ($\chi_m$), the product of the strength and gradient of the

magnetic field (($\mathbf{B}\cdot\nabla$)$\mathbf{B}$), and the absolute viscosity of the medium ($\eta$). Previously published work on free-flow magnetophoresis concerned studies into the effect of changes in $V_\mathrm{p}$, $\chi_\mathrm{p}$, and $r$ of the particles,[358,383] while further investigations looked into the use of different sizes and types of magnets with varying distance from the chamber to observe how changing ($\mathbf{B}\cdot\nabla$)$\mathbf{B}$ affected the particle deflection.[420] However, one parameter that has not received any attention is that of the solution viscosity. Here, an investigation was undertaken to study the effect of altering the viscosity of the liquids in the microfluidic chip on the deflection behaviour of particles through the chamber, and also on the separation resolution of two particle populations.

The velocity of a particle due to a magnetic field ($\mathbf{u_{mag}}$) is inversely proportional to the viscosity of the medium (Equation 30), meaning that as the viscosity increases the particles should experience lower velocities due to the increased viscous drag forces ($\mathbf{F_{vis}}$). One parameter that affects viscosity is temperature, and the correlation between these two terms is shown in Equation 40:[54,421]

$$\eta = A\, \exp^{(\Delta E_{vis}\,/\,RT)} \qquad\qquad \textbf{Equation 40}$$

where $A$ = a constant (kg m$^{-1}$ s$^{-1}$), $\Delta E_\mathrm{vis}$ = the activation energy for viscous flow (J mol$^{-1}$), $R$ = the gas constant (8.315 J K$^{-1}$ mol$^{-1}$), and $T$ = temperature (K). Thus, the viscosity of a medium is inversely proportional to its temperature, and the relationship is exponential. As a result, the viscosity was changed in the magnetophoresis experiments by controlling the temperature of the system, thereby allowing the effect of temperature and viscosity to be explored.

## 3.2 Results and Discussion

### 3.2.1 Absolute viscosity of the 0.1x glycine saline solution

The viscosity of the 0.1x glycine saline solution was determined over a temperature range of 5 to 50 °C in order to obtain accurate values for later calculations. As described in Section 2.5.3, a density meter was used to determine the density of the solution at the different temperatures, with an Ubbelohde viscometer used to measure the kinematic viscosity of the solution. The absolute viscosity ($\eta$) of a solution can be calculated from the density ($\rho$) and kinematic viscosity ($v_k$) of a solution by using Equation 41:

$$\eta = \rho \; v_k \hspace{4cm} \textbf{Equation 41}$$

Density values were simply read from the meter and recorded, while the kinematic viscosity was determined from viscometer measurements by Equation 42, where $K$ is a constant ($m^2 \; s^{-2}$) and $t$ is time (s):

$$v_k = K \; t \hspace{4cm} \textbf{Equation 42}$$

The constant, $K$, was determined for each temperature by first calculating the kinematic viscosity of pure water, which was achieved by rearranging Equation 41 to give $v_k$ and then using known values of the density and absolute viscosity of water at each of the desired temperatures.[422] These kinematic viscosities of water were then divided by the time taken for the water to pass between the two timing marks on the Ubbelohde viscometer at the corresponding temperatures, giving $K$ values of pure water over the temperature range. With the $K$ values determined for each temperature, they were used in Equation 42 to calculate kinematic viscosities by multiplying $K$ by the time taken for the 0.1x glycine saline solution to pass through the time marks. The kinematic viscosity

values were then multiplied by the density values (as per Equation 41) at the appropriate temperatures to give the absolute viscosity of 0.1x glycine saline at 5, 10, 20, 30, 40 and 50 °C. These absolute viscosity values are illustrated in Fig. 74.



The graph shows: $y = (1.419\, e^{-0.0366x} + 0.3391) \times 10^{-3}$, $R^2 = 0.9999$
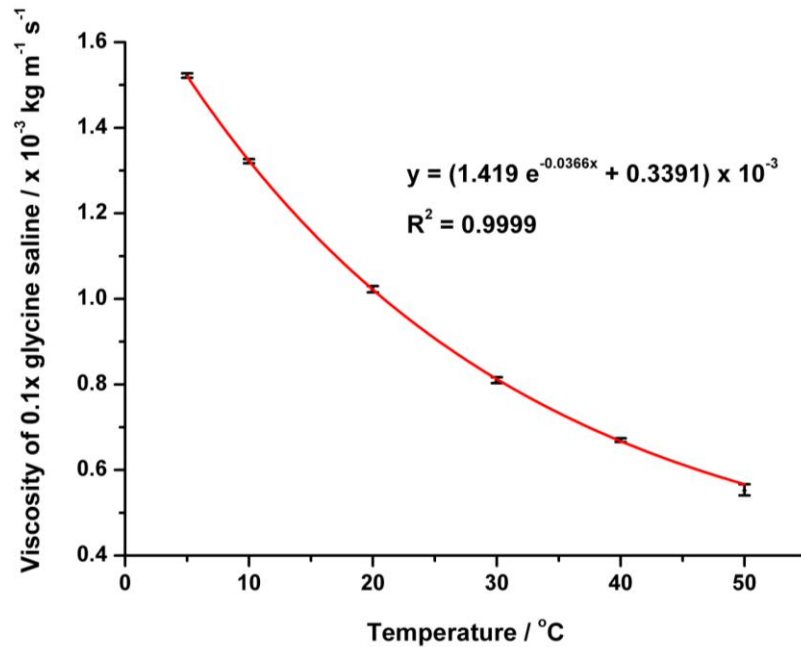
**Fig. 74** **Plot of the viscosity of 0.1x glycine saline solution between 5 and 50 °C. The viscosity decreased as the temperature increased.**

The results agreed with Equation 40, with the viscosity dropping exponentially as temperature increases, and the sharpest drop in viscosity occurring at changes over the lower temperatures, while changes at higher temperatures had less of an effect. The graph in Fig. 74 gives the equation of the line to be $y = (1.419\, \exp^{-0.0366x} + 0.3391) \times 10^{-3}$, corresponding to Equation 40 where y = the absolute viscosity ($\eta$), $A = 1.419 \times 10^{-3}$ kg m$^{-1}$ s$^{-1}$, $\Delta E_{vis}/R = -0.0366$ (thereby giving a value of -0.3043 J mol$^{-1}$ for $\Delta E_{vis}$), and x = the temperature ($T$) of the solution. As examples of how temperature would affect the deflection of particles in a microfluidic device, it can be seen that if the temperature of the solution was increased ten times from 5 to 50 °C, the viscosity would

decrease by around 2.75 times. This would in turn would increase the value of $\mathbf{u_{mag}}$ by 2.75 times (Equation 30), thereby increasing the deflection of particles across the separation chamber (Equation 31).

## 3.2.2   Flow in the chamber

Liquids pumped through a microchannel by hydrodynamic pressure exhibit a parabolic flow profile, which is to say that the flow velocity is highest at the centre of the channel, while the velocity at the walls is near zero. The flow velocity, $v$ (m s$^{-1}$) at different depths of the microfluidic chamber can be determined theoretically by the use of Equation 43.[423]

$$v = \frac{\Delta p}{4\, l\, \eta}\left[\left(\frac{d}{2}\right)^2 - x_c{}^2\right]$$

**Equation 43**

where $l$ = the length of the channel (m), $d$ = depth of the channel (m), $x_c$ = distance from the centre of the channel (m), and $\Delta p$ is the pressure drop (Pa) across the channel, which was determined to be 171.56 Pa for the chamber using Equations 35-39. Equation 43 was used to calculate the flow profile in the microfluidic chamber by determining the flow velocity ($v$) at different values of $x_c$ in the 20 μm deep microfluidic separation chamber (Fig. 75).

The maximum flow velocity of the fluid in the chamber was calculated as 699 μm s$^{-1}$, as shown by the maximum peak on the graph, while the average flow velocity was 454 μm s$^{-1}$. Therefore, particles flowing at different heights in the chamber would experience slightly different velocities through the chamber. Changes in viscosity have no bearing on the flow profile as the viscosity term in Equation 43 is cancelled out by the viscosity

term in the pressure drop (Equations 35 and 37). Hence, the velocity of the fluid does

not change when varying the system temperature.
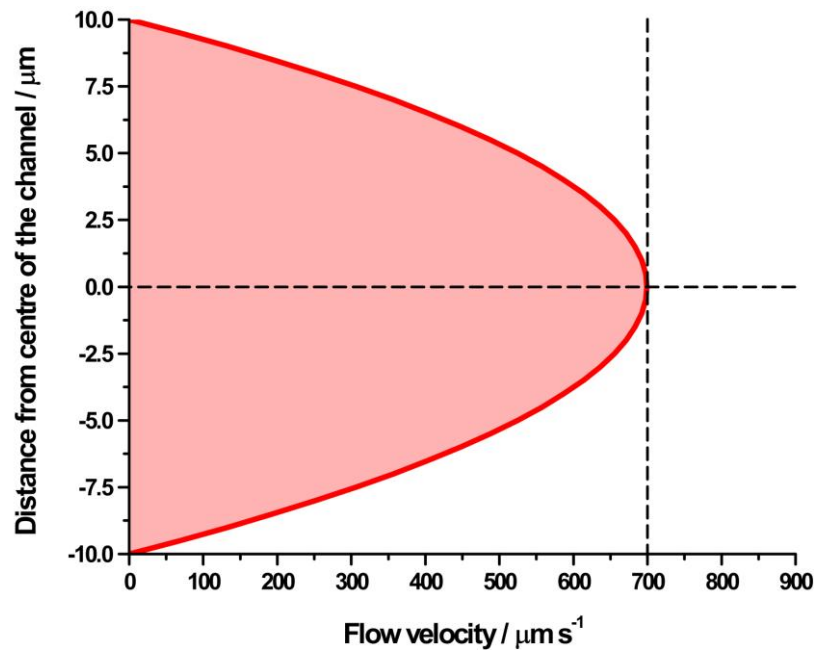


**Fig. 75  Parabolic flow profile over the 20 $\mu$m height of the microfluidic separation chamber at a flow rate of 400 $\mu$L h$^{-1}$.**

Another property of the flow regime to consider is whether the flow in the

magnetophoresis chip would be laminar. Hence,  the Reynolds number, Re, of the flow

in the device was calculated at room temperature using Equation 1 and found to be

0.036, well below the value required for flow to be laminar (Re < 2000). At the lowest

temperature of 5 °C, Re = 0.024, while at the highest temperature of 50 °C, Re = 0.066.

This showed that the flow would remain laminar throughout the temperature range

investigated in the free-flow magnetophoresis experiments. To confirm that flow in the

chamber was laminar, inks were pumped through the chip at 400 $\mu$L h$^{-1}$ as shown in

Fig. 76, with blue ink pumped from the buffer reservoir and red ink from the sample reservoir.

The photograph demonstrates that laminar flow was achieved in the chip, with the red ink flowing side-by-side with the blue ink across the chamber, thus agreeing with the theory. Therefore, it can be hypothesised that magnetic particles entering the chamber from the sample inlet without the presence of an external magnet would travel across the chamber in the direction of flow without migrating in a direction perpendicular to the flow, which was indeed observed experimentally. Additionally, further physical effects can also be considered that could potentially affect the movement of particles through the chamber without the presence of a magnetic field.
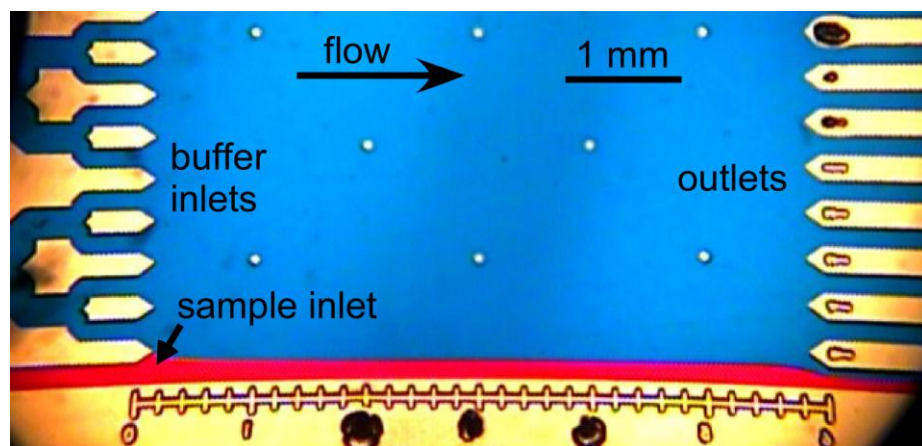


**Fig. 76 Visualisation of the laminar flow in chip design FFM1 at a flow rate of 400 $\mu$L h$^{-1}$, with blue ink pumped from the buffer reservoir and red ink pumped from the sample reservoir.**

### 3.2.3 Particle characteristics

Since particles in a parabolic flow regime could flow at a range of velocities depending on their height in the channel, as described in the previous section, the average velocity

($v_p$) of the 2.8 μm and 1 μm particles in the flow can be determined based on the depth of the channel ($d$) and the radius of the particle ($r$). The calculation for this is very similar to that for determining the fluid velocity in the chamber (Equation 43), and is given by Equation 44.[404]

$$v_p = \frac{\Delta p}{12\ l\ \eta}\left[\frac{d^2}{2} + dr - r^2\right]$$ **Equation 44**

Due to the larger size of the M-270 particles, they would not be able to flow through the microfluidic chamber as close to the upper and lower walls as the smaller MyOne particles. Therefore, the larger particles would not be able to enter the regions of lowest fluid velocity, which the smaller particles could do, and so would experience a higher average velocity through the chamber. Hence, the larger 2.8 μm particles (M-270) were calculated as having a greater velocity than the 1 μm particles (MyOne), with average velocities of 527 μm s$^{-1}$ and 500 μm s$^{-1}$, respectively. However, the difference between the velocities of the two particle types was not significantly large, meaning they would travel across the 6 mm chamber in roughly the same amount of time (~12 s). This has the consequence that neither particle type would be affected by an applied magnetic field for a longer period of time than the other, and so would not be separated as a result of residence time in the chamber rather than by their magnetic properties.

Other considerations when regarding the possibility of the two particle types separating by means other than magnetophoresis includes their diffusion across the chamber in a direction perpendicular to that of the applied flow. Equation 3, the Einstein-Smoluchowski equation, describes the diffusion of a species through a media due to Brownian motion; random zig-zag movements due to the thermal motion of the surrounding solvent molecules.[59] As well as simple molecules found in aqueous media, magnetic particles of the type used here also undergo Brownian motion, and are

therefore able to diffuse through a solution due to this random motion. The extent to which a particle will travel in a solution due to diffusion depends on its diffusion coefficient, $D$ ($m^2$ $s^{-1}$). Typical diffusion coefficients of molecules in liquids are in the order of $D \approx 10^{-9}$ $m^2$ $s^{-1}$, though larger species move more slowly and thus have smaller values of $D$, as given by the Stokes-Einstein equation (Equation 45), where $k_B$ is the Boltzmann constant ($1.38065 \times 10^{-23}$ J $K^{-1}$), and $T$ is the temperature (K).[53,59]

$$D = \frac{k_B\ T}{6\ \pi\ \eta\ r}$$
**Equation 45**

The $k_B T$ component is an estimate of the translational kinetic energy of a particle, while the lower expression of the equation refers to Stokes' law, as seen previously in Equation 8, since it describes the drag on a particle as it tries to move through a solution. The diffusion coefficient of Dynabeads M-270 particles in 0.1x glycine saline solution at 20 °C was determined to be $1.50 \times 10^{-13}$ $m^2$ $s^{-1}$. From this, the diffusion of particles due to Brownian motion whilst traversing the microfluidic chamber was calculated as 1.85 μm using Equation 3, assuming particles would spend an average of 11.4 s in the chamber at most (calculated from the particle velocities mentioned above). Corresponding figures for the Dynabeads MyOne particles were $D = 4.00 \times 10^{-13}$ $m^2$ $s^{-1}$, and a diffusion distance of 3.10 μm; only slightly greater numbers than the larger particles. This means that, without the presence of a magnet, the larger and smaller particles could only migrate about 1.85 μm and 3.10 μm, respectively, in the y-direction due to diffusion as they passed through the chamber, which would not be enough to cause the particles to move out of the sample stream and into the buffer stream without the application of a magnetic field.

### 3.2.4 Temperature dependence of magnetic particle deflection

Having established how the viscosity of the 0.1x glycine saline solution varied with temperature, a series of experiments were performed in which the deflection behaviour of Dynabeads M-270 was studied at different temperatures, as described in Section 2.5.8. Briefly, the 2.8 μm diameter particles were pumped into a microfluidic separation chamber at a flow rate of 400 μL h$^{-1}$ (930 μm s$^{-1}$), with a disc magnet placed halfway over the chamber and the chip situated on a Peltier heater. The percentage of particles exiting each outlet was counted over 4 min at temperatures of 5, 10, 15, 20, 25, 30, 43 and 50 °C, and a selection of these results is given in Fig. 77. Outlet 1 was situated directly opposite the particle inlet channel, hence particles exiting via this outlet would have experienced little or no deflection towards the magnet, while outlet 8 was the outlet nearest the edge of the disc magnet.

As expected by Equations 25 and 30, the deflection distances of the particles were smallest at the lowest temperature of 5 °C, where they experienced the highest viscous drag forces ($\mathbf{F_{vis}}$) and so only exited the chip via outlets 2 and 3. Increasing the temperature to 15 °C resulted in over 90 % of the particles exiting via outlet 3 with some at outlets 2 and 4. At room temperature (20 °C) most particles exited at outlet 3 but some reached as far as outlet 5. Higher temperatures of 43 °C led to particles exiting via outlets 5 and 6. At the highest temperature investigated (50 °C) particles experienced the least viscous drag effects and the majority now exited via outlet 6 with some even deflecting as far as outlet 8. Results obtained at temperatures not shown here followed the same trend. It should also be noted that only single particles were counted, while agglomerates of particles were not.
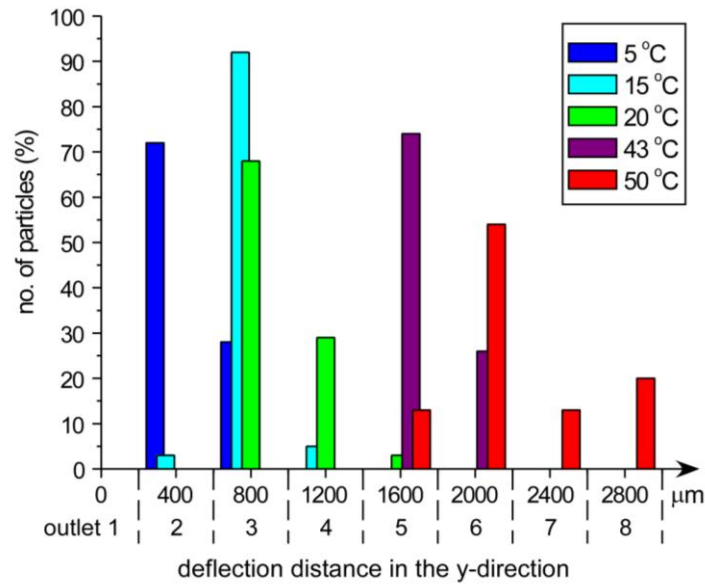
**Fig. 77 The observed deflection distances of Dynabeads M-270 magnetic particles at temperatures between 5 and 50 °C. The trend showed that at higher temperatures the particles deflected further due to the reduced viscosity of the solution.**

The spread of particles over the outlets was fairly consistent throughout the temperature range with particles typically exiting over two or three outlets, equivalent to a distribution of 400 to 800 μm, which was due to the spread of particles across the 100 μm wide inlet channel that allowed particles to experience different initial $\mathbf{u_{mag}}$ forces as they entered the chamber. The exception to this was the spread experienced at 50 °C, where particles exited over four outlets and more particles left the chamber at outlets 6 and 8 than did at 7. This effect was caused by the agglomeration of some particles at the side of the sample inlet channel due to their attraction to the magnet and the reduced viscosity, which meant that even particles in the inlet channel were more affected by the magnetic field at the high temperature. The agglomerated particle clusters grew until being dislodged and deflected across the chamber whereupon they disrupted the paths of other particles, thus affecting their trajectories slightly. This could be eliminated in

future experiments by incorporating particle focussing streams into the sample inlet channel, and by altering the angle with which the inlet channel connects to the chamber, such that the particles would not have the opportunity to become stuck to the sidewall of the channel.

The magnetically induced velocities ($u_{mag}$) of the particles were calculated to better illustrate how $u_{mag}$ changed with temperature. This was achieved by measuring the time taken for particles to cross a 500 µm horizontal section (in the x-direction) of the chamber, near to the outlets, whilst also calculating the distance travelled in the y-direction in this same region. The $u_{mag}$ values were calculated by dividing the distance travelled in the y-direction by the time taken. From these observed $u_{mag}$ results, the corresponding $F_{mag}$ values were calculated using Equation 30 and the glycine saline viscosities determined in Section 3.2.1. Theoretical $F_{mag}$ values were calculated using Equation 25, based on information given in Table 6. These $F_{mag}$ values were then used to calculate theoretical $u_{mag}$ velocities using Equation 30 and the glycine saline viscosities. These experimental and theoretical values are shown in Table 12.

**Table 12  The magnetic forces on the M-270 particles at different temperatures, and their magnetically induced velocity in the y-direction.**

| Temperature / °C | Theoretical $F_{mag}$ / pN | Experimental $F_{mag}$ / pN | Theoretical $u_{mag}$ / µm s$^{-1}$ | Experimental $u_{mag}$ / µm s$^{-1}$ |
|---|---|---|---|---|
| 5 | 3.79 | $3.78 \pm 0.19$ | 81 | $81 \pm 4$ |
| 20 | 3.79 | $3.32 \pm 0.56$ | 121 | $106 \pm 18$ |
| 30 | 3.79 | $3.10 \pm 0.43$ | 152 | $124 \pm 17$ |
| 43 | 3.79 | $2.90 \pm 0.08$ | 185 | $142 \pm 4$ |
| 50 | 3.79 | $4.53 \pm 0.19$ | 223 | $267 \pm 11$ |

The table shows that the theoretical $\mathbf{F_{mag}}$ value was 3.79 pN, assuming a $(\mathbf{B} \cdot \nabla)\mathbf{B}$ value of 2.16 $T^2$ $m^{-1}$ (as calculated in Section 2.5.5), and using the $V_m$ and $\chi_p$ values estimated in Table 6. However, the value of 2.16 $T^2$ $m^{-1}$ is only an estimate due to the inhomogeneous gradient generated across the chamber by the permanent magnet (see Fig. 18), with values varying depending upon the location in the chip. The average $\mathbf{F_{mag}}$ value determined experimentally was 3.53 pN, showing that the forces generated in the experiments were generally very similar to those expected. The forces observed at 50 °C were noticeably larger than the others, however, and this may be due to the particles at this temperature being closer to the magnet in the measuring region than particles at other temperatures, where they would have experienced larger values of $(\mathbf{B} \cdot \nabla)\mathbf{B}$ that were not accounted for in the theoretical $\mathbf{F_{mag}}$ and $\mathbf{u_{mag}}$ values. This may also be the reason that the experimental $\mathbf{u_{mag}}$ values at this temperature were greater than those expected, as even a slight change in flux density or gradient due to the position of a particle in the field could significantly affect the forces acting upon it. Typically, the experimental and theoretical $\mathbf{u_{mag}}$ values also compared very well, though the values at 30 , 43 and 50 °C were a little lower than expected, but again this may be due to slight changes in field strength and gradient experienced by the particles, depending where they were in the chamber in relation to the magnet when they were measured.

With regards to the general trend shown by Table 12, it clearly shows that an increase in temperature results in an increase in the velocity of the particles towards the magnet in the y-direction, which would have the effect of increasing the value of $\mathbf{u_{defl}}$ and therefore the deflection distance of particles across the chamber. As explained in Section 3.2.1, increasing the temperature ten times from 5 to 50 °C should in turn increase the $\mathbf{u_{mag}}$ velocities of the particles by 2.75 times. The increase observed experimentally between these temperatures was 3.30 times, a little higher than expected

but close nonetheless, and again this is due to the higher than expected $\mathbf{u_{mag}}$ value caused by the inhomogeneous gradient, as described above.

The theoretically expected deflection behaviour of the particles were also simulated in collaboration with Damien Robert from Université Paris-Diderot, France (Section 2.5.9). The expected trajectories of the particles are shown at 5, 20 and 50 °C as solid black lines on a map of the magnetic gradient across the chamber (Fig. 78). The coloured regions around each line illustrate the spread of the particles from the experimental results, and the blue arrows indicate the magnetic field gradient and its direction, with typical gradients near the outlets being around 10 T m$^{-1}$.
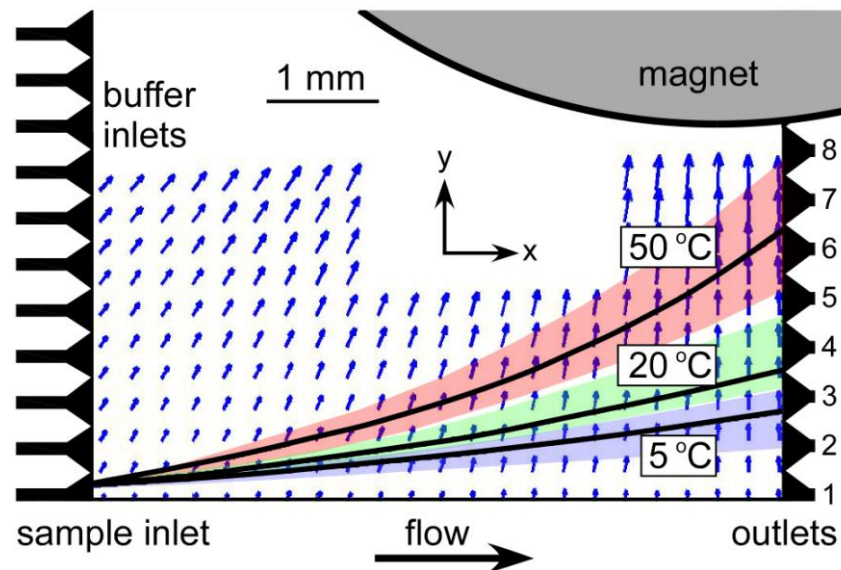


**Fig. 78 Calculated trajectories of Dynabeads M-270 particles, shown as solid black lines, at three different temperatures across the separation chamber. The coloured regions indicate the particle paths observed experimentally. The blue arrows show the magnetic field gradient, with typical values in the chamber being between 7 - 21 T m$^{-1}$, depending on the position in the chamber.**

The experimental results were found to compare very well with the theoretically expected particle trajectories, matching particularly well for the 20 and 50 °C temperatures, with most particles exiting the chamber at the expected outlets. However, the results for 20 °C show that the spread of particles does not fit the theoretical trajectory perfectly as the coloured region sits off-centre in relation to the black line. The results at 5 °C compare fairly well although there is a slight discrepancy in that the calculated trajectory shows most particles exiting via outlet 3, whilst experimentally most exited via outlet 2. This is likely due to the starting positions of the particles when they enter the chamber, as the simulated trajectories assume that all particles enter at the same position whereas the experimental starting positions varied across the width of the sample inlet channel. Hence, as particles entered the chamber at different positions they experienced different initial magnetic forces that affected their paths throughout the chamber. Generally, however, the theoretical trajectories give a very good indication of the distance a particle would be expected to travel towards the magnet at different temperatures, and the program could be used to calculate particle trajectories in future experiments that involve the deflection of magnetic particles perpendicular to fluid flow.

These results demonstrate not only how particle deflection increases with decreasing viscosity (and increasing temperature), but also the importance of maintaining good control over the temperature in order to achieve high reproducibility. In a wider context, this is also an important consideration of any other "free-flow" system, such as those utilising acoustic,[236] dielectrophoretic[227] and optical forces,[208] among others. Additionally, the technique also demonstrates potential for tuning the trajectories of magnetic particles such that certain particle types exit via only certain outlets. This could be useful for first directing particles of one type into one outlet at temperature

"A", and then switching to temperature "B" to direct them into a second outlet, whereupon the outlets lead to different downstream processes or collection vials.

### 3.2.5    Separation of two particle populations

Having established that an increase in temperature yields an increase in particle deflection distances, an investigation was undertaken to determine the effect of temperature on the separation of two magnetic particle populations. As detailed in Section 2.5.8, a mixture of Dynabeads M-270 (2.8 μm diameter) and Dynabeads MyOne (1 μm diameter) particles was pumped through the microchip at a flow rate of 400 μL h$^{-1}$ (930 μm s$^{-1}$). These particles were chosen since they are commercially available from Invitrogen and can be utilised for a number of separations due to the various surface functional groups that can be present, and as such are one of the most commonly used brands of magnetic particles. Additionally, as described previously, Dynabeads have been found to be more suitable to on-chip magnetophoresis applications,[395] hence their use here rather than particles from another supplier. Furthermore, the M-270 and MyOne particles are two of the main three types of Dynabeads available, the other being M-450 (4.5 μm diameter), and so it was decided to test the capability of the magnetophoresis technique for separation of the two smallest varieties since they experience the lowest magnetic forces of the three types.

The two different particle types (M-270 and MyOne) separate due to differences in magnetic material content (see Table 6), with the larger particles containing a greater volume of magnetic material ($V_m$) and deflecting further than the smaller particles (Equation 30). For example, the $V_m$ of the M-270 particles is 9.1 times that of the MyOne particles, as determined from the values in Table 6, which would mean that,

with constant values of $\eta$ and $(\mathbf{B} \cdot \nabla)\mathbf{B}$, the larger particles would experience a magnetic force ($\mathbf{F_{mag}}$) that was 9.1 times that of the smaller ones. In turn, the magnetically induced velocities ($\mathbf{u_{mag}}$) for the M-270 particles in a 20 μm deep channel would be 2.2 times greater than for the MyOne particles. As the particles then crossed the chamber, the larger ones would deflect 2.2 times further than the smaller ones, i.e. more than twice as far. Additionally, this situation only considers a homogeneous gradient across the chamber, whereas the inhomogeneous gradient created by the magnet (Fig. 54) would amplify the difference in deflection distances between the particle types.
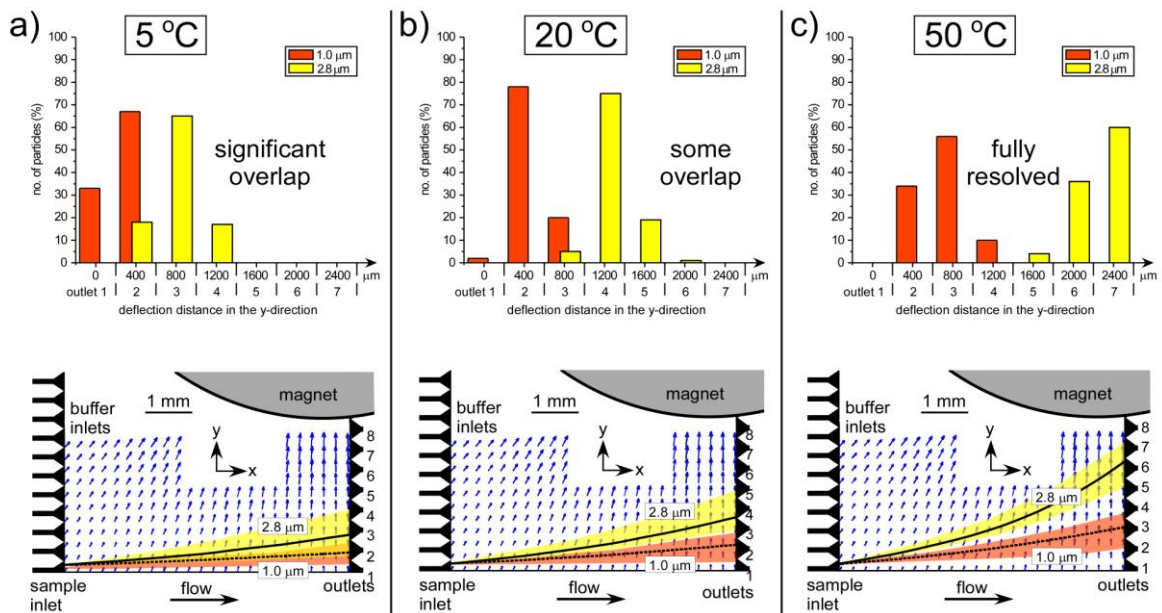


**Fig. 79 Separation of 1.0 μm and 2.8 μm diameter particles at a) 5 °C, b) 20 °C, and c) 50 °C. The images on the upper row show plots of the particle deflection distances at the different temperatures. The lower row of images illustrates the theoretical particles trajectories for the smaller (dotted lines) and larger (solid lines) particles, respectively, with the coloured regions showing the experimental particle spread.**

Thus, the different distances traversed by each particle type in the y-direction caused them to exit the chamber via different outlets, thereby achieving a separation.[358,383] In these experiments, the particle populations were separated at temperatures of 5, 20 and 50 °C, the results of which are shown as graphs in Fig. 79, alongside the theoretical particle trajectories (solid black lines = M-270 particles, dotted lines = MyOne particles) and the experimentally observed trajectories in the separation chamber (coloured regions).

At 5 °C the majority of both particle types were deflected into outlets 2 and 3. There was significant overlap of the two populations at outlet 2 and thus full separation could not be achieved. The separation was improved by increasing the temperature to 20 °C, whereupon most of the M-270 particles exited via outlet 4 while the majority of the MyOne particles exited at outlet 2. However, there was a still a small extent of crossover between the two particle populations at outlet 3. By increasing the temperature to 50 °C a full separation was achieved, with the M-270 particles exiting the chip via outlets 5, 6 and 7, whilst the MyOne particles exited via outlets 2, 3 and 4. Thus, the results showed how the resolution of a particle separation could be improved by simply increasing the temperature.

The theoretical particle trajectories (Fig. 79), determined as described in Section 2.5.9, compared very well with the experimentally observed particle paths, particularly at 5 and 20 °C. At these lower temperatures the majority of the particles were observed to exit via the outlets predicted by the theory, while at 50 °C the majority of the particles exited via outlet 7 while the theory predicted that most would exit at outlet 6. However, the theoretical path exits very close to outlet 7, suggesting that with a slight spread (due to different starting positions) a large number of particles would likely exit via outlets 6 and 7, as observed in the experimental results.

As in Section 3.2.4, the $\mathbf{u_{mag}}$ and $\mathbf{F_{mag}}$ values were calculated from the experimental results and compared to the theoretical values. As the experimental values were measured in a slightly different area than previously, a slight increase in experimental $\mathbf{u_{mag}}$ values for the M-270 particles was observed. Again, a $(\mathbf{B}{\cdot}\nabla)\mathbf{B}$ value of 2.16 $T^2$ $m^{-1}$ was used to calculate the theoretical values for the M-270 particles, while a slightly lower value of 1.60 $T^2$ $m^{-1}$ was used for the MyOne particle calculations due to the fact that these particles moved through a region further away from the magnet than the M-270 particles at all temperatures throughout the experiments. Despite the overall increase in experimental $\mathbf{F_{mag}}$ and $\mathbf{u_{mag}}$ values for the M-270 particles (Table 13, below) compared to those in the previous section (Table 12), the results at 5 and 20 °C supported the theoretical values very well, coming very close to matching the theory perfectly. With regards to the results at 50 °C, the experimental $\mathbf{F_{mag}}$ value was again notably higher than that expected by the theory. As mentioned, this may be due to the slightly different location of measurement, where a small increase of $\mathbf{B}$ or $\nabla\mathbf{B}$ may have affected the particles at the higher temperature.

The experimental and theoretical values for the MyOne particles (Table 14) show a significantly decreased amount of force on the particles compared to the M-270 particles, corresponding to lower values of $\mathbf{u_{mag}}$ as would be expected. The experimental $\mathbf{F_{mag}}$ values were generally in good agreement with the theoretical forces, although the value at the lowest temperature is a little low and this is reflected by a slightly lower than expected $\mathbf{u_{mag}}$ value. Despite this minor discrepancy, the values still agreed closely, indicating that the experimental results followed the expected theory.

**Table 13** **Experimental and theoretical values of $u_{mag}$ and $F_{mag}$ for the M-270 magnetic particles during the separation.**

| Temperature / °C | Theoretical $F_{mag}$ / pN | Experimental $F_{mag}$ / pN | Theoretical $u_{mag}$ / $\mu$m s$^{-1}$ | Experimental $u_{mag}$ / $\mu$m s$^{-1}$ |
|---|---|---|---|---|
| 5 | 3.79 | 4.29 ± 0.23 | 81 | 92 ± 5 |
| 20 | 3.79 | 3.92 ± 0.25 | 121 | 125 ± 8 |
| 50 | 3.79 | 5.80 ± 0.59 | 223 | 342 ± 35 |

**Table 14** **Experimental and theoretical values of $u_{mag}$ and $F_{mag}$ for the MyOne magnetic particles during the separation.**

| Temperature / °C | Theoretical $F_{mag}$ / pN | Experimental $F_{mag}$ / pN | Theoretical $u_{mag}$ / $\mu$m s$^{-1}$ | Experimental $u_{mag}$ / $\mu$m s$^{-1}$ |
|---|---|---|---|---|
| 5 | 0.45 | 0.32 ± 0.08 | 30 | 21 ± 5 |
| 20 | 0.45 | 0.47 ± 0.05 | 45 | 46 ± 5 |
| 50 | 0.45 | 0.40 ± 0.03 | 82 | 73 ± 6 |

Overall, the average experimental $F_{mag}$ values show that the forces experienced by the M-270 particles were 11.8 ± 0.7 times those experienced by the MyOne particles. This was very close to a theoretically expected increase of 9.2, which is likewise supported by the 9.1 times increase in the volume of magnetisable material determined using Table 6. The difference between experimental and theoretical values is likely due to the effect of the inhomogeneous gradient that amplifies the effect in regions closer to the magnet.

The increase in $u_{mag}$ due to changes in viscosity between 5 and 50 °C would theoretically be 2.75 times for both particle types, as described in the previous section.

The increases observed experimentally for the M-270 and MyOne particles were 3.72 and 3.48, respectively. The values are larger than expected in both cases, but can be explained for the M-270 particles because of the greater than expected $\mathbf{u_{mag}}$ value at 50 °C (as explained earlier), and for the MyOne particles because of the lower than expected $\mathbf{u_{mag}}$ velocity at 5 °C (also explained above). In both cases the differences between the expected and experimental $\mathbf{u_{mag}}$ values were likely due to the effect of the inhomogeneous gradient.

The results clearly show that by increasing the temperature of the magnetophoresis system, the resolution of the separation is also increased. Although both particle types experienced greater deflection, the effect was much more pronounced for the M-270 particles, allowing them to deflect much further than the MyOne particles at the higher temperatures. Whilst these two varieties of commercially available particles could not be separated at lower temperatures, their separation at higher temperatures is significant since they are two commonly used magnetic particle types. As such their simultaneous sorting at higher temperatures could be used for the separation of different target analytes from the same sample mixture by employing suitable functional groups on each particle type. In addition, control of the temperature could be used to fine tune separations, such that the separated species exit via only certain outlets, from which further downstream processing or collection could take place. A potential limitation of the procedure is that the application to biological species may not always be suitable since, for example, the viability and properties of cells are temperature dependant, as are other biomolecules, several of which are commonly used as surface functional groups on commercially available magnetic particles. Therefore, in the case of separations involving biological species, the setup of the system may need to be tailored to suit the temperature conditions required.

The system could be optimised by applying particle focussing techniques to the sample inlet channel, which would allow a narrow stream of particles to be introduced rather than a wide spread as was found in these experiments. A narrow stream would ensure that all particles experienced the same magnetic forces throughout the chip, such that they would follow a more reproducible path and exit by only one outlet rather than several. This would have the advantage that narrower outlet channels could be used to collect different particle types whose properties are only slightly different, such that their deflection distances are similar.

Overall, the method presents a simple yet efficient means of improving separation resolution by controlling the temperature of the buffer solution. While this technique was applied here to free-flow magnetophoresis, it could also be employed for a number of other continuous flow separation systems that involve the lateral deflection of particles or cells through flowing liquids via external forces.[145]

### 3.2.6   Summary

Two sets of experiments were performed to determine the effect of changing the buffer solution viscosity in on-chip free-flow magnetophoresis experiments, via control of the system temperature. In the first experiments, the particle deflection behaviour of 2.8 μm magnetic particles was observed over a range of 5 to 50 °C. Here, it was determined that increasing the temperature of the buffer solution, and in turn decreasing its viscosity, reduced the viscous drag force on the particles and allowed them to deflect further across the separation chamber in the y-direction, towards the region of highest magnetic field. This allowed particles to exit the chamber at outlets further away from the particle inlet than at lower temperatures. The deflection behaviour of the particles at

different temperatures was found to be predictable based on the expected theory, with particle trajectories comparing well with simulated particle paths.

The second series of experiments showed how the temperature control system could be used to improve the resolution of particle separations. 2.8 μm and 1 μm diameter magnetic particles were separated using the on-chip free-flow magnetophoresis system at temperatures of 5, 20 and 50 °C. At the lower temperatures, the viscosity of the solution was so great that the particles experienced very little deflection towards the magnet and could not be separated. At 50 °C, however, the two particle populations were fully resolved due to the much greater magnetically induced velocity of the larger particles compared to the smaller particles at this temperature, combined with the reduced drag force. Thus, this method presents a simple yet efficient means of improving the resolution of particle separations by controlling the temperature of the buffer solution.

# 4 Multilaminar flow procedures

The work described in this chapter concerns the determination of laminar flow and magnetic particle characteristics in a microfluidic device developed for performing multistep reactions and assays in continuous flow.

## *4.1 Introduction*

As described in Section 1.5, the principle of on-chip free-flow magnetophoresis was further developed such that continuous flow reactions and assays could be performed on mobile magnetic particles. Briefly, laminar flow is generated in the x-direction across a wide chamber, as in the magnetophoresis device, but with the flow now consisting of alternating streams of reagents and buffer solutions (Fig. 37). Functionalised magnetic particles are then introduced into the chamber and deflected sequentially through each of the streams, allowing consecutive reactions to take place on the particle surfaces.

At the outset of the work described in this thesis, a one-step proof-of-principle reaction had been performed by Peyman *et al*.,[394] in which streptavidin coated magnetic particles were deflected through a stream of fluorescently labelled biotin. While the results showed great promise for performing multistep reactions in rapid timeframes and using only a simple setup, there remained the necessity to take the work further and demonstrate its potential for different procedures, and developing the system towards more relevant chemical and biological uses. At this point, three types of useful processes were investigated by different members of the research group: (i) bioassays (by Sally Peyman),[424,425] (ii) DNA hybridisation (by Martin Vojtišék),[426] and (iii) chemical reactions/depositions (the work described in this thesis). The chemical

reactions and depositions were a significant departure from the more biology based studies pursued by the other members of the group, and were important to demonstrate the versatility of the system for important chemical procedures.

Here, a number of investigations were undertaken to determine the ability of the microfluidic platform for performing chemical reactions. The four chapters following this one describe the different areas to which the platform was applied. Firstly, a fluorescamine reaction (Chapter 5) was attempted as a simple one-step reaction to demonstrate a chemical reaction in the system, and this was followed by a more complicated amide bond synthesis (Chapter 6). Next, the adsorption of chemical species onto magnetic templates in continuous flow was explored by looking at a proof-of-principle layer-by-layer (LbL) deposition method of polyelectrolytes onto particles and cells (Chapter 7). Finally, at a late stage in the project, a clinically relevant two-step sandwich immunoassay of the inflammatory biomarker, C-reactive protein (CRP), was investigated for performing rapid clinical diagnostics after the departure of Sally Peyman from the project (Chapter 8). In each of these cases, the multilaminar flow system presented a means of reducing the large processing times to only a few minutes, with only a pumping mechanism and a simple permanent magnet. Before all of these applications are discussed, however, this chapter describes the operation of the multilaminar flow platform itself, including the laminar flow regime present in the system and the theoretical characteristics of the particles in the chamber.

## *4.2 Laminar flow*

Before performing particle experiments in the multilaminar flow chips, the flow regimes were tested to confirm that they were laminar. If the flow was not laminar then

the alternating reagent and buffer streams could not be generated. Additionally, the extent of diffusion between the streams was studied in order to determine whether the diffusion could be problematic. An investigation by Peyman *et al.*[424] had already established in previous work that the diffusion between the laminar streams was not sufficient to cause cross-contamination between reagents, but it was nonetheless studied briefly here to ensure that this was the case. Fig. 80 shows the laminar flow regime of alternating streams of water and blue ink in chip design MLF1 (captured using a black and white camera), with the liquids pumped through the chamber at 15 μL h$^{-1}$ (278 μm s$^{-1}$ in the chamber). The figure clearly shows that laminar flow was obtained, with the blue and colourless liquids flowing side-by-side through the microfluidic chamber. This corroborates with the theoretically calculated Reynolds number (Re) of 0.0110 as determined by Equation 1, much lower than the Re < 2000 threshold required for flow to be laminar.

The streams were forced in the y-direction from the particle inlet at the bottom of the chamber due to the high pressure in the particle inlet (determined to be 855 Pa by Equation 37) compared to the other inlets (255 to 358 Pa). Midway through the chamber the streams had stabilised and were of roughly equal widths, before they were again forced in the y-direction at the outlets due to extremely high pressure at the waste outlet (1157 Pa) compared to the particle outlet channel (292 Pa). It was for this reason that different lengths and diameters of capillary were used in the waste and particle outlet holes (the effect would have been even more pronounced without doing so), in order to increase the pressure at the particle outlet and force the solution towards the waste outlet to stabilise the flow in the chamber even more. Still, even with this scenario, the flows throughout the majority of the chamber were near horizontal, and this was seen as acceptable for a simple one-step reaction procedure. The diffusion between the streams across the width of the chamber was measured 600 μm from the

outlet channels, as shown by the red line in Fig. 80a. The diffusion was measured by plotting the grey scale against the distance across the channel, where the grey scale range was 0 (black) to 255 (white) (Fig. 80b). The plot shows very distinct regions of the blue and colourless solutions, with "plateaus" on the line graph that show there was little diffusion between the streams. The amount of diffusion between the colourless and blue streams in the centre of the chamber was determined as being ~ 200 μm, as shown on the graph.
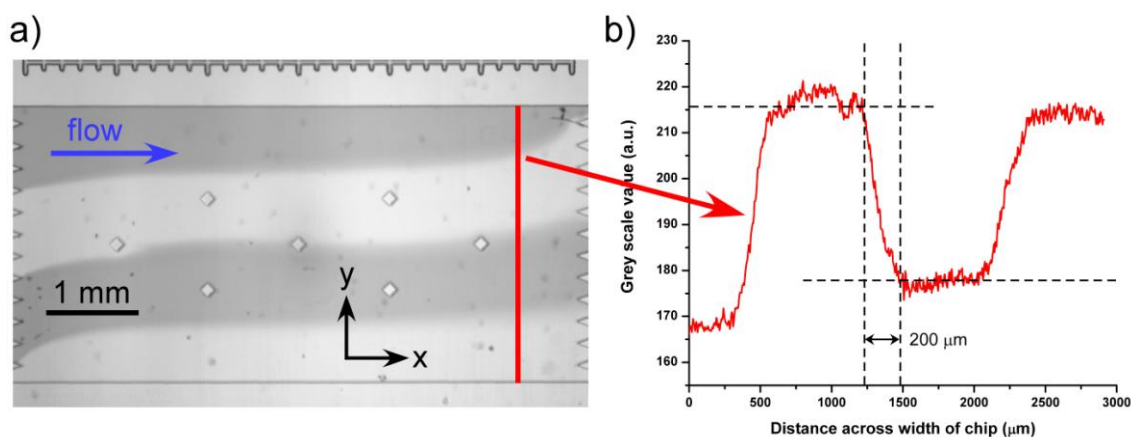


**Fig. 80 a) Laminar flow of alternating blue ink and water streams in multilaminar flow chip design MLF1. The diffusion across the width of the chamber was measured along the red line. b) Grey scale plot of the diffusion along the red line. The lower values correspond to the blue ink, and the higher values to the water. The distinct plateaus show that there was not a great deal of diffusion between the streams.**

Fig. 81a shows the laminar flow regime in chip design MLF2, observed using alternating red and yellow inks. The upper image demonstrates the flow at 232 μm s$^{-1}$ in the chamber (applied flow rate of 10 μL h$^{-1}$), which was typically used in experiments, and shows very well-defined, straight flow streams, proving that the flow

was laminar. This also correlates with the calculated Reynolds number (Re) of 0.0092. The yellow ink streams were slightly wider than the red streams, which was expected by theoretical calculations using Equation 37, whereby the increased flow resistance at inlets 2 and 4, as well as outlets 2 and 4, causes a larger pressure difference than at other channels, forcing the yellow ink to expand slightly more than the red ink as it entered the chamber.

As for chip design MLF1, the diffusion was measured across the chamber of MLF2, at a distance of 600 μm from the outlets as illustrated by the black line. The results are shown as the black line on the graph in Fig. 81b, which as before clearly shows distinct grey scale values for each of the coloured streams, indicating that there was little diffusion and certainly not enough for the reagent streams (from inlet 2 and 4) to diffuse across the central washing stream (from inlet 3) and cause cross-contamination. By performing the same type of analysis as shown in Fig. 81b, the average diffusion distances between streams were found to be 248 ± 40 μm. The lower image in Fig. 81a shows the laminar flow in MLF2 at a flow velocity of 23.2 μm s$^{-1}$ in the chamber (flow rate of 1 μL h$^{-1}$), which was never used when performing actual multilaminar flow experiments but was applied here as a comparison to the flow at 232 μm s$^{-1}$. At such a low flow rate, it can be seen that the laminar flow streams are less well-defined, and analysis of the diffusion (red line) in Fig. 81b clearly shows that the "yellow" streams have been contaminated by the red streams, hence the lower maximum grey scale values compared to those in the black line. Hence, the lower image exemplifies the importance of flow rate in controlling the extent of diffusion between streams (as described by Equation 3), a particularly important factor in the multilaminar flow studies.

These results show that, at the 15 μL h$^{-1}$ and 10 - 12 μL h$^{-1}$ flow rates for chip designs MLF1 and MLF2, respectively, stable laminar flow is achieved using both designs, with

minimal diffusion. With this, it was concluded that the designs were suitable for performing multilaminar flow experiments.
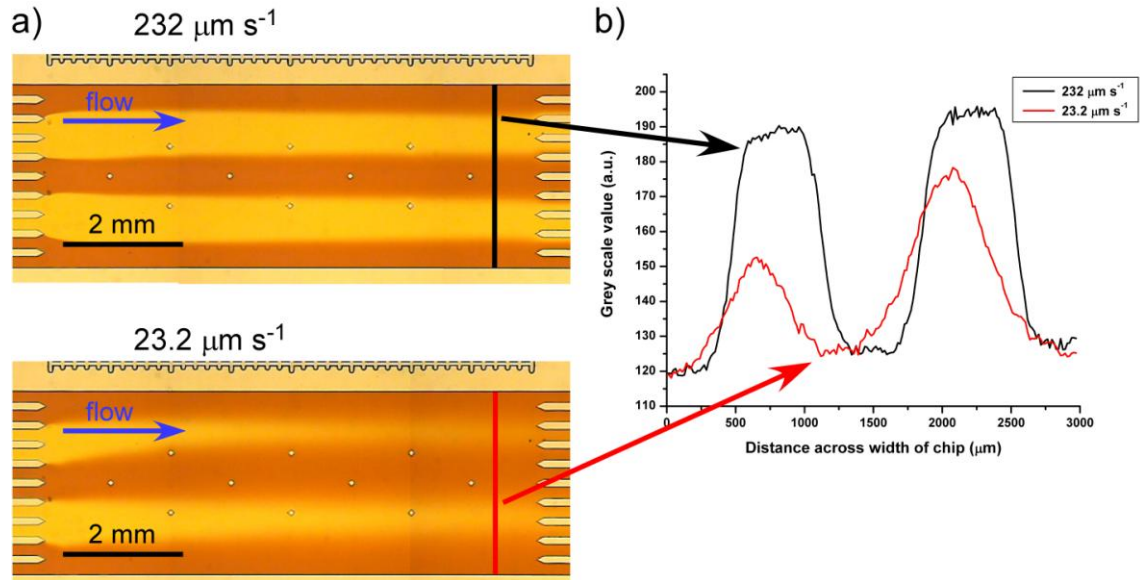


**Fig. 81  a) Laminar flow regime of red and yellow inks in chip design MLF2 at 232 $\mu$m s$^{-1}$ (upper image) and 23.2 $\mu$m s$^{-1}$ (lower image).  b) Diffusion of red and yellow inks across the width of the chamber at the faster and slower flow rates.**

## *4.3     Particle characteristics*

As well as ensuring that the laminar flow in the chamber was stable and that diffusion was not problematic, further considerations must be taken into account concerning the particles in the chamber. Firstly, the average velocity of the particles was calculated using Equation 44 to be 149 $\mu$m s$^{-1}$ and 115 $\mu$m s$^{-1}$ for MLF1 and MLF2, respectively. As described in Section 3.2.3, particles undergo Brownian motion that can cause them to diffuse through a liquid, an important factor to consider here since the particles should not be able to diffuse out of one laminar stream and into another when not under the influence of a magnetic field. The diffusion coefficient (*D*) of the M-270 particles

in water at 20 °C was calculated using the Stokes-Einstein equation (Equation 45) to be $1.53 \times 10^{-13}$ $m^2$ $s^{-1}$. Therefore, the diffusion of particles due to Brownian motion whilst traversing a microfluidic chamber was calculated via Equation 3 as 5.7 µm and 4.0 µm for MLF1 and MLF2, respectively. This means that, without the presence of a magnet, as the particles flowed across the chamber they would only migrate about 5.7 µm or 4.0 µm in the y-direction, which is not enough for particles to diffuse out of the their buffer stream and into a reagent stream without the assistance of a further force, i.e. magnetism.

Another factor to consider regarding the particles is their effect on the surrounding flow. As the particles pass from stream to stream, they have the potential to disrupt the flow around them, making it turbulent, and dragging solution in vortices behind it (a phenomena known as vortex shedding). To determine whether this was likely to occur, the Reynolds number of the particles ($Re_p$) was calculated using Equation 46.[427,428]

$$\text{Re}_p = \text{Re}\frac{(2r)^2}{r_h^{\ 2}} \qquad\qquad \textbf{Equation 46}$$

Here, Re is the Reynolds number of the channel (given by Equation 1), $r$ is the particle radius (m), and $r_h$ is the hydraulic diameter of the channel (m). Laminar flow only occurs around particles up to a $Re_p$ value of 0.1, above which vortex shedding will then take place, causing disruptions to the flow around it. Thus, Equation 46 was used to calculate the $Re_p$ of the M-270 particles in MLF1 and MLF2, where they were found to be $5.5 \times 10^{-5}$ and $4.5 \times 10^{-5}$, respectively. The determined values were much lower than the Re = 0.1 threshold, meaning that flow was laminar around the particles and there was no risk of solutions crossing from one stream to the next due to the movement of particles through them.

## *4.4    Summary*

This chapter described the generation of the multilaminar flow streams within the chambers of the two microfluidic devices, MLF1 and MLF2, and demonstrated that at the flow rates employed, the diffusion in the system was not sufficient to cause contamination of reagents across washing streams.  Additionally, it was shown that the magnetic particles exhibit low Reynolds numbers, such that the flow around them remained laminar, and that any noticeable translation of the particles in the y-direction would be due to their attraction to a magnetic field, and not due to diffusion as a result of Brownian motion.  With the chip parameters and particle behaviour established as being theoretically suitable for performing multilaminar flow experiments, procedures could then be undertaken for the application of the system to a number of processes, beginning with a one-step fluorescamine reaction.

# 5      Fluorescamine reaction

In this chapter, an investigation into the application of the multilaminar flow platform is described for performing a fluorescamine reaction on amine functionalised magnetic microparticles.

## *5.1      Introduction*

Prior to 1972, reactions used for the fluorescence analysis of amino acids peptides had to be performed in conditions that were "*severe enough to often impede its wider utility*", often resulting in limiting side reactions.[429] It was at this point, however, that Weigele *et al.*[429,430] developed fluorescamine (4-phenylspiro[furan-2(3*H*),1'-phthalan]-3,3'-dione), a compound that revolutionised the fluorescence detection of primary amine-containing species. Fluorescamine, which is non-fluorescent in its common state, reacts with primary amines in aqueous solutions at room temperature to form highly fluorescent products. It also reacts with water and other amines, but in these cases it only forms non-fluorescent products, making it a very specific analytical tool.[431]

The reaction with primary amines proceeds at pH 9 and at room temperature, with a half-time (the time required for the reagent concentration to be halved due to its reacting with a species) for most amino acids of 200 - 500 ms.[432] Excess fluorescamine is then hydrolysed with a half-time of 5 - 10 s, yielding non-fluorescent, water-soluble products and ensuring that all remaining reagent is rendered inert. However, due to its reactivity with water, fluorescamine cannot be stored as an aqueous solution. Therefore, it must be stored in a water-miscible solvent such as acetone (most common), acetonitrile,[433] chloroform,[434] or dimethylsulphoxide (DMSO),[435] then mixed with an aqueous solution

containing the primary amine species. The amine reacts first due to the small half-time, and the excess fluorescamine then reacts with water as described above, following the reaction scheme shown in Fig. 82. The exact mechanism of the fluorescamine reaction is not known, but it is believed to proceed via an intermediate as shown in the figure.[436,437]

Since primary amines can be found in a variety of molecules and biological samples, fluorescamine has been used for a wide range of applications and analysis. Examples include the analysis of <10 ng of proteins,[438,439] with detection of amino acids achieved in the picomole range.[432] It has also been applied to the determination of primary amine endgroups on polymers,[434] the analysis of functionalised polymer surfaces such as those treated with aminopropyltriethoxysilane (APTES),[440] and the surface properties of functionalised silica particles.[441,442]
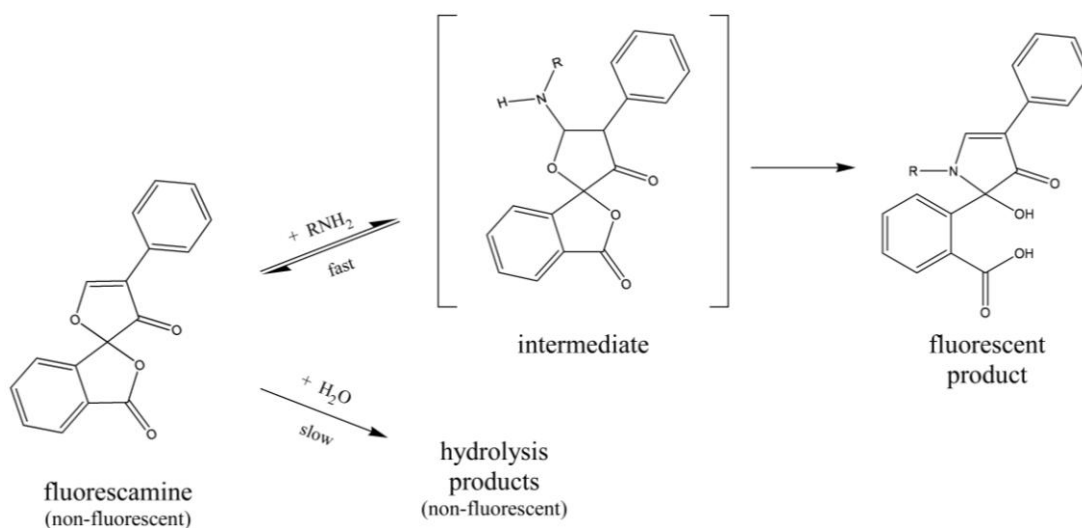


**Fig. 82 Fluorescamine reaction scheme, showing the fast reaction with primary amines to form a fluorescent product via an intermediate, and the slower formation of hydrolysis products.**[431,436,437]

With its usefulness made apparent, fluorescamine has inevitably found its use in microfluidic devices in numerous applications. These have included the prelabelling of proteins for performing electrophoretic separations in a chip-based hand-held microanalytical instrument, designed for field analysis, forensics, and point-of-care diagnostics.[433] A microfluidic device was also designed for use in extraterrestrial exploration in which a microfabricated capillary electrophoresis chip was used to separate and analyse fluorescamine-labelled amino acids for their composition and chirality.[443] The device was designated the Mars Organic Analyzer (MOA), developed for analysing surface organic molecules on Mars. After some development it was able to detect amino acids at 70 parts per trillion to 100 parts per billion in field tests of jarosite, a mineral recently detected on the red planet.[444,445] The developers of the MOA also applied it to the terrestrial analysis of bioamines in fermented beverages, and were able to separate and detect prelabelled amino acids in just 120 s, with detection limits below 1 $\mu$g mL$^{-1}$.

Here, the fluorescamine reaction was investigated using the multilaminar flow platform. However, fluorescamine was chosen simply for performing a chemical reaction with the system rather than the biological assays seen previously. Here, amine functionalised particles were to be introduced into the chamber and deflected through a stream of fluorescamine reagent, whereupon the chemical reaction would take place on the particle surfaces and render them fluorescent, signifying a successful procedure (Fig. 83).
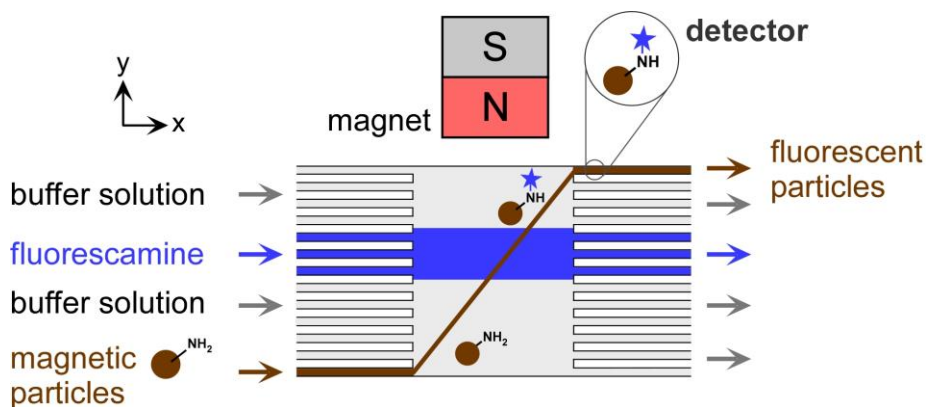
**Fig. 83** **Principle of the one-step multilaminar flow procedure for performing a fluorescamine reaction on amine functionalised particles by deflecting them through a reagent stream.**

## 5.2 Results and discussion

### 5.2.1 Off-chip tests

Prior to performing on-chip experiments, the fluorescamine reaction was performed off-chip at room temperature (20 °C) to ensure that the reaction occurred as expected. Particles in borate buffer were incubated with fluorescamine in acetone before being washed, then the particle intensities before and after the reaction were measured as described in Section 2.7.3. Unreacted amine coated particles exhibited no fluorescence signal under UV excitation, whereas particles having undergone the fluorescamine reaction (and subsequent washing in borate buffer) indeed displayed a signal, indicating that the fluorescamine reaction had successfully taken place on the amine functionalised magnetic particles, as illustrated in Fig. 84. Thus, the reaction was attempted using the multilaminar flow system.
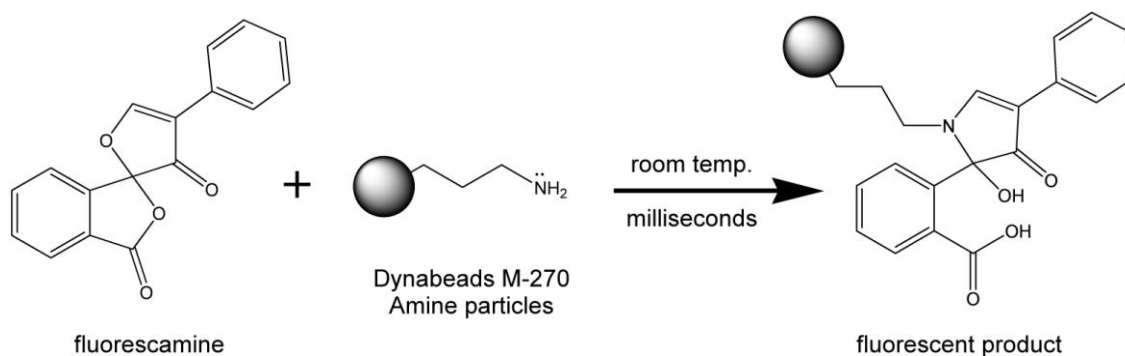
**Fig. 84  Fluorescamine reaction with amine functionalised magnetic particles at room temperature, giving a fluorescent product.**

## 5.2.2  On-chip tests

As detailed in Section 2.7.4, Dynabeads M-270 Amine particles were introduced into the microfluidic chamber of chip design MLF1 via inlet 1, with a stream of fluorescamine solution generated from inlet 3, and washing buffer streams from inlets 2 and 4.  The principle of the experiment is shown in Fig. 83, in which the amine particles would be deflected through the stream of fluorescamine, allowing the reaction to take place that would result in an increase in fluorescence signal.  However, in initial experiments, the particles simply stuck to the surface of the glass upon entering the chamber and would not move thereafter.  This likely occurred as a result of two factors, the first being that the particles would have experienced an upwards magnetic force due to the NdFeB magnet being placed on top of the chip, which would have drawn the particles towards the upper surface of the glass chamber.  Secondly, the amine particles had a positive charge at pH 9 (see Table 5) while the glass surface of the chip would have exhibited a negative charge, hence the particles would have experienced an electrostatic attraction to the surface.  When performing the free-flow magnetophoresis experiments prior to this, in which the magnet was also placed on top of the chamber,

particles were only observed to stick to the glass surface when very close to the position of the magnet, whereas for the fluorescamine experiment they became stuck as soon as they entered the chamber. Thus, it was thought that while the particles experience an upwards force due to the magnetic field, the electrostatic repulsion due to the negatively charged particles and surfaces in the free-flow magnetophoresis chamber was sufficient to stop adsorption of the particles to the glass. However, in the fluorescamine case, no such repulsive force is present, with the forces in fact being attractive, hence the sticking.

In an effort to reduce this effect, the glass channels were treated with octadecyltrichlorosilane (OTS) as described in Section 2.4 to render the chip surfaces uncharged, albeit hydrophobic. With the uncharged surface, it was found that when only borate buffer was present in the chip (i.e. without fluorescamine solution) the particles could be deflected across the entire chamber without any sticking occurring, due to the lack of electrostatic attraction. However, when the fluorescamine stream in acetone was introduced, the particles would flow through the borate buffer until encountering the acetone interface, whereupon they instantly stuck to the chip surface as before without crossing the acetone stream at all. An attempt to reduce the sticking involved using trichloro(1*H*,1*H*,2*H*,2*H*-perfluorooctyl)silane (FDTS) to treat the glass surfaces rather than OTS. FDTS features a perfluoroalkyl chain (Table 9) that, when coated onto the glass surfaces, formed uncharged and hydrophobic surfaces that prefer to be wetted by fluorinated species. As observed with the OTS treatment, however, the particles were able to flow through the chamber without sticking whilst in borate buffer, but upon encountering the acetone stream they simply stuck to the surface again.

Further attempts to manoeuvre the particles through the stream of solvent included changing the acetone stream to acetonitrile (a polar aprotic solvent like acetone), and

even to solvents such as ethanol and propan-2-ol that were tested since, like water, they are polar protic solvents (although this feature renders them unsuitable for the fluorescamine reaction). However, in each case the particles again became stuck to the surface of the chip (treated with FDTS in each case) upon encountering the borate buffer-to-solvent interface. In addition, the presence of Tween20 surfactant appeared to have no effect on the sticking of the particles compared to its absence.

This scenario of having hydrophilic particles suspended in a non-aqueous media in a hydrophobic channel presents a complex system with regards to both DLVO and non-DLVO theory. As such, the mechanism behind the sticking of the particles to the surface is not fully understood, other than to say that an apparent lack of repulsive forces causes the van der Waal's forces of attraction to dominate. Therefore, this remains an important factor to consider regarding the potential of the multilaminar flow system for applications in which solvents are required, including many types of organic synthesis. To overcome this limitation as it is at present, future work should involve a rigorous study into the electrostatic, van der Waal's, hydration, and hydrophobic forces at work in the system from a more physical chemistry-based viewpoint. This would include characterisation of the particles in different media, the effect of the glass surfaces with different treatments (e.g. hydrophilic, charged, and hydrophobic silanisation), and the influence of different surfactants at varying concentrations. With this type of information, a wider range of practical uses for the multilaminar flow technique could become available, with the possibility of tailoring the type of chip surface, particle functionalisation, and liquid media to suit specific processes.

## *5.3    Summary*

The multilaminar flow method of performing processes on mobile magnetic particles was applied to the fluorescamine reaction; a chemical synthesis rather than a biological binding procedure that had been used previously by Peyman *et al.*[394] The fluorescamine reaction was chosen since commercially available amine functionalised Dynabeads M-270 particles could be utilised, and because the reagent is non-fluorescent until the reaction has occurred.

However, while the reaction itself was successful in off-chip tests, it was found that when transferring the procedure to the microfluidic device the particles became stuck to the channel surfaces upon encountering the acetone stream. Despite testing the process with several solvents and two types of glass surface treatment, and the addition of Tween20 surfactant, the particles could not be deflected through the solvent stream, sticking at the water-solvent interface in each case. This was presumably due to a lack of repulsive forces between the particles and the chip surface, resulting in the domination of van der Waal's forces of attraction when the particles neared the upper surface of the chamber due to their movement towards the permanent magnet.

At present, this limited the application of the multilaminar flow system to completely aqueous systems in order to prevent sticking, while further physical investigations are required to determine the causes of the sticking in non-aqueous systems and the methods by which this effect could be reduced. However, at this stage in the development of the device, it was decided to focus on procedures that could be performed in water, while the solvent-based studies could be performed elsewhere. To this end, another type of chemical reaction was selected that could be performed in aqueous conditions: the synthesis of amide bonds.

# 6    Amide bond synthesis

In this chapter, the application of the multilaminar flow microfluidic system is described for performing one reaction-step and two reaction-step amide bond synthesis on carboxylic acid functionalised particles, via carbodiimide coupling, towards performing on-chip peptide synthesis. The one-step procedure has been published in the proceedings of the MicroTAS 2009 conference.[446]

## *6.1    Introduction*

Proteins are biological macromolecules that carry out the biofunctional processes of a cell and contribute to the cell structure.[447] The biological function of a protein is determined by its folded structure, which is itself defined by its polypeptide chain containing an amino acid structure. The structure of an amino acid consists of a central carbon atom, to which a basic primary amine group, an acidic carboxylic acid group, a hydrogen atom, and a side chain (R-group) are attached (Fig. 85). The presence of the basic and acidic groups means that an amino acid can be either positively charged at low pH, negatively charged at high pH, or zwitterionic (positive *and* negative) at physiological pH.[417]

Amino acids link together via peptide bonds (amide bonds), and amino acids that are part of a peptide or protein are referred to as "residues".[448] Peptides usually contain less than 50 residues, and those containing between 15 and 50 residues are known as polypeptides. Proteins, usually as either fibrous or globular structures, contain over 50 residues, and sometimes even over 1000.[417] Proteins, and in particular the polypeptides they contain, play very important roles in biological systems, but are also of great

interest for their pharmacological properties, provided the appropriate peptides can be isolated and synthesised. Peptide synthesis, and in particular the generation of peptide bonds, is widely used throughout the pharmaceutical industry for the production of drugs that perform specific tasks in the body. The synthesis of amide bonds between compounds that are not amino acids is also important for the production of drugs, with some of the top selling drugs worldwide containing amide bonds, including Atorvastin (sold as Lipitor by Pfizer),[449] which blocks the production of cholesterol, and Diltiazem (available under many brand names from several manufacturers),[450] which is used to treat angina and hypertension. Therefore, whether synthesising peptides or another type of drug molecule, the formation of peptide and amide bonds is an important and often essential part of the process.
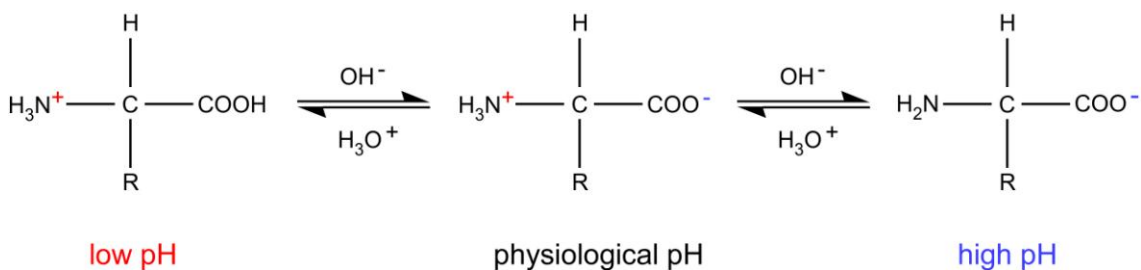


**Fig. 85  A typical amino acid exhibiting different charges depending on the pH: positive at low pH, negative at high pH, and zwitterionic at physiological pH.[417]**

Early methods of peptide synthesis were performed in solution, with all of the side-chain functional groups reversibly protected to prevent a host of unwanted byproducts being formed by reactions at unprotected functional groups.[447] However, this method gave rise to several problems when attempting to synthesise long polypeptide chains

like those found in proteins, including the poor solubility of fully-protected peptide segments in organic solvents, which led to slow, incomplete reactions and the generation of many by-products. It was also difficult to purify and characterise the protected peptide segments, hence it was necessary to deprotect them before analysis. Finally, activation of the *C*-terminal (the carboxylic acid end) of the amino acid gave rise to racemisation in the basic conditions used for condensation with another peptide segment. Despite the many drawbacks, however, a number of proteins were successfully synthesised, though the procedure was often arduous.

However, in 1963, Merrifield introduced the technique of solid-phase peptide synthesis, which greatly facilitated the synthesis of peptides.[451] Here, the *C*-terminal of an amino acid residue of a peptide chain is covalently attached to an insoluble polymer support, then the *N*-terminal (the amine end of the peptide chain) is deprotected. The resin-bound amino acid is filtered and washed, then a second amino acid added in *N*-protected, carboxyl-activated form to create a peptide bond with the resin-bound amino acid. This process could then be repeated a number of times to form a long chain, after which the chain would be cleaved from the resin and filtered to yield crude products containing a high proportion of the desired peptide. However, solid-phase synthesis has a few disadvantages, including the extra steps required to link a residue to the support and subsequently remove it, commonly via the use of hydrofluoric acid.[452]

In the last decade, microfluidic devices have been used increasingly for performing many types of organic synthesis with high yields, high purity, and short reaction times,[1,5,6] including common processes such as the Suzuki[453] and Wittig reactions.[454] The on-chip solution phase synthesis of peptides via amide bond formation was successfully achieved by Watts *et al.*,[452] in which reagents were introduced via reservoirs in a glass microfluidic chip and pumped via electroosmotic flow (EOF).

Several dipeptides were formed in quantitative yields via a carbodiimide coupling reaction[455] in only 20 min, a significant increase in yield compared to the moderate 40 – 50 % yields obtained in 24 h by batch reactions. Watts *et al.*[456] followed this work by performing more complex, multistep syntheses of *β*-peptides, via conversion from pentafluorophenyl ester. It was found that reactions in the microfluidic device generally resulted in increased reaction efficiencies compared to traditional batch methods. Furthermore, a tripeptide was synthesised using a revised system with more reservoirs, producing a 30 % yield. The work was later extended to an investigation into racemisation of synthesised α-peptides in the microreactor,[457] and the post-synthesis separation of peptides via EOF was also achieved in a microreactor.[458]

The above microfluidic peptide synthesis methods were performed in solution phase, but a solid phase was also reported on-chip. Murayama *et al.*[459] trapped resin beads in a microfluidic channel using a dam, whereupon they conducted the synthesis of a pentapeptide on the beads, though the yield was found to be only 20 %.

As magnetic particles are often utilised as solid supports in immunoassays and other bioanalytical procedures, so too can they be used as supports in solid phase peptide synthesis. Norén and Kempe synthesised magnetic nanoparticles from $Fe_3O_4$ nanopowder which were coated with a silane and then a polymer to make the magnetic support.[460] Onto this were loaded a cleavable linker onto which two different peptides were synthesised via carbodiimide coupling, one of which required 10 min coupling reactions, while the other much more challenging synthesis required 2 h couplings. The magnetic supports allowed the particles to be washed easily in-between coupling steps (as in Fig. 26). Finally, the peptides were cleaved from the magnetic supports using trifluoroacetic acid and the nanoparticle supports removed using a magnet, leaving the synthesised peptides in solution which were analysed by HPLC.

Amide bond formation is typically a lengthy and labour-intensive procedure to perform, and as with many batch processes it is dependent on diffusion of reagents to the surface of the solid-phase support. This means that, at the start of the process, the reagents can diffuse to the surface quite freely, but as the number of reactive sites diminishes and the nearby reagents are used up, the reaction slows down due to the need for reagents to diffuse further and react with fewer sites. In the work described in this thesis, microfluidic amide bond synthesis was combined with the use of magnetic particles as solid supports to demonstrate the application of the multilaminar flow system for performing chemical reactions, in particular the highly important formation of peptide (amide) bonds.
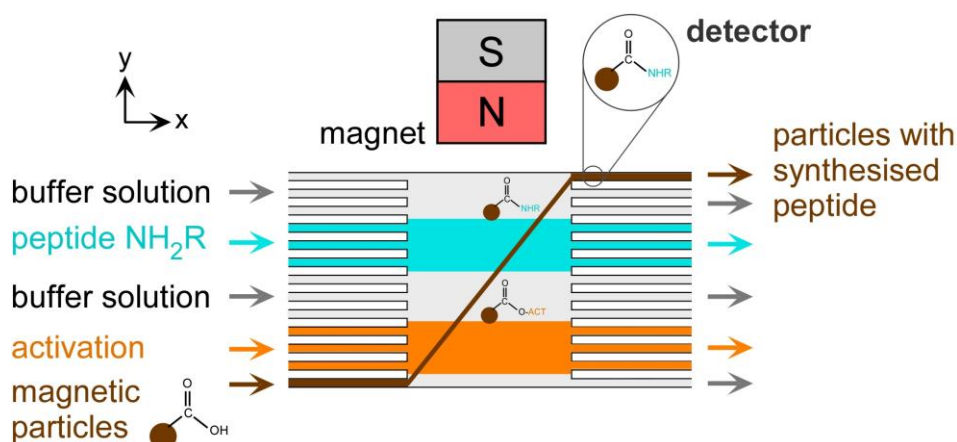


**Fig. 86  Envisaged multilaminar flow system for the synthesis of peptides. Carboxylic acid functionalised magnetic particles are first activated via a carbodiimide, then reacted with an amino acid or peptide to form a new peptide bond.**

This method has the advantage that, being in continuous flow whilst the particles are passing through the streams, fresh reagents are constantly transported directly to the particle surface, with any waste being immediately washed away. Thus, the multilaminar flow technique holds potential for performing amide bond synthesis with

short processing times, towards the multi-step synthesis of peptides on the magnetic particles (Fig. 86).

## 6.2 *Results and discussion*

## 6.2.1 Off-chip tests

A series of tests were performed to ensure that the magnetic particle-based amide bond synthesis worked as expected, the procedure of which is described in Section 2.8.3, and is based on the manufacturer's instructions. Briefly, carboxylic acid functionalised magnetic particles (Dynabeads M-270 Carboxylic Acid) were first activated with EDC carbodiimide (*N*-(3-dimethylaminopropyl)-*N*'-ethylcarbodiimide hydrochloride) in PBS buffer (pH 7.45), then washed and reacted with fluorescently labelled glycine (FGA, fluoresceinyl glycine amide) in MES buffer (pH 5). Successful peptide synthesis was indicated by an increase in fluorescence intensity compared to the unreacted particles. The reaction mechanism detailing the progress of the peptide bond formation is shown in Fig. 87.[461] Firstly, the carbodiimide undergoes nucleophilic attack by the carboxylic acid on the magnetic particle, taking a proton from the MES buffer in the process, thereby "activating" the carboxylic group by replacing the hydrogen on the hydroxyl group to give a better leaving group.[455] The amine group on the fluorescently labelled glycine then attacks the carbonyl group on the activated carboxyl group, and the structure loses the carbodiimide complex, leaving only the magnetic particle with an amide bond linking to the fluorescently labelled glycine (FGA).
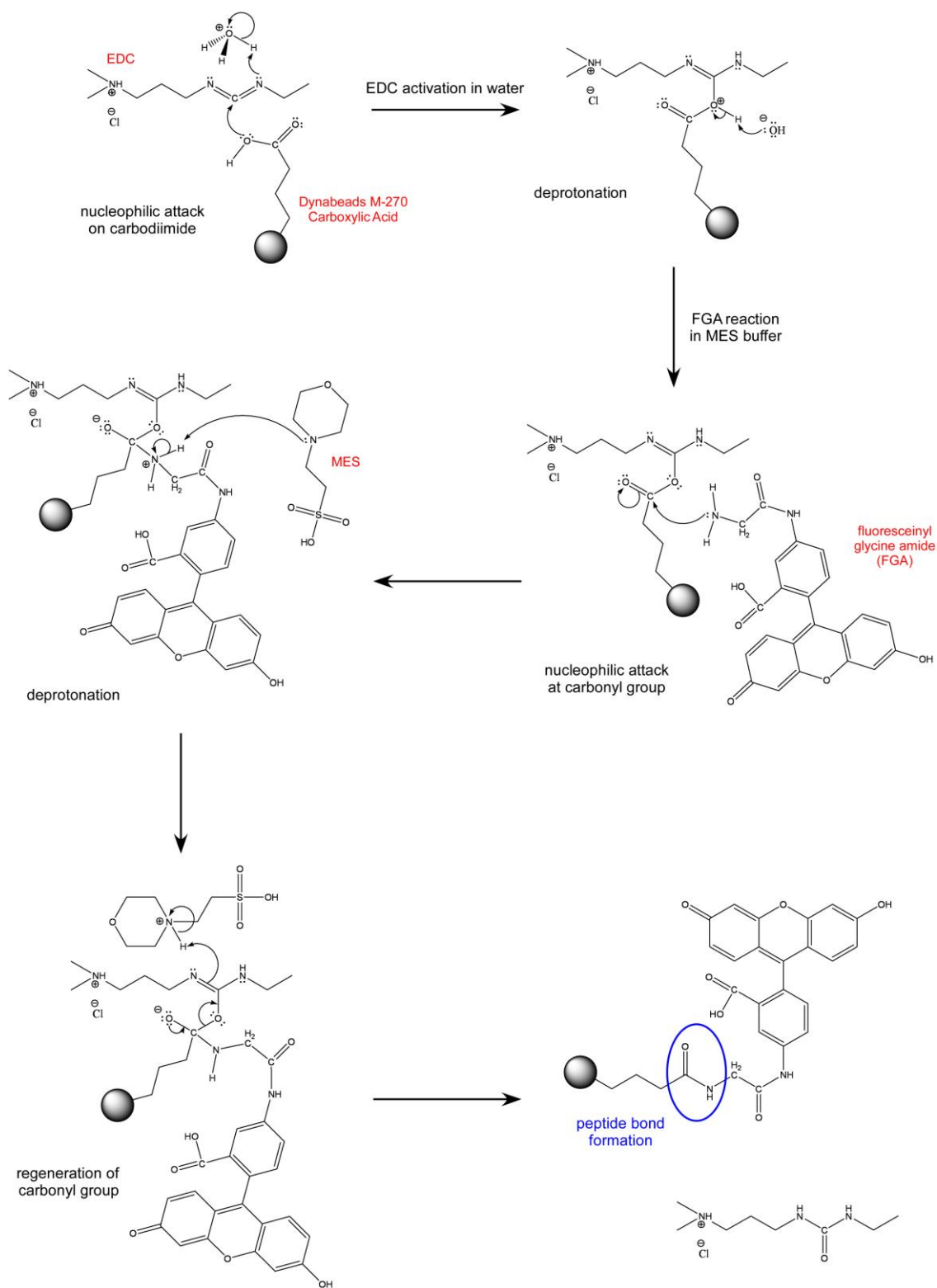
**Fig. 87 Reaction mechanism for the formation of an amide bond between a carboxylic acid functionalised magnetic particle and fluorescently labelled glycine, via a carbodiimide (EDC).**[461]

It should be noted that the pH of the MES buffer recommended by the manufacturer was pH 5, while the fluorescence of the label is known to be pH-dependent, exhibiting greater intensities at higher pH. This meant that during the on-chip procedures, particles would be required to traverse streams of differing pH in order to satisfy both the FGA reaction conditions and the ability to detect a good fluorescence signal. Ideally, it would be best to have the difference in pH be small, so at not to force the particles to migrate through very different pH environments. Therefore, off-chip tests were performed in which particles were reacted as normal, then suspended in MES and PBS buffer at different pH values to determine the effect on fluorescence intensity (Fig. 88a).
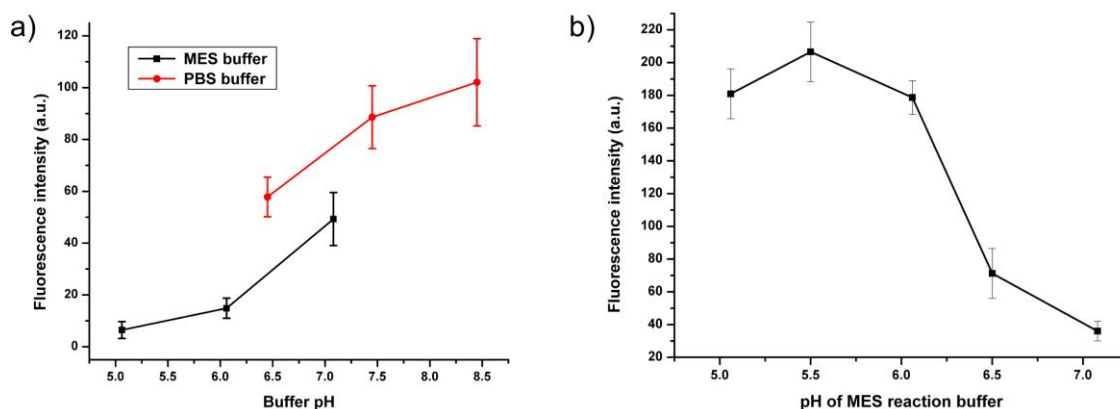


**Fig. 88  a) Fluorescence intensity of fully reacted particles in different detection buffers and at different pH values.  b) Fluorescence intensity of particles when the FGA reaction was performed at different pH values.**

It was found that in MES buffer, even at the highest pH value of 7, the fluorescence intensity of the particles was still less than the lower pH value of 6.45 used in PBS buffer, indicating that PBS was the better buffer for fluorescence. It was also

determined that the highest value of fluorescence was at a pH of 8.45 in PBS. Next, the MES buffer pH was tested for the FGA reaction itself, with the reaction performed in MES buffer from pH 5 to 7, then suspended in PBS buffer. Here, it was seen that the reaction worked best in pH 5.5 buffer, and at pH above 6 the reaction proceeded poorly (Fig. 88b). Therefore, it was decided that to keep the pH difference between the reaction (MES) and detection (PBS) buffers small but still maintain a high level of fluorescence intensity, the reaction would be performed in MES buffer at pH 6, then detected in PBS buffer at pH 7.45.

## 6.2.2    On-chip one-step reaction

Having decided to perform the reaction step in MES buffer (pH 6) and the detection in PBS buffer (pH 7.45), the peptide synthesis reaction was applied to a one-step procedure on-chip, using chip design MLF2 as described in Section 2.8.4. Here, the EDC activation step took place off-chip, and the activated particles were introduced into the chamber to be deflected through a stream of FGA, as illustrated in Fig. 89.
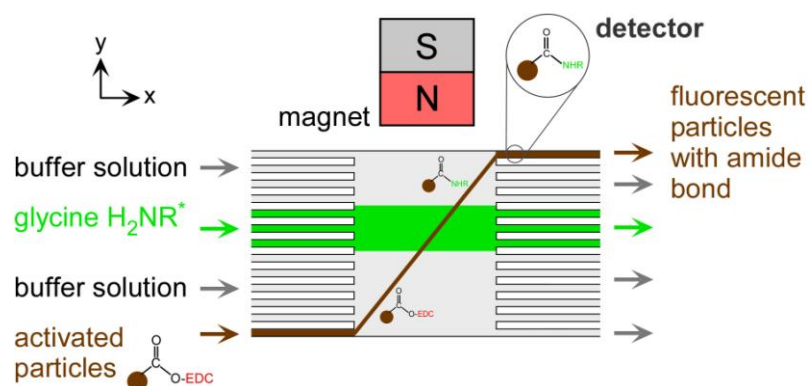


**Fig. 89   Schematic of the one-step peptide synthesis reaction, in which carbodiimide-activated particles are deflected through a stream of fluorescently labelled glycine.**

Initially, the activated particles, the first washing stream, and the FGA solution were all in MES buffer (pH 6), while the final two washing/detection streams contained PBS buffer (pH 7.45). However, upon entering the chamber (with untreated surfaces) it was found that the particles became stuck to the glass walls. This was likely due to the negative charge exhibited by the glass surfaces, while the amine groups present in the EDC compound would have made the particles positively charged, thereby causing electrostatic attraction to make the particles stick. In an attempt to reduce this effect, the particles were instead suspended in PBS buffer (pH 7.45), and the first washing stream was also replaced with PBS buffer, leaving the FGA reaction stream as the only solution in MES buffer in the chip. Off-chip tests were also performed to ensure that the change of solutions did not affect the reaction, which they did not. Now, the particles were able to deflect through the chip until the FGA interface since the nitrogen groups on the EDC were no longer protonated and thus the particles were not positively charged in PBS buffer. However, they simply became stuck again upon entering the FGA stream in the presence of MES buffer, likely due once more to electrostatic attraction to the surface.

As with the fluorescamine experiments, the next step in attempting to reduce the sticking was to test silanisation reagents. Therefore, experiments were performed using chip surfaces treated with uncharged hydrophobic (FDTS) and hydrophilic (PEG-silane or PEG-SPA, the latter of which contains more PEG groups than the former) silanes (deposited as described in Section 2.4), to determine if the sticking effect could be stopped by removing the surface charge. Here, it was found that the particles would still flow through the PBS buffer only to again stick at in the FGA stream. However, in both the hydrophilic and hydrophobic chips, the particles did not stick irreversibly to the glass surface as it was found that by flicking the inlet capillaries the sudden, if small, effect on the flow would allow the particles to "jump" slightly in the chip before

sticking again. Despite this, each jump was so small that deflecting the particles across the chip in this manner was not practical. Since sticking was still occurring with uncharged surfaces, and in cases of both hydrophilic and hydrophobic surface treatments, it was unclear what the cause of the sticking was, unless it was a case of the surface treatments not creating a monolayer across the entire chamber surface, leaving gaps of untreated glass.

Having tried using uncharged surface treatments, it was then decided to test a positively charged surface treatment (QAS, quaternary ammonium silane) that would actually repel the positively charged particles away from the surface. Additionally, a cationic surfactant, cetyltrimethylammonium bromide (CTAB), was added to each solution to a concentration of 0.1 % w/v. To ensure that the presence of CTAB did not have an adverse effect on the reaction, off-chip tests were performed with 0.1 % CTAB present in each step of the reaction, and the fluorescence intensity of the particles measured after each step. These measurements were compared to fluorescence intensities obtained for each step without the presence of CTAB, and it was found that the levels matched at each step of the reaction until after the final FGA reaction, whereupon the intensities were found to be significantly increased when CTAB was added. This is believed to be due to the electrostatic attraction of the cationic CTAB to the anionic fluorescein group, which stabilises the excited state of the fluorescein and results in enhanced fluorescence and longer fluorescence lifetimes.[462] Therefore, CTAB was added to solutions in the on-chip experiments to benefit from the increased fluorescence as well as to help reduce sticking.

When activated particles were now introduced into the chip (again with PBS in all streams apart from the FGA reaction stream), they were once again deflected through the chip until they encountered the FGA stream, at which point they again became stuck

to the chip surface. However, flicking the capillaries, as before, made the particles "jump" along the chamber, although the distances travelled by the particles as they did this were far greater than those observed when the chip was treated with FDTS, PEG-silane or PEG-SPA. It remained unclear as to why the particles kept sticking, but the theory behind using the QAS treatment appeared to benefit the system. Thus, by gently and rhythmically flicking the inlet capillaries, the particles could be made to jump across the FGA reaction stream, only briefly sticking a few times on the way. Once in the PBS washing streams they flowed more easily, as they had before entering the FGA stream.

With this, particles could now be deflected across the entire chip, albeit not in a smooth manner. Nonetheless, it allowed the EDC-activated particles to pass through the FGA stream and into the washing stream where their fluorescence intensities were measured and compared to those before the FGA stream. A typical result for this is shown in Fig. 90, which demonstrates that the average fluorescence intensity of the particles increased after the FGA reaction, suggesting that the peptide bond formation occurred to some degree, and that a chemical reaction had been successfully performed using the multilaminar flow system. However, the error bars were very large, even going below the average intensity of the unreacted particles, which strongly implied that many particles did not form amide bonds. Additionally, the average fluorescence increase was relatively small compared to the vast increases observed in the off-chip tests.

Initially it was thought that the residence time of the particles in the FGA stream may have been an issue, with particles taking around $20 - 30$ seconds to pass through the stream, a large decrease in reaction time compared to the off-chip tests in which they were incubated for 15 min. This timeframe may therefore have been too small to allow the reaction to occur. Hence, the residence time of the particles was increased by

adding additional FGA reagent streams to the system. This was achieved by simply replacing the PBS buffer solution in inlets 2 and 4 with FGA solution, which meant that as the particles entered the chip they immediately crossed through three concurrent streams of FGA and into the final remaining PBS washing/detection stream. The results of this are also shown in Fig. 90, alongside those for the single stream reaction.
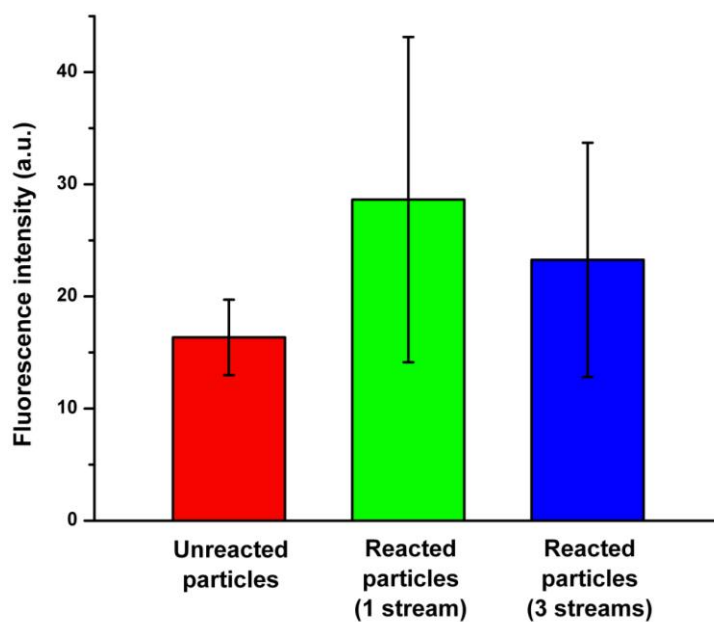


**Fig. 90 Fluorescence intensities of particles before the FGA reaction, after the reaction in one stream, and after the reaction over three streams.**

As the results show, an increase was observed in the average fluorescence of the particles after passing through the three reagent streams and reacting with the FGA, but the error remained large and the increase in fluorescence intensity was actually not even as great as that of the particles passing through the single stream. These results again showed successful chemical reaction in the case of some but not all particles, and that the problem was not one related to reaction time as first suspected. However, when looking down the objective of the inverted fluorescence microscope by eye (rather than

using the black and white CCD camera that was used to record videos/photographs of particles for analysis) it was found that some particles that had become stuck in the FGA stream were fluorescing green, indicating the reaction had been successful since the fluorescein label fluoresces green under blue light, while some particles were a yellow-orange colour. The yellow-orange colour was the same as that observed when the particles first entered the chip, before the FGA stream, which indicated that some particles in the FGA stream were reacting but others were not, despite being stuck and thus exposed to a great deal of FGA.

Therefore, it was thought that the problem was more likely to be due to the activated particles, with either some of the particles not being activated or the EDC losing its activity throughout an experiment. The former theory did not appear to be the case as, when performing off-chip tests, all of the particles displayed a large degree of fluorescence after the reaction step. The second theory was tested by activating a batch of particles with EDC, then performing the FGA reactions off-chip at 10 min intervals after the initial activation. The results for this are shown in Fig. 91.
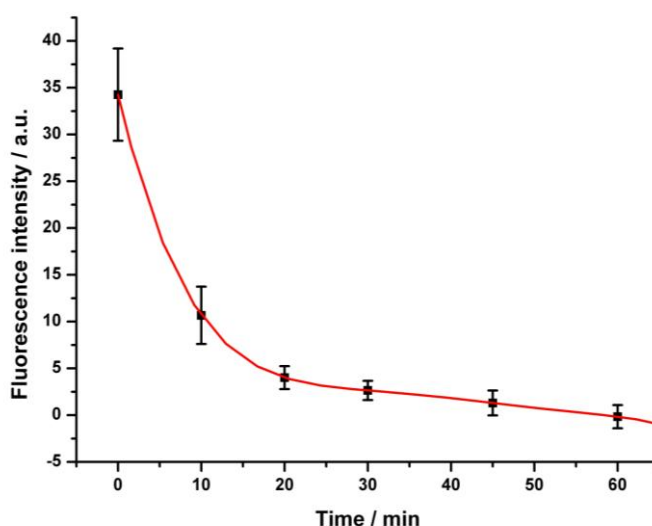


**Fig. 91 The activity of EDC-bound particles over time. The activity dropped sharply in only 10 min, and was reduced to nearly zero after 20 min.**

The results showed that within 10 minutes of their reaction with EDC, the particles showed a 69 % decrease in activity, while after 20 min the particles showed almost no activity. It is known that EDC, despite being an aqueous-based carbodiimide, forms hydrolysis products with water over time, hence particles cannot be stored for a long time and must be used immediately.[463] This was perfectly acceptable for the off-chip tests since the particles were activated, washed, and immediately reacted with FGA solution. When performing the on-chip experiments, however, the particles were activated, introduced into a syringe, and connected to the chip and syringe pump, whereupon the pump was started. Each solution had to first be pumped through the inlet capillaries and into the chamber, then the streams allowed to stabilise, and if air bubbles were present they had to be removed by applying some manual pressure, all of which typically required several minutes before the system was running normally.

Thus, even trying to introduce activated particles into the chip as quickly as possible, there was usually at least a few minutes before particles would enter the chamber itself. According to the results in Fig. 91, this gave only a small window of time in which activated particles would be able to react with the FGA in the reagent stream, resulting in initial measurements reacting successfully (although not in the optimal timeframe hence lower than expected fluorescence intensities) while measurements taken at a later time would show little to no signal since the particles would no longer be able to react. This explains why, according to the results in Fig. 90, the fluorescence signal for the particles that passed through three streams of FGA is smaller than that from a single FGA stream; the measurements in the former scenario likely took place at a later period than the latter, hence fewer particles would have been able to react with FGA despite the increased exposure to the reagent.

Therefore, the one-step amide bond synthesis reaction showed that a chemical reaction could be performed successfully, but it was not an ideal example due to the rapid loss of EDC activity. Thus, this particular type of reaction seems to remain better suited to batch methods in which the reagents are added to the particles in a single step, rather than on a particle-by-particle basis as in the one-step reaction method. However, it was considered that the amide bond synthesis might work better if the entire procedure were performed in continuous flow on-chip, rather than only the FGA reaction step. By performing both the EDC activation *and* the FGA reaction in a two-step procedure, the amount of time between the activation of the particles and their subsequent reaction would be minimised, thereby increasing the number of particles on which the amide bond synthesis could be performed.

### 6.2.3 On-chip two-step reaction

A series of two-step amide bond synthesis experiments were performed as described in Section 2.8.5. Briefly, carboxylic acid functionalised particles were pumped into the chamber of an MLF2 chip, where they were to be deflected through streams of (i) *N*-(3-dimethylaminopropyl)-*N*'-ethylcarbodiimide hydrochloride (EDC) solution, (ii) washing buffer, (iii) fluoresceinyl glycine amide (FGA) in MES buffer, and (iv) washing buffer, as shown in Fig. 92.

As with the one-step procedure, particles sticking to the chip surface was a problem encountered when performing the two-step experiments. In an untreated chip, the carboxylic acid particles would enter the EDC stream and stick to the chamber surface, presumably because having reacted with the EDC they exhibited a positive charge and stuck to the negative surface. A number of surface treatments as in the one-step

experiments were tried, with the particles typically flowing well until encountering the FGA stream. When the QAS surface treatment and the addition of CTAB surfactant was found to allow particles to deflect most easily in the one-step experiments, the same setup was used for the two-step reaction.
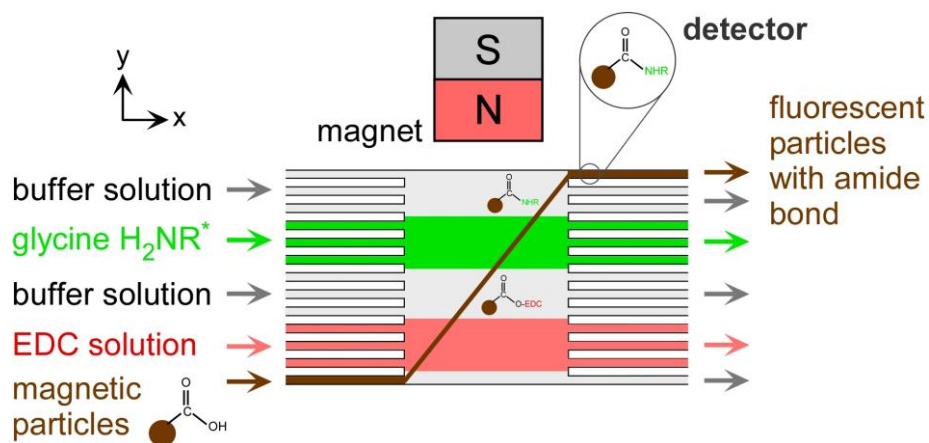
**Fig. 92 Principle of the two-step amide bond synthesis procedure using the multilaminar flow system. Carboxylic acid particles were activated in a stream of carbodiimide (EDC), before reacting with fluorescently labelled glycine in a second reagent stream to form a peptide bond.**

It was found that many carboxylic acid particles (negatively charged) became stuck to the surface as they entered the chamber, presumably due to electrostatic attraction to the now positive surface, but since the EDC stream was positioned alongside the particle stream, some of the particles were able to enter the EDC solution without sticking. Additionally, the positively charged CTAB surfactant may have become electrostatically attracted to the particles before entering the EDC stream, reducing the extent of the negative charge slightly and thus the extent of the sticking to some degree. However, this may also have resulted in a slightly lesser amount of EDC being able to

react on the particle surface. As with the one-step reaction, the inlet capillaries needed to be gently and rhythmically flicked to allow the particles to jump across sections of the chip where they were sticking. With this setup, some particles were able to cross the stream and were analysed, with the fluorescence intensities of the particles before and after the FGA reagent stream given in Fig. 93. It should be noted that the particles analysed were stuck to the chamber surfaces.
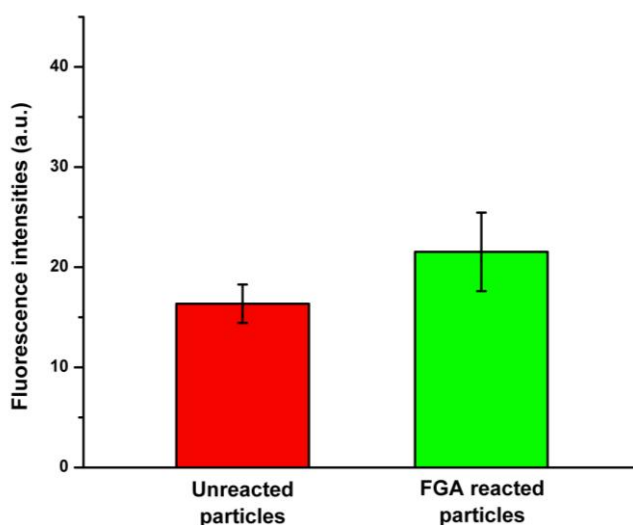


**Fig. 93  Fluorescence intensities of magnetic particles before and after passing through the fluoresceinyl glycine amide (FGA) reagent stream.  Particles showed slightly higher fluorescence after passing through the stream, suggesting the reaction was reasonably successful.**

The results show that a slight increase in fluorescence occurred for the particles having crossed the FGA stream compared to those before the stream, indicating that the two-step reaction had, to some degree, been successful. However, the error bars on the two bar graphs overlapped, showing that the results were not definitive, but nonetheless the average showed at least some evidence of the reaction working as intended. Part of the reason why the fluorescence increase was so small may be due to the addition of CTAB,

which may have blocked some of the active sites as described above. Another possible cause is the short lifetime of the EDC, as described in Section 6.2.2, since trying to deflect the particles across the chamber took a considerable amount of time to achieve due to the sticking problems.

Thus, the two-step reaction worked to a degree, in that a fluorescence increase was observed after the particles had passed through both reagent streams, but the increase was only small. One of the major problems encountered was the sticking of the particles to the surface of the chip, making it difficult to deflect particles across the chamber despite the employment of different surfaces treatments and added surfactant. This shows that the effectiveness of the multilaminar flow technique for performing reactions is, in its current state at least, hindered by processes that cause significant changes to the surface chemistry of the particles. Hence, this results in the scenario whereby particles can flow freely when they first enter a chip, but then stick once a reaction has taken place and formed new chemical groups on their surfaces.

At present, this means care must be taken that reactions selected to be performed using the multilaminar flow procedure exhibit no changes in the particle surfaces that would result in their adhering to the chip surfaces. However, this does not mean that such reactions are entirely unfeasible for future implementation via a multilaminar flow approach. As concluded in the findings of the fluorescamine reaction, in which the particles were unable to cross solvent streams without sticking, more investigation is required into the sticking effects of different types of particle surface functionalities on glass surfaces modified with different treatments. With a thorough investigation into the mechanism behind the sticking in different scenarios, and the determination of which surface treatments, surfactants, and buffer solutions are suitable for which particles, a database could be generated that would allow the appropriate combination of

parameters for unhindered particle deflection. Such an investigation would greatly increase the potential of the system for performing a wide variety of processes. Thus, the two-step amide bond synthesis procedure may yet be viable after future studies have been conducted.

## 6.3    Summary

Investigations were performed into one-step and two-step amide bond syntheses using the multilaminar flow system, as examples of the ability of the platform for performing chemical reactions and with a view towards peptide synthesis in continuous flow. However, due to the charge of the particles at various points in the chamber, the charge of the chamber surface itself, and perhaps further as yet unknown reasons, deflecting particles across the chamber proved difficult as they would stick to the surface, thus preventing them from crossing the reagent stream. By employing a positively charged chip surface and a positively charged surfactant in the one-step procedure, EDC-activated particles could be deflected across the FGA reagent stream, whereupon an increase in the average fluorescence intensity was observed. This indicated that a chemical reaction had been successfully performed using the multilaminar flow platform, a first for this type of system, although the signal increase was not as high as expected. Tests of the carbodiimide (EDC) lifetime revealed that in only 10 minutes its activity dropped by 69 %, and almost reaching zero activity after 20 min. Thus, with the time required to set up the platform to the point that particles were being deflected across the chamber, the EDC activity would already be very diminished.

A two-step reaction was studied using the same surface treatment and surfactant and, despite greater difficulties in deflecting particles across the chip, the reaction was again

shown to be successful to an extent due to the increase in particle fluorescence. However, the multilaminar flow system was not an ideal platform for amide bond synthesis in it current state, and further work will be required to develop it to the point at which high yield, reproducible amide bond synthesis can be performed. Such a development would in turn lead to the application of the system to rapid on-chip peptide synthesis on the surfaces of the mobile magnetic particles.

# 7 Polyelectrolyte deposition

In this chapter, proof-of-principle experiments were performed in which negatively charged magnetic templates were deflected through a stream of positively charged polyelectrolyte solution using the multilaminar flow platform, towards the layer-by-layer fabrication of drug capsules. This initial study has been published in the proceedings of the MicroTAS 2010 conference.[464]

## *7.1 Introduction*

Polyelectrolytes are polymer chains that contain an electrolyte in the repeating units, with the electrolytes dissolving in aqueous solution to yield charged species.[465] Thus, a polyelectrolyte is essentially a charged polymer. Common polyelectrolytes include polycations such as poly(allylamine hydrochloride) (PAH) (Fig. 94a),[466] and its fluorescently labelled counterpart poly(fluorescein isothiocyanate allylamine hydrochloride) (PAH-FITC) (Fig. 94c), poly(diallyldimethylammonium chloride) (PDADMAC),[467] and poly(ethyleneimine) (PEI),[468] as well as polyanions like poly(4-styreneslufonic acid) (PSS) (Fig. 94b),[466] and poly(acrylic acid) (PAA).[469]

In recent years, the fabrication of capsules prepared from polyelectrolytes has seen a great deal of interest for drug delivery.[466,470] With new drugs becoming available based on peptides, proteins and oligonucleotides, it is ever more challenging to introduce these into the body and have them reach the area of interest without being destroyed by enzymes and other species during their transport. Thus, the encapsulation of therapeutic drugs has been explored as a method of creating drug delivery vesicles, with the use of polyelectrolytes being one of the more promising materials with which to prepare such

capsules. The fabrication proceeds via a technique known as Layer-by-Layer (LbL) deposition, in which alternating layers of oppositely charged polyelectrolytes are coated onto a sacrificial core template, followed by the dissolution of the core to leave a hollow shell into which drugs can be introduced.
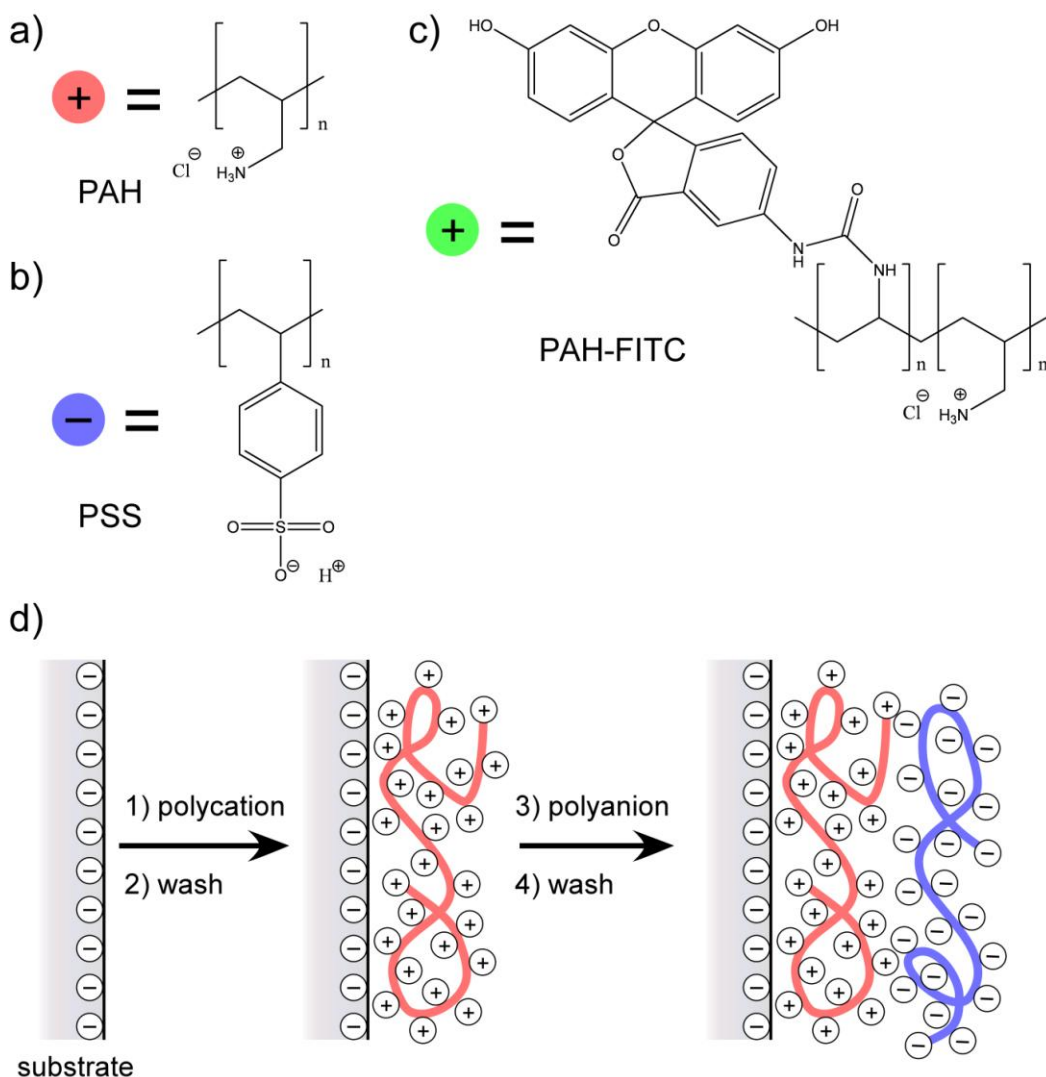


**Fig. 94 a) Structure of the repeating unit of the polycation, poly(allylamine hydrochloride) (PAH). b) Repeating unit of the polyanion, poly(4-styrenesulfonic acid) (PSS). c) Repeating units of fluorescently labelled polycation, PAH-FITC. The ratio of PAH to FITC units is 50:1. d) Layer-by-Layer (LbL) deposition of polycations and polyanions onto a negatively charged substrate. The process can be repeated over and over to build a multilayered film.**

The LbL technique also allows the option of having different functionalities incorporated within the layers of the shell, such as macromolecular drugs or nanoparticles,[467] enzymes,[471] and DNA.[472] By adding different properties to the polyelectrolyte layers, the capsules can be made to "open" in order to add or release drugs from within the shell. This effect can be achieved using stimuli such as pH,[473] salt concentration,[472] light,[474] and magnetic fields,[475] among others. Fig. 94d shows the LbL method of adhering a polycation onto a negatively charged substrate, followed by a polyanion.

The LbL method for forming alternating polyelectrolyte layers was first described by Decher, in which a charged wafer was immersed in a beaker of oppositely charged polyelectrolyte solution for a period of time, before being removed and rinsed thoroughly to remove excess polyelectrolyte.[476,477] The wafer now exhibited a surface charge opposite to that which it originally featured. It could then be immersed in a second polyelectrolyte with an opposite charge to the first, and again be removed and washed. This process could be repeated as many times as required until the desired number of layers were prepared.

Polyelectrolyte capsules were first produced in 1998 by Möhwald's research group, in which the LbL method of Decher was applied to colloidal templates.[467,478-481] In some instances the core material was a polystyrene particle, onto which layers of $SiO_2$ nanoparticles and PDADMAC were deposited,[467] while in other cases the core was prepared from melamine formaldehyde particles that were coated with layers of PAH and PSS.[479] The latter two polyelectrolytes are a particularly popular pair for forming multilayered films due to the reproducibility of the layers, and because capsules fabricated using them do not suffer from aggregation or decomposition upon removal of the core.[466] There are many types of core materials that can be used to form capsules,

with common criteria being that they are spherical, have a narrow size distribution during fabrication of a batch of capsules, and that they can be easily dissolved without damage to the polyelectrolyte layers. A selection of popular template materials are shown in Table 15, alongside the solvents used to dissolve the core after deposition of the multilayers.

**Table 15   Examples of core template materials and the solutions used to dissolve them after the production of multiple polyelectrolyte layers.**

| Core template material | Dissolution method |
|---|---|
| Polystyrene particles | Tetrahydrofuran (THF)[467] |
| Melamine formaldehyde particles | Low pH aqueous solution[479] |
| Calcium carbonate crystals | Ethylenediaminetetraacetic acid (EDTA)[482] |
| Calcium phosphate crystals | Hydrochloric acid[483] |
| Manganese carbonate crystals | Low pH aqueous solution[484] |
| Cadmium carbonate crystals | Low pH aqueous solution[484] |
| Silica particles | Hydrofluoric acid[485] |

Typically, polyelectrolyte capsules are prepared by the formation of around five to eight bilayers, with each layer being ~1 - 2 nm thick in order to make the capsules stable after core dissolution.[486]   During the LbL procedure for capsule formation, the particles/crystals are suspended in polyelectrolyte solution before being separated via

centrifugation,[487,488] although in some cases membrane filtration has been used.[489] The templates are then washed several times before being suspended in the next solution. Typically this step-by-step process is very laborious and time-consuming, with adsorption times of 20 min per layer, and three washings steps requiring centrifugation in between each layer deposition taking several minutes each. Thus, to generate even just one bilayer would take at least 1 h.

Recently, however, polymer capsules have been prepared by the LbL method using microfluidic devices. In 2008, while the study presented in this thesis was underway, Priest *et al.*[490] demonstrated a microfluidic device to generate liquid crystal droplets that were subsequently coated with a polymer by the surrounding medium (Fig. 95a). Downstream, the polymer solution was diverted to a waste channel while the droplets were rinsed and introduced into a second polymer solution. This was an efficient means of performing continuous flow capsule production with a high throughput, and the liquid crystal cores were easily removed using ethanol. However, the capsules were not formed from polyelectrolytes, instead using polymers that were bonded together via hydrogen bonding. As such, the usefulness of these capsules as drug delivery vesicles is unclear, but the technique could be used to form multilayered polyelectrolyte capsules at a later date.

Also in 2008, Zhang *et al.*[491] developed a microfluidic device in which mineral oil droplets were generated in PSS solution and encapsulated in the channel (Fig. 95b). The PSS solution was drained out of an outlet, while the droplets were deflected into a different stream by a series of pillars. This second stream contained a washing stream of water to remove any unbound polyelectrolyte, then the droplets deflected by a second series of pillars into a stream containing PAH-FITC. In total, four layers were produced, with fluorescence analysis used to observe the now fluorescent droplets,

indicating that the adsorption process was successful. However, photographs supplied by the authors of the final products showed that there was a large degree of size variation of the capsules, hence the method was not very reproducible at that time.
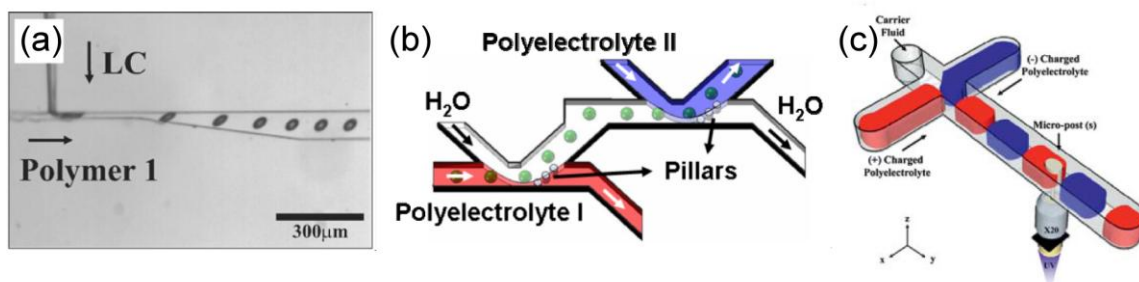


**Fig. 95  Photographs of microfluidic devices used to generate multilayered templates, as featured in recent articles.  a) System developed by Priest *et al*.[490] in which liquid crystal droplets were generated in a polymer solution, then rinsed downstream and introduced into a new polymer solution.  b) Zhang *et al*.[491] demonstrated a device in which mineral oil droplets were deflected into and out of polyelectrolyte and washing streams via a series of pillars.  c) A chip fabricated by Lee *et al*.[492] featured a post in the channel, onto which polyelectrolyte layers were built up by having PAH and PSS droplets continuously striking the post in flow.**

In 2010, Lee *et al*.[492] fabricated a microfluidic chip with a main channel that featured a single poly(ethylene glycol) diacrylate (PEG-DA) post positioned in the centre of the channel (Fig. 95c).  Polyelectrolyte solution was introduced into this channel in the form of droplets in an immiscible carrier fluid, with alternating droplets containing either PAH or PSS.  As the droplets traversed the channel they struck the post in turn, such that each droplet split in two and went around the post before continuing down the remainder of the channel.  As each droplet contacted the post it deposited a film of polyelectrolyte, such that alternating layers of positive and negative polyelectrolytes

were built up on the post at a frequency of 5 to 102 droplet pairs (PAH and PSS) per second. This rapidly built a thick multilayered film around the post, measuring 1 μm in thickness after 60,000 droplets had passed over the post. However, one issue with this method was that the layers were thicker at the "front" of the post, where the droplets first made contact, and were thinner at the back. This was addressed to some extent by altering the shape of the post, but the effect remained present to a degree. Additionally, this technique was only able to form cylindrical films (after removal of the post) rather than capsules and so would not be suitable for the production of drug delivery vesicles in its current setup.

To date, only a few microfluidic methods have been utilised to form multilayered polymer constructs, but each has its own problems that limit their use for drug capsule fabrication. The Layer-by-Layer method is potentially an ideal application for the multilaminar flow platform, since magnetic particles could be used as the core material of the capsule. By simply deflecting particles through streams of alternately charged polyelectrolytes it is theoretically possible to produce a multilayered film, as demonstrated in Fig. 96, after which the core could be dissolved to leave hollow capsules. This would conceivably reduce processing times from several hours to only a few minutes for the formation of multiple bilayers. Fakhrullin and Paunov have recently developed magnetically functionalised yeast cells via the application of magnetic nanoparticles and polyelectrolyte layers (as described in Section 2.9.2).[419,482] Such magnetic, negatively charged yeast cells could also used as cores, since the cells themselves mostly consist of water, hence would be easy to remove after the deposition steps. To determine the viability of the multilaminar flow system for the fabrication of polyelectrolyte capsules, a one-step proof-of-principle experiment was performed in which negatively charged magnetic templates were deflected through a single stream of positively charged, fluorescent polyelectrolyte in the microfluidic device.
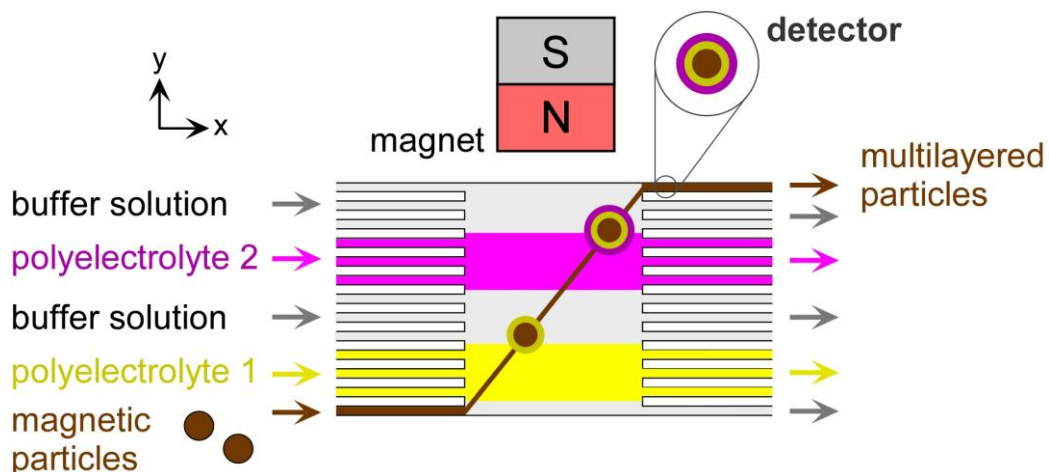
**Fig. 96 Principle of the proposed layer-by-layer formation of multiple polyelectrolytes on the surface of magnetic particles, using the multilaminar flow system. By increasing the number of polyelectrolyte and washing streams, more layers would be added to the particles. The particles could then be dissolved to yield hollow microcapsules.**

## 7.2 Results and discussion

### 7.2.1 Off-chip tests

The polyelectrolyte coating of PAH-FITC onto carboxylic acid functionalised magnetic particles was first tested off-chip to ensure that the deposition was successful, using the method described in Section 2.9.3. Particles were incubated with PAH-FITC, washed several times, and fluorescence images taken before and after the treatment. The results showed an increase in fluorescence intensity, indicating successful adsorption of the PAH-FITC onto the particle surface (as illustrated in Fig. 97, also see Fig. 94). A similar experiment was performed on the negatively charged, magnetic yeast cells, although this test was performed by Dr Rawil Fakhrullin, who produced the magnetic cells. Again, exposure to PAH-FITC resulted in an increased fluorescence signal, signifying successful polyelectrolyte adsorption.
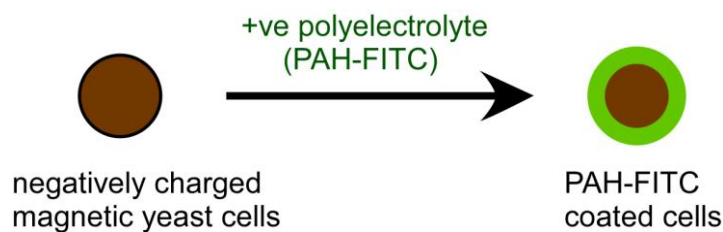
**Fig. 97  Adsorption of the fluorescently labelled, positively charged polyelectrolyte (PAH-FITC) onto templates such as magnetic particles and magnetically labelled cells.**

## 7.2.2   On-chip tests

As explained in Section 2.9.4, on-chip experiments consisted of trying to coat either M-270 Carboxylic Acid magnetic particles or magnetically-coated yeast cells with PAH-FITC in continuous flow, by passing them through a single stream of the polyelectrolyte solution (Fig. 98).  Chip design MLF2 was employed for these experiments.  Initial experiments utilised a 4 x 4 x 5 mm$^3$ NdFeB block magnet placed on top of the chip, next to the chamber (Figs. 57 and 58).  The results for the particles and cells are explained in separate sections.
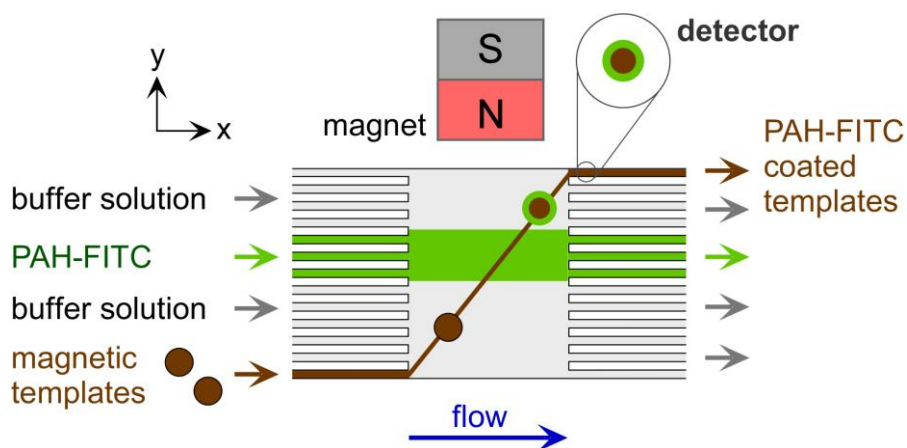


**Fig. 98   Principle of the one-step deposition of positively charged PAH-FITC onto negatively charged magnetic templates using the multilaminar flow platform.**

*Dynabeads M-270 Carboxylic Acid particles*

When the chip was untreated, particles were able to flow freely in the salt solution while being deflected across the chip, but upon encountering the interface with the PAH-FITC stream they immediately stuck to the chip surface. The reason for this may be that, since the chip surface exhibits a negative charge, the positively charged polyelectrolyte deposited a layer on the chip surface, thereby reversing the surface charge so that it was now positive. As the negatively charged particles traversed the chamber, they may have been drawn upward by the magnet on top of the chip, such that when they entered the PAH-FITC stream they immediately adhered electrostatically to the chamber before they could be coated with the polyelectrolyte. A schematic of how this may occur is shown in Fig. 99a, while Fig. 99b shows a photograph of particles sticking at the NaCl/PAH-FITC interface.
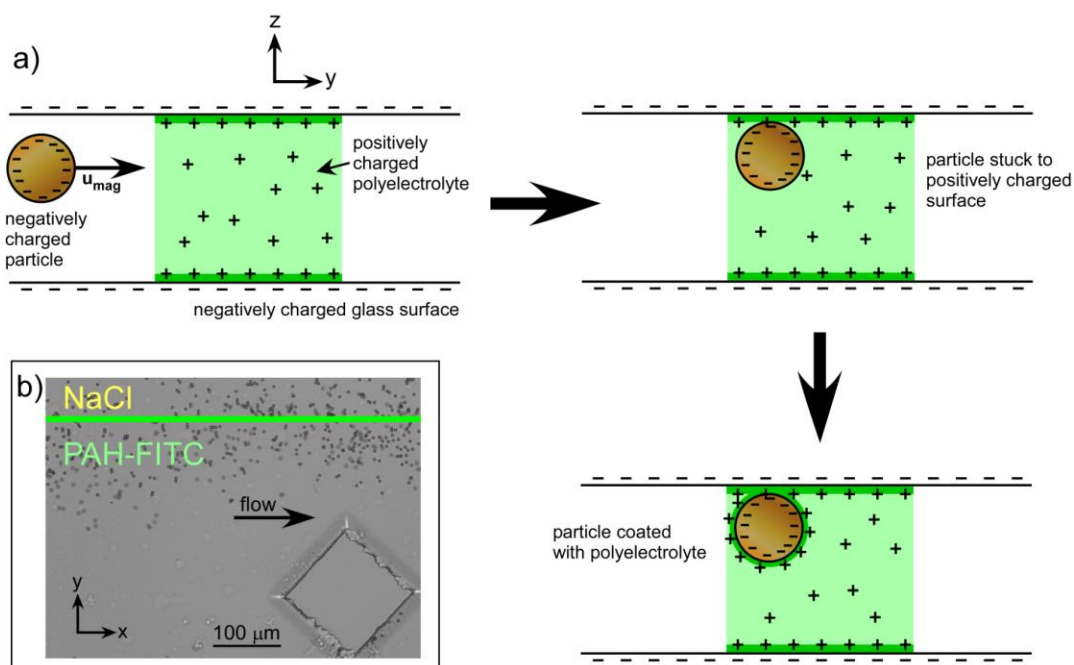


**Fig. 99  a) Schematic of the suspected cause of negatively charged particles sticking in the stream of PAH-FITC on-chip.  b) Photograph of particles sticking at the NaCl/PAH-FITC interface in the reaction chamber.**

In order to prevent this scenario from occurring, the chip was coated with FDTS (trichloro(1$H$,1$H$,2$H$,2$H$-perfluorooctyl)silane) silanising agent to render the surfaces uncharged. However, the same particle sticking was observed, and it was found that if there was a pulse in the system (due to capillaries being knocked or air bubbles in the chip) the PAH-FITC would coat the surface anywhere it contacted. Even when the laminar flow then stabilised, these areas would remain affected by the PAH-FITC despite being constantly washed with NaCl solution, as could be seen via the fluorescence of the surface. In extreme cases, the entire surface of the chamber could be coated with PAH-FITC, whereupon the particles would immediately stick to the surface as soon as they encountered a coated patch. This effect can be seen in Fig. 100, where in photograph (a) the streams are stable and the PAH-FITC can be clearly seen, while in photograph (b) the entire chip surface has been coated with the polyelectrolyte, which remains even when flushed thoroughly with washing solution.
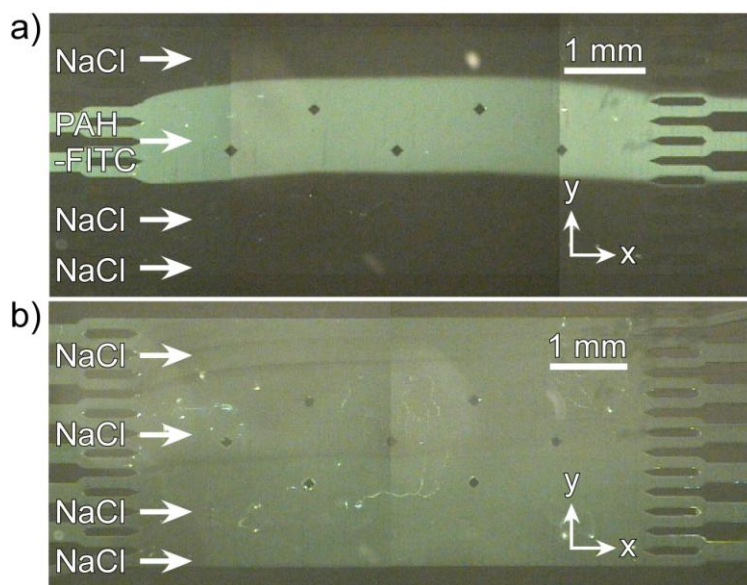


**Fig. 100  Fluorescence images of PAH-FITC in the microfluidic device.  a)  The PAH-FITC laminar stream is clearly visible next to the dark background consisting of NaCl streams.  b) In this instance, the PAH-FITC has been accidentally coated onto the entire surface of the chamber, rendering the chamber fluorescent.**

After some literature research, it was found that polyelectrolytes actually adhere to hydrophobic surfaces even when such surfaces are uncharged.[493] This effect is not due to electrostatic forces as would usually be expected when dealing with polyelectrolytes, but is actually due to very strong short-range attraction between the hydrophobic surface and the hydrophobic backbone (the polymer chain) of the polyelectrolyte, as described by the non-DLVO theory in Section 1.2.2. Hence, the use of hydrophobic surface treatments in the chip would result in PAH-FITC adhering to the surface, as seen with the FDTS coating. This in turn provides a means for causing negatively charged particles to stick to the now positively charged surface.

A possible solution to the problem was thought to be the application of an uncharged hydrophilic surface treatment that would allow particles to traverse the chamber without sticking, since there would be no electrostatic or hydrophobic attraction of the polyelectrolyte to the surface. To this end, chip coatings of PEG-silane and PEG-SPA, containing poly(ethylene glycol) chains, were tested (Section 2.4). However, it was found that the surfaces in each case could still be coated PAH-FITC as was seen with the untreated and FDTS treated chips. One possible reason for this may be due to the hydrophilic nature of the PEG chain, in which the polyether groups (hydrogen bond acceptors) may have formed hydrogen bonds with the hydrated nitrogen groups (hydrogen bond donors) on the PAH-FITC molecule (see Fig. 94), thereby allowing some adsorption to occur. Another reason may be that, with no electrostatic repulsion generated as a result of the uncharged PEG chains, the van der Waal's forces of attraction may have dominated, resulting in adsorption as per DLVO theory (Section 1.2.2). Hence, when performing polyelectrolyte deposition experiments with the hydrophilic surface treatments, the particles were found to still stick to the chamber surface upon encountering the PAH-FITC stream.

However, by employing the method of flicking the capillaries, as had been done in the amide bond formation experiments (Chapter 6), it was found to be possible for the particles to "jump" short distances before sticking again. However, the distance travelled with each jump was not sufficient to allow their deflection across the entire polyelectrolyte stream. Nonetheless, the hydrophilic surface treatments were investigated further since the particles were not permanently adhered to the surface, with PEG-silane used to treat the surface as the preparation was easier and the use of PEG-SPA did not appear to offer any greater benefits.

In addition to the hydrophilic coating, it was thought that by applying the magnetic field in the same vertical plane as the microfluidic chamber, the particles would move only in the y-direction, rather than also moving in the z-direction when the magnet was placed on top of the chip. Therefore, with a magnet placed in line with the chamber, particles would not experience forces that would make them migrate to the top of the chamber, theoretically allowing them to deflect through the chip without getting near to the surface and sticking (as explained in Section 2.6.2, see Fig. 59). To this end, holes were cut out of the glass next to the chamber, allowing the 4 x 4 x 5 mm$^3$ NdFeB block magnet to be placed in the hole. However, it was found that the particles would now struggle to get into the chip as the magnet now provided a stronger force that caused them to simply be pulled against the side of the particle inlet channel before entering the chamber.

To stop this from occurring, the block magnet was replaced with a 6 mm Ø x 3 mm NdFeB disc magnet (Section 2.6.2) which exhibited slightly less force on the particles, allowing them to enter the chamber. After entering the chamber, the particles again flowed well in the NaCl solution, only to again stick at the PAH-FITC interface. However, by flicking the capillaries, some of the particles were able to jump across the

PAH-FITC stream, although at very different speeds, and so there was a great deal of variation in residence time. The particles that were deflected through the entire stream and into the washing stream had their fluorescence intensities measured and compared to those of the particles before the reagent stream, and these results are shown in Fig. 101. The graph shows that the average fluorescence intensity of the particles increased after passing through the PAH-FITC stream, indicating that the positively charged polyelectrolyte had successfully been adsorbed to the surface of the negatively charged particles. However, the standard deviation of the fluorescence intensity was very large, which may be due to the different residence times of the particles in the streams, with those that stuck more having higher fluorescence intensities than those that stuck less.
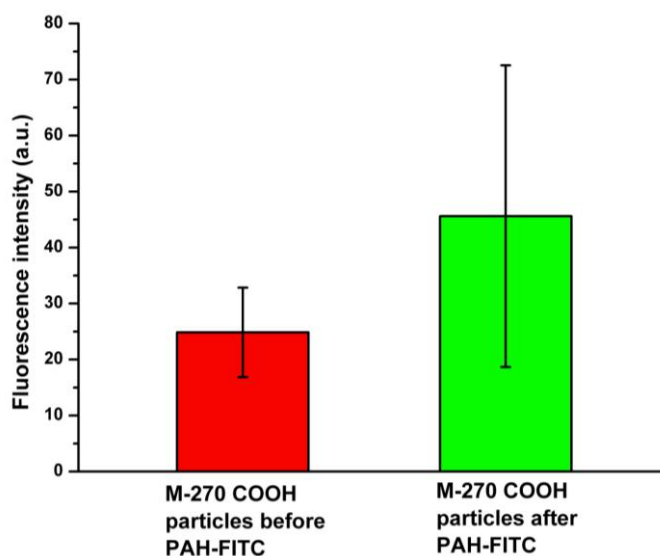


**Fig. 101   Fluorescence intensities of carboxylic acid functionalised magnetic particles before and after passing through a stream of PAH-FITC in the multilaminar flow device.**

Nonetheless, these initial results demonstrated that magnetic particles could be coated with a layer of polyelectrolyte using the multilaminar flow system, though further

studies into the sticking mechanisms are required in order that the particles be deflected through the stream without sticking at all. Once this issue is overcome, it should then be possible to simply increase the number of alternately charged polyelectrolyte streams such that a multilayered structure could be formed, before dissolving the particle core to produce a hollow capsule. As concluded in previous chapters, an important factor in achieving this will be a determination via future work of the particle and chip surface characteristics for different scenarios to give a better understanding of the types of surface treatments that can be used with different particles. Another parameter that could be investigated is the use of deeper chips in order to increase the distance between particles and the walls of the microfluidic chamber. A further alternative to polyelectrolyte deposition that could be considered is the use of polymers that form layers due to hydrogen bonding rather than electrostatic attraction, as demonstrated by Priest *et al.*.[490] This would potentially negate the problems caused by the sticking of the negatively charged particles to positively charged polyelectrolytes.

*Magnetic yeast cells*

Magnetic yeast cells were introduced into the multilaminar flow chips in exactly the same manner as the magnetic particles had been, in experiments run in parallel during the particle-based deposition tests. Initially, the cells were used in a chip coated with hydrophobic FDTS, with a 4 x 4 x 5 mm$^3$ NdFeB block magnet placed on top of the chip, next to the chamber. The cells showed excellent magnetic properties, deflecting through the first NaCl streams. The cells were found to stick to the chip surface at the polyelectrolyte interface, as had been seen with the particles, although it was possible to get some of them through the PAH-FITC stream by flicking the capillaries. The fluorescence intensity was measured of those that were deflected through the

polyelectrolyte stream, the results of which are shown in Fig. 102 (in this case shown as a plot of fluorescence intensity across the surface of the cells). Unlike the magnetic particles, the yeast cells did not exhibit any background fluorescence at all, while after passing through the reagent stream they had a definite fluorescence signal, indicating successful coating of the negatively charged cells with PAH-FITC.
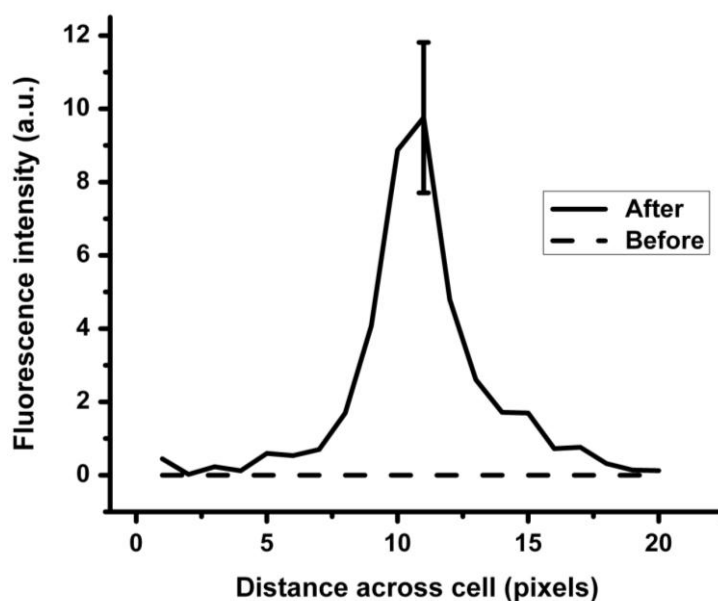


**Fig. 102 Fluorescence intensity of magnetic yeast cells before and after passing through a stream of PAH-FITC in the multilaminar flow system. The increase in fluorescence signal indicated successful polyelectrolyte deposition onto the magnetic templates.**

Following this result, the cells were pumped through a chip coated with agarose to make the surface hydrophilic. In this case, it was observed that the cells in general were able to deflect across the entire width of the chamber, including through the PAH-FITC stream without much sticking. However, before measurements could be taken in this particular experiment, a problem arose with the system that prevented cells from

entering the chamber. When the attempts were made to repeat this experiment, it was found to be too difficult to coat the chip surfaces with a layer of agarose, as patches of gel would remain stuck in the chamber that prevented stable flow streams from being generated and affected the deflection of cells.

Thus, the agarose gel surface treatments seemed to be very suitable for performing polyelectrolyte deposition onto magnetic cells, but further work is required to investigate the optimisation of the agarose coating. This may then lead to the Layer-by-Layer coating of magnetic yeast cells with multiple coatings of polyelectrolyte, after which the core could be removed and the capsules used as drug delivery vesicles.

## 7.3    *Summary*

Proof-of-principle one-step polyelectrolyte deposition onto magnetic templates was demonstrated using the multilaminar flow platform. Commercially available magnetic particles and yeast cells that had been rendered magnetic, both featuring negatively charged surfaces, were introduced into the microfluidic chamber and deflected through a single stream of fluorescently labelled, positively charged polyelectrolyte (PAH-FITC). These experiments were designed to demonstrate the ability of the system to perform Layer-by-Layer deposition onto mobile templates, with a view to the fabrication of hollow, multilayered capsules, and also to show the versatility of the multilaminar flow device in a method that involved neither chemical reactions nor biological assays.

As proof-of-principle experiments the studies were a success, with both the particles and cells being deflected through the PAH-FITC and into a washing stream, whereupon they exhibited increased fluorescence signals that indicated the polyelectrolyte had

adsorbed onto their surface. However, difficulties were encountered concerning the deflection of particles through the reagent as substantial sticking of the templates to the chip surface was encountered, requiring manual intervention to allow the particles to "jump" across the PAH-FITC stream. Multiple surface treatments were tested, and it was found that agarose gel shows promise as a coating for the microfluidic chamber in order to reduce the extent of the particle sticking problems, though this requires further investigation and optimisation. As with the work shown in previous chapters, it will be important for subsequent polyelectrolyte deposition experiments that the physical properties of the particles and chip surface treatments be thoroughly explored, such that conditions can be applied to the procedure to allow unhindered passage of the particles through the chip. Further alternatives include the use of polymers that are not electrolytes and form layers via hydrogen bonding, thereby eliminating the issue of electrostatic attraction of negatively charged templates to a positively charged channel wall.

# 8    C-reactive protein sandwich immunoassay

In this chapter, the application of the multilaminar flow platform is described for performing a clinically relevant, two-step sandwich immunoassay for the inflammatory biomarker, C-reactive protein (CRP).  These preliminary results have been published in the proceedings of the MicroTAS 2010 conference.[464]

## *8.1    Introduction*

C-reactive protein (CRP) is an inflammatory biomarker found in blood.  It is an acute phase protein, with its concentration increasing in response to inflammation or infection.[494]  CRP is a pentamer of about ~118 kDa molecular weight,[494] consisting of five identical subunits (each with a molecular weight of 20-28 kDa)[495] arranged symmetrically around a central pore, forming a circular structure.[496]   As an inflammatory response biomarker it is now routinely measured in clinical diagnostics, and it is also believed that chronic, minor elevations in CRP are an indicator of cardiovascular disease (CVD) and in predicting cardiovascular events.[497,498]

Normal levels of CRP in the serum of healthy humans are typically between 1-10 $\mu$g mL$^{-1}$, with levels of 10-40 $\mu$g mL$^{-1}$ indicating mild inflammation or viral infection, while levels of 40-200 $\mu$g mL$^{-1}$ suggest active inflammation or bacterial infection.[494,499] Values over 100 $\mu$g mL$^{-1}$ are more likely to indicate bacterial infection (though viral infections have caused CRP levels this high), and levels over 200 $\mu$g mL$^{-1}$ are commonly due to severe bacterial infections and burns, with levels peaking at around 400 $\mu$g mL$^{-1}$.  Thus, standard CRP tests for the determination of inflammation and infection typically only require detection of the biomarker in a range from 1 $\mu$g mL$^{-1}$ to

400 µg mL$^{-1}$. However, as mentioned above, CRP can also be used as an indicator of cardiovascular disease (CVD), for which highly sensitive CRP (hs-CRP) assays are employed, using nephelometry or ELISA methods. The American Heart Association have defined hs-CRP levels below 1 µg mL$^{-1}$ as suggesting a person has a low risk of developing CVD, while levels between 1-3 µg mL$^{-1}$ indicate an average risk, and levels higher than 3 µg mL$^{-1}$ suggest high risk.[500] They also state that a person having constant, unexplained elevated levels of hs-CRP (>10 µg mL$^{-1}$) should be evaluated as having non-CVD causes. Elevated levels are also observed in people with autoimmune diseases and cancer.

Thus, CRP is a biomarker whose detection is important not only for determination of inflammation and infection, but also for CVD using highly sensitive analytical methods. However, the detection limits using of nephelometry are commonly higher than 5 µg mL$^{-1}$,[501] and while ELISA detection limits are lower (1 ng mL$^{-1}$),[502] both methods typically require >12 hours and so cannot be used to give rapid analysis.[495] Therefore, a number of magnetic particle-based and microfluidic methods have been developed to reduce procedural times while maintaining low limits of detection, a number of which are given below. Magnetic particle-based methods are described first, followed by microfluidic techniques, and finally combinations of the two.

Kriz *et al.*[503] used magnetic particles in a sandwich immunoassay of CRP in whole blood, where the particles were allowed to sediment before being analysed by a single magnetic resonant coil. Analysis required only 11.5 min to perform a hs-CRP assay, with detection limits of 0.2 µg mL$^{-1}$. Ibraimi *et al.*,[504] of the same research group, developed this technique further, to the point that they could perform the analysis in 5.5 min with a detection limit of 3 µg mL$^{-1}$, sacrificing sensitivity for rapid analysis. Meyer *et al.*[498] developed a similar CRP analysis method in which two magnetic resonant coils

were used rather than one, and a "frequency mixing" technique used to determine the concentration of magnetic particles that had become bound to CRP on a surface. Although this method required a rather long analysis time of 30 min, the detection limit was very low at 25 ng mL$^{-1}$, which was far lower than actually is required for CRP analysis.

Wang *et al*.[505] utilised magnetic nanoparticles conjugated with CRP antibodies in order to extract CRP from human serum, at which point the particles were mixed with a matrix solution and analysed by MALDI-TOF MS (matrix-assisted laser desorption/ionisation-time of flight mass spectrometry). Analysis required 30 min, though sample preparation took longer, and the limit of detection was found to be lower than that of ELISA. Zhu *et al*.[506] performed a CRP sandwich assay on magnetic particles, using magnetism for reaction and washing steps (as in Fig. 26), before labelling the bound the secondary CRP antibodies with quantum dots. This application of quantum dots allowed highly sensitive fluorescence detection to be performed with a detection limit of 0.01 nM (1 ng mL$^{-1}$) and a linear range up to around 2.5 μg mL$^{-1}$. This detection limit was far lower than needed for CRP detection, but nonetheless demonstrated the benefits of magnetic particle based methods when utilised with highly fluorescent species such as quantum dots.

Several microfluidic systems have been developed for detecting CRP.[507] Pultar *et al*.[508] developed an on-chip sandwich immunoassay that used single stranded RNA aptamers on the chip surface to immobilise CRP, before it was tagged with a fluorescently labelled antibody. The authors stated that their device was superior to antibody-based chips in terms of the CRP concentration that could be measured (0.01 to 100 μg mL$^{-1}$), although the antibody-based chips showed better reproducibility. Hosokawa *et al*.[509] used a "power-free" microfluidic chip to perform a wall-based CRP sandwich assay in

20 min, with a detection limit of 0.42 nM (0.042 μg mL$^{-1}$). Rather than using a syringe pump or electroosmotic flow to pump liquids through the PDMS chip, air was removed from the system via a vacuum desiccator, thus drawing liquids through the chip to replace the air.

Gervais and Delamarche[510] developed a capillary force-driven chip that delivered a CRP-containing analyte from a loading pad through several chambers, in which a sandwich immunoassay was allowed to take place. The system required a 5 μL sample, and was able to yield a limit of detection of 10 ng mL$^{-1}$ in only 3 min, with a limit of 1 ng mL$^{-1}$ after 14 min. Baldini *et al.*[499] developed an optical PMMA chip based on fluorescence anisotropy for measuring CRP within a range of 0.1-50 μg mL$^{-1}$, though this sequential procedure required several long reaction and washing steps. A microchip for measuring CRP in human saliva rather than serum was used by Christodoulides *et al.*[495] to detect CRP down to 10 pg mL$^{-1}$. The device consisted of a microwell array containing a particle in each well, and the array was fixed between two plates to form a flow cell. Reagents and washing buffers were pumped sequentially through the flow cell, allowing a sandwich assay to be performed using fluorescence or colorimetric detection, although the procedural time required 12 min.

Bhattacharyya and Klapperich[502] designed and tested a device for detecting CRP via chemiluminescence. Detection limits of 0.1 μg mL$^{-1}$ were achieved in 25 min by binding the channel surfaces with the CRP antigen, before labelling with a primary antibody followed by a secondary antibody labelled with horseradish peroxidase (HRP). The HRP was then used to catalyse the oxidation of luminol in the presence of hydrogen peroxide, yielding a chemiluminescent signal.

The group of Gwo-Bin Lee developed systems that incorporated the use of magnetic particles in microfluidic devices for working with CRP. In 2009, Yang *et al.*[501]

demonstrated the use of magnetic particles coated with CRP-specific aptamers that were reacted with CRP in a chamber and washed using conventional trap-and-release methodology (Section 1.4.2 and Fig. 27), with labelling achieved via acridinium ester-tagged antibodies that allowed chemiluminescent detection. An analysis time of 25 min was achieved, with a good detection limit of 12.5 ng mL$^{-1}$, but one of the more important aspects of this setup was the integrated chip setup, featuring a number of micropumps and vortex-type micromixers that allowed the process to be automated.

The detection of C-reactive protein is important in clinical practice. While many magnetic particle and microfluidic methods have been demonstrated that reduce procedural times and offer excellent limits of detection, the multilaminar flow system offers the potential of reducing the procedural time to around 90 seconds for serum analysis. If successful, this could open the door to a number of further clinical diagnostic tests where rapid analysis is an important factor. To this end, the potential of a two-step CRP sandwich immunoassay was investigated by performing analysis of spiked sample solutions, with a view to later studies into CRP detection in human serum and perhaps even blood samples.

This study was originally begun by Sally Peyman, who found that while some particles could be deflected across the chip and analysed, most became stuck to the untreated chip surface.[420] She was able obtain some data for a 10 μg mL$^{-1}$ concentration of CRP, proving that the immunoassay was possible in the multilaminar flow device, but reliability was hampered by issues with the particles sticking. Here, the investigation focussed on deflecting the particles through the chamber with minimal sticking in order to attain high reliability and reproducibility of the particle trajectories and the amount of time they spent in the reagent streams, a crucial factor since residence time affects the

amount of CRP that binds to the particle surfaces. In addition, the ability to perform a quantitative analysis was an important objective for the CRP immunoassay.

## 8.2 *Results and discussion*

### 8.2.1 Off-chip tests

To check that the CRP sandwich immunoassay method was viable, off-chip tests were performed as described in Section 2.10.3. Briefly, streptavidin functionalised Dynabeads M-270 magnetic particles were reacted with biotinylated primary CRP antibody and washed with buffer solution, then CRP allowed to bind to the surface and the particles washed again. A fluorescently labelled secondary antibody added, and after washing the particles for the final time their fluorescence intensities were measured. Fig. 103 shows the two main reaction steps for the CRP assay.
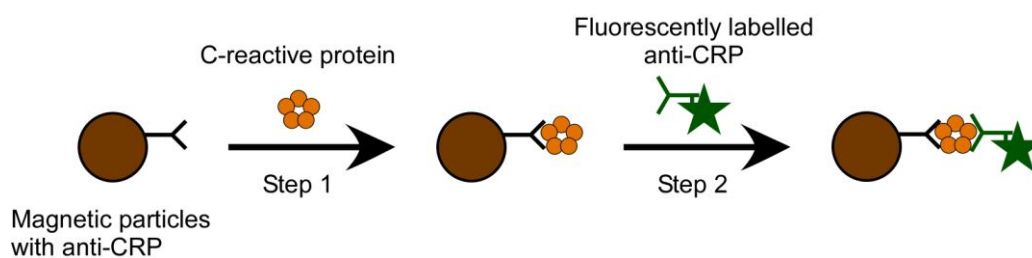


**Fig. 103 A two reaction-step CRP sandwich immunoassay. Magnetic particles functionalised with primary antibody are used to capture CRP in solution, which is then labelled via a fluorescently tagged secondary antibody.**

The fluorescence intensities of the particles after all the reaction steps were found to be greater than those of the particles before the reaction, indicating that the CRP sandwich

assay had been successful. Not only that, but there was no difference observed in fluorescence intensity after each step until after the final step, i.e. there was no other cause of increased fluorescence at any point in the reaction until after the labelling step. Negative tests were also performed by leaving out certain steps in the process and measuring the fluorescence afterwards. It was found that no increase in fluorescence was observed when no CRP was added, or when the particles were not functionalised with primary antibody. Hence, the increase in fluorescence only occurred when CRP was able to bind to antibodies on the particle surfaces, and when a subsequent labelling step was performed.

With the sandwich assay tests establishing that CRP could be bound and detected on the magnetic particles, the two-step reaction was applied to the multilaminar flow system.

## 8.2.2   On-chip tests

The CRP sandwich immunoassay was set up for the multilaminar flow system as described in Section 2.10.4. Anti-CRP coated magnetic particles were introduced via inlet 1, CRP solution (10 µg mL$^{-1}$) via inlet 2, secondary antibody with fluorescent label via inlet 4, and washing buffer via inlets 3 and 5. When a magnet was placed opposite the particle inlet (in the y-direction), particles would be deflected first through the CRP stream, allowing the reagent to bind to the particle surface, then washed, labelled with the secondary antibody, and washed again in the final stream. This process is illustrated in Fig. 104. A chip holder was used throughout most of these experiments, which greatly reduced setting up times and the number of air bubbles in the system once all of the tubing and syringes were connected. A 4 x 4 x 5 mm$^3$ NdFeB block magnet was placed on top of the chip, next to the chamber.

Initial experiments were performed in an uncoated chip that was first flushed with IPA/KOH solution to render the surfaces negatively charged, followed by water and then buffer solution before introducing the final reagents. It was important to maintain a negative charge on the glass surface since the IgG antibody used (present on the surface of the particles and also as the secondary antibody in the labelling stream) had an isoelectric point (pI) of ~6.9, as informed via personal communication with the manufacturers, and the CRP itself had a pI of 5.28, as calculated using an on-line program (http://www.expasy.org/tools/pi_tool.html). This meant that when suspended in the pH 7.45 PBS buffer solution, all of the reagents in the system would be negatively charged and thus repelled from the glass surface of the chip, reducing the possibility of the particles sticking as they deflected through each reagent stream.
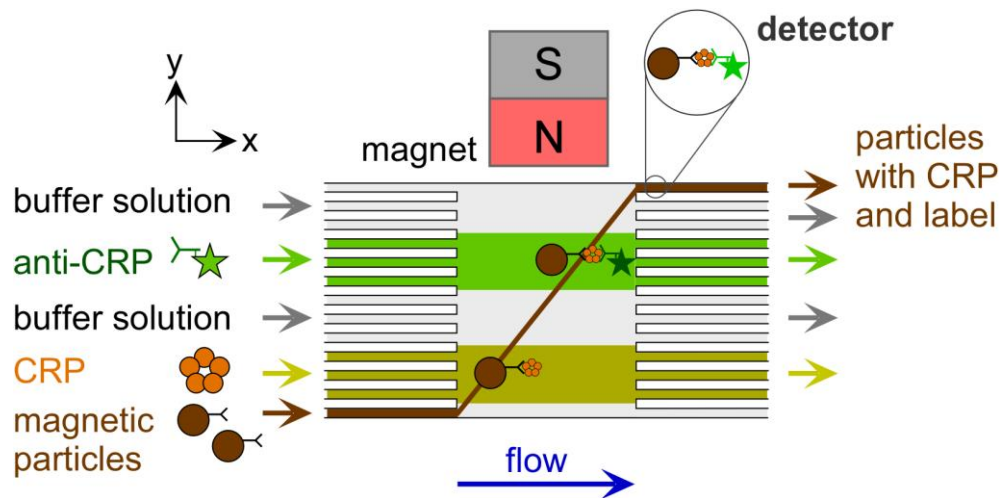


**Fig. 104  Schematic of the two-step CRP sandwich immunoassay in the multilaminar flow system. Anti-CRP coated magnetic particles were deflected through consecutive streams of CRP and fluorescently labelled secondary anti-CRP.**

Using this setup, it was found that particles could enter the chip and be deflected well until reaching the interface with the secondary antibody stream, at which point they

would start to stick to the surface. However, flicking the capillaries as had previously been done (Sections 6.2 and 7.2) allowed the particles to cross the labelling stream and enter the washing stream, where the fluorescence intensities were measured and compared to those before the reaction had occurred. It was found that the fluorescence intensity increased after the particles had passed through the final 2° Ab-FITC reagent stream, indicating that the sandwich assay was successful. However, the particle sticking was not ideal as it meant the particles passing through the reagents streams had very varied residence times. Ideally, the particles should follow the same path through the streams without sticking, giving each one an identical residence time that would provide better reproducibility in results.

Immunoglobulin G is known to be hydrophobic,[508] which may have been part of the reason that the particles became temporarily stuck to the surface upon reaching the 2° Ab-FITC interface. When first entering the chip, the particles already featured a surface functionalised with IgG, but the magnetic field at this point may not have been strong enough to draw the particles near the surface before having CRP become bound to them in the first reagent stream. However, when the particles then reached the second reagent stream, the labelled IgG became bound to the surface, rendering the particles hydrophobic. IgG has been shown to stick far less to more hydrophilic surfaces, such as those expressing PEG groups, than to untreated glass or hydrophobic surfaces (the latter of which increases the amount of sticking greatly).[511] Therefore, the surfaces inside the chips were coated with a hydrophilic layer to reduce the amount of particle sticking compared to that seen in the untreated glass chips, though some degree of sticking was still expected to occur.

To make the surfaces hydrophilic, the chips were coated with a layer of agarose gel (Section 2.4) as the procedure had been refined with practice to be more reliable since

the first attempts (Section 7.2.2). With the coating in place, particles were able to deflect across the chip far more easily, requiring less flicking of the capillaries and allowing particles to cross the stream with more similar residence times than when they "jumped" across to different extents. With this, some initial studies were performed on detecting CRP in the prepared sample stream. A CRP concentration of 10 μg mL$^{-1}$ was chosen for the first experiments since up to this value there is no indication of inflammation or infection, and so if this concentration could be detected then the device would be suitable for normal CRP analysis (rather than hs-CRP). The result of this is shown in Fig. 105, with an increase in fluorescence intensity demonstrating that the multilaminar flow system was capable of measuring an important concentration of CRP. Not only that, but the particles required less than 90 s from entering the chamber to leaving it, a great reduction in procedural time compared to other methods.
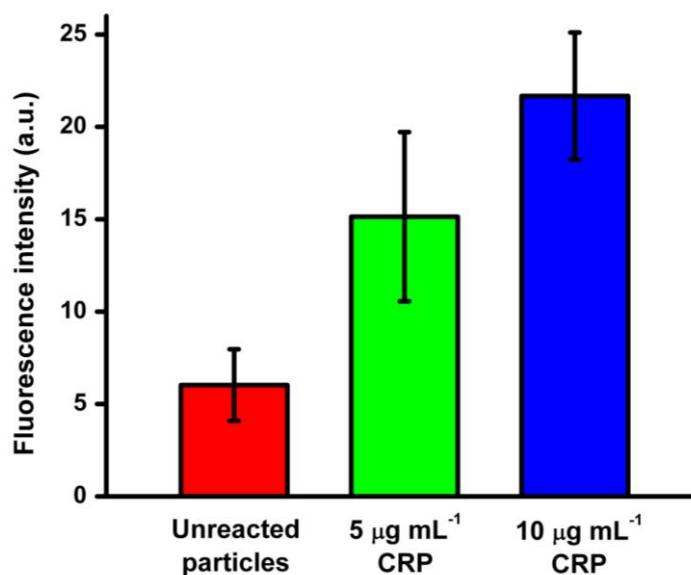


**Fig. 105 Fluorescence intensities of unreacted particles versus those that have passed through the reagent streams in the multilaminar device, with CRP concentrations of 5 μg mL$^{-1}$ and 10 μg mL$^{-1}$.**

The intention was to then explore a concentration range above 10 μg mL$^{-1}$ to show that the system could be used for quantification in the case of infection and inflammation, whilst also exploring concentrations below this value to see whether hs-CRP detection was possible. However, due to time constraints at the end of the project, only one more CRP concentration was tested, 5 μg mL$^{-1}$, the results of which are also shown in Fig. 105. The results show an increase in fluorescence compared to the unreacted particles, demonstrating that the assay was successful, and that the intensity was less than for the 10 μg mL$^{-1}$ concentration. This suggests that, as would be expected, the fluorescence intensity increases with increasing concentration, and although only two data points are not enough to give a definite correlation, they nonetheless show that the system holds potential for performing quantitative analysis.

These initial results showed that the multilaminar flow platform was capable of performing the detection of C-reactive protein, with agarose coated channel surfaces allowing particles to cross the chamber with minimal sticking. Not only that, they indicate that quantitative detection would be possible with some refinement of the system, potentially down to concentrations required for hs-CRP analysis. However, this represented an ideal setup with known concentrations of CRP in a prepared buffer solution. As such, a more thorough study needs to be performed on serum samples, including the production of a calibration curve, the testing of real samples, and comparisons to normal ELISA tests.

## 8.3 *Summary*

The multilaminar flow platform was applied to the detection of C-reactive protein, an important biomarker for detecting inflammation and infection, as well as an indicator of

cardiovascular disease. In initial experiments, it was found that particles stuck to the chip surface as in previous applications, though this effect was greatly reduced by the application of a hydrophilic surface treatment. CRP was detected at concentrations of 5 $\mu g\ mL^{-1}$ and 10 $\mu g\ mL^{-1}$ in only 90 seconds, demonstrating the potential of the system for performing clinically relevant diagnostics in rapid time. The detection limits have not yet been thoroughly investigated, but the concentrations studied are already in an important clinical range for CRP, while the residence time of the particles in the chamber is far less than the procedural times of comparative methods. Thus, the system shows a great deal of promise for biological analysis, and thus could be applied to the detection of a number of other biomarkers where immediate measurements are required.

However, before this can be achieved the setup requires a great deal more investigation for CRP detection, including the efforts to eliminate particle sticking entirely, the determination of calibration graphs across the relevant CRP concentration ranges, the analysis of real human serum samples, and direct comparisons to conventional methods. If these goals can be achieved, it may also be possible to then look into performing analysis of whole or diluted blood samples, thereby cutting out time-consuming sample preparation steps.

# 9    Diamagnetic repulsion

In the following chapter, the use of the diamagnetic repulsion phenomena on polystyrene particles was investigated in microfluidic devices, enhanced by their suspension in a paramagnetic medium, as a means of particle and cell manipulation without the need for magnetic labelling.

## *9.1    Introduction*

The use of diamagnetic repulsion in microfluidics offers numerous applications, as described in Section 1.4.4, though most commonly in the separation of materials based on their intrinsic properties. Employing such forces has the advantage that the objects of interest do not require magnetic labelling, though this also means that it is more challenging to generate the same forces as those seen in magnetic attraction since diamagnetic repulsion is a weak force. Despite the different trapping and separation techniques shown in Section 1.4.4, there are still a great deal of potential applications that can be explored using this fascinating effect.

Here, a number of experiments are described in which diamagnetic repulsion is applied to particles in microfluidic devices for performing different applications: (i) the study of particle deflection behaviour in a microfluidic chamber, towards continuous flow separations by diamagnetophoresis, (ii) the repulsion of particles out of a reagent stream, with a view to performing multilaminar flow reactions on diamagnetic particles, and (iii) the flow focussing of polymer particles and untreated cells using a simple diamagnetic setup.

## *9.2 Particle deflection behaviour*

In this subchapter, the deflection behaviour of diamagnetic polystyrene particles in a high magnetic field is described, towards the continuous flow separation of diamagnetic species. This work was published in the Institute of Physics journal, Science and Technology of Advanced Materials.[385] The experiments were performed in the Tsukuba Magnet Laboratory at the National Institute for Materials Science (NIMS) in Tsukuba, Japan.

## 9.2.1 Introduction

On-chip free-flow magnetophoresis has been demonstrated as a useful method of separating magnetic particles of different properties in continuous flow, requiring only a simple setup but allowing separations among different types of magnetic particles as well as from non-magnetic material (Chapter 3).[316,358] Its potential has also been demonstrated for the separation of cells, a process for which it was very successful.[360] However, this last step in particular presents extra required steps as samples must first be labelled with magnetic particles before separation can take place. Since most materials are inherently diamagnetic, a separation method that offers the manipulation of objects based entirely on their intrinsic properties, without the need for labelling, would be ideal. Because of this, diamagnetic repulsion holds potential for performing on-chip free-flow *dia*magnetophoresis separations, in which materials would be separated in continuous flow in a microfluidic chamber, based on their repulsion from an applied magnetic field (Fig. 106). Thus, this would essentially be the opposite of normal on-chip free-flow magnetophoresis (Fig. 33).
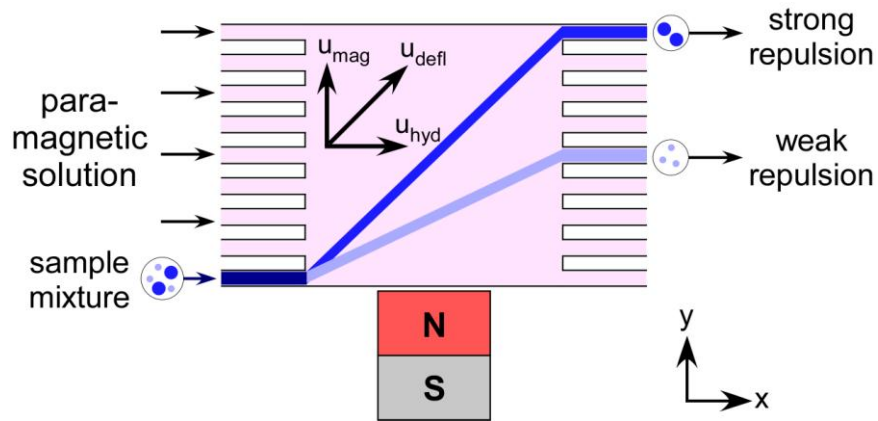
**Fig. 106 Principle of on-chip free-flow diamagnetophoresis for the continuous separation of particles via diamagnetic repulsion. The particles are suspended in a paramagnetic medium and repelled by the magnetic field as they traverse the microfluidic chamber, with some particles migrating further in the y-direction than others, thereby allowing their separation.**

To this end, the deflection behaviour of two sizes of diamagnetic particles and in solutions with different magnetic susceptibility were investigated in a high magnetic field, in order to study the particles and their velocities prior to attempting actual separations.

### 9.2.2 Results and discussion

**Particle characteristics**

As described in Section 3.2.3, when performing experiments in which particles are deflected it is important that their movement be due to the force being applied to them, rather than simply their diffusion due to Brownian motion. As such, the diffusion coefficients of the particles in 6 % and 10 % $MnCl_2$ were determined using Equation 45.

The results are given in Table 16, which also shows the expected diffusion distances as the particles cross the microfluidic chamber of the FFM2 chip.

**Table 16  Diffusion coefficients and diffusion distances of the polystyrene particles over a 6 mm long microfluidic chamber.**

| $MnCl_2$ concentration (% w/v) | Particle diameter ($\mu$m) | Diffusion coefficient ($m^2 s^{-1}$) | Diffusion distance ($\mu$m) |
|---|---|---|---|
| 6 | 10 | $3.58 \times 10^{-14}$ | 1.70 |
|   | 5 | $7.16 \times 10^{-14}$ | 2.40 |
| 10 | 10 | $3.11 \times 10^{-14}$ | 1.58 |
|   | 5 | $6.22 \times 10^{-14}$ | 2.24 |

Diffusion coefficients and distances were smaller for the polystyrene particles compared to the Dynabeads M-270 and MyOne magnetic particles (Section 3.2.3) due to the larger sizes of the former, thereby increasing the viscous drag on them as they move through a solution.  The diffusion distances are very small, hence the movement of the particles in the y-direction would be practically unnoticeable and so any observed movement in this direction would be only due to magnetic forces.

**On-chip deflection behaviour**

The setup and experimental procedure for the deflection experiments is described in Section 2.11.1.  Briefly, 5 $\mu$m and 10 $\mu$m polystyrene particles were introduced into a microfluidic chamber in either 6 % or 10 % w/v $MnCl_2$ solution, and the chip placed at

either position (A) or (B) in the bore of a 10 T superconducting magnet. Particles were pumped through the chip at a flow rate of 400 μL h$^{-1}$. The magnetic field product, $(\mathbf{B} \cdot \nabla)\mathbf{B}$, had the same magnitude but opposite directions at positions (A) and (B), as shown in Fig. 69.
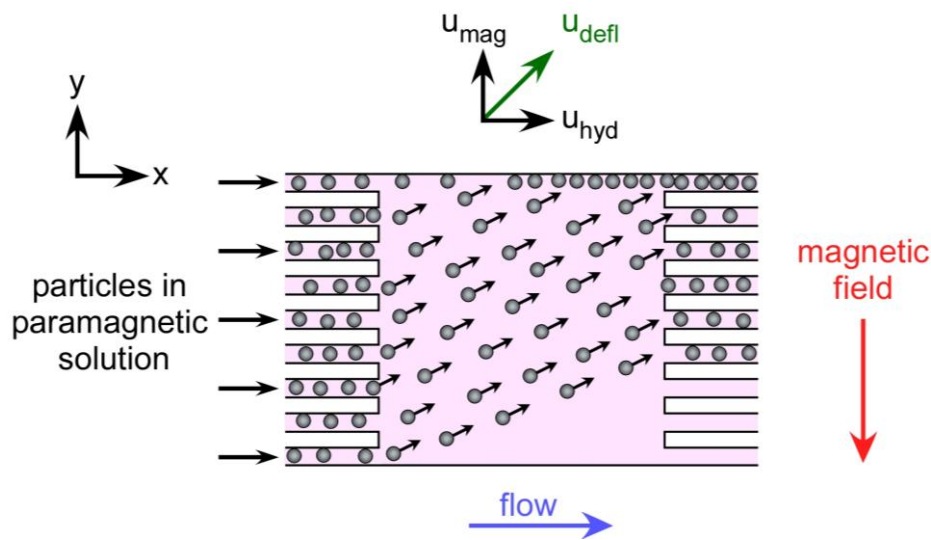


**Fig. 107    Principle of the particle deflection behaviour experiments.    When the diamagnetic polystyrene particles entered the chamber they were repelled from the region of highest magnetic field.    Particles were introduced across the width of the chamber for easier visualisation of them and their movement.**

When positioned inside the superconducting magnet, the polystyrene particles were deflected in the y-direction, across the chamber, away from the region of highest magnetic field (Fig. 107). The velocities of the particles in the y-direction due to the magnetic field, $\mathbf{u_{mag}}$, were measured for each of the conditions using ImageJ software to determine the distance migrated by a particle in a certain time. The final $\mathbf{u_{mag}}$ values were taken as an average of twelve particles per experiment, unless otherwise stated. Unfortunately the resolution of the camera, as well as the conversions required to

transfer the images to a format that could be used for analysis, resulted in difficulties in being able to see the particles in the videos, and so in some cases twelve particles could not be analysed. On some occasions there were also simply too few particles entering the chamber, possibly due to the repulsive force of the magnet that hindered their approach to the chip through the capillaries. Particle trajectories for each of the parameters are shown in Fig. 108, which shows how particles were deflected to the top of the chamber (in the y-direction) at position (A), and to the bottom edge at position (B). The theoretical and experimental $u_{mag}$ (velocity due to the magnetic field) and $F_{mag}$ (magnetic force) values are summarised in Table 17, using Equation 30.
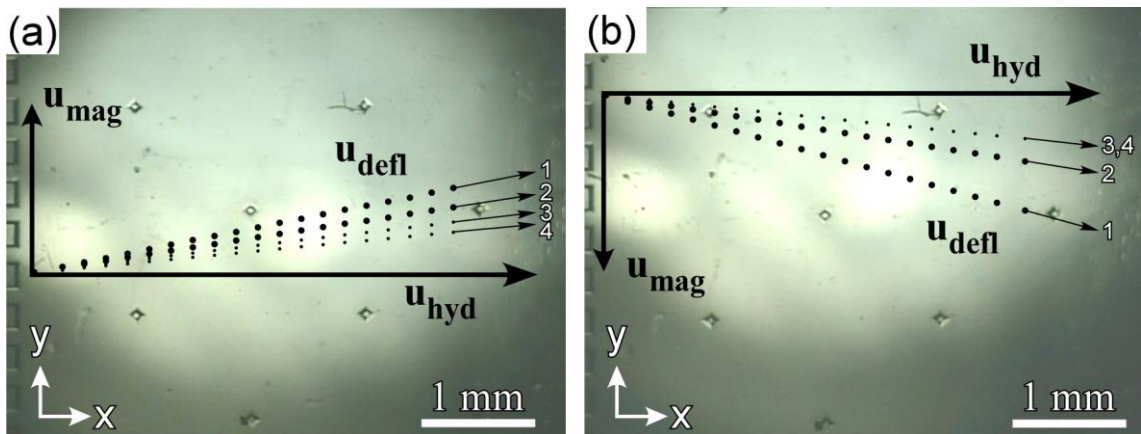


**Fig. 108 Particle trajectories through the microfluidic chamber when the chip was at (a) position (A), and (b) position (B) in the superconducting magnet. The numbered paths correspond to the following parameters: (1) 10 μm particles in 10 % MnCl$_2$, (2) 10 μm particles in 6 % MnCl$_2$, (3) 5 μm particles in 6 % MnCl$_2$, and (4) 5 μm particles in 6 % MnCl$_2$. Particle paths 3 and 4 at position (B) were almost identical.**

**Table 17  The theoretical and experimental values of the magnetically induced velocity, $u_{mag}$, and magnetic force, $F_{mag}$, on the polystyrene particles in the superconducting magnet.**

| MnCl$_2$ conc. (%) | Particle diameter (μm) | Bore position | Theoretical $u_{mag}$ (μm s$^{-1}$) | Experimental $u_{mag}$ (μm s$^{-1}$) | Theoretical $F_{mag}$ (pN) | Experimental $F_{mag}$ (pN) |
|---|---|---|---|---|---|---|
| 6 | 10 | A | 63.9 | 67.9 ± 22.0 | 12.9 | 13.7 ± 4.5 |
| | | B | -63.9 | -66.8 ± 18.5[a] | -12.9 | -13.5 ± 3.7[a] |
| | 5 | A | 21.7 | 52.7 ± 23.9 | 1.6 | 3.9 ± 1.8 |
| | | B | -21.7 | -43.8 ± 21.1[b] | -1.6 | -3.3 ± 1.6[b] |
| 10 | 10 | A | 95.8 | 87.5 ± 19.1 | 22.3 | 20.4 ± 4.5 |
| | | B | -95.8 | -117.6 ± 25.4 | -22.3 | -27.4 ± 5.9 |
| | 5 | A | 32.5 | 42.0 ± 19.0 | 2.8 | 3.6 ± 1.6 |
| | | B | -32.5 | -45.8 ± 16.4[c] | -2.8 | -3.9 ± 1.4[c] |

[a]8 particles analysed; [b]7 particles analysed; [c]2 particles analysed

The experimental results showed that repulsion of the 10 μm particles was greater than that of the 5 μm particles in both concentrations of MnCl$_2$. This was due to the larger volume of material ($V_p$) being affected by the magnetic field, since the 10 μm particles had twice the diameter of the 5 μm particles, hence eight times the value of $V_p$, and therefore experience eight times the magnetic force ($F_{mag}$), as per Equation 30. This effect was observed in both concentrations of MnCl$_2$, though it was much more pronounced in the higher concentration.

The reason for the greater $u_{mag}$ values of the 10 μm particles in the 10 % MnCl$_2$ solution compared to the 6 % solution was that the difference in magnetic susceptibilities between the particles and media ($\chi_p - \chi_m$) was greater for the 10 % medium, resulting in a larger force on the particles (Equation 30). The 5 μm particles, however, did not show much difference in $u_{mag}$ when suspended in the different MnCl$_2$ concentrations. When

10 % $MnCl_2$ was used, the $\mathbf{u_{mag}}$ values of the 10 μm particles were nearly double that of the 5 μm particles, while comparatively the increase in $\mathbf{u_{mag}}$ of the larger particles was only 1.3 times that of the smaller particles when suspended in 6 % $MnCl_2$.

It should also be noted that, although the magnitude of $\mathbf{u_{mag}}$ should be identical whether the chip was situated at position (A) or (B) (with only the direction being different), there were some discrepancies between the results, particularly for the 10 μm particles in 10 % $MnCl_2$. This may have been due to the chip being slightly out of place, as the rail was inserted manually into the bore, up to a mark. This issue could be overcome by using a more sophisticated system of moving the rail. In general, the theoretical and experimental results match well, and although in some cases the experimental $\mathbf{u_{mag}}$ and $\mathbf{F_{mag}}$ values are higher than their theoretical counterparts, the expected values were all within the experimental error. Additionally, the $\mathbf{F_{mag}}$ and $\mathbf{u_{mag}}$ values of the 10 μm and 5 μm particles were found to be in a similar range to those of the 2.8 μm (M-270) and 1.0 μm (MyOne) superparamagnetic particles, shown in Section 3.2.5.

An experiment was also performed in which 10 μm particles were pumped through the chip in 20 % $MnCl_2$ to determine whether this would increase $\mathbf{u_{mag}}$ values further. However, due to the increased density of the solution, the particles creamed to the top of the chamber (see Section 1.2.2), where they "dragged" along the glass surface. Thus, the particles had an apparent $\mathbf{u_{mag}}$ velocity of around 6 μm s$^{-1}$ due to their restricted movement, and this showed that the ability to increase the deflection by increasing the $MnCl_2$ content was limited to a paramagnetic salt concentration of less than 20 %.

In order to explore the results further, a number of additional theoretical calculations were performed using the experimental $\mathbf{u_{mag}}$ and $\mathbf{F_{mag}}$ values. In the 13 seconds the particles spent in the chamber, the distance travelled in the y-direction was calculated.

If the particles were then introduced into chip design FFM1, the outlet by which they would exit the chip was determined for each parameter using the calculated distances, which are given in Table 18. Additionally, Equation 30 was used to calculate the theoretical $u_{mag}$ values, distance travelled, and outlet by which they would exit, of 1 μm, 2 μm, 3 μm and 4 μm polystyrene particles in 6 % and 10 % $MnCl_2$. As a further comparison, the theoretical deflection distances of 5 μm and 10 μm graphite particles were calculated using Equation 30, as graphite has a larger magnetic susceptibility ($\chi_p$ = -4.19 x $10^{-4}$) than polystyrene ($\chi_p$ = -8.21 x $10^{-6}$), giving a much greater value of $\Delta\chi$ that in turn gives increased values of $u_{mag}$ and $F_{mag}$. These calculations would therefore indicate the sizes of polystyrene particles that could be separated using a magnetophoresis system, and whether separation between diamagnetic particles of different materials could be achieved. These values are given in Table 19.

**Table 18 Theoretical deflection distances of particles in 13 seconds, based on the experimental results, and the corresponding outlet by which they would exit in a magnetophoresis separation system such as chip design FFM1.**

| MnCl₂ conc. (%) | Particle diameter (μm) | Bore position | Experimental $u_{mag}$ (μm s⁻¹) | Deflection distance (μm) | Outlet |
|---|---|---|---|---|---|
| 6 | 10 | A | 68 ± 22 | 884 | 3 |
| | | B | -67 ± 18 | 871 | 3 |
| | 5 | A | 53 ± 24 | 689 | 3 |
| | | B | -44 ± 21 | 572 | 3 |
| 10 | 10 | A | 88 ± 19 | 1144 | 4 |
| | | B | -118 ± 25 | 1534 | 5 |
| | 5 | A | 42 ± 19 | 546 | 2 |
| | | B | -46 ± 16 | 598 | 3 |

**Table 19  Theoretical $u_{mag}$ values, deflection distances, and corresponding outlet by which the particles would exit for 1-4 $\mu$m polystyrene particles, plus 10 $\mu$m and 5 $\mu$m graphite particles.**

| MnCl$_2$ conc. (%) | Particle material | Particle diameter ($\mu$m) | Theoretical $u_{mag}$ ($\mu$m s$^{-1}$) | Deflection distance ($\mu$m) | Outlet |
|---|---|---|---|---|---|
| 6 | Polystyrene | 1 | 0.6 | 8.3 | 1 |
| | | 2 | 4.6 | 59 | 1 |
| | | 3 | 5.8 | 75 | 1 |
| | | 4 | 18.3 | 238 | 2 |
| | Graphite | 5 | 121.2 | 1573 | 5 |
| | | 10 | 357.5 | 4641 | 13 |
| 10 | Polystyrene | 1 | 0.9 | 12 | 1 |
| | | 2 | 6.9 | 89 | 1 |
| | | 3 | 8.6 | 112 | 1 |
| | | 4 | 27.43 | 357 | 2 |
| | Graphite | 5 | 118.9 | 1547 | 5 |
| | | 10 | 350.8 | 4563 | 13 |

The results in Table 18 show that if an on-chip free-flow magnetophoresis experiment were performed using diamagnetic repulsion, the 5 $\mu$m and 10 $\mu$m polystyrene particles would both exit by outlet 3 when suspended in 6 % MnCl$_2$, hence a separation would not be achieved.  However, when suspended in 10 % MnCl$_2$, the larger particles would have exited at outlet 4 and the smaller particles by outlet 2 when the chip was at position (A), while at position (B) they would have left the chamber via outlets 5 and 3, respectively.  This shows that, in the higher concentration of paramagnetic salt solution, the particles would be separated based on their size by the use of diamagnetic repulsion. This confirms, theoretically, that diamagnetic repulsion could be a useful means of separating diamagnetic objects based on their size.   Table 19 shows that 4 $\mu$m

polystyrene particles would be deflected as far as outlet 2, but those particles which were smaller would be deflected very little and only exit the chamber via outlet 1, directly opposite the inlet. Hence, particles with diameters of 3 μm and smaller could not be separated from each other.

To determine if it would be possible to separate particles based on their magnetic susceptibility rather than their size, the theoretical deflection distances of 5 μm and 10 μm graphite particles were calculated as shown in Table 19. These showed that, whether suspended in 6 % or 10 % $MnCl_2$, the larger particles would exit via outlet 13 and the smaller ones by outlet 5. Firstly, this show that they would be separated from each other based on size, as expected from the polystyrene particle experiments. Secondly, it shows that if particles of the same size but different materials were present in a mixture, they could be separated based on their magnetic susceptibility. As an example, in 10 % $MnCl_2$ the 10 μm polystyrene particles would exit via outlet 5 (at position (B)), while the 10 μm graphite particles would exit via outlet 13. Similarly, the 5 μm particles would have exited via outlets 3 and 5 for polystyrene and graphite, respectively, when suspended in 10 % $MnCl_2$ at position (B). This shows that, in theory, the diamagnetophoretic separation of materials based on their magnetic susceptibility is feasible.

### 9.2.3 Summary

Polystyrene particles of 5 μm and 10 μm diameter were suspended in a paramagnetic solution of manganese (II) chloride and pumped through a microfluidic chamber whilst inside the bore of a 10 T superconducting magnet. The particle deflection behaviour due to diamagnetic repulsion was studied in each scenario, and it was determined that

the larger particles were deflected further than the smaller particles, while a higher concentration of $MnCl_2$ (10 % w/w) enhanced the effect further due to the increased difference in magnetic susceptibility between the particles and the medium. The experimental results compared very well with the theoretically expected behaviour, and the theory was used to determine the expected effects on smaller diameter polystyrene particles, and particles made from graphite. These findings indicated that separations of diamagnetic particles in a microfluidic chamber were feasible, and that a proposed on-chip free-flow diamagnetophoresis system showed potential for the separation of materials, including biological cells, based on their intrinsic properties and without the need for magnetic labelling.

Indeed, shortly after this initial investigation, the topic was studied further by members of our research group. Peyman *et al.*[512] used the on-chip free-flow magnetophoresis chip (FFM1) to perform size-based separations of 10 μm and 5 μm polystyrene particles in 10 % $MnCl_2$, based on the findings described in this chapter. However, rather than using a superconducting magnet, a large NdFeB disc magnet was placed along the edge of the chamber nearest the particle inlet. As the particles entered the chamber they were immediately repelled by the magnetic field, with the larger particles travelling further in the y-direction than the smaller ones, thus allowing their separation into different outlets as they exited the chamber. However, the applied volumetric flow rate required to achieve a full separation was 40 μL h$^{-1}$ or less, compared to the much higher flow rate of 400 μL h$^{-1}$ that was employed when using the superconducting magnet. Nonetheless, the work demonstrated the implementation of several of the findings from the original investigation described in this chapter, and showed that diamagnetic particles could not only be separated by using diamagnetic repulsion, but also that it could be achieved using a conventional NdFeB permanent magnet.

## *9.3      Repulsion from a reagent stream*

In this sub-chapter, a proof-of-principle experiment is described in which streptavidin-coated particles were introduced into a stream of biotin before being deflected into a washing stream via diamagnetic repulsion. This represents preliminary work with a view to performing multilaminar flow reactions using diamagnetic repulsion rather than magnetic attraction, and has been published in the proceedings of the MicroTAS 2010 conference.[464]

## 9.3.1   Introduction

The previous sub-chapter described how polystyrene particles suspended in paramagnetic manganese (II) chloride solution can be deflected laterally across a microfluidic chamber via diamagnetic repulsion.[385]   Additionally, Peyman *et al*. demonstrated that the effect could be achieved using simple, permanent NdFeB magnets and low flow rates.[512]   In the same work, Peyman *et al*. also showed that streptavidin-biotin assays could be performed by trapping streptavidin functionalised particles in 10 % $MnCl_2$ between two magnets, then flushing fluorescently labelled biotin over the particle plug. An increase in particle fluorescence showed that the binding had occurred on the surface of the particles.

Having established that diamagnetic repulsion can be used to deflect particles across a microfluidic chamber, and that reactions can take place on particles suspended in $MnCl_2$, these two principles were combined to determine whether it was feasible for multilaminar flow reactions to be performed using diamagnetic repulsion rather than magnetic attraction, as illustrated in Fig. 109. As an initial investigation, the deflection

of streptavidin coated polystyrene particles out of a fluorescently labelled biotin stream was studied.
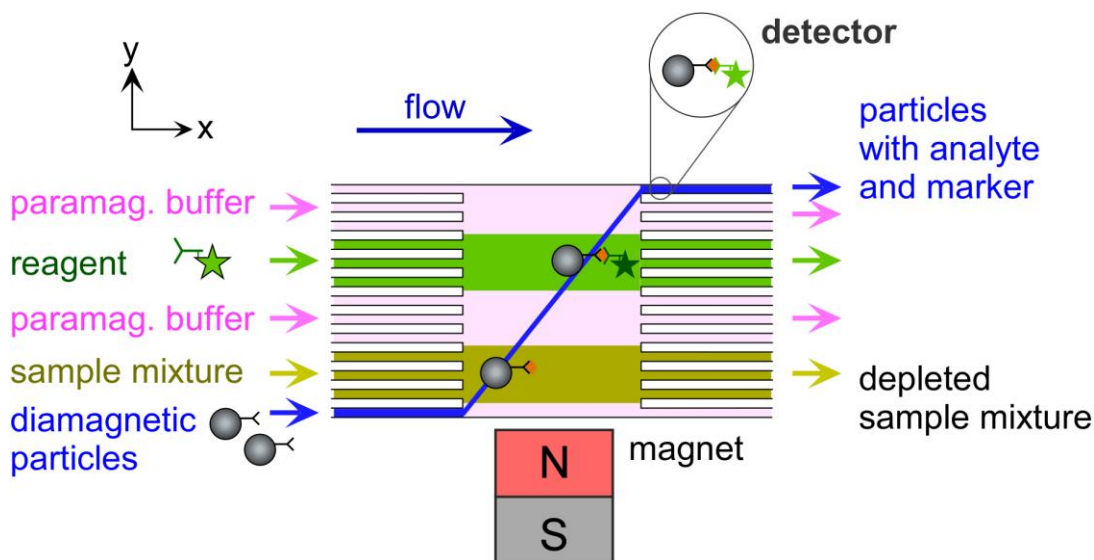


**Fig. 109  Principle of a two-step sandwich assay performed using the multilaminar flow system, but in which polystyrene particles are deflected through the streams via diamagnetic repulsion rather than magnetic attraction.**

## 9.3.2   Results and discussion

**Off-chip tests**

In order to ensure that the reaction would take place on-chip, an off-chip test was first performed as described in Section 2.11.2.  Briefly, 10 $\mu$m polystyrene particles coated with streptavidin were reacted with fluorescently labelled biotin in 10 % $MnCl_2$ solution.  The fluorescence intensity of the particles after the reaction and washing steps was found to be greater than those before the reaction, demonstrating that the streptavidin-biotin binding assay had successfully taken place on the surface of the

particles while suspended in paramagnetic solution. Hence, the reaction was adapted for use on-chip.

## On-chip tests

The on-chip reaction procedure is described in Section 2.11.2. 10 μm polystyrene particles, functionalised with streptavidin, were introduced into the MLF3 multilaminar flow device. This chip design was chosen due to the particle focussing section, which allowed the particles to be introduced into the chamber between two narrow streams of fluorescently labelled biotin (10 μg mL$^{-1}$). All solutions were prepared in 10 % MnCl$_2$. At the entrance to the chamber the particles were exposed to the biotin at the narrow inlet channel (Fig. 110).
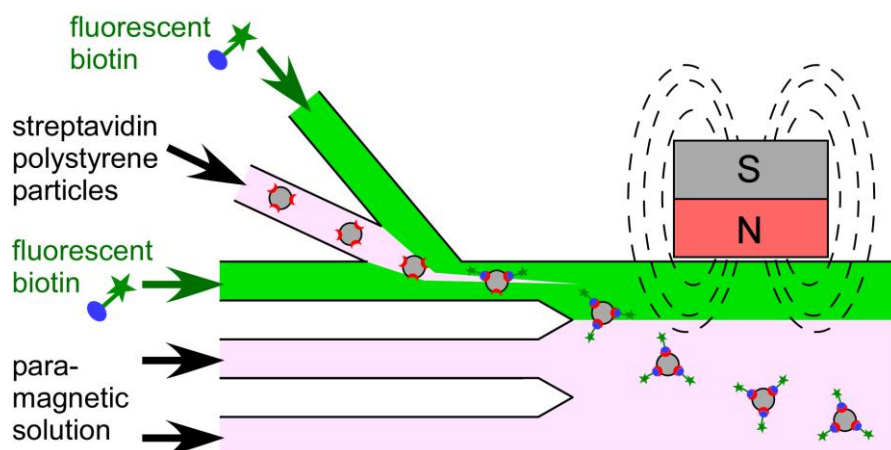


**Fig. 110   Principle of the diamagnetic repulsion of particles out of a reagent stream. Streptavidin coated polystyrene particles are introduced into a reagent stream where fluorescently labelled biotin becomes bound to the particle surfaces.  The particles are then deflected out of the reagent stream and into a washing stream.**

As the particles traversed the chamber, they were repelled by a 20 mm Ø x 5 mm NdFeB disc magnet and deflected through the lower biotin stream, before entering the washing stream containing only 10 % $MnCl_2$. Fig. 111 shows photographs of this process, with particles entering the biotin stream before being deflected into the washing stream. To ensure that the reaction itself was achieved, fluorescence intensities of particles before and after the reagent stream were measured, with the results shown in Fig. 112. The fluorescence of the particles was found to increase after passing through the biotin stream, indicating the reaction was successful. No sticking of the particles occurred on the chip surface.
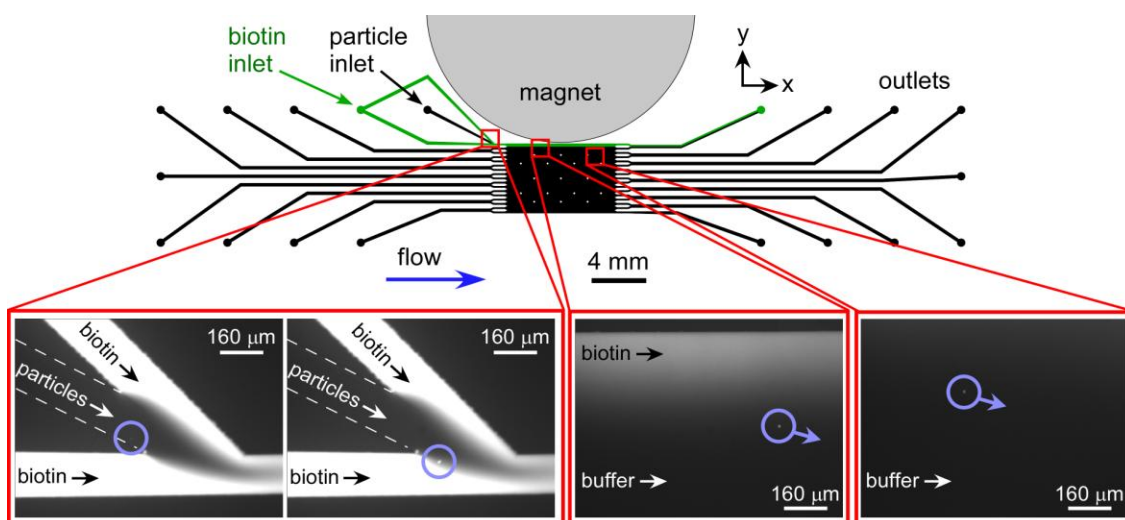


**Fig. 111 Photographs showing the migration of streptavidin coated polystyrene particles through a stream of biotin, before being deflected out of the reagent stream and into a washing stream via diamagnetic repulsion.**
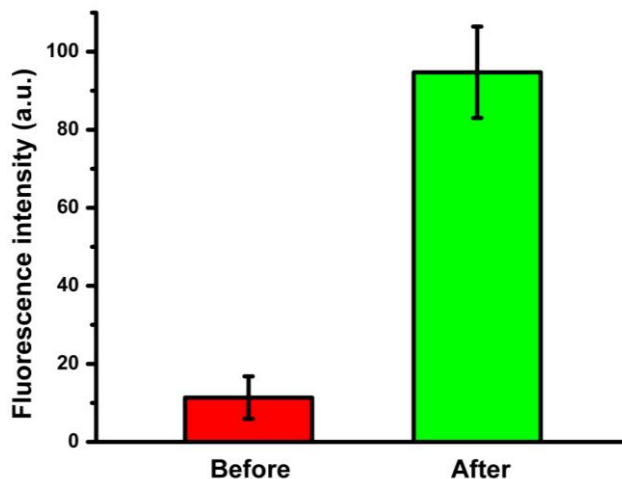
**Fig. 112  Fluorescence intensities of the particles before and after passing through the biotin reagent stream.  The increase in fluorescence signal indicates the reaction was successful.**

Although only a simple proof-of-principle demonstration of how diamagnetic particles can be repelled out of a reagent stream, this experiment nonetheless demonstrates the potential of the system for performing multilaminar flow processes on materials without needing to label them magnetically.  With further investigation into a purpose built setup, such as dedicated chip designs and optimised magnetic field characteristics, it may be possible to adapt this procedure to perform full multi-step reactions as have already been demonstrated with great success using magnetic attraction.[394,424-426]

### 9.3.3   Summary

Diamagnetic repulsion was used to continuously deflect streptavidin coated polystyrene particles out of a biotin reagent stream and into a washing buffer stream, after allowing streptavidin-biotin binding to take place on the surface of the particles.  This represents

the first application of diamagnetic repulsion in this manner, and hints at further development into a multilaminar flow reaction system such as that previously demonstrated using magnetic attraction (Chapters 4-8). Further considerations are required before this goal can be achieved, such as the improvement of the chip design and optimisation of the magnetic setup, but the resultant microfluidic platform would potentially allow multi-step reactions to be performed on diamagnetic particles or cells without their need for prior labelling.

## *9.4      Flow focussing of particles and cells*

In the following sub-chapter, the application of diamagnetic repulsion for the focussing of particles in continuous flow is described, with a preliminary study into the focussing of living cells. The experiments were performed by Angeles Ivón Rodríguez-Villarreal, a visiting PhD student from the University of Barcelona, under close supervision from the author of this thesis. This work has been published in Lab on a Chip.[513]

## 9.4.1   Introduction

The focussing of particles and cells is often an important factor in continuous flow procedures, involving the forcing of objects into narrow, well-defined streams that allows them to be processed and sorted in a precise and reproducible manner. The most common applications of focussing are in the use of flow cytometry and fluorescence activated cell sorting (FACS) for the detection, counting and sorting of cells.[514] With the advent of microfluidic technology there has been a surge of interest in the miniaturisation of FACS procedures and in the continuous flow processing of particles and cells within the confined spaces of a microchannel.[145-147,176,515]

There are two main types of devices for the focussing of particles: sheath flow focusers and sheathless focusers (Fig. 113). Sheath flow focusers employ hydrodynamic[359,516,517] or electrokinetic[518,519] forces to generate laminar flow streams that surround the sample stream, forcing particles into a narrow region. This method allows well-controlled and reproducible particle trajectories, but only with careful channel design and flow rate control since it is the stream of particle solution that is being focussed, rather than the particles themselves.

Sheathless focusers operate by affecting the particles directly rather than the fluid around them. Here, the particles are pumped through a microfluidic channel and an external force field is applied laterally to the particles, causing them to migrate into a narrow space in the channel. Methods of achieving this have been through the use of dielectrophoretic,[520,521] acoustic,[231,522] and optical forces.[523] However, these techniques often require complicated setups of electrodes and power supplies, channels of certain widths or sophisticated laser assemblies, respectively.
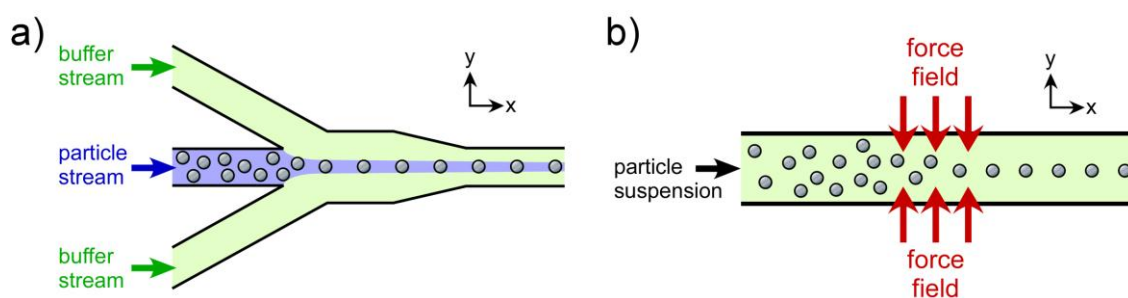


**Fig. 113   Principle of particle focussing via a) sheath flow methods, in which buffer streams are used to focus a particle solution into a narrow region, and b) sheathless methods, whereby a field of force is applied directly to the particles to manipulate them into a well-defined stream.**

Magnetic attraction is not feasible for continuous flow focussing as magnetic particles would be attracted towards the region of strongest field, which is always outside of the channel. James *et al.*[524] used magnetic attraction to aid particle focussing, whereby magnetic particles were drawn close to the microfluidic chip surface via a magnetic field, but the lateral focussing of the particles was still performed using dielectrophoresis. Very recently, Afshar *et al.*[525] demonstrated a system in which

particles were trapped in a plug against the side of a channel wall via an electromagnet. The particles were then released and a sheath flow introduced that forced the particles into the centre of the channel, achieving three-dimensional focussing. However, while this showed that magnetic forces could be applied to the focussing of particles, the need to trap them meant that it was not a true continuous flow system.

An earlier demonstration in our group was a proof-of-principle experiment in which sheathless focussing of particles was achieved using diamagnetic repulsion (Fig. 114).[512] 10 μm polystyrene particles, suspended in 10 % $MnCl_2$, were pumped through a capillary between a pair of NdFeB magnets, with the two magnets having their like poles facing each other. The magnets were fixed in place close together, forming a region of low magnetic field between them, such that as the particles passed between the magnets they were repelled from the magnet surfaces towards the field minima along the central plane of the capillary. Thus, as the particles passed through the magnetic field region, they were continuously focussed into a narrow stream, demonstrating successful focussing via the application of diamagnetic repulsion.
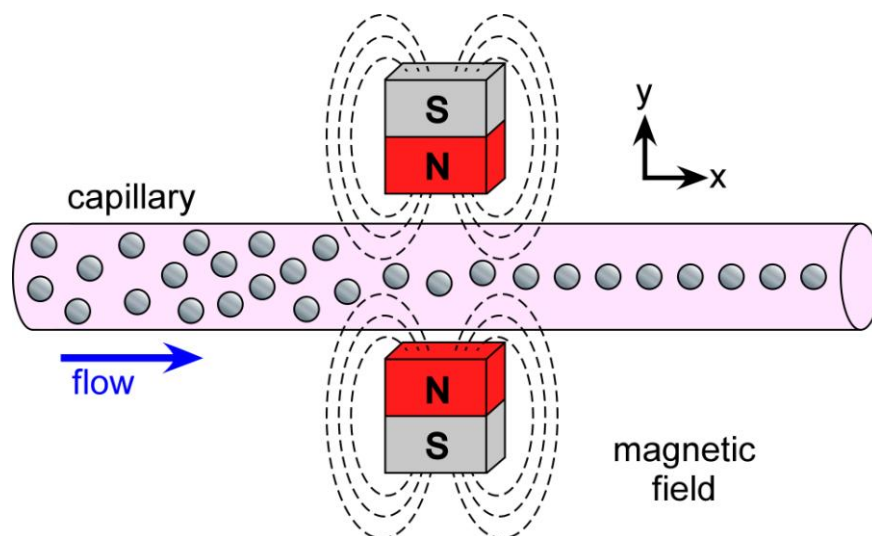


**Fig. 114 Principle of flow focussing via diamagnetic repulsion. As diamagnetic particles pass between the magnets they are repelled into the centre of the capillary.**

In the work described in this chapter, the focussing of particles via diamagnetic repulsion was more thoroughly explored by varying the parameters affecting the forces acting on the particles. These parameters include the polystyrene particle size, the type and concentration of paramagnetic salt in the solution, flow rate, and residence time of the particles in the magnetic field. As an extension of this work, and to demonstrate the potential of the system for biological studies in microfluidic chips, the findings of the particle studies were applied to the continuous flow focussing of living cells.

## 9.4.2 Results and discussion

**Particle size**

As shown by Equation 30, and experimentally in Sections 3.2.5 and 9.2.2, the extent of particle deflection in a magnetic field depends on the size of the particle, or more accurately the volume of material affected by the magnetic field ($V_p$). In order to determine how particle size affected the flow focussing of diamagnetic materials in a paramagnetic buffer, 10 μm and 20 μm diameter polystyrene particles were suspended in 0.039 M $MnCl_2$ solution and pumped through a capillary at a flow rate of 30 μL $h^{-1}$, as described in Section 2.11.3. A pair of 4 x 4 x 5 $mm^3$ rectangular NdFeB magnets were positioned around the capillary with their like poles facing, such that an area of low magnetic field was generated between them (as demonstrated in Fig. 73). Before the particles encountered the magnetic field region, they were dispersed across the width of the capillary. However, as the particles passed between the magnets they were repelled away from the magnet surfaces towards the central axis of the capillary, such that as they exited the magnetic field region they were confined to a narrower region than before. A typical example of this is shown in Fig. 115.
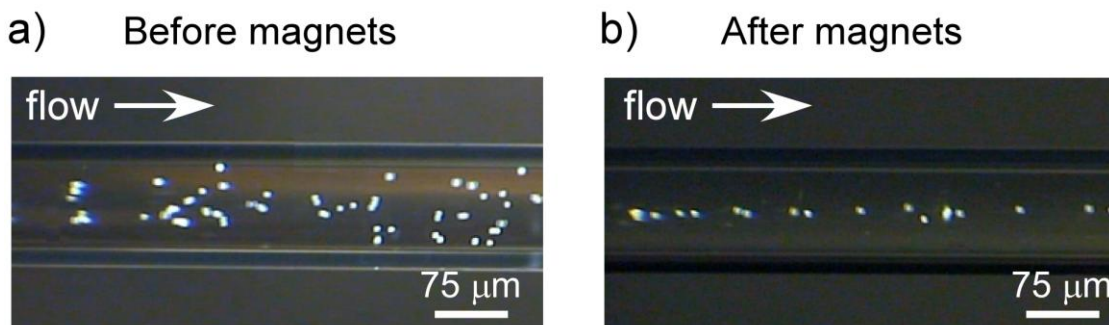
**Fig. 115 Principle of flow focussing via diamagnetic repulsion. As diamagnetic particles pass between the magnets they are repelled into the centre of the capillary. The photographs show a typical focussing experiment, with particle distribution across the width of the capillary a) before the magnet pair, and b) after the magnet pair.**
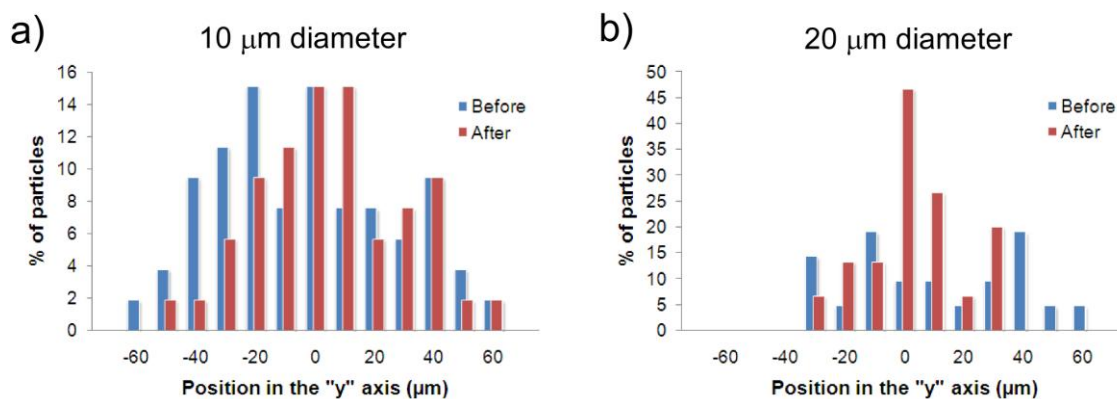


**Fig. 116 Histograms showing the distribution of particles across the width of a capillary before (blue) and after (red) the pair of magnets. The graphs show the focussing of a) 10 μm diameter, and b) 20 μm diameter polystyrene particles in 0.039 M MnCl$_2$ solution, pumped at 30 μL h$^{-1}$ between two 4 x 4 x 5 mm$^3$ NdFeB magnets.**

Fig. 116 shows the results for the focussing of the two different sized particles. When suspended in 0.039 M MnCl$_2$, the 10 μm particles did not display much of a focussing effect after passing through the pair of magnets. This indicated that the forces ($\mathbf{F_{mag}}$) on

the particles were not strong enough to sufficiently repel them towards the centre of the capillary. However, when the 20 μm particles were used instead, the volume of magnetisable material was increased to eight times that of the 10 μm particles, yielding an eight times increase in $\mathbf{F_{mag}}$ as per Equation 30. The increase in the force resulted in much better focussing, with nearly 50 % of the 20 μm particles being deflected into the central axis of the capillary (y = 0 μm), with the remaining population focussed to within 30 μm of the centre.

This demonstrated the large effect that particle volume ($V_p$) has on the focussing of particles using diamagnetic repulsion. However, many biological cells have diameters around 10 μm, and so subsequent experiments were performed with a view to obtaining better focussing for particles of this size.

**Paramagnetic salt type and concentration**

As shown above, when the 10 μm particles were suspended in a low concentration of $MnCl_2$ (0.039 M) they showed very little focussing. Hence, at a flow rate of 30 μL h$^{-1}$ and when using 4 x 4 x 5 mm$^3$ NdFeB magnets, the difference in magnetic susceptibility ($\Delta\chi$) was too small between the particles and the media, resulting in too small a force to repel the particles significantly. However, by increasing the magnetic susceptibility of the medium ($\chi_m$), $\Delta\chi$ becomes larger and so a greater $\mathbf{F_{mag}}$ force is experienced by the particles. Therefore, a range of salt concentrations were studied between 0.79 M and 0.079 M for two different paramagnetic salt species: manganese (II) chloride ($MnCl_2$) and gadolinium (III) chloride ($GdCl_3$). $Gd^{3+}$ has seven unpaired electrons compared to the five of $Mn^{2+}$, meaning that at the same concentration the gadolinium salt has a higher magnetic susceptibility. To test the effect of magnetic

susceptibility, 10 μm particles were pumped through the capillary at 30 μL h$^{-1}$ between two 4 x 4 x 5 mm$^3$ NdFeB magnets.

Figs. 117a and 117b show the results for the 0.079 M concentrations of MnCl$_2$ and GdCl$_3$, respectively. In MnCl$_2$ ($\chi_m$ = 5.40 x 10$^{-6}$) the particles only experienced a slight focussing effect, whereas in the more paramagnetic GdCl$_3$ solution ($\chi_m$ = 1.92 x 10$^{-5}$) over half of the particles were focussed to the centre line of the capillary (y = 0 μm), with the remainder focussed to within 20 μm of the centre. By suspending the particles in GdCl$_3$ rather than MnCl$_2$, with 3.56 times greater magnetic susceptibility, they experienced twice the theoretical **F$_{mag}$** force from the magnets. This represented a large increase in focussing efficiency by simply using a salt with a higher $\chi_m$.
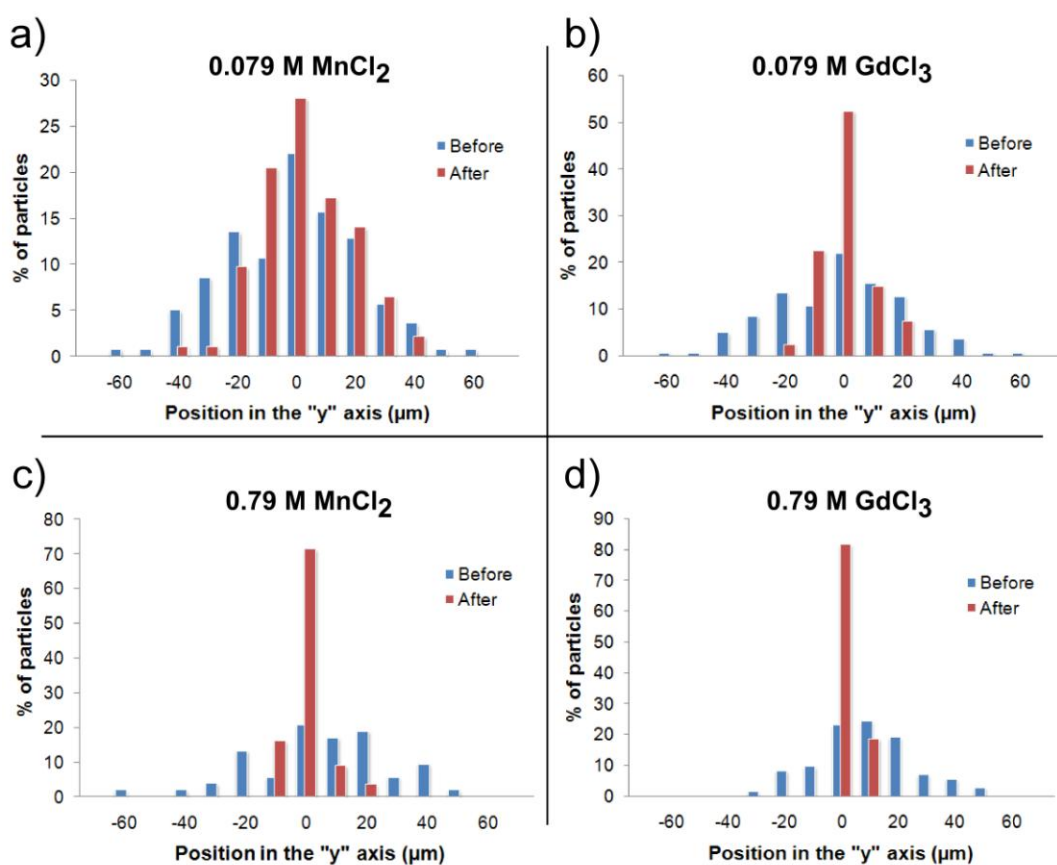


**Fig. 117** **Particle distributions across the width of the capillary before and after passing between the magnets. The 10 μm particles were suspended in a) 0.079 M MnCl$_2$, b) 0.079 M GdCl$_3$, c) 0.79 M MnCl$_2$, and d) 0.79 M GdCl$_3$.**

The concentrations of $MnCl_2$ and $GdCl_3$ were increased to 0.79 M, and the results for these are shown in Figs. 117c and 117d, respectively. When suspended in the $MnCl_2$ solution ($\chi_m = 1.46$ x $10^{-4}$), over 71 % of the particles were focussed to the centre line (y = 0), with the remainder focussed to within 20 μm of the centre. However, in $GdCl_3$ ($\chi_m = 3.20$ x $10^{-4}$), more than 80 % of the particle population was focussed to y = 0, with the rest of the particles within 10 μm of the centre. By increasing the concentration of $MnCl_2$ by a factor of 10, from 0.079 M to 0.79 M, the magnetic susceptibility of the solution was increased 2.7 times, which resulted in a theoretical $\mathbf{F_{mag}}$ increase of 11.3 times. When the concentration of $GdCl_3$ was raised by a factor of 10, the magnetic susceptibility of the solution was increased 1.67 times, which resulted in 12 times the $\mathbf{F_{mag}}$ force on the particles in the higher concentration.

This confirmed that increasing the paramagnetic salt concentration resulted in better focussing, since both $MnCl_2$ and $GdCl_3$ yielded better results at the higher concentrations, as expected by the theory. Additionally, the superiority of the $GdCl_3$ to the $MnCl_2$ was further reinforced by the results at the higher concentration. It was also found, however, that when using high concentrations of $GdCl_3$ at relatively low flow rates, the particles became trapped in the regions before the magnets and before leaving the area between them (Fig. 118).

The trapping effect was caused as result of the high magnetic fields generated at the corners of the magnets, creating a barrier of sorts that the particles struggled to pass. As more particles enter the first region of high field a plug is formed, growing in size over time. However, at the same time particles were also being released, as they simply circulated in the plug until they reached an optimum position where the force due to the applied flow was greater than the force repelling them from the magnets. This allowed a constant stream of particles to leave the first plug, flowing between the magnets until

they encountered the second region of high field, where the same scenario was observed of particles recirculating until they could leave the plug in a narrow stream. This trap-and-release method of focussing was an interesting effect in itself as it allowed particles to be focussed into very narrow streams and warrants further investigation. It was found that higher flow rates could be used to avoid the trapping of particles, though it may be possible to optimise the magnetic field design such that low flow rates could be applied without having trapping occur. This could potentially be achieved by using magnets in the same orientation but with curved edges so that there are no regions of particularly high field like those observed when using magnets with square edges.
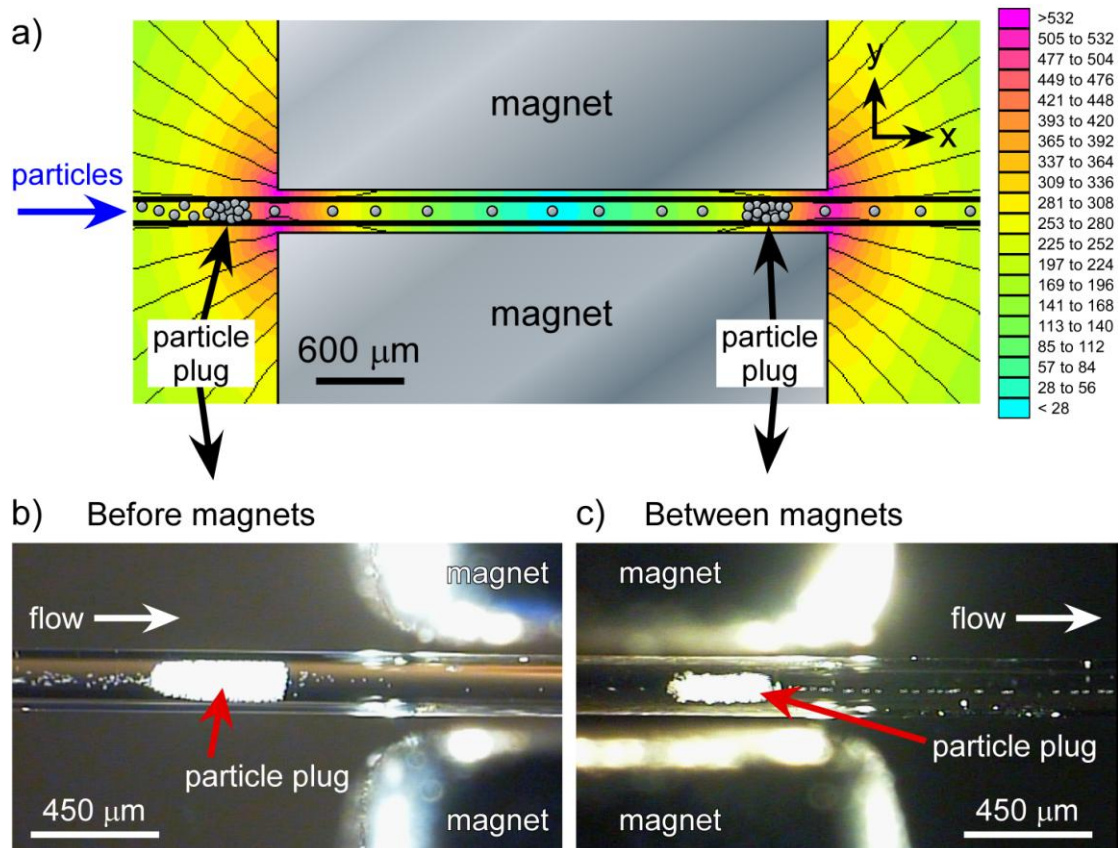


**Fig. 118 The trapping of particle plugs at the regions of high magnetic field. a) FEMM simulation showing the highest field strengths (in purple) generated at the corners of the magnets, creating a barrier of force against the flow of the particles. The scale on the right-hand side of the image shows the magnetic flux density in mT. b) Photograph of particles trapped before the magnets, and c) particles trapped between the magnets.**

The experiments in this section showed how the focussing of particles depends greatly on the type and concentration of paramagnetic salt solution being used, with greater magnetic susceptibilities yielding improved focussing effects.

## Flow rate

The deflection velocity of particles, $\mathbf{u_{defl}}$, is dependent on both the velocity due to the hydrodynamic flow, $\mathbf{u_{hyd}}$, and the velocity due to the magnetic field, $\mathbf{u_{mag}}$, as shown by Equation 31 and Fig. 33. Hence, if the parameters influencing $\mathbf{u_{mag}}$ are kept constant (i.e. particle size, magnetic susceptibilities, magnetic field characteristics), the extent of deflection depends only on the applied hydrodynamic flow, $\mathbf{u_{hyd}}$. Since better focussing was achieved using gadolinium (III) salt compared to manganese (II) salt solution, 10 μm particles were suspended in 0.79 M and 0.079 M $GdCl_3$ solution and pumped through the capillary at flow rates of 30, 40 and 50 μL h$^{-1}$, equivalent to linear velocities ($\mathbf{u_{hyd}}$) of 0.47, 0.63 and 0.78 mm s$^{-1}$, respectively. The particles were pumped between a pair of 4 x 4 x 5 m$^3$ NdFeB magnets, as before.
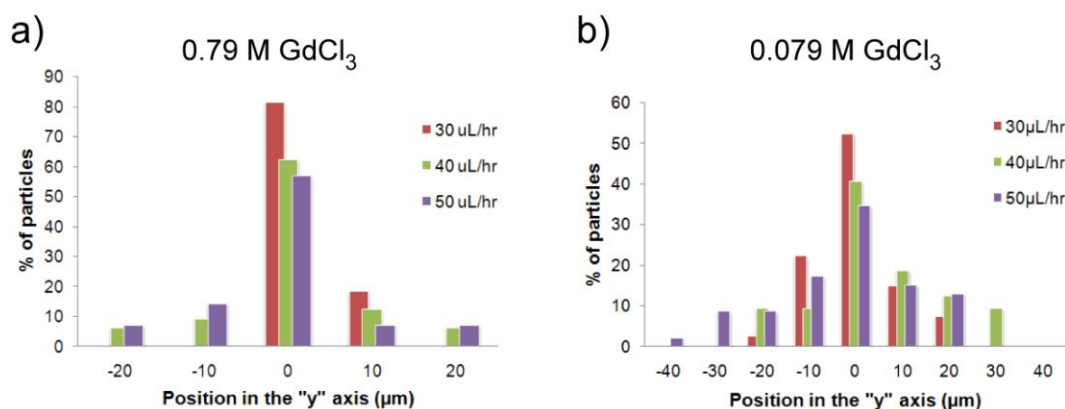


**Fig. 119  Particle distribution across the capillary at flow rates of 30, 40 and 50 μL h$^{-1}$ (0.47, 0.63 and 0.78 mm s$^{-1}$) in a) 0.79 M $GdCl_3$, and b) 0.079 M $GdCl_3$.**

The results for focussing at different flow rates in 0.79 M GdCl$_3$ are shown in Fig. 119a. At a flow rate of 30 μL h$^{-1}$, over 80 % of the particles were focussed to y = 0. As the flow rate increased to 40 μL h$^{-1}$, the percentage of particles being focussed to y = 0 was slightly more than 60 %, decreasing to under 60 % at a flow rate of 50 μL h$^{-1}$. At each flow rate the particles were focussed to within 20 μm of the centre line, showing that a substantial amount of focussing was seen in each case, though the distribution was wider at the two highest flow rates. The reason that the lowest flow rate gave the best results was that the particles had a greater amount of time to interact with the magnetic field as they passed between the magnets, allowing them to deflect towards the centre of the capillary for a longer period of time than those at higher flow rates. For example, the distance along the capillary in the x-direction in which particles experience the magnetic field was approximately 8 mm, as determined from the FEMM simulation in Figs. 73 and 118. Thus, at a flow rate of 50 μL h$^{-1}$ the particles would spend ~10 s in the magnetic field region, while at 30 μL h$^{-1}$ they would be in this same region for ~17 s, a 1.7 times increase in the residence time. Therefore, when performing focussing experiments there is an option of either using low flow rates to gain a high degree of focussing but a low throughput, or employing high flow rates that give greater particle throughput but less efficient focussing.

Paramagnetic salt solutions are typically toxic to biological cells, hence when such solutions are used in medical processes (e.g. MRI scans) the concentration of a solution is in the order of mM (e.g. 500 mM in an injected dose, with concentrations varying in the body).[526] To determine whether focussing of particles could be achieved with increasing flow rates in lower concentration of GdCl$_3$, experiments were also performed in 0.079 M solution and the results are shown in Fig. 119b. Focussing was observed at each of the flow rates, again with the lowest flow rate giving the best results as over 50

% of the particles were focussed to y = 0 at 30 $\mu$L h$^{-1}$, and the remaining particles to within 20 $\mu$m. At 40 $\mu$L h$^{-1}$, around 40 % of particles were focussed to y = 0, with a spread of 30 $\mu$m around the centre, whereas at 50 $\mu$L h$^{-1}$ about 35 % of the particles were focussed to y = 0 with a spread of 40 $\mu$m. As before, this showed that as the flow rate increased the degree of focussing worsened, but nonetheless demonstrated that focussing was achievable at low GdCl$_3$ concentrations over a range of flow rates.

**Magnetic field**

As described above, paramagnetic salt solutions are toxic to cells. Therefore, while increasing the concentration of the salt solution is acceptable for improving the focussing of particles, this is not an effective method when using cells. In order to attain continuous flow focussing of cells, other factors must be considered that allow deflection when using fixed diameters (since cells are typically ~10 $\mu$m) and the low paramagnetic salt concentrations required to maintain cell viability. One such factor is the design of the magnetic field. While employing stronger magnetic fields and gradients would seem a simple solution for improving particle deflection into the centre of the capillary, this would also lead to more instances of the trap-and-release focussing observed previously, and it may also be the case that particles could not pass between the magnets at all and are simply trapped. Therefore, another option is to extend the amount of time the particles spend in the magnetic field region without having to reduce the flow rate of the solution, an effect that could be achieved by using larger magnets of similar strength to those used previously.

To study this effect, 10 $\mu$m particles in 0.039 M GdCl$_3$ (a low concentration was chosen in anticipation of performing cell studies) were pumped through the capillary at a flow

rate of 30 $\mu$L h$^{-1}$ between either a pair of 4 x 4 x 5 mm$^3$ NdFeB rectangular magnets (particle residence time between the magnets $\approx$ 17 s), or a pair of 10 mm Ø x 5 mm NdFeB disc magnets (particle residence time $\approx$ 35 s).  Fig. 120 shows the results for the particle focussing using both of these magnet setups.
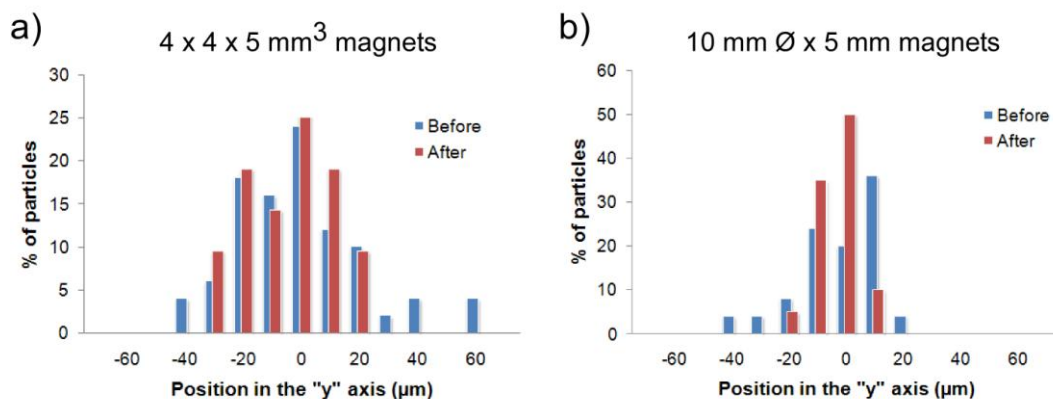


**Fig. 120  Focussing of 10 $\mu$m particles in 0.039 M GdCl$_3$ at 30 $\mu$L h$^{-1}$, using a) 4 x 4 x 5 mm$^3$ NdFeB rectangular magnets, and b) 10 mm Ø x 5 mm NdFeB disc magnets.**

The magnetic field values of $(\mathbf{B}\cdot\nabla)\mathbf{B}$, which affect the $\mathbf{F_{mag}}$ force on the particles, varied only slightly between the two setups.  The $(\mathbf{B}\cdot\nabla)\mathbf{B}$ value at a distance of 1 mm before the magnet pairs was 16 T$^2$ m$^{-1}$ for both setups, while the values at the edges of the magnets were 740 and 517 T$^2$ m$^{-1}$ for the 4 x 4 x 5 mm$^3$ and 10 mm Ø x 5 mm magnets, respectively.  The values at a distance 1 mm into the space between the magnets were 47 and 46 T$^2$ m$^{-1}$, respectively.  Therefore, as the particles passed between the rectangular magnets they experienced a slightly greater force, but as they passed between the disc magnets they experienced a somewhat smaller force but for approximately twice the length of time.

When using the 4 x 4 x 5 mm$^3$ magnets, less than 30 % of the particles were focussed to the centre line with the remainder within 30 μm, which was only a slight improvement to the distribution before the magnets. However, when using the 10 mm Ø x 5 mm magnets, nearly 50 % of the particles were focussed to y = 0, with most of the remaining particles within 10 μm of the centre and only a few percent as far as 20 μm.

These results show that when using low concentrations of paramagnetic salt solution, as would be required when using cells, a good degree of focussing can be achieved by increasing the amount of time the particles/cells spend in the magnetic field. When lowering the flow rate of the particles is not a viable option, this could still be achieved by using different sizes of magnets, or by building arrays of small magnets, which presents a very economical method of increasing focussing efficiency since small NdFeB magnets are inexpensive.

## Viability of cells in paramagnetic media

With a number of particle based focussing studies having been performed, the system was next applied to the focussing of HaCaT (spontaneously immortalised human skin keratinocyte) cells. As mentioned in previous sections, the toxicity of paramagnetic salt solutions is an important factor to consider when using cells, and so a series of tests was performed on the cells to determine their viability in paramagnetic media. This was achieved by using MTS assays as described in Section 2.11.3.

Firstly, the cells were tested in DMEM culture media that contained either $MnCl_2$, $GdCl_3$ or Gd-DTPA. As previously mentioned, Gd-DTPA is a biologically benign MRI contrast agent, approved by the Food and Drug Administration (FDA). It was reported by Winkleman et al.[128] as being suitable for their cell work at a concentration of 0.04 M

and a pH of 7.2. Therefore, Gd-DTPA was used here to determine whether it could be used to maintain the viability of HaCaT cells.

However, when the cells were suspended in any of the paramagnetic salt modified DMEM solutions, they immediately died. In the subsequent test, the paramagnetic salts were prepared in PBS buffer, but it was found that neither $MnCl_2$ nor $GdCl_3$ would dissolve properly, with only Gd-DTPA forming a suitable solution. Three concentrations of Gd-DTPA were prepared: 0.24 M, 0.079 M, and 0.039 M. When the cells were suspended in the 0.24 M solution they died within one hour, but survived a far greater amount of time in the two lower concentrations, as shown in Table 20.

**Table 20  Percentage of living HaCaT cells in 0.079 M and 0.039 M concentrations of Gd-DTPA over four hours.**

| Hours | Percentage of living cells (%) | |
|:---:|:---:|:---:|
| | 0.079 M | 0.039 M |
| 1 | 95.8 | 98.7 |
| 2 | 87.5 | 92.6 |
| 3 | 86.8 | 90.0 |
| 4 | 43.6 | 54.4 |

After three hours in the 0.079 M solution, 86.8 % of the cells were still alive, before decreasing to 43.6 % after the fourth hour. By comparison, when the cells were suspended in 0.039 M solution, 90 % of the particles were still viable after three hours, with 54.4 % still alive after the fourth. These results demonstrate that within the timeframe required to perform the focussing experiments (typically requiring less than one hour), the majority of particles would still be alive. To maintain as high a rate of living cells as possible whilst performing cell focussing experiments, cells were

suspended in 0.039 M Gd-DTPA solution. However, it could not be commented on as to how stable the cells were in this medium.

**Flow focussing of HaCaT cells**

With cells able to stay viable for a number of hours in 0.039 M Gd-DTPA, a preliminary experiment was performed in which the HaCaT cells were introduced into the capillary to determine whether living cells could be focussed. The findings of the previous particle studies were incorporated into this experiment, with a flow rate of 30 μL h$^{-1}$ applied and the larger 10 mm Ø x 5 mm NdFeB disc magnets used to allow longer residence times. The results of this are shown in Fig. 121.
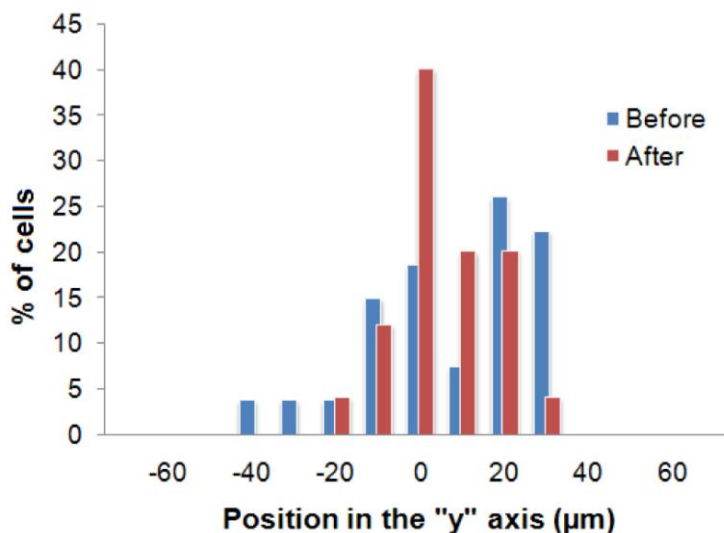


**Fig. 121  Flow focussing of living HaCaT cells (~10 μm) in 0.039 M Gd-DTPA, and pumped at 30 μL h$^{-1}$ between a pair of 10 mm Ø x 5 mm NdFeB disc magnets.**

Before passing between the magnets, the cells were distributed across a 70 μm region in the capillary, with 20 % of the cells in the y = 0 plane and the highest percentage of cells (27 %) in the y = +20 μm plane. However, after the cells had passed between the two magnets, the percentage in the y = 0 μm plane was doubled to 40 %, with 56 % of the remaining cells within 20 μm of the centre line and only 4 % being as far as 30 μm from the centre.

This successfully demonstrated the flow focussing of living cells via the use of diamagnetic repulsion forces, using a paramagnetic salt solution and simple, inexpensive permanent magnets. These preliminary findings demonstrate the potential of the system for the focussing of cells without the need for any labelling, with deflection based on the intrinsic properties of the cells (being composed mostly of water and therefore being diamagnetic). However, as well as further investigation into the actual focussing of cells, future studies will also require an assessment of the toxic effects of the paramagnetic medium on the cells, as the HaCaT cells used here were only able to survive for a few hours in Gd-DTPA. With this, a more suitable medium could be developed in which the cells would be more stable and survive for longer periods of time.

## Summary

An investigation was performed into the potential of flow focussing of particles and cells via the use of diamagnetic repulsion, without the need for prior labelling. This initially involved a thorough study into the focussing of diamagnetic polystyrene particles, which were suspended in paramagnetic salt solution containing either $MnCl_2$ or $GdCl_3$, and pumped through a capillary between a pair of permanent NdFeB magnets.

The particles were focussed by the magnets into the central axis of the capillary, and the effect was found to be enhanced with (i) increased particle size (and thus increased volume of magnetisable material), (ii) paramagnetic salt solution with a high magnetic susceptibility, determined by the salt type (e.g. $GdCl_3$ rather than $MnCl_2$) and at higher concentrations, (iii) decreased flow rate in order to allow a longer period of time between the magnets, and (iv) further increasing the residence time of the particles in the magnetic field by using larger magnets.

These findings were applied to the focussing of living HaCaT cells via diamagnetic repulsion. This result demonstrates the potential of the system for the flow focussing of cells by magnetic forces without being labelled, and with further optimisation could be used to focus different types of cells for performing a number of downstream processes including sorting and analysis in microfluidic devices. Although the experiments here were performed in a capillary, they could easily be adapted to lab-on-a-chip platforms by simply cutting out sections of chip material next to the channels, allowing magnets to be placed directly beside the microchannels.

# 10    Conclusions

The aim of this PhD project was to investigate the on-chip continuous flow processing of microparticles via the use of magnetic forces. This included studies into the effects of temperature on magnetophoresis separations, and the development of a multilaminar flow reactor to perform different types of reactions, coatings, and assays. Additionally, the use of diamagnetic repulsion as a viable means of performing similar continuous flow procedures was investigated. In this chapter, the major findings and achievements in each of these areas will be summarised, and considerations made for future work in these areas.

## 10.1    On-chip free-flow magnetophoresis

While parameters such as particle size and magnetic field characteristics had been studied previously, one important factor in the deflection of particles that had not been considered in magnetophoresis, or any other method of continuous flow processing for that matter, was the effect of temperature. Hence experiments were undertaken in which the temperature of the buffer solution was varied between 5 and 50 °C.

In the first experiment, the deflection behaviour of 2.8 μm magnetic particles was studied over the given temperature range, whereupon it was determined that increasing the temperature of the system resulted in lower solution viscosity, and therefore lower viscous drag forces on the particles. This had the effect of increasing the magnetically induced velocity of the particles perpendicular to the direction of fluid flow, resulting in them deflecting further across the microfluidic chamber at higher temperatures.

Secondly, two particle populations (2.8 μm and 1 μm particles) were separated at temperatures of 5, 20 and 50 °C. Here, the greater volume of magnetic material in the larger particles resulted in their deflecting further than the smaller particles, but at the lowest two temperatures there were some particles from both populations that exited the chamber via the same outlet. However, increasing the temperature, whilst increasing the deflection distances of both particles, had the greater effect on the 2.8 μm variety, which were deflected much further than the smaller particles. This allowed the separation resolution to be increased at higher temperatures. Additionally, theoretically calculated particle trajectories compared very well with the experimentally observed paths. This demonstrated that the effect of temperature followed the theory well, and that it is possible to predict the particle paths based on the parameters utilised in the experiments.

The results demonstrate the importance of temperature control during particle separations, as fluctuations in the system temperature could lead to poor reproducibility. Additionally, while this technique was used here for magnetophoretic separations, on the wider scale it could also be applied to any number of on-chip continuous flow methods that involve the lateral deflection of particles through flowing liquid via the use of external forces (e.g. acoustic, optical, dielectrophoretic). Despite the type of force employed, adjusting the temperature should nonetheless improve the deflection of particles, the resolution of a separation, and potentially the speed of other continuous flow processing techniques, such as the multilaminar flow system. However, its applicability may be limited for some biological species, such as cells, where they can only be used in a narrow temperature range.

Future work would involve using a flow focussing effect prior to particles entering the chamber, such that they would all follow reproducible trajectories. A further

improvement could also be the use of narrower outlets to collect fractions that are only slightly separated. It would also be interesting to actually tune the temperature of the system in order to direct particles to specific outlets, then change it slightly so that they exit via a different outlet, which would allow different downstream procedures to be performed simultaneously on the same particle types.

## 10.2    Multilaminar flow procedures

A multilaminar flow microreactor has been described in which magnetic particles can be deflected through alternating streams of reagents to perform rapid reactions and assays in only 90 s. Previously, the platform had been applied to proof-of-principle bioassays[394,424] and DNA hybridisation,[425,426] to great effect. Here, studies were undertaken to determine its applicability to a number of different areas, including its use for (i) chemical reactions such as the fluorescamine reaction and peptide synthesis, (ii) the deposition of polyelectrolyte layers onto magnetic templates, and (iii) clinically relevant sandwich immunoassays such as the detection of the C-reactive protein biomarker.

Despite encountering difficulties, some of the main goals of this work were achieved to a degree, including the ability to perform a chemical reaction (amide bond formation) on the surface of mobile magnetic particles, and the deposition of a polyelectrolyte layer onto magnetic templates in continuous flow. In several of these investigations it was found that the reaction/coating/assay itself was successful, but on most occasions the studies were hindered by the sticking of particles to the chip surfaces. Therefore, to build on these initial findings a more thorough study into this sticking phenomena should be performed from a more physical chemistry orientated viewpoint. Once the

causes and solutions to these problems can be determined, the multilaminar flow device will show far greater diversity in what it can be used to achieve, and this remains a priority for future investigations otherwise the system will find its applicability somewhat limited.

The most promising investigation was that of the C-reactive protein (CRP) assay, in which a hydrophilic surface treatment of the microchannels was determined to allow particles to cross the chamber with minimal sticking. The beginnings of a clinically relevant calibration curve for CRP were demonstrated, though time constraints meant that this work could not be continued further. The main benefits of the system are its ability to perform rapid processes, with particles taking less than 90 s to cross the chamber, while requiring only a simple setup and minimal input from the user once the system is running. However, the rapid processing does not take into account the setup time, which commonly takes around half an hour or more, though the chip holder was found to speed the process up somewhat. In future, it should be possible to engineer the device such that its setup is minimal, and in which the reagents and particle suspensions can be injected into the system, possibly via the use of a HPLC-style sample injector.

Some future applications of the multilaminar flow device may also require longer residence times for particles, or more reagent streams if there are a large number of steps in a reaction/assay. In both of these cases the number of inlets can simply be increased to allow a greater number of reagent streams. Future devices would also benefit from a particle focussing inlet channel, as the current devices suffer from having a great deal of particle spread as they traverse the channel due to the variation in starting position when they enter the chamber. By focussing the particles when they enter the chamber they would each have the same starting position, hence they would experience the same magnetic forces and follow the same trajectory through the chamber, thereby

increasing reproducibility in the results. Example of both of these design features can be seen in Fig. 122, with red and yellow ink used to show the laminar flow streams in chip design MLF3. A detailed description of MLF3 can be found in Section 2.2.

With a better understanding of the particle sticking effects, further improvements in chip design, and a more advanced setup, the multilaminar flow microreactor could become a powerful tool for performing rapid analysis, synthesis and particle coating, among other applications, while requiring little input from the operator and using minimal volumes of expensive reagents.
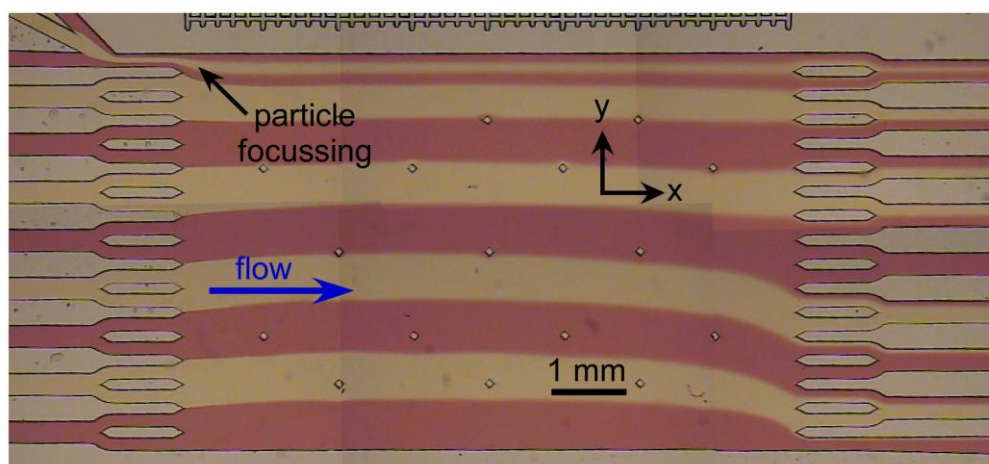


**Fig. 122  Photograph of chip design MLF3, featuring a particle focussing inlet channel and multiple reagent/washing streams. Such a design could be used to perform up to four consecutive reactions, while the flow focussing channel would allow particles to enter the chamber in a narrow stream, such that their trajectories across the chamber would be more reproducible and experience less of a spread.**

## 10.3    *Diamagnetic repulsion*

There are many methods of manoeuvring particles in continuous flow microfluidic devices. However, most techniques require complex chip designs and/or complicated and expensive setups. Magnetism allows the manipulation of particles via inexpensive, powerful, permanent neodymium-iron-boron magnets, which can be easily placed next to a microchannel to give a simple setup. One drawback of using magnetism conventionally, though, is that the objects of interest (be they particles or cells etc.) must feature some kind of magnetic labelling in order that they can be attracted towards the source of the magnetic field. In some instances this may not be ideal, for example it adds to the number of steps when cells must be labelled with magnetic nanoparticles, and in some cases may alter some properties of the species being labelled. Additionally, it may also be necessary to remove the magnetic label once the desired process has taken place, further increasing the number of steps required.

Thus, an investigation was performed into the ability to use diamagnetic repulsion, based on the intrinsic properties of materials, to perform continuous flow processes on polystyrene particles and cells that have not been magnetically labelled. An initial investigation involved studying the effect of particle size and paramagnetic medium on the particle deflection behaviour across a microfluidic chamber in the high magnetic field of a superconducting magnet. The results showed that larger particle deflected further due to the greater volume of material, while suspending them in a higher concentration of paramagnetic manganese (II) chloride enhanced the effect further. However, it was also found that a 20 % w/w $MnCl_2$ solution caused the particles to cream to the surface of the chip, restricting their movement, hence a 10 % w/w concentration was determined to be the most suitable. This showed promise for performing size based separations of diamagnetic particles, and indeed the findings here

were utilised by Peyman *et al.*[512] to perform continuous flow separations of polystyrene particles by on-chip free-flow diamagnetophoresis.

In a short set of experiments that followed, streptavidin functionalised polystyrene particles in $MnCl_2$ solution were introduced into reagent stream of fluorescently labelled biotin which became bound to the particle surfaces. Diamagnetic repulsion was achieved using simple permanent magnets, and the particles were deflected out of the reagent stream into a washing buffer stream in continuous flow. This demonstrated the possibility of performing multilaminar flow reactions on mobile polystyrene particles or cells via diamagnetic forces, without the need for magnetic labelling.

Finally, a thorough investigation into the use of diamagnetic repulsion for the focussing of particles was performed, with a number of parameters studied that showed the focussing was improved with increased residence time between two magnets, larger particles, and higher magnetic susceptibility of the paramagnetic solution. These findings were then applied to the continuous flow focussing of living cells, the first time this has been achieved using such forces.

These describe a handful of the possible processes that could be performed using diamagnetic repulsion for controlling the migration of unlabelled species such as particles and cells. Future work would include the optimisation of the setups for carrying out separations of a variety of diamagnetic species, including cells, as well as multi-step reactions using a modified multilaminar flow system. These could be achieved by further investigation into different types of paramagnetic salt solution, and in particular suitable concentrations, especially when using living cells. Magnets could be designed with high strength and/or gradients, in order to focus the field into a desired area in order to better control the movement of diamagnetic particles and cells.

# References

1.  P. Watts and S. J. Haswell, *Chemical Engineering & Technology*, 2005, **28**, 290-301.

2.  G. M. Whitesides, *Nature*, 2006, **442**, 368-373.

3.  D. Mark, S. Haeberle, G. Roth, F. von Stetten and R. Zengerle, *Chemical Society Reviews*, 2010, **39**, 1153-1182.

4.  S. Haeberle and R. Zengerle, *Lab on a Chip*, 2007, **7**, 1094-1110.

5.  S. J. Haswell, R. J. Middleton, B. O'Sullivan, V. Skelton, P. Watts and P. Styring, *Chemical Communications*, 2001, 391-398.

6.  P. Watts and S. J. Haswell, *Chemical Society Reviews*, 2005, **34**, 235-246.

7.  K. M. Horsman, J. M. Bienvenue, K. R. Blasier and J. P. Landers, *Journal of Forensic Sciences*, 2007, **52**, 784-799.

8.  E. Verpoorte, *Electrophoresis*, 2002, **23**, 677-712.

9.  J. A. Oakley, K. J. Shaw, P. T. Docker, C. E. Dyer, J. Greenman, G. M. Greenway and S. J. Haswell, *Lab on a Chip*, 2009, **9**, 1596-1600.

10. K. J. Shaw, L. Thain, P. T. Docker, C. E. Dyer, J. Greenman, G. M. Greenway and S. J. Haswell, *Analytica Chimica Acta*, 2009, **652**, 231-233.

11. J. O. Tegenfeldt, C. Prinz, H. Cao, R. L. Huang, R. H. Austin, S. Y. Chou, E. C. Cox and J. C. Sturm, *Analytical and Bioanalytical Chemistry*, 2004, **378**, 1678-1692.

12. K. J. Shaw, P. T. Docker, J. V. Yelland, C. E. Dyer, J. Greenman, G. M. Greenway and S. J. Haswell, *Lab on a Chip*, 2010, **10**, 1725-1728.

13. S. Lindstrom and H. Andersson-Svahn, *Lab on a Chip*, 2010, **10**, 3363-3372.

14. S. M. Hattersley, C. E. Dyer, J. Greenman and S. J. Haswell, *Lab on a Chip*, 2008, **8**, 1842-1846.

15. A. H. C. Ng, U. Uddayasankar and A. R. Wheeler, *Analytical and Bioanalytical Chemistry*, 2010, **397**, 991-1007.

16. S. Vyawahare, A. D. Griffiths and C. A. Merten, *Chemistry & Biology*, 2010, **17**, 1052-1065.

17. L. Marle and G. M. Greenway, *TrAC - Trends in Analytical Chemistry*, 2005, **24**, 795-802.

18. J. G. E. Gardeniers and A. van den Berg, *Analytical and Bioanalytical Chemistry*, 2004, **378**, 1700-1703.

19. P. A. Greenwood and G. M. Greenway, *TrAC - Trends in Analytical Chemistry*, 2002, **21**, 726-740.

20. A. Rios, A. Escarpa, M. C. Gonzalez and A. G. Crevillen, *TrAC - Trends in Analytical Chemistry*, 2006, **25**, 467-479.

21. S. C. Terry, J. H. Jerman and J. B. Angell, *IEEE Transactions on Electron Devices*, 1979, **26**, 1880-1886.

22. A. Manz, Y. Miyahara, J. Miura, Y. Watanabe, H. Miyagi and K. Sato, *Sensors and Actuators B - Chemical*, 1990, **1**, 249-255.

23. A. Manz, N. Graber and H. M. Widmer, *Sensors and Actuators B - Chemical*, 1990, **1**, 244-248.

24. P. A. Auroux, D. Iossifidis, D. R. Reyes and A. Manz, *Analytical Chemistry*, 2002, **74**, 2637-2652.

25. P. S. Dittrich, K. Tachikawa and A. Manz, *Analytical Chemistry*, 2006, **78**, 3887-3907.

26. D. R. Reyes, D. Iossifidis, P. A. Auroux and A. Manz, *Analytical Chemistry*, 2002, **74**, 2623-2636.

27. T. Vilkner, D. Janasek and A. Manz, *Analytical Chemistry*, 2004, **76**, 3373-3385.

28. J. West, M. Becker, S. Tombrink and A. Manz, *Analytical Chemistry*, 2008, **80**, 4403-4419.

29. A. Arora, G. Simone, G. B. Salieb-Beugelaar, J. T. Kim and A. Manz, *Analytical Chemistry*, 2010, **82**, 4830-4847.

30. G. B. Salieb-Beugelaar, G. Simone, A. Arora, A. Philippi and A. Manz, *Analytical Chemistry*, 2010, **82**, 4848-4864.

31. Y. Kim, B. Kuczenski, P. R. LeDuc and W. C. Messner, *Lab on a Chip*, 2010, **10**, 3428-3428.

32. J. P. McMullen and K. F. Jensen, *Organic Process Research & Development*, 2010, **14**, 1169-1176.

33. Y. Kim, B. Kuczenski, P. R. LeDuc and W. C. Messner, *Lab on a Chip*, 2009, **9**, 2603-2609.

34. J. W. Choi, K. W. Oh, J. H. Thomas, W. R. Heineman, H. B. Halsall, J. H. Nevin, A. J. Helmicki, H. T. Henderson and C. H. Ahn, *Lab on a Chip*, 2002, **2**, 27-30.

35. R. Tornay, T. Braschler and P. Renaud, *Lab on a Chip*, 2009, **9**, 657-660.

36. K. W. Oh and C. H. Ahn, *Journal of Micromechanics and Microengineering*, 2006, **16**, R13-R39.

37. B. D. Iverson and S. V. Garimella, *Microfluidics and Nanofluidics*, 2008, **5**, 145-174.

38. P. Watts and C. Wiles, *Organic & Biomolecular Chemistry*, 2007, **5**, 727-732.

39. T. McCreedy, *TrAC - Trends in Analytical Chemistry*, 2000, **19**, 396-401.

40. T. McCreedy, *Analytica Chimica Acta*, 2001, **427**, 39-43.

41. T. McCreedy and N. G. Wilson, *Analyst*, 2001, **126**, 21-23.

42. H. Shadpour, M. L. Hupert, D. Patterson, C. G. Liu, M. Galloway, W. Stryjewski, J. Goettert and S. A. Soper, *Analytical Chemistry*, 2007, **79**, 870-878.

43. L. Martynova, L. E. Locascio, M. Gaitan, G. W. Kramer, R. G. Christensen and W. A. MacCrehan, *Analytical Chemistry*, 1997, **69**, 4783-4789.

44. J. A. Thompson and H. H. Bau, *Journal of Chromatography B*, 2010, **878**, 228-236.

45. R. Kellner, J.-M. Mermet, M. Otto, M. Valcarcel and H. M. Widmer, *Analytical Chemistry: A Modern Approach To Analytical Science*, 2nd edn., Wiley-VCH, Weinheim, 2004.

46. H. Becker and L. E. Locascio, *Talanta*, 2002, **56**, 267-287.

47. A. de Mello, *Lab on a Chip*, 2002, **2**, 31N-36N.

48. R. M. McCormick, R. J. Nelson, M. G. Alonso-Amigo, J. Benvegnu and H. H. Hooper, *Analytical Chemistry*, 1997, **69**, 2626-2630.

49. H. Becker and U. Heim, *Sensors and Materials*, 1999, **11**, 297-304.

50. H. Qi, T. Chen, L. Y. Yao and T. C. Zuo, *Optics and Lasers in Engineering*, 2009, **47**, 594-598.

51. D. C. Duffy, J. C. McDonald, O. J. A. Schueller and G. M. Whitesides, *Analytical Chemistry*, 1998, **70**, 4974-4984.

52. J. C. McDonald, D. C. Duffy, J. R. Anderson, D. T. Chiu, H. K. Wu, O. J. A. Schueller and G. M. Whitesides, *Electrophoresis*, 2000, **21**, 27-40.

53. S. E. Ong, S. Zhang, H. J. Du and Y. Q. Fu, *Frontiers in Bioscience*, 2008, **13**, 2757-2773.

54. P. Atkins and J. de Paula, *Atkins' Physical Chemistry*, 7th edn., Oxford University Press, Oxford, 2002.

55. E. Verpoorte, *Lab on a Chip*, 2003, **3**, 60N-68N.

56. H. Kawaguchi, *Progress in Polymer Science*, 2000, **25**, 1171-1210.

57. M. B. Meza, *Drug Discovery Today*, 2000, 38-41.

58. L. B. Bangs, *Pure and Applied Chemistry*, 1996, **68**, 1873-1879.

59. I. W. Hamley, *Introduction to Soft Matter: Polymers, Colloids, Amphiphiles and Liquid Crystals*, John Wiley & Sons, Ltd., Chichester, 2000.

60. E. Dickinson and G. Stainsby, *Colloids in Food*, Applied Science Publishers, Ltd., Essex, 1982.

61. R. Tadmor, E. Hernandez-Zapata, N. H. Chen, P. Pincus and J. N. Israelachvili, *Macromolecules*, 2002, **35**, 2380-2388.

62. D. F. Evans and H. Wennerstrom, *The Colloidal Domain: Where Physics, Chemistry, Biology, and Technology Meet*, VCH Publishers (UK) Ltd., Cambridge, 1994.

63. D. Grasso, K. Subramaniam, M. Butkus, K. Strevett and J. Bergendahl, *Reviews in Environmental Science and Biotechnology*, 2002, **1**, 17-38.

64. T. Cosgrove, *Colloid Science: Principles, methods and applications*, 2nd edn., John Wiley & Sons, Ltd., Chichester, 2010.

65. J. Israelachvili, *Intermolecular and Surface Forces*, 2nd edn., Academic Press, Inc., London, 1991.

66. I. E. Dunlop, W. H. Briscoe, S. Titmuss, R. M. J. Jacobs, V. L. Osborne, S. Edmondson, W. T. S. Huck and J. Klein, *Journal of Physical Chemistry B*, 2009, **113**, 3947-3956.

67. B. Liberelle and S. Giasson, *Langmuir*, 2008, **24**, 1550-1559.

68. D. S. Peterson, *Lab on a Chip*, 2005, **5**, 132-139.

69. C. T. Lim and Y. Zhang, *Biosensors & Bioelectronics*, 2007, **22**, 1197-1204.

70. J. Nilsson, M. Evander, B. Hammarstrom and T. Laurell, *Analytica Chimica Acta*, 2009, **649**, 141-157.

71. K. Sato, M. Tokeshi, T. Odake, H. Kimura, T. Ooi, M. Nakao and T. Kitamori, *Analytical Chemistry*, 2000, **72**, 1144-1147.

72. R. D. Oleschuk, L. L. Shultz-Lockyear, Y. B. Ning and D. J. Harrison, *Analytical Chemistry*, 2000, **72**, 585-590.

73. A. B. Jemere, R. D. Oleschuk, F. Ouchen, F. Fajuyigbe and D. J. Harrison, *Electrophoresis*, 2002, **23**, 3537-3544.

74. A. B. Jemere, R. D. Oleschuk and D. J. Harrison, *Electrophoresis*, 2003, **24**, 3018-3025.

75. M. C. Breadmore, K. A. Wolfe, I. G. Arcibal, W. K. Leung, D. Dickson, B. C. Giordano, M. E. Power, J. P. Ferrance, S. H. Feldman, P. M. Norris and J. P. Landers, *Analytical Chemistry*, 2003, **75**, 1880-1886.

76.     H. Andersson, W. van der Wijngaart, P. Enoksson and G. Stemme, *Sensors and Actuators B - Chemical*, 2000, **67**, 203-208.

77.     L. Ceriotti, N. F. de Rooij and E. Verpoorte, *Analytical Chemistry*, 2002, **74**, 639-647.

78.     H. Andersson, C. Jonsson, C. Moberg and G. Stemme, *Electrophoresis*, 2001, **22**, 3876-3882.

79.     H. Andersson, C. Jonsson, C. Moberg and G. Stemme, *Talanta*, 2002, **56**, 301-308.

80.     J. P. Murrihy, M. C. Breadmore, A. M. Tan, M. McEnery, J. Alderman, C. O'Mathuna, A. P. O'Neill, P. O'Brien, N. Advoldvic, P. R. Haddad and J. D. Glennon, *Journal of Chromatography A*, 2001, **924**, 233-238.

81.     V. Sivagnanam, B. Song, C. Vandevyver and M. A. M. Gijs, *Analytical Chemistry*, 2009, **81**, 6509-6515.

82.     N. Malmstadt, A. S. Hoffman and P. S. Stayton, *Lab on a Chip*, 2004, **4**, 412-415.

83.     G. L. Lettieri, A. Dodge, G. Boer, N. F. de Rooij and E. Verpoorte, *Lab on a Chip*, 2003, **3**, 34-39.

84.     B. R. Lutz, J. Chen and D. T. Schwartz, *Analytical Chemistry*, 2006, **78**, 5429-5435.

85.     M. Tanyeri, E. M. Johnson-Chavarria and C. M. Schroeder, *Applied Physics Letters*, 2010, **96**, 224101.

86.     C. M. Lin, Y. S. Lai, H. P. Liu, C. Y. Chen and A. M. Wo, *Analytical Chemistry*, 2008, **80**, 8937-8945.

87.     J. Guck, S. Schinkinger, B. Lincoln, F. Wottawah, S. Ebert, M. Romeyke, D. Lenz, H. M. Erickson, R. Ananthakrishnan, D. Mitchell, J. Kas, S. Ulvick and C. Bilby, *Biophysical Journal*, 2005, **88**, 3689-3698.

88.     H. C. Hunt and J. S. Wilkinson, *Microfluidics and Nanofluidics*, 2008, **4**, 53-79.

89.     A. Jonas and P. Zemanek, *Electrophoresis*, 2008, **29**, 4813-4851.

90.     M. Ozkan, M. Wang, C. Ozkan, R. Flynn, A. Birkbeck and S. Esener, *Biomedical Microdevices*, 2003, **5**, 61-67.

91.     A. L. Birkbeck, R. A. Flynn, M. Ozkan, D. Q. Song, M. Gross and S. C. Esener, *Biomedical Microdevices*, 2003, **5**, 47-54.

92.     R. A. Flynn, A. L. Birkbeck, M. Gross, M. Ozkan, B. Shao, M. M. Wang and S. C. Esener, *Sensors and Actuators B - Chemical*, 2002, **87**, 239-243.

93.     A. Terray, J. Arnold and S. J. Hart, *Optics Express*, 2005, **13**, 10406-10415.

94. S. J. Hart, A. Terray, J. Arnold and T. A. Leski, *Optics Express*, 2007, **15**, 2724-2731.

95. S. Cran-McGreehin, T. F. Krauss and K. Dholakia, *Lab on a Chip*, 2006, **6**, 1122-1124.

96. S. J. Cran-McGreehin, K. Dholakia and T. F. Krauss, *Optics Express*, 2006, **14**, 7723-7729.

97. R. Pethig, *Biomicrofluidics*, 2010, **4**, 039901.

98. R. Pethig, *Biomicrofluidics*, 2010, **4**, 022811.

99. K. Khoshmanesh, S. Nahavandi, S. Baratchi, A. Mitchell and K. Kalantar-zadeh, *Biosensors and Bioelectronics*, 2011, **26**, 1800-1814.

100. B. H. Lapizco-Encinas and M. Rito-Palomares, *Electrophoresis*, 2007, **28**, 4521-4538.

101. T. Muller, G. Gradl, S. Howitz, S. Shirley, T. Schnelle and G. Fuhr, *Biosensors & Bioelectronics*, 1999, **14**, 247-256.

102. Q. Ramadan, V. Samper, D. Poenar, Z. Liang, C. Yu and T. M. Lim, *Sensors and Actuators B - Chemical*, 2006, **113**, 944-955.

103. N. Markarian, M. Yeksel, B. Khusid, K. Farmer and A. Acrivos, *Applied Physics Letters*, 2003, **82**, 4839-4841.

104. N. Markarian, M. Yeksel, B. Khusid, K. Farmer and A. Acrivos, in *Proceedings of the IEEE 29th Annual Northeast Bioengineering Conference*, eds. S. Reisman, R. Foulds and B. Mantilla, 2003, pp. 152-153.

105. T. Yasukawa, M. Suzuki, T. Sekiya, H. Shiku and T. Matsue, *Biosensors & Bioelectronics*, 2007, **22**, 2730-2736.

106. J. V. Norris, M. Evander, K. M. Horsman-Hall, J. Nilsson, T. Laurell and J. P. Landers, *Analytical Chemistry*, 2009, **81**, 6089-6095.

107. T. Lilliehorn, U. Simu, M. Nilsson, M. Almqvist, T. Stepinski, T. Laurell, J. Nilsson and S. Johansson, *Ultrasonics*, 2005, **43**, 293-303.

108. T. Lilliehorn, M. Nilsson, U. Simu, S. Johansson, M. Almqvist, J. Nilsson and T. Laurell, *Sensors and Actuators B - Chemical*, 2005, **106**, 851-858.

109. M. Evander, L. Johansson, T. Lilliehorn, J. Piskur, M. Lindvall, S. Johansson, M. Almqvist, T. Laurell and J. Nilsson, *Analytical Chemistry*, 2007, **79**, 2984-2991.

110. S. S. Guo, L. B. Zhao, K. Zhang, K. H. Lam, S. T. Lau, X. Z. Zhao, Y. Wang, H. L. W. Chan, Y. Chen and D. Baigl, *Applied Physics Letters*, 2008, **92**, 213901.

111. O. Manneberg, B. Vanherberghen, J. Svennebring, H. M. Hertz, B. Onfelt and M. Wiklund, *Applied Physics Letters*, 2008, **93**, 063901.

112. T. Laurell, F. Petersson and A. Nilsson, *Chemical Society Reviews*, 2007, **36**, 492-506.

113. J. Y. Liu, S. Lin, D. W. Qi, C. H. Deng, P. Y. Yang and X. M. Zhang, *Journal of Chromatography A*, 2007, **1176**, 169-177.

114. S. Bronzeau and N. Pamme, *Analytica Chimica Acta*, 2008, **609**, 105-112.

115. M. A. Hayes, N. A. Polson, A. N. Phayre and A. A. Garcia, *Analytical Chemistry*, 2001, **73**, 5896-5902.

116. K. Y. Lien, J. L. Lin, C. Y. Liu, H. Y. Lei and G. B. Lee, *Lab on a Chip*, 2007, **7**, 868-875.

117. G. F. Jiang and D. J. Harrison, *Analyst*, 2000, **125**, 2176-2179.

118. Z. H. Fan, S. Mangru, R. Granzow, P. Heaney, W. Ho, Q. P. Dong and R. Kumar, *Analytical Chemistry*, 1999, **71**, 4851-4859.

119. K. Smistrup, B. G. Kjeldsen, J. L. Reimers, M. Dufva, J. Petersen and M. F. Hansen, *Lab on a Chip*, 2005, **5**, 1315-1319.

120. T. Lund-Olesen, M. Dufva and M. F. Hansen, *Journal of Magnetism and Magnetic Materials*, 2007, **311**, 396-400.

121. M. Slovakova, N. Minc, Z. Bilkova, C. Smadja, W. Faigle, C. Futterer, M. Taverna and J. L. Viovy, *Lab on a Chip*, 2005, **5**, 935-942.

122. Z. Bilkova, M. Slovakova, N. Minc, C. Futterer, R. Cecal, D. Horak, M. Benes, I. le Potier, J. Krenkova, M. Przybylski and J. L. Viovy, *Electrophoresis*, 2006, **27**, 1811-1824.

123. A. Le Nel, N. Minc, C. Smadja, M. Slovakova, Z. Bilkova, J. M. Peyrin, J. L. Viovy and M. Taverna, *Lab on a Chip*, 2008, **8**, 294-301.

124. L. G. Rashkovetsky, Y. V. Lyubarskaya, F. Foret, D. E. Hughes and B. L. Karger, *Journal of Chromatography A*, 1997, **781**, 197-204.

125. H. Watarai and M. Namba, *Journal of Chromatography A*, 2002, **961**, 3-8.

126. H. Watarai and M. Namba, *Analytical Sciences*, 2001, **17**, 1233.

127. H. Watarai, M. Suwa and Y. Iiguni, *Analytical and Bioanalytical Chemistry*, 2004, **378**, 1693-1699.

128. A. Winkleman, K. L. Gudiksen, D. Ryan, G. M. Whitesides, D. Greenfield and M. Prentiss, *Applied Physics Letters*, 2004, **85**, 2411.

129. T. Kimura, Y. Sato, F. Kimura, M. Iwasaka and S. Ueno, *Langmuir*, 2005, **21**, 830.

130. T. Kimura, M. Yamato and A. Nara, *Langmuir*, 2004, **20**, 572.

131. C. Wang, R. Oleschuk, F. Ouchen, J. J. Li, P. Thibault and D. J. Harrison, *Rapid Communications in Mass Spectrometry*, 2000, **14**, 1377-1383.

132. H. Andersson, W. van der Wijngaart and G. Stemme, *Electrophoresis*, 2001, **22**, 249-257.

133. A. Russom, A. Ahmadian, H. Andersson, P. Nilsson and G. Stemme, *Electrophoresis*, 2003, **24**, 158-161.

134. A. Russom, N. Tooke, H. Andersson and G. Stemme, *Journal of Chromatography A*, 2003, **1014**, 37-45.

135. A. Ahmadian, A. Russom, H. Andersson, M. Uhlen, G. Stemme and P. Nilsson, *Biotechniques*, 2002, **32**, 748-754.

136. M. L. Frisk, E. Berthier, W. H. Tepp, E. A. Johnson and D. J. Beebe, *Lab on a Chip*, 2008, **8**, 1793-1800.

137. T. Buranda, J. M. Huang, V. H. Perez-Luna, B. Schreyer, L. A. Sklar and G. P. Lopez, *Analytical Chemistry*, 2002, **74**, 1149-1156.

138. Y. Murakami, T. Endo, S. Yamamura, N. Nagatani, Y. Takamura and E. Tamiya, *Analytical Biochemistry*, 2004, **334**, 111-116.

139. Y. Jeong, K. Choi, J. Kim, D. S. Chung, B. Kim, H. C. Kim and K. Chun, *Sensors and Actuators B - Chemical*, 2008, **128**, 349-358.

140. T. Satoh, Y. Shinoda, S. Tokonami, R. Hirota, K. Noda, A. Kuroda and Y. Murakami, *Sensors and Actuators B - Chemical*, 2009, **142**, 118-122.

141. S. A. Bowden, J. M. Cooper, F. Greub, D. Tambo and A. Hurst, *Lab on a Chip*, 2010, **10**, 819-823.

142. J. Bergkvist, S. Ekstrom, L. Wallman, M. Lofgren, G. Marko-Varga, J. Nilsson and T. Laurell, *Proteomics*, 2002, **2**, 422-429.

143. G. H. Seong, W. Zhan and R. M. Crooks, *Analytical Chemistry*, 2002, **74**, 3372-3377.

144. M. B. Kerby, R. S. Legge and A. Tripathi, *Analytical Chemistry*, 2006, **78**, 8273-8280.

145. N. Pamme, *Lab on a Chip*, 2007, **7**, 1644-1659.

146. A. Lenshof and T. Laurell, *Chemical Society Reviews*, 2010, **39**, 1203-1217.

147. M. Kersaudy-Kerhoas, R. Dhariwal and M. P. Y. Desmulliez, *IET Nanobiotechnology*, 2008, **2**, 1-13.

148. H. Tsutsui and C. M. Ho, *Mechanics Research Communications*, 2009, **36**, 92-103.

149. D. R. Gossett, W. M. Weaver, A. J. Mach, S. C. Hur, H. T. K. Tse, W. Lee, H. Amini and D. Di Carlo, *Analytical and Bioanalytical Chemistry*, 2010, **397**, 3249-3267.

150. L. R. Huang, E. C. Cox, R. H. Austin and J. C. Sturm, *Science*, 2004, **304**, 987-990.

151. J. A. Davis, D. W. Inglis, K. J. Morton, D. A. Lawrence, L. R. Huang, S. Y. Chou, J. C. Sturm and R. H. Austin, *Proceedings of the National Academy of Sciences of the United States of America*, 2006, **103**, 14779-14784.

152. D. W. Inglis, K. J. Morton, J. A. Davis, T. J. Zieziulewicz, D. A. Lawrence, R. H. Austin and J. C. Sturm, *Lab on a Chip*, 2008, **8**, 925-931.

153. D. W. Inglis, *Applied Physics Letters*, 2009, **94**.

154. D. W. Inglis, J. A. Davis, R. H. Austin and J. C. Sturm, *Lab on a Chip*, 2006, **6**, 655-658.

155. K. J. Morton, K. Lotherback, D. W. Inglis, O. K. Tsui, J. C. Sturm, S. Y. Chou and R. H. Austin, *Proceedings of the National Academy of Sciences of the United States of America*, 2008, **105**, 7434-7438.

156. S. Choi and J. K. Park, *Lab on a Chip*, 2007, **7**, 890-897.

157. S. Choi, S. Song, C. Choi and J. K. Park, *Lab on a Chip*, 2007, **7**, 1532-1538.

158. P. B. Lillehoj, H. Tsutsui, B. Valamehr, H. Wu and C. M. Ho, *Lab on a Chip*, 2010, **10**, 1678-1682.

159. M. T. Blom, E. Chmela, J. G. E. Gardeniers, R. Tijssen, M. Elwenspoek and A. van den Berg, *Sensors and Actuators B - Chemical*, 2002, **82**, 111-116.

160. M. T. Blom, E. Chmela, R. E. Oosterbroek, R. Tijssen and A. van den Berg, *Analytical Chemistry*, 2003, **75**, 6761-6768.

161. M. Yamada, M. Nakashima and M. Seki, *Analytical Chemistry*, 2004, **76**, 5465-5471.

162. J. Takagi, M. Yamada, M. Yasuda and M. Seki, *Lab on a Chip*, 2005, **5**, 778-784.

163. Y. Sai, M. Yamada, M. Yasuda and M. Seki, *Journal of Chromatography A*, 2006, **1127**, 214-220.

164. T. Kawamata, M. Yamada, M. Yasuda and M. Seki, *Electrophoresis*, 2008, **29**, 1423-1430.

165. M. Yamada and M. Seki, *Lab on a Chip*, 2005, **5**, 1233-1239.

166. M. Yamada and M. Seki, *Analytical Chemistry*, 2006, **78**, 1357-1362.

167. A. A. S. Bhagat, S. S. Kuntaegowdanahalli and I. Papautsky, *Lab on a Chip*, 2008, **8**, 1906-1914.

168. A. A. S. Bhagat, S. S. Kuntaegowdanahalli and I. Papautsky, *Microfluidics and Nanofluidics*, 2009, **7**, 217-226.

169. A. A. S. Bhagat, S. S. Kuntaegowdanahalli, N. Kaval, C. J. Seliskar and I. Papautsky, *Biomedical Microdevices*, 2010, **12**, 187-195.

170. Z. G. Wu, B. Willing, J. Bjerketorp, J. K. Jansson and K. Hjort, *Lab on a Chip*, 2009, **9**, 1193-1199.

171. Y. Shirasaki, H. Sugino, M. Tatsuoka, J. Mizuno, S. Shoji and T. Funatsu, *Ieee Journal of Selected Topics in Quantum Electronics*, 2007, **13**, 223-227.

172. H. Sugino, T. Arakawa, Y. Nara, Y. Shirasaki, K. Ozaki, S. Shoji and T. Funatsu, *Lab on a Chip*, 2010, **10**, 2559-2565.

173. H. Sugino, K. Ozaki, Y. Shirasaki, T. Arakawa, S. Shoji and T. Funatsu, *Lab on a Chip*, 2009, **9**, 1254-1260.

174. R. D. Jaggi, R. Sandoz and C. S. Effenhauser, *Microfluidics and Nanofluidics*, 2007, **3**, 47-53.

175. S. Yang, A. Undar and J. D. Zahn, *Lab on a Chip*, 2006, **6**, 871-880.

176. A. I. Rodriguez-Villarreal, M. Arundell, M. Carmona and J. Samitier, *Lab on a Chip*, 2010, **10**, 211-219.

177. J. C. Giddings, *Separation Science and Technology*, 1966, **1**, 123-125.

178. K. D. Caldwell, J. C. Giddings, M. N. Myers and L. F. Kesner, *Science*, 1972, **176**, 296-298.

179. W. J. Cao, P. S. Williams, M. N. Myers and J. C. Giddings, *Analytical Chemistry*, 1999, **71**, 1597-1609.

180. M. E. Hovingh, G. H. Thompson and J. C. Giddings, *Analytical Chemistry*, 1970, **42**, 195-203.

181. P. J. P. Cardot, J. Gerota and M. Martin, *Journal of Chromatography - Biomedical Applications*, 1991, **568**, 93-103.

182. F. Carpino, M. Zborowski and P. S. Williams, *Journal of Magnetism and Magnetic Materials*, 2007, **311**, 383-387.

183. A. H. Latham and M. E. Williams, *Abstracts of Papers of the American Chemical Society*, 2005, **230**, U275.

184. A. H. Latham, R. S. Freitas, P. Schiffer and M. E. Williams, *Analytical Chemistry*, 2005, **77**, 5055-5062.

185. S. Mori, *Chromatographia*, 1986, **21**, 642-644.

186. T. M. Vickrey and J. A. Garciaramirez, *Separation Science and Technology*, 1980, **15**, 1297-1304.

187. S. K. R. Williams, H. Lee and M. M. Turner, *Journal of Magnetism and Magnetic Materials*, 1999, **194**, 248-253.

188. B. Roda, A. Zattoni, P. Reschiglian, M. H. Moon, M. Mirasoli, E. Michelini and A. Roda, *Analytica Chimica Acta*, 2009, **635**, 132-143.

189. P. Reschiglian, A. Zattoni, B. Roda, E. Michelini and A. Roda, *Trends in Biotechnology*, 2005, **23**, 475-483.

190. S. K. R. Williams and D. Lee, *Journal of Separation Science*, 2006, **29**, 1720-1732.

191. J. C. Giddings, *Science*, 1993, **260**, 1456-1465.

192. J. C. Giddings, *Separation Science and Technology*, 1985, **20**, 749-768.

193. C. B. Fuh and J. C. Giddings, *Separation Science and Technology*, 1997, **32**, 2945-2967.

194. C. Ratier and M. Hoyos, *Analytical Chemistry*, 2010, **82**, 1318-1325.

195. J. J. Hawkes, R. W. Barber, D. R. Emerson and W. T. Coakley, *Lab on a Chip*, 2004, **4**, 446-452.

196. N. Tantidanai, W. Veerasai and R. Beckett, *Separation Science and Technology*, 2006, **41**, 3003-3025.

197. M. H. Moon, D. J. Kang, S. Y. Kwon and S. Lee, *Journal of Separation Science*, 2003, **26**, 1675-1682.

198. C. B. Fuh and J. C. Giddings, *Journal of Microcolumn Separations*, 1997, **9**, 205-211.

199. J. Zhang, P. S. Williams, M. N. Myers and J. C. Giddings, *Separation Science and Technology*, 1994, **29**, 2493-2522.

200. C. B. Fuh, H. Y. Tsai and J. Z. Lai, *Analytica Chimica Acta*, 2003, **497**, 115-122.

201. C. B. Fuh, J. Z. Lai and C. M. Chang, *Journal of Chromatography A*, 2001, **923**, 263-270.

202. C. B. Fuh and S. Y. Chen, *Journal of Chromatography A*, 1998, **813**, 313-324.

203. M. Zborowski, P. S. Williams, L. Sun, L. R. Moore and J. J. Chalmers, *Journal of Liquid Chromatography & Related Technologies*, 1997, **20**, 2887-2905.

204. C. Contado, F. Dondi, R. Beckett and J. C. Giddings, *Analytica Chimica Acta*, 1997, **345**, 99-110.

205. Y. H. Zhang, R. W. Barber and D. R. Emerson, *Current Analytical Chemistry*, 2005, **1**, 345-354.

206. A. Ashkin, J. M. Dziedzic, J. E. Bjorkholm and S. Chu, *Optics Letters*, 1986, **11**, 288-290.

207. C. Piggee, *Analytical Chemistry*, 2009, **81**, 16-19.

208. M. P. MacDonald, G. C. Spalding and K. Dholakia, *Nature*, 2003, **426**, 421-424.

209. M. P. MacDonald, S. Neale, L. Paterson, A. Richies, K. Dholakia and G. C. Spalding, *Journal of Biological Regulators and Homeostatic Agents*, 2004, **18**, 200-205.

210. G. Milne, D. Rhodes, M. MacDonald and K. Dholakia, *Optics Letters*, 2007, **32**, 1144-1146.

211. R. F. Marchington, M. Mazilu, S. Kuriakose, V. Garces-Chavez, P. J. Reece, T. F. Krauss, M. Gu and K. Dholakia, *Optics Express*, 2008, **16**, 3712-3726.

212. K. Ladavac, K. Kasza and D. G. Grier, *Physical Review E*, 2004, **70**, 010901.

213. D. Kohlheyer, J. C. T. Eijkel, A. van den Berg and R. B. M. Schasfoort, *Electrophoresis*, 2008, **29**, 977-993.

214. D. Kohlheyer, J. C. T. Eijkel, S. Schlautmann, A. van den Berg and R. B. M. Schasfoort, *Analytical Chemistry*, 2007, **79**, 8190-8198.

215. H. A. Pohl, *Journal of Applied Physics*, 1951, **22**, 869-871.

216. H. A. Pohl, *Dielectrophoresis: the behaviour of neutral matter in non-uniform electric field*, Cambridge University Press, Cambridge, 1978.

217. S. Choi and J. K. Park, *Lab on a Chip*, 2005, **5**, 1161-1167.

218. K. H. Kang, Y. J. Kang, X. C. Xuan and D. Q. Li, *Electrophoresis*, 2006, **27**, 694-702.

219. K. H. Kang, X. C. Xuan, Y. J. Kang and D. Q. Li, *Journal of Applied Physics*, 2006, **99**.

220. S. Chang and Y. H. Cho, *Lab on a Chip*, 2008, **8**, 1930-1936.

221. X. Y. Hu, P. H. Bessette, J. R. Qian, C. D. Meinhart, P. S. Daugherty and H. T. Soh, *Proceedings of the National Academy of Sciences of the United States of America*, 2005, **102**, 15757-15761.

222. P. H. Bessette, X. Y. Hu, H. T. Soh and P. S. Daugherty, *Analytical Chemistry*, 2007, **79**, 2174-2178.

223. M. S. Pommer, Y. T. Zhang, N. Keerthi, D. Chen, J. A. Thomson, C. D. Meinhart and H. T. Soh, *Electrophoresis*, 2008, **29**, 1213-1218.

224. I. Doh and Y. H. Cho, *Sensors and Actuators A - Physical*, 2005, **121**, 59-65.

225. Y. L. Li, C. Dalton, H. J. Crabtree, G. Nilsson and K. Kaler, *Lab on a Chip*, 2007, **7**, 239-248.

226. T. Braschler, N. Demierre, E. Nascimento, T. Silva, A. G. Oliva and P. Renaud, *Lab on a Chip*, 2008, **8**, 280-286.

227. U. Kim, J. R. Qian, S. A. Kenrick, P. S. Daugherty and H. T. Soh, *Analytical Chemistry*, 2008, **80**, 8656-8661.

228.     W. T. Coakley, *Trends in Biotechnology*, 1997, **15**, 506-511.

229.     J. J. Hawkes and W. T. Coakley, *Sensors and Actuators B - Chemical*, 2001, **75**, 213-222.

230.     N. R. Harris, M. Hill, S. Beeby, Y. Shen, N. M. White, J. J. Hawkes and W. T. Coakley, *Sensors and Actuators B - Chemical*, 2003, **95**, 425-434.

231.     A. Nilsson, F. Petersson, H. Jonsson and T. Laurell, *Lab on a Chip*, 2004, **4**, 131-135.

232.     F. Petersson, A. Nilsson, C. Holm, H. Jonsson and T. Laurell, *Lab on a Chip*, 2005, **5**, 20-22.

233.     F. Petersson, A. Nilsson, C. Holm, H. Jonsson and T. Laurell, *Analyst*, 2004, **129**, 938-943.

234.     A. Lenshof, A. Ahmad-Tajudin, K. Jaras, A. M. Sward-Nilsson, L. Aberg, G. Marko-Varga, J. Malm, H. Lilja and T. Laurell, *Analytical Chemistry*, 2009, **81**, 6030-6037.

235.     C. Grenvall, P. Augustsson, J. R. Folkenberg and T. Laurell, *Analytical Chemistry*, 2009, **81**, 6195-6200.

236.     F. Petersson, L. Aberg, A. M. Sward-Nilsson and T. Laurell, *Analytical Chemistry*, 2007, **79**, 5117-5123.

237.     S. Kapishnikov, V. Kantsler and V. Steinberg, *Journal of Statistical Mechanics - Theory and Experiment*, 2006.

238.     R. Piazza and A. Parola, *Journal of Physics-Condensed Matter*, 2008, **20**, 153102.

239.     R. Piazza, *Soft Matter*, 2008, **4**, 1740-1744.

240.     R. Piazza, *Journal of Physics-Condensed Matter*, 2004, **16**, S4195-S4211.

241.     S. Wiegand, *Journal of Physics-Condensed Matter*, 2004, **16**, R357-R379.

242.     J. G. Shackman, M. S. Munson and D. Ross, *Analytical and Bioanalytical Chemistry*, 2007, **387**, 155-158.

243.     D. Ross and L. E. Locascio, *Analytical Chemistry*, 2002, **74**, 2556-2564.

244.     P. F. Geelhoed, R. Lindken and J. Westerweel, *Chemical Engineering Research & Design*, 2006, **84**, 370-373.

245.     D. Vigolo, R. Rusconi, H. A. Stone and R. Piazza, *Soft Matter*, 2010, **6**, 3489-3493.

246.     D. Huh, J. H. Bahng, Y. B. Ling, H. H. Wei, O. D. Kripfgans, J. B. Fowlkes, J. B. Grotberg and S. Takayama, *Analytical Chemistry*, 2007, **79**, 1369-1376.

247.     A. H. Morrish, *The Physical Principles of Magnetism*, IEEE Press, New York, 2001.

248. D. Jiles, *Introduction to Magnetism and Magnetic Materials*, 2nd edn., Chapman & Hall, London, 1998.

249. B. Bederson, *Physical Review Letters*, 2008, **101**, 010002.

250. G. E. Uhlenbeck and S. Goudsmit, *Naturwissenschaften*, 1925, **13**, 953-954.

251. G. E. Uhlenbeck and S. Goudsmit, *Nature*, 1926, **117**, 264-265.

252. Q. A. Pankhurst, J. Connolly, S. K. Jones and J. Dobson, *Journal of Physics D - Applied Physics*, 2003, **36**, R167-R181.

253. W. J. Duffin, *Electricity and Magnetism*, 4th edn., McGraw-Hill Book Company Europe, Maidenhead, UK, 1990.

254. Magnet Sales & Manufacturing, Inc., *http://www.magnetsales.com/Design/DesignG.htm*, accessed 2010.

255. M. A. M. Gijs, *Microfluidics and Nanofluidics*, 2004, **1**, 22-40.

256. M. A. M. Gijs, F. Lacharme and U. Lehmann, *Chemical Reviews*, 2010, **110**, 1518-1563.

257. E. Beaugnon and R. Tournier, *Nature*, 1991, **349**, 470.

258. M. V. Berry and A. K. Geim, *European Journal of Physics*, 1997, **18**, 307-313.

259. K. Guevorkian and J. M. Valles, *Review of Scientific Instruments*, 2005, **76**, 103706.

260. K. Guevorkian and J. M. Valles, *Proceedings of the National Academy of Sciences of the United States of America*, 2006, **103**, 13051-13056.

261. K. Guevorkian and J. M. Valles, *Applied Physics Letters*, 2004, **84**, 4863-4865.

262. J. M. Valles and K. Guevorkian, in *Proceedings of the European Symposium on Life in Space for Life on Earth*, ed. B. Warmbein, 2002, vol. 501, pp. 7-10.

263. J. M. Valles and K. Guevorkian, in *Materials Processing in Magnetic Fields*, eds. H. J. S. Muntau and H. Wada, 2005, pp. 257-265.

264. J. M. Valles, K. Lin, J. M. Denegre and K. L. Mowry, *Biophysical Journal*, 1997, **73**, 1130-1133.

265. J. M. Valles, H. J. Maris, G. M. Seidel, J. Tang and W. Yao, in *Low Gravity Phenomena and Condensed Matter Experiments in Space*, eds. R. Narayanan and T. C. P. Chui, 2005, vol. 36, pp. 114-118.

266. C. Lorin and A. Mailfert, *Journal of Applied Physics*, 2008, **104**.

267. H. M. Lu, D. C. Yin, H. S. Li, L. Q. Geng, C. Y. Zhang, Q. Q. Lu, Y. Z. Guo, W. H. Guo, P. Shang and N. I. Wakayama, *Review of Scientific Instruments*, 2008, **79**.

268. C. Lorin, A. Mailfert and D. Chatain, *Microgravity Science and Technology*, 2010, **22**, 71-77.

269. Y. Liu, D.-M. Zhu, D. M. Strayer and U. E. Israelsson, *Advances in Space Research*, 2010, **45**, 208-213.

270. A. Yamagishi, *Journal of Magnetism and Magnetic Materials*, 1990, **90-91**, 43-46.

271. D. C. Yin, H. M. Lu, L. Q. Geng, Z. H. Shi, H. M. Luo, H. S. Li, Y. J. Ye, W. H. Guo, P. Shang and N. I. Wakayama, *Journal of Crystal Growth*, 2008, **310**, 1206-1212.

272. M. Motokawa, K. Watanabe and S. Awaji, *Current Applied Physics*, 2003, **3**, 367-376.

273. L. Quettier, O. Vincent-Viry, A. Mailfert and F. P. Juster, *European Physical Journal - Applied Physics*, 2003, **22**, 69-73.

274. M. Tagami, M. Hamai, I. Mogi, K. Watanabe and M. Motokawa, *Journal of Crystal Growth*, 1999, **203**, 594-598.

275. N. Kitamura, M. Makihara, T. Sato, M. Hamai, I. Mogi, S. Awaji, K. Watanabe and M. Motokawa, *Journal of Non-Crystalline Solids*, 2001, **293-295**, 624-629.

276. T. Kimura and M. Yamato, in *Materials Processing in Magnetic Fields*, eds. H. J. S. Muntau and H. Wada, 2005, pp. 321-329.

277. T. Kimura, *Polymer Journal*, 2003, **35**, 823-843.

278. E. Beaugnon, D. Bourgault, D. Braithwaite, P. Derango, R. P. Delabathie, A. Sulpice and R. Tournier, *Journal De Physique I*, 1993, **3**, 399-421.

279. I. Mogi, K. Takahashi, S. Awaji, K. Watanabe and M. Motokawa, in *Materials Processing in Magnetic Fields*, eds. H. J. S. Muntau and H. Wada, 2005, pp. 278-284.

280. M. Motokawa, M. Hamai, T. Sato, I. Mogi, S. Awaji, K. Watanabe, N. Kitamura and M. Makihara, *Journal of Magnetism and Magnetic Materials*, 2001, **226-230**, 2090-2093.

281. M. Motokawa, M. Hamai, T. Sato, I. Mogi, S. Awaji, K. Watanabe, N. Kitamura and M. Makihara, *Physica B: Condensed Matter*, 2001, **294-295**, 729-735.

282. M. Motokawa, I. Mogi, M. Tagami, M. Hamai, K. Watanabe and S. Awaji, *Physica B: Condensed Matter*, 1998, **256-258**, 618-620.

283. M. Yamaguchi and Y. Tanimoto, *Magneto-Science*, Springer, Berlin, 2006.

284. A. H. Lu, E. L. Salabas and F. Schuth, *Angewandte Chemie - International Edition*, 2007, **46**, 1222-1244.

285. T. Osaka, T. Matsunaga, T. Nakanishi, A. Arakaki, D. Niwa and H. Iida, *Analytical and Bioanalytical Chemistry*, 2006, **384**, 593-600.

286.    E. Palecek and M. Fojta, *Talanta*, 2007, **74**, 276-290.

287.    Z. M. Saiyed, S. D. Telang and C. N. Ramchand, *BioMagnetic Research and Technology*, 2003, **1**, 2.

288.    I. Safarik and M. Safarikova, *BioMagnetic Research and Technology*, 2004, **2**, 7.

289.    A. G. Wu, P. Ou and L. Y. Zeng, *Nano*, 2010, **5**, 245-270.

290.    K. M. Krishnan, *IEEE Transactions on Magnetics*, 2010, **46**, 2523-2558.

291.    B. Jeyadevan, *Journal of the Ceramic Society of Japan*, 2010, **118**, 391-401.

292.    A. Ito, M. Shinkai, H. Honda and T. Kobayashi, *Journal of Bioscience and Bioengineering*, 2005, **100**, 1-11.

293.    C. Billotey, C. Wilhelm, M. Devaud, J. C. Bacri, J. Bittoun and F. Gazeau, *Magnetic Resonance in Medicine*, 2003, **49**, 646-654.

294.    C. Wilhelm, F. Gazeau, J. Roger, J. N. Pons and J. C. Bacri, *Langmuir*, 2002, **18**, 8148-8155.

295.    C. Wilhelm and F. Gazeau, *Biomaterials*, 2008, **29**, 3161-3174.

296.    C. Wilhelm, F. Gazeau and J. C. Bacri, *European Biophysics Journal with Biophysics Letters*, 2002, **31**, 118-125.

297.    O. W. Ronning and A. C. Christophersen, *Hybridoma*, 1991, **10**, 641-645.

298.    S. G. Gundersen, I. Haagensen, T. O. Jonassen, K. J. Figenschau, N. Dejonge and A. M. Deelder, *Journal of Immunological Methods*, 1992, **148**, 1-8.

299.    M. V. Kiselev, A. K. Gladilin, N. S. Melik-Nubarov, P. G. Sveshnikov, P. Miethe and A. V. Levashov, *Analytical Biochemistry*, 1999, **269**, 393-398.

300.    V. Kourilov and M. Steinitz, *Analytical Biochemistry*, 2002, **311**, 166-170.

301.    L. Dorgan, R. Magnotti, J. M. Hou, T. Engle, K. Ruley and B. Shull, *Journal of Magnetism and Magnetic Materials*, 1999, **194**, 69-75.

302.    J. A. Itak, M. Y. Selisker, S. W. Jourdan, J. R. Fleeker and D. P. Herzog, *Journal of Agricultural and Food Chemistry*, 1993, **41**, 2329-2332.

303.    J. A. Itak, M. Y. Selisker, D. P. Herzog, J. R. Fleeker, E. R. Bogus and R. O. Mumma, *Journal of AOAC International*, 1994, **77**, 86-91.

304.    M. Kala, K. Bajaj and S. Sinha, *Analytical Biochemistry*, 1997, **254**, 263-266.

305.    M. A. Sommerfelt, I. Ohlsson, I. Flolid, R. Thorstensson and B. Sorensen, *Journal of Virological Methods*, 2004, **115**, 191-198.

306.    X. Y. Guo, Y. P. Guan, B. Yang, Y. N. Wang, H. L. Lan, W. T. Shi, Z. H. Yang and Z. H. Lu, *International Journal of Molecular Sciences*, 2006, **7**, 274-288.

307. A. P. Fan, C. W. Lau and J. Z. Lu, *Analytical Chemistry*, 2005, **77**, 3238-3242.

308. R. P. Liu, J. T. Liu, L. Xie, M. X. Wang, J. P. Luo and X. X. Cai, *Talanta*, 2010, **81**, 1016-1021.

309. M. Tudorache and C. Bala, *Sensors*, 2008, **8**, 7571-7580.

310. A. Hernandez-Santana, A. Yavorskyy, A. Olinyole, G. M. McCarthy and G. P. McMahon, *Chemical Communications*, 2008, 2686-2688.

311. A. Grützkau and A. Radbruch, *Cytometry Part A*, 2010, **77A**, 643-647.

312. S. Miltenyi, W. Muller, W. Weichel and A. Radbruch, *Cytometry*, 1990, **11**, 231-238.

313. N. Pamme, *Lab on a Chip*, 2006, **6**, 24-38.

314. M. Brandl, M. Mayer, J. Hartmann, T. Posnicek, C. Fabian and D. Falkenhagen, *Journal of Magnetism and Magnetic Materials*, 2010, **322**, 2454-2464.

315. W. S. Chang, H. Shang, R. M. Perera, S. M. Lok, D. Sedlak, R. J. Kuhn and G. U. Lee, *Analyst*, 2008, **133**, 233-240.

316. J. N. Krishnan, C. Kim, H. J. Park, J. Y. Kang, T. S. Kim and S. K. Kim, *Electrophoresis*, 2009, **30**, 1457-1463.

317. K. Smistrup, M. Q. Bu, A. Wolff, H. Bruus and M. F. Hansen, *Microfluidics and Nanofluidics*, 2008, **4**, 565-573.

318. A. L. Gassner, M. Abonnenc, H. X. Chen, J. Morandini, J. Josserand, J. S. Rossier, J. M. Busnel and H. H. Girault, *Lab on a Chip*, 2009, **9**, 2356-2363.

319. M. Abonnenc, A. L. Gassner, J. Morandini, J. Josserand and H. H. Girault, *Analytical and Bioanalytical Chemistry*, 2009, **395**, 747-757.

320. K. Smistrup, O. Hansen, H. Bruus and M. F. Hansen, *Journal of Magnetism and Magnetic Materials*, 2005, **293**, 597-604.

321. J. W. Choi, T. M. Liakopoulos and C. H. Ahn, *Biosensors & Bioelectronics*, 2001, **16**, 409-416.

322. Q. Ramadan, V. Samper, D. Poenar and C. Yu, *Journal of Magnetism and Magnetic Materials*, 2004, **281**, 150-172.

323. K. Smistrup, P. T. Tang, O. Hansen and M. F. Hansen, *Journal of Magnetism and Magnetic Materials*, 2006, **300**, 418-426.

324. A. Sinha, R. Ganguly and I. K. Puri, *Journal of Magnetism and Magnetic Materials*, 2009, **321**, 2251-2256.

325. K. Smistrup, T. Lund-Olesen, M. F. Hansen and P. T. Tang, *Journal of Applied Physics*, 2006, **99**.

326. H. T. Chen, M. D. Kaminski, P. L. Caviness, X. Q. Liu, P. Dhar, M. Torno and A. J. Rosengart, *Physics in Medicine and Biology*, 2007, **52**, 1185-1196.

327. T. Deng, M. Prentiss and G. M. Whitesides, *Applied Physics Letters*, 2002, **80**, 461-463.

328. T. Deng, G. M. Whitesides, M. Radhakrishnan, G. Zabow and M. Prentiss, *Applied Physics Letters*, 2001, **78**, 1775-1777.

329. P. S. Doyle, J. Bibette, A. Bancaud and J. L. Viovy, *Science*, 2002, **295**, 2237-2237.

330. M. C. Huang, H. Ye, Y. K. Kuan, M. H. Li and J. Y. Ying, *Lab on a Chip*, 2009, **9**, 276-285.

331. R. H. Liu, J. N. Yang, R. Lenigk, J. Bonanno and P. Grodzinski, *Analytical Chemistry*, 2004, **76**, 1824-1831.

332. V. I. Furdui and D. J. Harrison, *Lab on a Chip*, 2004, **4**, 614-618.

333. M. M. Caulum and C. S. Henry, *Lab on a Chip*, 2008, **8**, 865-867.

334. F. Carpino, L. R. Moore, M. Zborowski, J. J. Chalmers and P. S. Williams, *Journal of Magnetism and Magnetic Materials*, 2005, **293**, 546-552.

335. P. S. Williams, F. Carpino and M. Zborowski, *Journal of Magnetism and Magnetic Materials*, 2009, **321**, 1446-1451.

336. L. P. Sun, M. Zborowski, L. R. Moore and J. J. Chalmers, *Cytometry*, 1998, **33**, 469-475.

337. M. Zborowski, L. P. Sun, L. R. Moore, P. S. Williams and J. J. Chalmers, *Journal of Magnetism and Magnetic Materials*, 1999, **194**, 224-230.

338. P. S. Williams, M. Zborowski and J. J. Chalmers, *Analytical Chemistry*, 1999, **71**, 3799-3807.

339. R. Hartig, M. Hausmann and C. Cremer, *Electrophoresis*, 1995, **16**, 789-792.

340. R. Hartig, M. Hausmann, J. Schmitt, D. B. J. Herrmann, M. Riedmiller and C. Cremer, *Electrophoresis*, 1992, **13**, 674-676.

341. G. Blankenstein and U. D. Larsen, *Biosensors & Bioelectronics*, 1998, **13**, 427-438.

342. K. S. Kim and J. K. Park, *Lab on a Chip*, 2005, **5**, 657-664.

343. N. Xia, T. P. Hunt, B. T. Mayers, E. Alsberg, G. M. Whitesides, R. M. Westervelt and D. E. Ingber, *Biomedical Microdevices*, 2006, **8**, 299-308.

344. C. W. Yung, J. Fiering, A. J. Mueller and D. E. Ingber, *Lab on a Chip*, 2009, **9**, 1171-1177.

345. J. J. Lai, K. E. Nelson, M. A. Nash, A. S. Hoffman, P. Yager and P. S. Stayton, *Lab on a Chip*, 2009, **9**, 1997-2002.

346. K. H. Han and A. B. Frazier, *Journal of Applied Physics*, 2004, **96**, 5797-5802.

347. K. H. Han and A. B. Frazier, *IEE Proceedings - Nanobiotechnology*, 2006, **153**, 67-73.

348. K. H. Han and A. B. Frazier, *Lab on a Chip*, 2006, **6**, 265-273.

349. K. H. Han and A. B. Frazier, *Journal of Microelectromechanical Systems*, 2005, **14**, 1422-1431.

350. B. Y. Qu, Z. Y. Wu, F. Fang, Z. M. Bai, D. Z. Yang and S. K. Xu, *Analytical and Bioanalytical Chemistry*, 2008, **392**, 1317-1324.

351. D. W. Inglis, R. Riehn, R. H. Austin and J. C. Sturm, *Applied Physics Letters*, 2004, **85**, 5093-5095.

352. D. W. Inglis, R. Riehn, J. C. Sturm and R. H. Austin, *Journal of Applied Physics*, 2006, **99**.

353. J. D. Adams, U. Kim and H. T. Soh, *Proceedings of the National Academy of Sciences of the United States of America*, 2008, **105**, 18165-18170.

354. C. Derec, C. Wilhelm, J. Servais and J. C. Bacri, *Microfluidics and Nanofluidics*, 2010, **8**, 123-130.

355. A. C. Siegel, S. S. Shevkoplyas, D. B. Weibel, D. A. Bruzewicz, A. W. Martinez and G. M. Whitesides, *Angewandte Chemie - International Edition*, 2006, **45**, 6877-6882.

356. S. H. Song, H. L. Lee, Y. H. Min and H. I. Jung, *Sensors and Actuators B - Chemical*, 2009, **141**, 210-216.

357. X. H. Lou, J. R. Qian, Y. Xiao, L. Viel, A. E. Gerdon, E. T. Lagally, P. Atzberger, T. M. Tarasow, A. J. Heeger and H. T. Soh, *Proceedings of the National Academy of Sciences of the United States of America*, 2009, **106**, 2989-2994.

358. N. Pamme and A. Manz, *Analytical Chemistry*, 2004, **76**, 7250-7256.

359. N. Pamme, R. Koyama and A. Manz, *Lab on a Chip*, 2003, **3**, 187-192.

360. N. Pamme and C. Wilhelm, *Lab on a Chip*, 2006, **6**, 974-980.

361. E. Al-Hetlani, O. J. Hatt, M. Vojtisek, M. D. Tarn, A. Iles and N. Pamme, *AIP Conference Proceedings*, 2010, **1311**, 167-175.

362. E. Al-Hetlani, O. J. Hatt, M. Vojtisek, M. D. Tarn and N. Pamme, *Proceedings of the MicroTAS 2010 Conference*, 2010, 1817-1819.

363. H. Song, D. L. Chen and R. F. Ismagilov, *Angewandte Chemie - International Edition*, 2006, **45**, 7336-7356.

364. A. B. Theberge, F. Courtois, Y. Schaerli, M. Fischlechner, C. Abell, F. Hollfelder and W. T. S. Huck, *Angewandte Chemie - International Edition*, 2010, **49**, 5846-5868.

365. K. Zhang, Q. L. Liang, S. Ma, X. A. Mu, P. Hu, Y. M. Wang and G. A. Luo, *Lab on a Chip*, 2009, **9**, 2992-2999.

366. T. Schneider, S. Karl, L. R. Moore, J. J. Chalmers, P. S. Williams and M. Zborowski, *Analyst*, 2010, **135**, 62-70.

367. T. Schneider, L. R. Moore, Y. Jing, S. Haam, P. S. Williams, A. J. Fleischman, S. Roy, J. J. Chalmers and M. Zborowski, *Journal of Biochemical and Biophysical Methods*, 2006, **68**, 1-21.

368. C. Carr, M. Espy, P. Nath, S. L. Martin, M. D. Ward and J. Martin, *Journal of Magnetism and Magnetic Materials*, 2009, **321**, 1440-1445.

369. M. A. Espy, H. Sandin, C. Carr, C. J. Hanson, M. D. Ward and R. H. Kraus, *Cytometry Part A*, 2006, **69A**, 1132-1142.

370. N. Hirota, M. Kurashige, M. Iwasaka, M. Ikehata, H. Uetake, T. Takayama, H. Nakamura, Y. Ikezoe, S. Ueno and K. Kitazawa, *Physica B*, 2004, **346**, 267.

371. A. Winkleman, R. Perez-Castillejos, K. L. Gudiksen, S. T. Phillips, M. Prentiss and G. M. Whitesides, *Analytical Chemistry*, 2007, **79**, 6542-6550.

372. D. E. Bergbreiter, *Nature*, 2009, **457**, 805-805.

373. K. A. Mirica, S. T. Phillips, S. S. Shevkoplyas and G. M. Whitesides, *Journal of the American Chemical Society*, 2008, **130**, 17678-17680.

374. K. A. Mirica, S. S. Shevkoplyas, S. T. Phillips, M. Gupta and G. M. Whitesides, *Journal of the American Chemical Society*, 2009, **131**, 10049-10058.

375. K. A. Mirica, S. T. Phillips, C. R. Mace and G. M. Whitesides, *Journal of Agricultural and Food Chemistry*, 2010, **58**, 6565-6569.

376. Y. Iiguni, M. Suwa and H. Watarai, *Journal of Chromatography A*, 2004, **1032**, 165-171.

377. E. P. Furlani, *Journal of Physics D - Applied Physics*, 2007, **40**, 1313-1319.

378. J. H. Kang, S. Choi, W. Lee and J. K. Park, *Journal of the American Chemical Society*, 2008, **130**, 396-397.

379. H. Chetouani, C. Jeandey, V. Haguet, H. Rostaing, C. Dieppedale and G. Reyne, *IEEE Transactions on Magnetics*, 2006, **42**, 3557-3559.

380. P. Kauffmann, H. Chetouani, P. Pham, V. Haguet and G. Reyne, *Sensor Letters*, 2009, **7**, 470-474.

381. G. P. Hatch and R. E. Stelter, *Journal of Magnetism and Magnetic Materials*, 2001, **225**, 262-276.

382. S. S. Shevkoplyas, A. C. Siegel, R. M. Westervelt, M. G. Prentiss and G. M. Whitesides, *Lab on a Chip*, 2007, **7**, 1294-1302.

383. N. Pamme, J. C. T. Eijkel and A. Manz, *Journal of Magnetism and Magnetic Materials*, 2006, **307**, 237-244.

384. J. Happel and H. Brenner, *Low Reynolds number hydrodynamics*, 2nd revised edn., Noordhoff International Publishing, Leyden, 1973.

385. M. D. Tarn, N. Hirota, A. Iles and N. Pamme, *Science and Technology of Advanced Materials*, 2009, **10**, 014611.

386. T. Baier, S. Mohanty, K. S. Drese, F. Rampf, J. Kim and F. Schonfeld, *Microfluidics and Nanofluidics*, 2009, **7**, 205-216.

387. S. Mohanty, T. Baier and F. Schonfeld, *Biochemical Engineering Journal*, 2010, **51**, 110-116.

388. S. Takayama, E. Ostuni, P. LeDuc, K. Naruse, D. E. Ingber and G. M. Whitesides, *Nature*, 2001, **411**, 1016-1016.

389. U. Seger, S. Gawad, R. Johann, A. Bertsch and P. Renaud, *Lab on a Chip*, 2004, **4**, 148-151.

390. G. Boer, R. Johann, J. Rohner, F. Merenda, G. Delacretaz, P. Renaud and R. P. Salathe, *Review of Scientific Instruments*, 2007, **78**, 116101.

391. E. Eriksson, K. Sott, F. Lundqvist, M. Sveningsson, J. Scrimgeour, D. Hanstorp, M. Goksor and A. Graneli, *Lab on a Chip*, 2010, **10**, 617-625.

392. E. Eriksson, J. Enger, B. Nordlander, N. Erjavec, K. Ramser, M. Goksor, S. Hohmann, T. Nystrom and D. Hanstorp, *Lab on a Chip*, 2007, **7**, 71-76.

393. T. Kim, L. J. Cheng, M. T. Kao, E. F. Hasselbrink, L. J. Guo and E. Meyhofer, *Lab on a Chip*, 2009, **9**, 1282-1285.

394. S. A. Peyman, A. Iles and N. Pamme, *Chemical Communications*, 2008, 1220-1222.

395. M. D. Tarn, S. A. Peyman, D. Robert, A. Iles, C. Wilhelm and N. Pamme, *Journal of Magnetism and Magnetic Materials*, 2009, **321**, 4115-4122.

396. R. L. Tornay, T. Braschler, N. Demierre, B. Steitz, A. Finka, H. Hofmann, J. A. Hubbell and P. Renaud, *Lab on a Chip*, 2008, **8**, 267-273.

397. K. J. Morton, K. Loutherback, D. W. Inglis, O. K. Tsui, J. C. Sturm, S. Y. Chou and R. H. Austin, *Lab on a Chip*, 2008, **8**, 1448-1453.

398. P. Augustsson, L. B. Aberg, A. M. K. Sward-Nilsson and T. Laurell, *Microchimica Acta*, 2009, **164**, 269-277.

399. R. Ganguly, T. Hahn and S. Hardt, *Microfluidics and Nanofluidics*, 2010, **8**, 739-753.

400. L. A. Sasso, A. Undar and J. D. Zahn, *Microfluidics and Nanofluidics*, 2010, **9**, 253-265.

401. M. Karle, J. Miwa, G. Czilwik, V. Auwarter, G. Roth, R. Zengerle and F. von Stetten, *Lab on a Chip*, 2010, **10**, 3284-3290.

402. G. Fonnum, C. Johansson, A. Molteberg, S. Mørup and E. Aksnes, *Journal of Magnetism and Magnetic Materials*, 2005, **293**, 41-47.

403. D. R. Lide, *CRC Handbook of Chemistry and Physics*, 83rd edn., CRC Press LLC, London, 2002-2003.

404. N. Pamme, *PhD Thesis: Single Particle Analysis in Microfluidic Chips*, Imperial College London, London, 2004.

405. R. K. Shah and A. L. London, *Laminar Flow Forced Convection in Ducts: A Source Book for Compact Heat Exchanger Analytical Data*, Academic Press, New York, 1979.

406. A. Iles, A. Oki and N. Pamme, *Microfluidics and Nanofluidics*, 2007, **3**, 119-122.

407. B. H. Lee and M. M. Sung, *Bulletin of the Korean Chemical Society*, 2005, **26**, 127-130.

408. M. H. Park, Y. J. Jang, H. M. Sung-Suh and M. M. Sung, *Langmuir*, 2004, **20**, 2257-2260.

409. H. Hartshorne, C. J. Backhouse and W. E. Lee, *Sensors and Actuators B - Chemical*, 2004, **99**, 592-600.

410. L. S. Roach, H. Song and R. F. Ismagilov, *Analytical Chemistry*, 2005, **77**, 785-796.

411. Z. P. Chen, R. Z. Xu, Y. Zhang and N. Gu, *Nanoscale Research Letters*, 2009, **4**, 204-209.

412. Y. J. Chuang, J. W. Huang, H. Makamba, M. L. Tsai, C. W. Li and S. H. Chen, *Electrophoresis*, 2006, **27**, 4158-4165.

413. J. J. H. Oosterhof, K. Buijssen, H. J. Busscher, B. van der Laan and H. C. van der Mei, *Applied and Environmental Microbiology*, 2006, **72**, 3673-3677.

414. *Silane Coupling Agent Guide*, United Chemical Techologies, Bristol, PA.

415. B. Arkles, in *Gelest Catalog for Silicon Compounds: Silanes and Silicones*, eds. B. Arkles and G. Larson, Gelest, Inc., Morrisville, 2nd edn., 2008.

416. B. Arkles, *Chemtech*, 1977, **7**, 766-778.

417. A. Manz, N. Pamme and D. Iossifidis, *Bioanalytical Chemistry*, Imperial College Press, London, 2004.

418. J. Clayden, N. Greeves, S. Warren and P. Wothers, *Organic Chemistry*, Oxford University Press, Oxford, 2001.

419. R. F. Fakhrullin, J. Garcia-Alonso and V. N. Paunov, *Soft Matter*, 2010, **6**, 391-397.

420. S. A. Peyman, *PhD Thesis*, University of Hull, Hull, 2010.

421. W. J. Moore, *Physical Chemistry*, 4th edn., Longmans Green & Co. Ltd., London, 1962.

422. Physical characteristics of water (at atmospheric pressure), *http://thermexcel.com/english/tables/eau_atm.htm*, Thermexcel, accessed 2008.

423. H. Kuchling, *Taschenbuch der Physik*, 14th edn., Fachbuchverlag Leipzig-Köln, Leipzig, 1994.

424. S. A. Peyman, A. Iles and N. Pamme, *Lab on a Chip*, 2009, **9**, 3110-3117.

425. S. A. Peyman, H. Patel, N. Belli, A. Iles and N. Pamme, *Magnetohydrodynamics*, 2009, **45**, 361-370.

426. M. Vojtisek, A. Iles and N. Pamme, *Biosensors & Bioelectronics*, 2010, **25**, 2172-2176.

427. J. Berthier and P. Silberzan, *Microfluidics for Biotechnology*, Artech House Publishers, London, 2006.

428. J.-S. Park, S.-H. Song and H.-I. Jung, *Lab on a Chip*, 2009, **9**, 939-948.

429. M. Weigele, S. L. DeBernardo, J. P. Tengi and W. Leimgruber, *Journal of the American Chemical Society*, 1972, **94**, 5927-5928.

430. M. Weigele, J. P. Tengi, J. F. Blount, R. C. Czajkowski and W. Leimgrub, *Journal of the American Chemical Society*, 1972, **94**, 4052-4054.

431. S. Udenfriend, S. Stein, P. Bohlen and W. Dairman, *Science*, 1972, **178**, 871-872.

432. S. Stein, P. Bohlen, J. Stone, W. Dairman and S. Udenfriend, *Archives of Biochemistry and Biophysics*, 1973, **155**, 202-212.

433. R. F. Renzi, J. Stamps, B. A. Horn, S. Ferko, V. A. VanderNoot, J. A. A. West, R. Crocker, B. Wiedenman, D. Yee and J. A. Fruetel, *Analytical Chemistry*, 2005, **77**, 435-441.

434. Y. Eckstein and P. Dreyfuss, *Analytical Chemistry*, 1980, **52**, 537-541.

435. C. N. Jayarajah, A. M. Skelley, A. D. Fortner and R. A. Mathies, *Analytical Chemistry*, 2007, **79**, 8162-8169.

436. R. F. Chen, P. D. Smith and M. Maly, *Archives of Biochemistry and Biophysics*, 1978, **189**, 241-250.

437. S. Stein, P. Bohlen and S. Udenfriend, *Archives of Biochemistry and Biophysics*, 1974, **163**, 400-403.

438. P. Bohlen, S. Stein and W. Dairman, *Federation Proceedings*, 1973, **32**, 647.

439. P. Bohlen, S. Stein, W. Dairman and S. Udenfriend, *Archives of Biochemistry and Biophysics*, 1973, **155**, 213-220.

440. A. Hollander, S. Kropke and F. Pippig, *Surface and Interface Analysis*, 2008, **40**, 379-385.

441. G. Deng, M. A. Markowitz, P. R. Kust and B. P. Gaber, *Materials Science & Engineering C - Biomimetic and Supramolecular Systems*, 2000, **11**, 165-172.

442. M. A. Markowitz, P. E. Schoen, P. Kust and B. P. Gaber, *Colloids and Surfaces A - Physicochemical and Engineering Aspects*, 1999, **150**, 85-94.

443. A. M. Skelley and R. A. Mathies, *Journal of Chromatography A*, 2003, **1021**, 191-199.

444. A. M. Skelley, H. J. Cleaves, C. N. Jayarajah, J. L. Bada and R. A. Mathies, *Astrobiology*, 2006, **6**, 824-837.

445. A. M. Skelley, J. R. Scherer, A. D. Aubrey, W. H. Grover, R. H. C. Ivester, P. Ehrenfreund, F. J. Grunthaner, J. L. Bada and R. A. Mathies, *Proceedings of the National Academy of Sciences of the United States of America*, 2005, **102**, 1041-1046.

446. M. Vojtisek, M. D. Tarn, A. Iles and N. Pamme, *Proceedings of the MicroTAS 2009 Conference*, 2009, 1497-1499.

447. S. B. H. Kent, *Chemical Society Reviews*, 2009, **38**, 338-351.

448. P. D. Bailey, *An Introduction to Peptide Chemistry*, John Wiley & Sons, Chichester, 1992.

449. Lipitor website, *www.lipitor.com*, Pfizer, accessed 2010.

450. Diltiazem website, *www.diltiazem.com*, accessed 2010.

451. R. B. Merrifield, *Journal of the American Chemical Society*, 1963, **85**, 2149-2154.

452. P. Watts, C. Wiles, S. J. Haswell, E. Pombo-Villar and P. Styring, *Chemical Communications*, 2001, 990-991.

453. G. M. Greenway, S. J. Haswell, D. O. Morgan, V. Skelton and P. Styring, *Sensors and Actuators B - Chemical*, 2000, **63**, 153-158.

454. V. Skelton, G. M. Greenway, S. J. Haswell, P. Styring, D. O. Morgan, B. H. Warrington and S. Y. F. Wong, *Analyst*, 2001, **126**, 11-13.

455. E. Valeur and M. Bradley, *Chemical Society Reviews*, 2009, **38**, 606-631.

456. P. Watts, C. Wiles, S. J. Haswell and E. Pombo-Villar, *Tetrahedron*, 2002, **58**, 5427-5439.

457. P. Watts, C. Wiles, S. J. Haswell and E. Pombo-Villar, *Lab on a Chip*, 2002, **2**, 141-144.

458. V. George, P. Watts, S. J. Haswell and E. Pombo-Villar, *Chemical Communications*, 2003, 2886-2887.

459. T. Maruyama, J. Uchida, T. Ohkawa, F. Kubota, N. Kamiya and M. Goto, *Kagaku Kogaku Ronbunshu*, 2004, **30**, 180-182.

460. K. Noren and M. Kempe, *International Journal of Peptide Research and Therapeutics*, 2009, **15**, 287-292.

461. S. N. Ege, *Organic chemistry: Structure and reactivity*, 3rd edn., D. C. Heath and Company, Lexington, MA, 1994.

462. A. M. Song, J. H. Zhang, M. H. Zhang, T. Shen and J. A. Tang, *Colloids and Surfaces a-Physicochemical and Engineering Aspects*, 2000, **167**, 253-262.

463. Invitrogen, *Dynabeads M-270 Carboxylic Acid data sheet*, accessed 2010.

464. M. D. Tarn, S. A. Peyman, R. F. Fakhrullin, A. Iles, V. N. Paunov and N. Pamme, *Proceedings of the MicroTAS 2010 Conference*, 2010, 1679-1681.

465. T. Radeva, *Physical Chemistry of Polyelectrolytes*, CRC Press LLC, London, 2001.

466. B. G. De Geest, N. N. Sanders, G. B. Sukhorukov, J. Demeester and S. C. De Smedt, *Chemical Society Reviews*, 2007, **36**, 636-649.

467. F. Caruso, R. A. Caruso and H. Mohwald, *Science*, 1998, **282**, 1111-1114.

468. S. Leporatti, C. Gao, A. Voigt, E. Donath and H. Mohwald, *European Physical Journal E*, 2001, **5**, 13-20.

469. H. P. Yap, J. F. Quinn, A. P. R. Johnston and F. Caruso, *Macromolecules*, 2007, **40**, 7581-7589.

470. A. P. R. Johnston, C. Cortez, A. S. Angelatos and F. Caruso, *Current Opinion in Colloid & Interface Science*, 2006, **11**, 203-209.

471. D. G. Shchukin, T. Shutava, E. Shchukina, G. B. Sukhorukov and Y. M. Lvov, *Chemistry of Materials*, 2004, **16**, 3446-3451.

472. C. Schuler and F. Caruso, *Biomacromolecules*, 2001, **2**, 921-926.

473. G. B. Sukhorukov, A. A. Antipov, A. Voigt, E. Donath and H. Mohwald, *Macromolecular Rapid Communications*, 2001, **22**, 44-46.

474. X. Tao, J. B. Li and H. Mohwald, *Chemistry - A European Journal*, 2004, **10**, 3397-3403.

475. Z. H. Lu, M. D. Prouty, Z. H. Guo, V. O. Golub, C. Kumar and Y. M. Lvov, *Langmuir*, 2005, **21**, 2042-2050.

476. G. Decher, J. D. Hong and J. Schmitt, *Thin Solid Films*, 1992, **210-211**, 831-835.

477. G. Decher, *Science*, 1997, **277**, 1232-1237.

478.  F. Caruso, H. Lichtenfeld, M. Giersig and H. Mohwald, *Journal of the American Chemical Society*, 1998, **120**, 8523-8524.

479.  E. Donath, G. B. Sukhorukov, F. Caruso, S. A. Davis and H. Mohwald, *Angewandte Chemie - International Edition*, 1998, **37**, 2202-2205.

480.  G. B. Sukhorukov, E. Donath, S. Davis, H. Lichtenfeld, F. Caruso, V. I. Popov and H. Mohwald, *Polymers for Advanced Technologies*, 1998, **9**, 759-767.

481.  G. B. Sukhorukov, E. Donath, H. Lichtenfeld, E. Knippel, M. Knippel, A. Budde and H. Mohwald, *Colloids and Surfaces A - Physicochemical and Engineering Aspects*, 1998, **137**, 253-266.

482.  R. F. Fakhrullin and V. N. Paunov, *Chemical Communications*, 2009, 2511-2513.

483.  J. Schwiertz, W. Meyer-Zaika, L. Ruiz-Gonzalez, J. M. Gonzalez-Calbet, M. Vallet-Regi and M. Epple, *Journal of Materials Chemistry*, 2008, **18**, 3831-3834.

484.  A. A. Antipov, D. Shchukin, Y. Fedutik, A. I. Petrov, G. B. Sukhorukov and H. Mohwald, *Colloids and Surfaces A - Physicochemical and Engineering Aspects*, 2003, **224**, 175-183.

485.  P. Schuetz and F. Caruso, *Advanced Functional Materials*, 2003, **13**, 929-937.

486.  D. Y. Wang and F. Caruso, *Chemistry of Materials*, 2002, **14**, 1909-1913.

487.  H. Ai, S. A. Jones, M. M. de Villiers and Y. M. Lvov, *Journal of Controlled Release*, 2003, **86**, 59-68.

488.  L. Dahne, S. Leporatti, E. Donath and H. Mohwald, *Journal of the American Chemical Society*, 2001, **123**, 5431-5436.

489.  A. Voigt, H. Lichtenfeld, G. B. Sukhorukov, H. Zastrow, E. Donath, H. Baumler and H. Mohwald, *Industrial & Engineering Chemistry Research*, 1999, **38**, 4037-4043.

490.  C. Priest, A. Quinn, A. Postma, A. N. Zelikin, J. Ralston and F. Caruso, *Lab on a Chip*, 2008, **8**, 2182-2187.

491.  S. Zhang, L. Yobas and D. Trau, *Proceedings of the MicroTAS 2008 Conference*, 2008, 1402-1404.

492.  M. Lee, W. Park, C. Chung, J. Lim, S. Kwon, K. H. Ahn, S. J. Lee and K. Char, *Lab on a Chip*, 2010, **10**, 1160-1166.

493.  J. Park and P. T. Hammond, *Macromolecules*, 2005, **38**, 10542-10550.

494.  B. Clyne and J. S. Olshaker, *Journal of Emergency Medicine*, 1999, **17**, 1019-1025.

495.    N. Christodoulides, S. Mohanty, C. S. Miller, M. C. Langub, P. N. Floriano, P. Dharshan, M. F. Ali, B. Bernard, D. Romanovicz, E. Anslyn, P. C. Fox and J. T. McDevitt, *Lab on a Chip*, 2005, **5**, 261-269.

496.    M. Motie, S. Brockmeier and L. A. Potempa, *Journal of Immunology*, 1996, **156**, 4435-4441.

497.    W. K. Lagrand, C. A. Visser, W. T. Hermens, H. W. M. Niessen, F. W. A. Verheugt, G. J. Wolbink and C. E. Hack, *Circulation*, 1999, **100**, 96-102.

498.    M. H. F. Meyer, M. Hartmann, H. J. Krause, G. Blankenstein, B. Mueller-Chorus, J. Oster, P. Miethe and M. Keusgen, *Biosensors & Bioelectronics*, 2007, **22**, 973-979.

499.    F. Baldini, A. Carloni, A. Giannetti, G. Porro and C. Trono, *Sensors and Actuators B - Chemical*, 2009, **139**, 64-68.

500.    The role of C-reactive protein, *www.americanheart.org/presenter.jhtml? identifier=4648*, American Heart Association, accessed 2010.

501.    Y. N. Yang, H. I. Lin, J. H. Wang, S. C. Shiesh and G. B. Lee, *Biosensors & Bioelectronics*, 2009, **24**, 3091-3096.

502.    A. Bhattacharyya and C. M. Klapperich, *Biomedical Microdevices*, 2007, **9**, 245-251.

503.    K. Kriz, F. Ibraimi, M. Lu, L. O. Hansson and D. Kriz, *Analytical Chemistry*, 2005, **77**, 5920-5924.

504.    F. Ibraimi, D. Kriz, M. Lu, L. O. Hansson and K. Kriz, *Analytical and Bioanalytical Chemistry*, 2006, **384**, 651-657.

505.    K. Y. Wang, S. A. Chuang, P. C. Lin, L. S. Huang, S. H. Chen, S. Ouarda, W. H. Pan, P. Y. Lee, C. C. Lin and Y. J. Chen, *Analytical Chemistry*, 2008, **80**, 6159-6167.

506.    X. S. Zhu, D. Y. Duan and N. G. Publicover, *Analyst*, 2010, **135**, 381-389.

507.    T. G. Henares, F. Mizutani and H. Hisamoto, *Analytica Chimica Acta*, 2008, **611**, 17-30.

508.    J. Pultar, U. Sauer, P. Domnanich and C. Preininger, *Biosensors & Bioelectronics*, 2009, **24**, 1456-1461.

509.    K. Hosokawa, M. Omata, K. Sato and M. Maeda, *Lab on a Chip*, 2006, **6**, 236-241.

510.    L. Gervais and E. Delamarche, *Lab on a Chip*, 2009, **9**, 3330-3337.

511.    B. Lassen, K. Holmberg, C. Brink, A. Carlen and J. Olsson, *Colloid and Polymer Science*, 1994, **272**, 1143-1150.

512.    S. A. Peyman, E. Y. Kwan, O. Margarson, A. Iles and N. Pamme, *J. Chromatogr. A*, 2009, **1216**, 9055-9062.

513. A. I. Rodriguez-Villarreal, M. D. Tarn, L. A. Madden, J. B. Lutz, J. Greenman, J. Samitier and N. Pamme, *Lab on a Chip*, 2011, **11**, 1240-1248.

514. H. R. Hulett, W. A. Bonner, J. Barrett and L. A. Herzenberg, *Science*, 1969, **166**, 747-749.

515. X. C. Xuan, J. J. Zhu and C. Church, *Microfluidics and Nanofluidics*, 2010, **9**, 1-16.

516. J. Kruger, K. Singh, A. O'Neill, C. Jackson, A. Morrison and P. O'Brien, *Journal of Micromechanics and Microengineering*, 2002, **12**, 486-494.

517. A. Kummrow, J. Theisen, M. Frankowski, A. Tuchscheerer, H. Yildirim, K. Brattke, M. Schmidt and J. Neukammer, *Lab Chip*, 2009, **9**, 972-981.

518. S. C. Jacobson and J. M. Ramsey, *Anal. Chem.*, 1997, **69**, 3212-3217.

519. L. T. Liang, S. Qian and X. C. Xuan, *Journal of Colloid and Interface Science*, 2010, **350**, 377-379.

520. D. Holmes, H. Morgan and N. G. Green, *Biosensors & Bioelectronics*, 2006, **21**, 1621-1630.

521. J. J. Zhu, T. R. J. Tzeng, G. Q. Hu and X. C. Xuan, *Microfluidics and Nanofluidics*, 2009, **7**, 751-756.

522. J. J. Shi, X. L. Mao, D. Ahmed, A. Colletti and T. J. Huang, *Lab Chip*, 2008, **8**, 221-223.

523. Y. Q. Zhao, B. S. Fujimoto, G. D. M. Jeffries, P. G. Schiro and D. T. Chiu, *Optics Express*, 2007, **15**, 6167-6176.

524. C. D. James, J. McClain, K. R. Pohl, N. Reuel, K. E. Achyuthan, C. J. Bourdon, K. Rahimian, P. C. Galambos, G. Ludwig and M. S. Derzon, *Journal of Micromechanics and Microengineering*, 2010, **20**, 045015.

525. R. Afshar, Y. Moser, T. Lehnert and M. A. M. Gijs, *Analytical Chemistry*, 2011, **83**, 1022-1029.

526. M. Ishida, H. Sakuma, S. Murashima, J. Nishida, M. Senga, S. Kobayasi, K. Takeda and N. Kato, *Journal of Magnetic Resonance Imaging*, 2009, **29**, 205-210.

# Publications

## <u>Journal articles</u>

A. I. Rodríguez-Villarreal, <u>M. D. Tarn</u>, L. A. Madden, J. B. Lutz, J. Greenman, J. Samitier and N. Pamme, "Flow focussing of particles and cells based on their intrinsic properties using a simple diamagnetic repulsion setup", *Lab on a Chip,* 2011*,* **11**, 1240 - 1248, doi: 10.1039/c0lc00464b.

<u>M. D. Tarn</u>, S. A. Peyman, D. Robert, A. Iles, C. Wilhelm and N. Pamme, "The importance of particle type selection and temperature control for on-chip free-flow magnetophoresis", *Journal of Magnetism and Magnetic Materials*, 2009, **321**, 4115 - 4122, doi: 10.1016/j.jmmm.2009.08.016.

<u>M. D. Tarn</u>, N. Hirota, A. Iles and N. Pamme, "On-chip diamagnetic repulsion in continuous flow", *Science and Technology of Advanced Materials*, 2009, **10**, 014611, doi: 10.1088/1468-6996/10/1/014611.

## <u>Oral presentations</u>

<u>M. D. Tarn</u>, S. A. Peyman, A. Iles and N. Pamme, "On-chip continuous flow processing utilising multilaminar flow streams and magnetic microparticles", *Analytical Research Forum 2010*, Loughborough (UK), 26 - 28 July 2010, Book of Abstracts, p. O19.

M. D. Tarn, S. A. Peyman, A. Iles and N. Pamme, "On-chip continuous flow sandwich immunoassays on magnetic particles", *Clinical Biosciences Institute Research Day*, Cottingham (UK), 21 July 2010, Book of Abstracts, p. 7.

*Oral presentation prize awarded.*

M. D. Tarn, S. A. Peyman and N. Pamme, "Continuous magnetic microparticle-based sandwich immunoassays in a multilaminar flow microreactor", *Scientific and Clinical Applications of Magnetic Carriers 2010; 8th International Conference*, Rostock (Germany), 25 - 29 May 2008, Abstract Booklet, p. 38.

M. D. Tarn, D. Robert, S. A. Peyman, A. Iles, C. Wilhelm and N. Pamme, "Temperature-based tuning of magnetic particle separation by on-chip free-flow magnetophoresis", *2nd Micro and Nano Flows Conference*, Uxbridge (UK), 1 - 2 September 2009.

M. D. Tarn, S. A. Peyman, M. Vojtíšek, A. Iles and N. Pamme, "The generation of multi-laminar reagent streams for rapid, sequential (bio)chemical reactions on magnetic particles in a continuous flow microreactor", *2nd Micro and Nano Flows Conference*, Uxbridge (UK), 1 - 2 September 2009.

## Poster presentations

M. D. Tarn, S. A. Peyman, R. F. Fakhrullin, A. Iles, V. N. Paunov and N. Pamme, "Magnetically-actuated particle-based procedures in continuous flow", *The 14th International Conference of Miniaturized Systems for Chemistry and Life Sciences*

*(MicroTAS 2010)*, Groningen (Netherlands), 3 - 7 October 2010, The Proceedings of the µTAS 2010 Conference, p. 1679 - 1681.

M.Vojtíšek, <u>M. D. Tarn</u>, A. Iles and N. Pamme, "Rapid and continuous on-chip multistep chemical processing on magnetic particles", *The 13<sup>th</sup> International Conference of Miniaturized Systems for Chemistry and Life Sciences (MicroTAS 2009)*, Jeju (Korea), 1 - 5 November 2009, The Proceedings of the µTAS 2009 Conference, p. 1497 - 1499.

S. A. Peyman, E.-Y. Kwan, O. Margarson, <u>M. D. Tarn</u>, A. Iles and N. Pamme, "Diamagnetic repulsion – A versatile means for the manipulation of objects in microfluidic devices", *The 13<sup>th</sup> International Conference of Miniaturized Systems for Chemistry and Life Sciences (MicroTAS 2009)*, Jeju (Korea), 1 - 5 November 2009, The Proceedings of the µTAS 2009 Conference, p. 1458 - 1460.

<u>M. D. Tarn</u>, D. Robert, S. A. Peyman, A. Iles, C. Wilhelm and N. Pamme, "Temperature-based tuning of magnetic particle separations", *The 13<sup>th</sup> International Conference of Miniaturized Systems for Chemistry and Life Sciences (MicroTAS 2009)*, Jeju (Korea), 1 - 5 November 2009, The Proceedings of the µTAS 2009 Conference, p. 1449 - 1451.

<u>M. D. Tarn</u>, "The effect of temperature on the manipulation and separation of magnetic particles via on-chip free-flow magnetophoresis", *Biomagnetic Sensing Workshop*, Cambridge (UK), 25 September 2009, Book of Abstracts, p. 27.

S. A. Peyman, <u>M. D. Tarn</u> and N. Pamme, "On-chip deflection of magnetic microparticles in continuous flow. A comparative study", *Scientific and Clinical Applications of Magnetic Carriers 2008; 7th International Conference*, Vancouver (Canada), 21 - 24 May 2008, Book of Abstracts, p. 36.

<u>M. D. Tarn</u>, A. Iles, N. Pamme and N. Hirota, "On-chip diamagnetic repulsion for the continuous flow sorting of particles", *Analytical Research Forum 2008*, Hull (UK), 21 - 23 July 2008, Book of Abstracts, p. P46.

<u>M. D. Tarn</u>, A. Iles, N. Pamme and N. Hirota, "On-chip diamagnetic repulsion in continuous flow", *3rd International Workshop on Materials Analysis and Processing in Magnetic Fields (MAP3)*, Tokyo (Japan), 14 - 16 May 2008, Book of Abstracts, p. 58.

<u>M. D. Tarn</u>, D. Robert, S. A. Peyman, A. Iles and N. Pamme, "Temperature dependence of magnetic particle separations via on-chip free-flow magnetophoresis", *22nd International Symposium on MicroScale Bioseparations & Methods for Systems Biology (MSB 2008)*, Berlin (Germany), 9 - 13 March 2008, Book of Abstracts, p. 277.